The interplay of cardiac developmental factors T-box transcription factor 20 (Tbx20) and Bone morphogenetic protein 2 (Bmp2) and their cross-talk with miR-101-3p in regulating cardiac homeostasis in rodent cardiomyopathy model

Thesis submitted for the Degree of Doctor of Philosophy (Science)
in Life Science and Biotechnology

By

SHREYA DAS

Under the supervision of

DR. ARUNIMA SENGUPTA

Assistant Professor

Department of Life Science and Biotechnology

Jadavpur University

2025

যাদবপুর বিশ্ববিদ্যালয়
কলকাতা-৭০০০৩২, ভারত

*JADAVPUR UNIVERSITY
KOLKATA-700 032, INDIA

DEPARTMENT OF LIFE SCIENCE AND BIOTECHNOLOGY

CERTIFICATE FROM THE SUPERVISOR(S)

This is to certify that the thesis entitled "**The interplay of cardiac developmental factors T-box transcription factor 20 (Tbx20) and Bone morphogenetic protein 2 (Bmp2) and their cross-talk with miR-101-3p in regulating cardiac homeostasis in rodent cardiomyopathy model**" Submitted by **Smt. Shreya Das** who got her name registered on **09.10.2020** for the award of Ph. D. (Science) Degree of Jadavpur University, is absolutely based upon her own work under the supervision of **Dr. Arunima Sengupta** and that neither this thesis nor any part of it has been submitted for either any degree / diploma or any other academic award anywhere before.

Arunima Sengupta 01/07/2025

Dr. Arunima Sengupta,
Assistant Professor,
Department of Life Science and Biotechnology,
Jadavpur University,
Kolkata.

Dr. Arunima Sengupta
UGC – Assistant Professor
Dept. of Life science and Bio-technology
JADAVPUR UNIVERSITY, KOLKATA

DECLARATION

I hereby declare that the work reported in this thesis entitled "**The interplay of cardiac developmental factors T-box transcription factor 20 (Tbx20) and Bone morphogenetic protein 2 (Bmp2) and their cross-talk with miR-101-3p in regulating cardiac homeostasis in rodent cardiomyopathy model**" is entirely original and was performed by me under the supervision of **Dr. Arunima Sengupta**, Assistant Professor, Department of Life Science and Biotechnology, Jadavpur University, Kolkata- 700032, India.

Furthermore, I declare that the contents of this thesis have not been submitted for the award of any degree, diploma, fellowship, associateship or any other similar title of any University or Institution.

Date: 01.07.2025

Shreya Das

SHREYA DAS

Department of Life Science and Biotechnology

Jadavpur University

Kolkata- 700032, India

Dedicated to "Baba" and "Maa," whose unwavering support, countless sacrifices, and constant faith in me have been instrumental in completing my doctoral studies. I also dedicate my work to my husband, "Safirul," for his selfless support, immense motivation, and insightful contributions throughout my PhD journey.

ACKNOWLEDGEMENTS

As I conclude my PhD journey, I want to extend my sincere gratitude to everyone involved for their unwavering guidance and support in their respective capacities, which were pivotal for shaping this research work into its current form. My Ph.D journey has not been short of a true roller coaster ride, filled with bumps and unprecedented turns at every step. Standing at the verge of this adventurous ride, as I look back, I see a younger me who has always been very ambitious and determined to take up this journey and finish it and giving up was never an option. I have literally dreamt of this day with open eyes, and seeing it come true feels overwhelming.

First and foremost, the individual who truly deserves the top position on this acknowledgement list is my mentor and supervisor, ***Dr. Arunima Sengupta***, Assistant Professor, Jadavpur University, Kolkata. Not a single success I have achieved in my scientific career would have been possible without her giving me a chance when I needed it the most. There is an abundance of lessons to learn from Ma'am and much to admire. She has ignited my passion for research and encouraged me to look beyond surface-level details, urging me to delve deeper until clarity is reached. Her insightful feedback throughout my research has significantly enhanced the quality of my work. I especially appreciate her vast knowledge, logical thinking, and leadership skills. She consistently highlights the fundamental importance of honesty in both science and life. She has instilled immense courage and confidence in me, convincing me to attend scientific conferences and seminars, big or small and even abroad. She has always given me full freedom while conducting the experiments, which in turn has instilled in me the traits of becoming an independent researcher. Expressing gratitude to someone who has impacted your life so significantly and whom you respect so highly feels insufficient. No words can truly capture the depth of Ma'am's influence in my life. I will continually strive to embody the scientific wisdom she has instilled in me and uphold the lessons she has taught. My ambition is to make her proud by embracing and applying her values correctly and to one day reflect the exceptional scientist and remarkable person she is. I also thank Ma'am for introducing me to the two most wonderful, adorable and talented kids, ***Anushka*** and ***Shreyan***. I wish and hope they always thrive in life with great success and flying colours.

I am extremely grateful to our present HOD, ***Prof. Biswadip Das,*** and former HODs, ***Prof. Parimal Karmakar*** and ***Prof. Ratan Gachhui***, for allowing me the resources and facilities to conduct my research smoothly at this respected university. I sincerely thank ***Prof.***

Biswadip Das for letting me use his laboratory instrumentation facilities. His willingness to help with departmental processes and quickly address problems has played a crucial role in facilitating my PhD journey.

I sincerely thank other faculty members of the Department of Life Science and Biotechnology, ***Dr. Paltu Kumar Dhal***, ***Dr. Arghya Adhikary***, ***Dr. Sougata Roy Chowdhury,*** ***Dr. Satarupa Das*** and ***Dr. Gouranga Upadhyaya***. I would also like to thank all the Staff members of the department for their cooperation and assistance.

I extend my sincere gratitude to our collaborator and my Research Advisory Committee member, ***Dr. Santanu Chakraborty,*** who is one of the most positive person I have come across in my life. I thank Sir for his unceasing scientific input and motivation in my research work. His insights and varied viewpoints have enhanced this thesis in the best possible way. I sincerely thank Sir for letting me use his laboratory instrumentation facilities. I also thank his lab members ***Riffat Khanam***, ***Madhurima Ghosh***, ***Ipshit Dey*** and ***Pabitra Mandal*** for their cooperation and assistance.

I sincerely thank our other collaborators, ***Dr. Alok Ghosh***, ***Dr. Mijanur Rahaman Molla***, ***Dr. Samit Guha,*** and ***Dr. Pabitra Kumar Paul,*** for their guidance and assistance in the experiments. I also thank their lab members for their cooperation.

I am extremely grateful to all my past and present labmates ***Jayeeta Samanta***, ***Arunima Mondal***, and ***Anuprerna Gangadhar,*** for being extremely helpful and cooperative throughout this journey and maintaining a healthy and friendly laboratory environment. I especially thank ***Madhuchhanda Das*** for being a wonderful friend and labmate one could have asked for. She has always extended her helping hand whenever I needed it. I thank her for her wholehearted assistance in the animal experiments. We have supported one another through the strangest situations and faced situations with broad grins on our faces. Hope our friendship stays like this forever.

I am grateful to ***Annesha Guray*** and ***Upasona Barui*** for being colleagues who quickly turned into great friends. I extend my gratitude to my colleagues and fellow researchers of the Life Science and Biotechnology department who have played a significant role in my research journey in their respective capacities- ***Soumita Paul***, ***Sunirmal Paira***, ***Bhaswar Nandy***, ***Mayukh Bannerjea***, ***Rajlaxmi Gaine***, ***Arnab Kundu***, ***Indraneel Sengupta***, ***Ishita Saha***, ***Rachayeeta Ray***, ***Swarupa Sarkar***, and ***Sontu Halder***. I acknowledge all the other scholars of

the department for their kind cooperation and help. Thank you all for making this PhD journey smoother.

I am sincerely thankful to the Department of Pharmaceutical Technology, Jadavpur University, for providing access to the animal house facility.

I am extremely grateful to my little companions (***Mice and Rats***), who sacrificed their lives for this project; without their contributions, none of this work would have been achievable.

I express my gratitude to the ***University Grant Commission*** research fellowship from the Government of India, New Delhi, for providing financial assistance that has made it possible for me to carry out my research effectively.

The two most happiest people today, who have dreamt of this day along with me, are my parents, ***Mr. Swapan Kumar Das*** and ***Mrs. Mithu Das***. I can't thank them enough for being my pillars of strength in this tumultuous journey. Their love, motivation, sacrifices, encouragement, and support is what have kept me going throughout this rough journey. They have brought me up to be a resilient and independent person, and they have always encouraged my academic pursuits and personal growth without any doubts. The values that my parents have instilled in me have always kept me grounded and motivated me to become a good human being. I aspire to eventually bring them joy and pride by becoming the ideal daughter they have always envisioned, as they truly deserve nothing but the best, forever. The prefix "Dr" before my name is the first step towards this journey. I also thank my other family members for their blessings and love. A special appreciation to my chotomama, ***Mr. Arun Mondal,*** for always motivating and boosting me during this PhD journey.

Another person who has firmly stood by me like a true companion during this journey is my husband, ***Safirul Islam***. I want to convey my deep affection and gratitude to him for his unwavering love and support. Being from the same profession, he is the one who has consistently supported me in every way possible whenever I stumbled upon anything. His scientific wisdom and suggestions have always positively guided my research. His collected demeanor has encouraged me to tackle challenging issues with confidence. I aspire for both of us to achieve esteemed scientific careers in the future, as we have always envisioned. I also thank my in-laws for their blessings and support.

I offer my homage to the ***Almighty*** for guiding me and granting me the endurance and courage to keep my head held high every day and pursue my objectives steadily with

unwavering concentration during my PhD tenure. I also thank my grandparents for always blessing me from their heavenly abode.

As I wrap up this chapter, I feel a deep sense of appreciation for all those who have played a role in it. Whether your name was specifically mentioned or not, each of you has made a lasting impact on my life. As I reflect on the past, I realize that all the difficult experiences I faced were necessary in more ways than one. No matter how devastated I felt at the time, they played a significant role in teaching me the true nature of this world and have made me more resilient than before. As I approach the conclusion of one of the most eventful chapters of my life, the weight of the memories I carry grows heavier each day. I will gather all those memories and keep them safely stored, allowing me to fondly recall moments of joy during times of deep loneliness. I am eternally grateful to everyone for being with me during this journey called "***PhD***"

Shreya Das
Department of Life Science and Biotechnology
Jadavpur University
Kolkata-700032

Contents

Page Numbers

List of Figures

A. Chapter 1

B. Chapter 3

C. Chapter 4

D. Chapter 5

E. Chapter 6

List of Tables

A. Chapter 1

B. Chapter 3

Abbreviations and Acronyms

ACM	Arrhythmogenic Cardiomyopathy
AEBSF	4-(2-Aminoethyl)benzene sulfonyl fluoride hydrochloride
ANF	Atrial Natriuretic Factor
AP	Arterial Pole
Ago	Argonaut
AHF	Anterior Heart Field
APD	Action Potential Duration
Atf	Activating transcription factor
ASK1	Apoptosis Signal-regulating Kinase 1
ATP	Adenosine Triphosphate
AV	Atrioventricular
AVC	Atrioventricular Canal
Bcl_{XL}	B cell lymphoma-extra large
Bax	Bcl2-associated X
Bmp	Bone morphogenetic protein
β-MHC	β-Myosin Heavy Chain
BNP	Brain Natriuretic Peptide
CAD	Coronary Artery Disease
CCN2	Chemokine (C-C) motif ligand 2
CDK	Cyclin Dependent Kinase
ChIP	Chromatin Immunoprecipitation
Chop	C/EBP homologous protein
CS	Carnegie Stage
COUP-TFII	Chicken Ovalbumin Upstream Promoter Transcription Factor 2
CSPG	Chondroitin Sulfate Proteoglycans
CVD	Cardiovascular Disease
Cx	Connexin
DCM	Dilated Cardiomyopathy
DGCR8	DiGeorge Syndrome Critical Region 8
DMP	Dorsal Mesocardial Protrusion
DTT	Dithiothreitol

EC	Endothelial Cell
ECG	Electrocardiograph
ECM	Extracellular Matrix
eIF2α	Eukaryotic Initiation Factor 2 alpha
EMT	Epithelial Mesenchymal Transition
ER	Endoplasmic Reticulum
ErbB	Erb-B2 receptor tyrosine kinase
ERK1/2	Extracellular Signal-Regulated Protein Kinases 1 and 2
ERSR	Endoplasmic Reticulum Stress Response
FAR1	Fatty Acyl-CoA Reductase 1
FGF	Fibroblast Growth Factor
FHF	First Heart Field
Grem2	Gremlin 2
Grp78	Glucose regulated protein 78
GSK-3β	Glycogen Synthase Kinase 3 beta
hESC-CMs	Human Embryonic stem cell-derived cardiomyocytes
hiPSC-CMs	Human induced pluripotent stem cell-derived cardiomyocytes
Hand	Heart and neural crest derivatives
HCM	Hypertrophic Cardiomyopathy
Hcn4	Hyperpolarization activated cyclic nucleotide gated potassium channel 4
Hey	Hairy/Enhancer-of-split related to the YRPW motif protein
HGF	Hepatocyte Growth Factor
Hopx	HOP homeobox
IC	Inner Curvature
Id	Inhibitor of DNA binding
IL	Interleukin
IFT	Inflow Tract
IGF	Insulin-like Growth Factor 1
I/R	Ischemia/ Reperfusion
Ire1α	Inositol-requiring enzyme 1 alpha
IRS-1	Insulin Receptor Substrate 1
Irx4	Iroquois homeobox 4
Isl1	Islet1

JNK	c-Jun-N-terminal kinase
KCNH2	Potassium voltage-gated channel subfamily H member 2
LQTS	Long QT Syndrome
LV	Left Ventricle
LVDP	Left Ventricular Developed Pressure
LVH	Left Ventricular Hypertrophy
LVNC	Left Ventricular Non-compaction
ROS	Reactive Oxygen Species
RV	Right Ventricle
MAPK	Mitogen-Activated Protein Kinase
MCP-1	Monocyte Chemoattractant Protein-1
Mef2	Myocyte enhancer factor 2
MI	Myocardial Infarction
miRNA	MicroRNA
miRISC	miRNA-Induced Silencing Complex
Mlc3f	Fast Myosin light chain 3
Mlc1v/ Mlc2v	Myosin light chain 1, ventricular/ Myosin light chain 2, ventricular
MMP	Matrix Metalloproteinase
Msx1	Msh homeobox 1
MV	Mitral Valve
NET	Neutrophil Extracellular Traps
NFκB	Nuclear Factor kappa B
Nmyc1	N-myc proto-oncogene protein 1
Nog	Noggin
Nr2f2	Nuclear receptor subfamily 2, group F, member 2
Nrg1	Neuregulin 1
Nkx2.5	NK2 Homeobox 5
Notch1	Neurogenic locus notch homolog protein 1
OFT	Outflow Tract
Perk	Protein kinase RNA-activated like ER kinase
PI3K	Phosphatidylinositol 3-kinase
Pitx2	Paired-like homeodomain transcription factor 2
RCM	Restrictive Cardiomyopathy

RecBmp2	Recombinant Bmp2
SA-β-Gal	Senescence Associated-β-Galactosidase
SAHF	Senescence Associated Heterochromatin Foci
SASP	Senescence Associated Secretory Phenotype
α-SMA	alpha Smooth Muscle Actin
Serca	Sarcoplasmic/Endoplasmic Reticulum Calcium ATPase
SHF	Second Heart Field
shRNA	short hairpin RNA
SM	Stomatopharyngeal Membrane
SMC	Smooth Muscle Cell
STEMI	ST elevation Myocardial Infarction
NSTEMI	Non-ST elevation Myocardial Infarction
T2DM	Type 2 Diabetes Mellitus
T2MI	Type 2 Myocardial Infarction
Tbx	T-box transcription factor
Tcf21	Transcription factor 21
TGF	Transforming Growth Factor
Tg	Thapsigargin
TNF	Tumor Necrosis Factor
Tun	Tunicamycin
TV	Tricuspid Valve
UPR	Untranslated Region
URL	Upper Reference Limit
UTR	Untranslated Region
Vcan	Versican
VEGF	Vascular Endothelial Growth Factor
Vim	Vimentin
WGA	Wheat Germ Agglutinin
WHO	World Health Organization
Wt1	Wilms' tumor 1
Yap	Yes associated protein
Xbp1	X-box binding protein 1

Synopsis

This thesis highlights the original findings of the novel role of cardiac T-box transcription factor 20 (Tbx20) and Bone morphogenetic protein 2 (Bmp2) and their cross-talk with miR-101-3p in regulating cardiac homeostasis during Endoplasmic Reticulum (ER) stress and diabetes-induced cardiomyopathy.

Cardiovascular diseases (CVDs) rank as the leading cause of mortality globally. The World Health Organization reports that nearly 75% of individuals with CVD succumb to strokes and heart attacks, with roughly a third of these fatalities occurring in those under 70 years. Hence, the early identification of CVDs has the potential to prevent numerous premature deaths.

The Endoplasmic Reticulum (ER) is an organelle that deliberates the synthesis and proper folding of different proteins. Any disruption in this machinery due to external mediators or internal factors often results in the build-up of unfolded or misfolded proteins. The excessive accumulation of misfolded or unfolded proteins results in the generation of ER stress. ER stress in turn stimulates the Unfolded Protein Response (UPR), which consists of three signaling pathways: Activating transcription factor 6 (Atf6), Protein kinase RNA-activated like ER kinase (Perk), and Inositol-requiring enzyme 1 alpha (Ire1α). The UPR is a two-headed sword with a very intricate balance between the protective and harmful effects of UPR. The UPR signaling is initially beneficial as it helps in the restoration of homeostasis; however, a prolonged ER stress eventually leads to increased programmed cell death due to increased activity of UPR signaling pathway molecules. ER stress has been implicated in the development of CVDs. Studies have reported elevated UPR signaling in patients with heart failure. Increased ER stress results in cardiac hypertrophy, ischemic heart disease and arrhythmias. Therefore, targeting ER stress can serve as an effective therapeutic strategy for curing CVDs.

Tbx20 is a cardiac transcription factor that is indispensable for proper heart development. The neonatal heart is highly proliferative; however, the proliferation ceases in the adult heart. Therefore, the lack of proliferation in the adult heart often results in the generation of heart disorders due to stress or injury. Tbx20 was shown to drive adult heart proliferation post-oxidative stress and hypoxia, however, the role of Tbx20 in ER stress-induced cardiomyopathy was still elusive.

This work was undertaken to elucidate the role of Tbx20 during ER stress-induced cardiomyopathy. Since ER stress is also shown to be involved in the pathogenesis of diabetic cardiomyopathy, therefore, to validate our results in an actual disease model we also

corroborated our findings in a diabetic model. Our study, for the first time, highlighted the novel role of Tbx20 in tilting the balance of UPR towards pro-survival, thereby restoring homeostasis of cardiomyocytes during mild ER stress/diabetes-induced cardiomyopathy. We found a novel signaling pathway of how Tbx20 is increased during ER stress involving the Atf6 arm of UPR signaling. Our *in vivo* data, in concert with the *in vitro* data for the time, showed increased proliferation of cardiomyocytes during mild ER stress/diabetes involving the Tbx20-Bmp2/pSmad1/5/8 signaling axis. However, prolonging ER stress/diabetes resulted in amelioration of Tbx20 with a concomitant decrease in cardiomyocyte proliferation. This prompted us to investigate the function of non-coding RNAs in modulating Tbx20 expression. We uncovered a new role for miR-101-3p in controlling Tbx20 expression in the context of extended ER stress or diabetes, which contributes to increased cardiomyocyte senescence and reduced cardiomyocyte proliferation. Our research also revealed an elevated expression of Bone morphogenetic protein 2 (Bmp2) in cardiac fibroblasts during prolonged ER stress or diabetes, leading to an enhanced inflammatory response that exacerbates cardiomyopathy. We characterized the novel function of miR-101-3p in reducing the expression of the Noggin (Nog) gene, a Bmp2 antagonist, during extended ER stress or diabetes, thus indirectly raising Bmp2 expression and subsequently the inflammatory response. Therefore, our findings establish Tbx20 as a dominant factor in the maintenance of cardiac homeostasis during ER stress-induced cardiomyopathy. Our study further extrapolated the novel role of miR-101-3p and Bmp2 as plausible biomarkers in the early detection of cardiomyopathy.

This thesis is comprised of seven chapters that present the original findings of our research work in a structured manner that is congruous with the topic of the thesis.

- ***Chapter 1 (Review of Literature)*** emphasises the different phases of heart development. It also focuses on the different cell types of the heart, the cross-talk between cardiomyocytes and cardiac fibroblasts and the newer developments in research concerning cardiac regeneration. It highlights a brief overview of cardiac disorders with a special focus on ER stress-mediated cardiomyopathy and diabetic cardiomyopathy. This chapter also highlights the importance of Tbx20 and Bmp2 in cardiac development and diseases. This chapter encompasses the importance of non-coding RNAs, specifically microRNAs (miRNAs), in regulating gene expression resulting in disease progression. This chapter, in short, focuses on an exhaustive study of background findings and the unanswered questions that led to the current study.

- ***Chapter 2 (Hypothesis and Objectives)*** highlights the structured hypothesis, aims and objectives that led to the abstraction and development of this study.

- ***Chapter 3 (Materials and Methods)*** details the methods that were implemented and reagents used while performing the different experimental procedures as discussed in the subsequent chapters.

- ***Chapter 4 (ER stress induces upregulation of transcription factor Tbx20 and downstream Bmp2 signaling to promote cardiomyocyte survival)*** focuses on the novel role of Tbx20 during ER stress-induced cardiomyopathy. In this chapter, we highlight how Tbx20 helps in the restoration of homeostasis during mild ER stress. We show here a novel signaling pathway where Tbx20 is upregulated by the Atf6 arm of UPR signaling. Atf6 directly interacted with Tbx20 to accentuate its expression during ER stress, which was further corroborated by AEBSF (Atf6 inhibitor) treatment. Upregulation of Tbx20 during ER stress induced for a short duration resulted in increased proliferation of cardiomyocytes via the Bmp2-pSmad/1/5/8 pathway, which was corroborated by knockdown of Tbx20. Bmp2, in turn, escalated the expression of Tbx20 via a feed-forward loop mechanism. Interestingly, prolonging the ER stress resulted in the decrease of Tbx20 with concomitant downregulation of Bmp2-pSmad1/5/8 pathway molecules, thereby decreasing the proliferative capacity of cardiomyocytes. Amelioration of Tbx20 during prolonged ER stress was accompanied by an increase in cardiomyocyte apoptosis, thereby shifting the balance from homeostasis to cardiomyopathy. Downregulation of Tbx20 during prolonged ER stress also resulted in alteration of cardiac function in rodents, thereby highlighting the importance of Tbx20 in the maintenance of homeostasis. Another important observation was a sustained increase in the expression of Bmp2 in cardiac fibroblasts during prolonged ER stress, the mechanism of which was delineated in subsequent chapters. Therefore, our study unravels a novel signaling pathway where Atf6 increases the expression of Tbx20 during ER stress, which in turn potentiates cardiomyocyte proliferation via the Bmp2-pSmad1/5/8 axis, thereby restoring cardiac homeostasis.

- ***Chapter 5 (MiR-101-3p mediated regulation of Tbx20 in cardiomyocytes and Bmp2 in cardiac fibroblasts perturb cardiac homeostasis)*** emphasises the role of non-coding RNA, specifically microRNA (miRNA) in regulating the expression of Tbx20 and Bmp2 during prolonged ER stress. The decrease in levels of Tbx20 in cardiomyocytes and heightened expression of Bmp2 in cardiac fibroblasts during prolonged ER stress prompted us to look into the possible role of miRNAs in regulating their expression pattern. We found miR-101-3p to

be upregulated during prolonged ER stress/diabetes. Interestingly, we observed direct binding of miR-101-3p to the 3'UTR of the *tbx20* gene. Using miR-101-3p mimics and inhibitors, we substantiated the regulation of Tbx20 by miR-101-3p. mir-101-3p-mediated attenuation of Tbx20 was associated with increased senescence of cardiomyocytes. The direct role of Tbx20 in repressing the senescence response during ER stress/diabetes in cardiac cells was corroborated by knockdown of Tbx20. Interestingly, miR-101-3p was also shown to target Noggin (Nog), a Bmp2 antagonist. We found direct binding of miR-101-3p to the *nog* gene. Differential expression studies of Nog in cardiomyocytes and fibroblasts revealed higher levels of Nog in fibroblasts compared to cardiomyocytes. miR-101-3p was found to be elevated in fibroblasts during increasing ER stress. Furthermore, mimic and inhibitor studies substantiated miR-101-3p targeting Nog, thereby increasing the expression of Bmp2 during prolonged or increasing ER stress in cardiac fibroblasts. Elevated Bmp2 caused increased inflammatory response in fibroblasts, thereby exacerbating the progression of cardiomyopathy. Therefore, our finding establishes miR-101-3p as a potential ER stress-induced cardiomyopathy detection biomarker. The robust increase of Bmp2 throughout disease progression also makes it a plausible biomarker for the early detection of cardiomyopathy. These results have broader implications since the identification of early biomarkers for cardiac diseases is of utmost importance, since it is the leading cause of mortality worldwide.

- ***Chapter 6 (Conclusions)*** provides a consolidated overview of the conclusions drawn from the results obtained from Chapter 4 and Chapter 5. It highlights the importance of Tbx20 in maintaining cardiac homeostasis during ER stress/diabetes-induced cardiomyopathy. It also emphasizes the role of miR-101-3p in regulating the expression of Tbx20 and Bmp2 during ER stress to induce cardiac senescence and inflammation, thereby making it a potential biomarker for the detection of cardiomyopathy.

- ***Chapter 7 (Bibliography)*** provides the consolidated lists of the illustrated bibliography consisting of research articles, reviews and book chapters, that were considered while conducting the experiments and writing the thesis.

Funding Agencies

- Central University Grant Commission StartUp Grant [No. F.4.5 (192-FRP)/2015 (BSR) to Dr. Arunima Sengupta

- Project Grant sponsored by the Department of Biotechnology (grant no.: BT/Bio-CARe/01/9686/2013-14) to Dr. Arunima Sengupta

- RUSA 2.0 Grant to Dr. Arunima Sengupta

- Project Grant sponsored by the Department of Science and Technology-Science and Engineering Research Board (grant no.: CRG/2020/000348) to Dr. Arunima Sengupta

- Project Grant sponsored by the Department of Science and Technology-Science and Engineering Research Board (grant no.: EMR/2017/001382) to Dr. Santanu Chakraborty

- Project Grant sponsored by Council of Scientific and Industrial Research (grant no.: 37WS(0007)/2023-24/EMR-II/ASPIRE) to Dr. Arunima Sengupta

- Project Grant sponsored by Government of West Bengal Science & Technology and Biotechnology Department (grant no.: 130 (Sanc.)/STBT-13015/9/2025-WBSCST SEC) to Dr. Arunima Sengupta

- University Grants Commission (UGC NET-JRF) Fellowship to Shreya Das

Chapter 1

Review of Literature

1.1 The development of the heart

1.1.1 Linear heart tube formation

Heart development initiates during gastrulation at Carnegie Stage 7 (CS7), marking approximately two weeks of human development (Figure 1). During gastrulation, the bilaminar embryo-blast transforms into a trilaminar structure, consisting of the endoderm, mesoderm, and ectoderm. The mesoderm is separated by the intra-embryonic coelom into a layer called the somatopleuric, which is adjacent to the ectoderm, and a layer known as the splanchnopleuric, which is next to the endoderm. The splanchnopleuric section of the mesoderm develops into the heart. The heart primarily originates from mesoderm, with some areas, like the outflow tract (OFT) cushions, deriving from ectoderm. By CS8, in the trilaminar embryonic layer, cardiac precursor cells are located in two symmetrical mesodermal regions lateral to the stomatopharyngeal membrane (SM), which eventually evolves into the mouth.

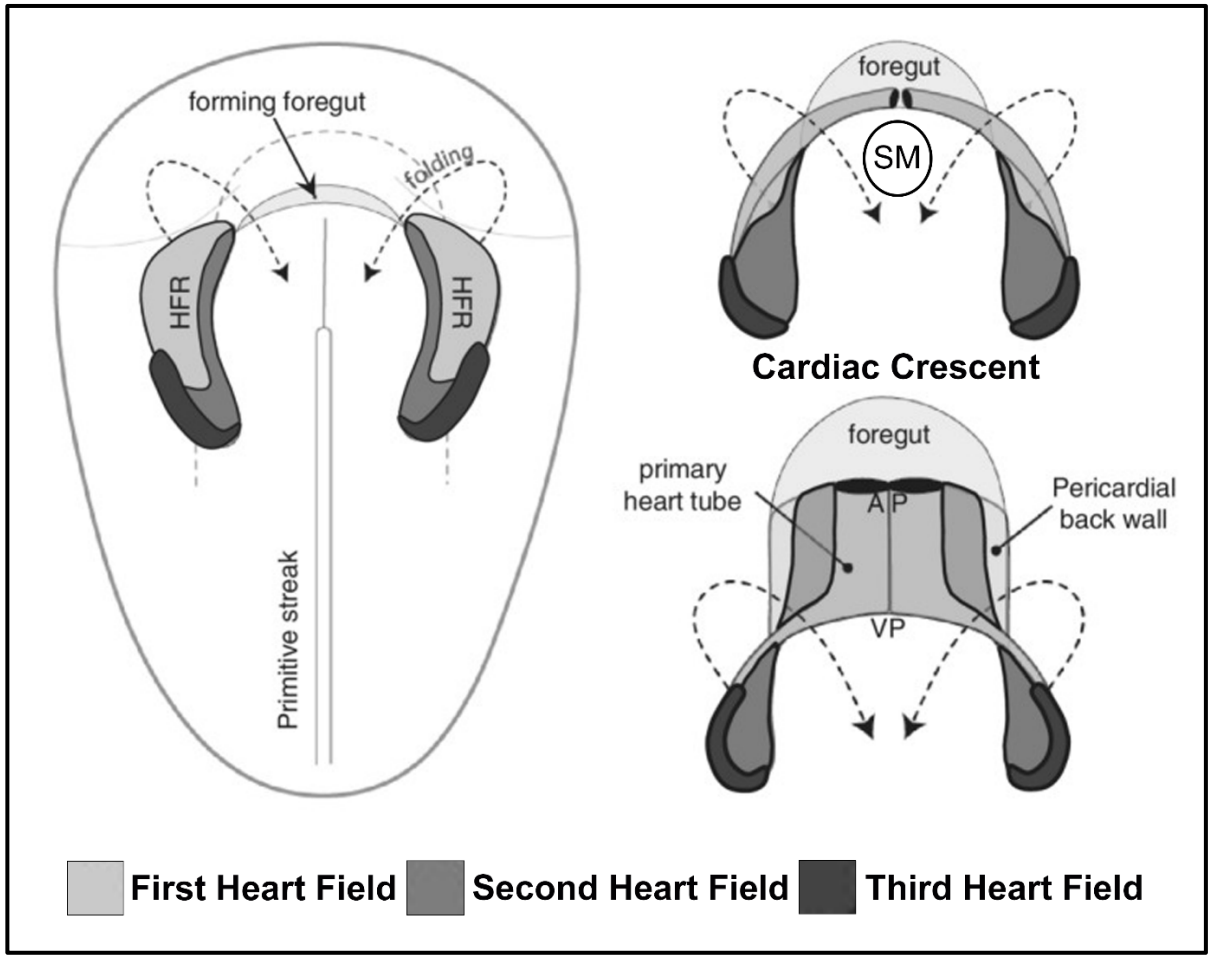

Figure 1. Primary heart tube formation from the heart forming region (HFR). A, Schematic representation depicting the development of the linear heart tube originating from the heart forming region (HFR), viewed from the ventral perspective. The first heart field forms the linear heart tube. The second heart field stays connected to the first heart field throughout further development, and

contributes cardiomyocytes to the forming heart. Abbreviations: HFR, Heart Forming Region; SM, stomatopharyngeal membrane; AP, arterial pole; VP, venous pole. (*Adopted from Buijtendijk et al., 2020*)

These precursor cells converge at the midline, cranial (anterior) to the stomatopharyngeal membrane, forming a horseshoe-shaped structure known as the cardiac crescent (also heart-forming region) (Sizarov et al., 2011). Their differentiation into cardiomyocytes is influenced by growth factor signals from the adjacent endoderm (Harvey, 2002).

During gastrulation, wingless-related integration site (Wnt) growth factors inhibit mesodermal cell differentiation. However, as these cells migrate anteriorly, they exit the Wnt-expressing region and enter the active Wnt inhibition zone, allowing them to develop into cardiac lineages. At CS8, ectodermal and endodermal cells along the lateral margins of the flat embryo produce Bone morphogenetic proteins (Bmps), coordinating the transformation of the cardiac crescent into cardiomyocytes. Additionally, the endoderm expresses Fibroblast Growth Factor (FGF), which defines the heart's posterior boundary. The cardiac crescent also showcases transcription factors like Islet1 (Isl1) and NK2 Homeobox 5 (Nkx2.5). Cardiomyocytes at this stage not only express transcription factors but also sarcomeric genes. The presence of these sarcomeric genes, along with ion channels and pumps in the membrane, facilitates cardiomyocyte contraction (Harvey, 2002; Moorman et al., 2000, 2007; Moorman & Christoffels, 2003; Sizarov et al., 2011). Meanwhile, as mesodermal cells migrate, a subset undergoes epithelial-mesenchymal transition (EMT) to create the endocardial cells, which later develop into channels through ongoing development.

1.1.2 Folding of the embryo

During CS9, which marks the end of week three of human development, the flat embryo begins to fold. Folding of the anterior part of the embryo into the ventro-caudal (posterior) direction results in the formation of a Y-shaped heart tube with two caudo-lateral inlets, also known as the venous pole (VP) and one cranio-medial outlet, also known as the arterial pole (AP). While the peripheral portion of the cardiac crescent forms the venous pole, the central part forms the OFT bordering the pharyngeal mesenchyme (Lescroart et al., 2010). The heart tube consists of about two to three outer strata of cardiomyocytes and a single stratum of endocardial cells on the inside, separated by cardiac jelly (Buijtendijk et al., 2020; Sylva et al., 2014).

1.1.3 Growth and Looping of the Heart

At CS10, which signals the beginning of the fourth week of human heart development,

marks the onset of heart tube looping. During this stage, the dorsal mesocardium ruptures, and the heart tube bends into a C-shaped structure. As it progresses, the intricate structure of heart tube results in it taking on an S-shape (Bayraktar & Manner, 2014). As the heart tube undergoes looping, it continues to grow to about five-fold by incorporating differentiated cardiomyocytes from the surrounding pool of proliferating mesodermal cells near the venous pole. Elevated proliferation rates are controlled by Wnt/β-catenin signaling (Ruiz-Villalba et al., 2016). The cardiac precursor cells are categorized into two groups: the cells forming the initial heart tube are known as first heart field (FHF) cells whereas the cells that are added to the heart tube (cardiac progenitor cells) are known as the second heart field (SHF) cells although, demarcation between the two heart field cells is controversial (Moorman et al., 2007). During addition to the heart tube, the SHF cells express Isl1; however, upon differentiation, the cells express less Isl1 and more Nkx2.5 (Buckingham et al., 2005; Cai et al., 2003). T-box transcription factor 1 (Tbx1) controls the demarcation of SHF progenitor cells to the inflow and outflow pole of the heart (De Bono et al., 2018).

1.1.4 Formation of the four-chambered Heart

Between CS9 and CS10, the S-shaped heart forms distinct inner and outer curvatures (Figure 2). The outer curvature contributes to the development of ventricles by facilitating the re-entry of cardiomyocyte cell division, which promotes both proliferation and differentiation. Similarly, the venous pole of the heart tube contributes to the bilateral extension of atrial appendages through proliferation and differentiation. While the atria form dorsolaterally, they grow cranially on either side of the OFT during development. The formation of cardiac chambers becomes evident as the cardiac jelly between the endocardium and myocardium vanishes, revealing conspicuous myocardial protrusions (trabeculations) on the endocardial side. Chamber myocytes begin expressing various genes, such as atrial natriuretic factor (ANF) and gap-junction protein Connexin 40 (Cx40/Gja5), enabling the creation of conduction channels (Houweling et al., 2002). Important transcription factors like Tbx5 and Tbx20 activate gene expression in ventricular cardiomyocytes, while Tbx2 and Tbx3 repress the ventricular myocardium's gene expression in the atrioventricular region (Greulich et al., 2011). The orientation of mitotic spindles influences trabeculation formation (Passer et al., 2016). In cardiomyocytes, spindles aligned with the heart tube lumen foster heart tube growth, while those oriented along the lumen promote trabeculation formation (Le Garrec et al., 2013).

Endocardial expression of Neurogenic locus notch homolog protein 1 (Notch1) and Neuregulin 1 (Nrg1) regulates the patterning of trabeculation, shaping the endocardium into

dome-like structures enriched with cardiac jelly. Nrg1 from endocardial cells interacts with cardiomyocyte Erb-B2 receptor tyrosine kinase 2 (ErbB2) to stimulate extracellular matrix (ECM) synthesis (del Monte-Nieto et al., 2018). Notch1 signaling facilitates touchdown/dome formation during trabeculation by degrading ECM (del Monte-Nieto et al., 2018). It also plays a pivotal role in ventricle trabeculation and chamber development by directly influencing the EphrinB2/EphB4 pathway, which regulates endocardial Nrg1 synthesis and subsequent ErbB2/ErbB4 production in myocardial cells (Grego-Bessa et al., 2007).

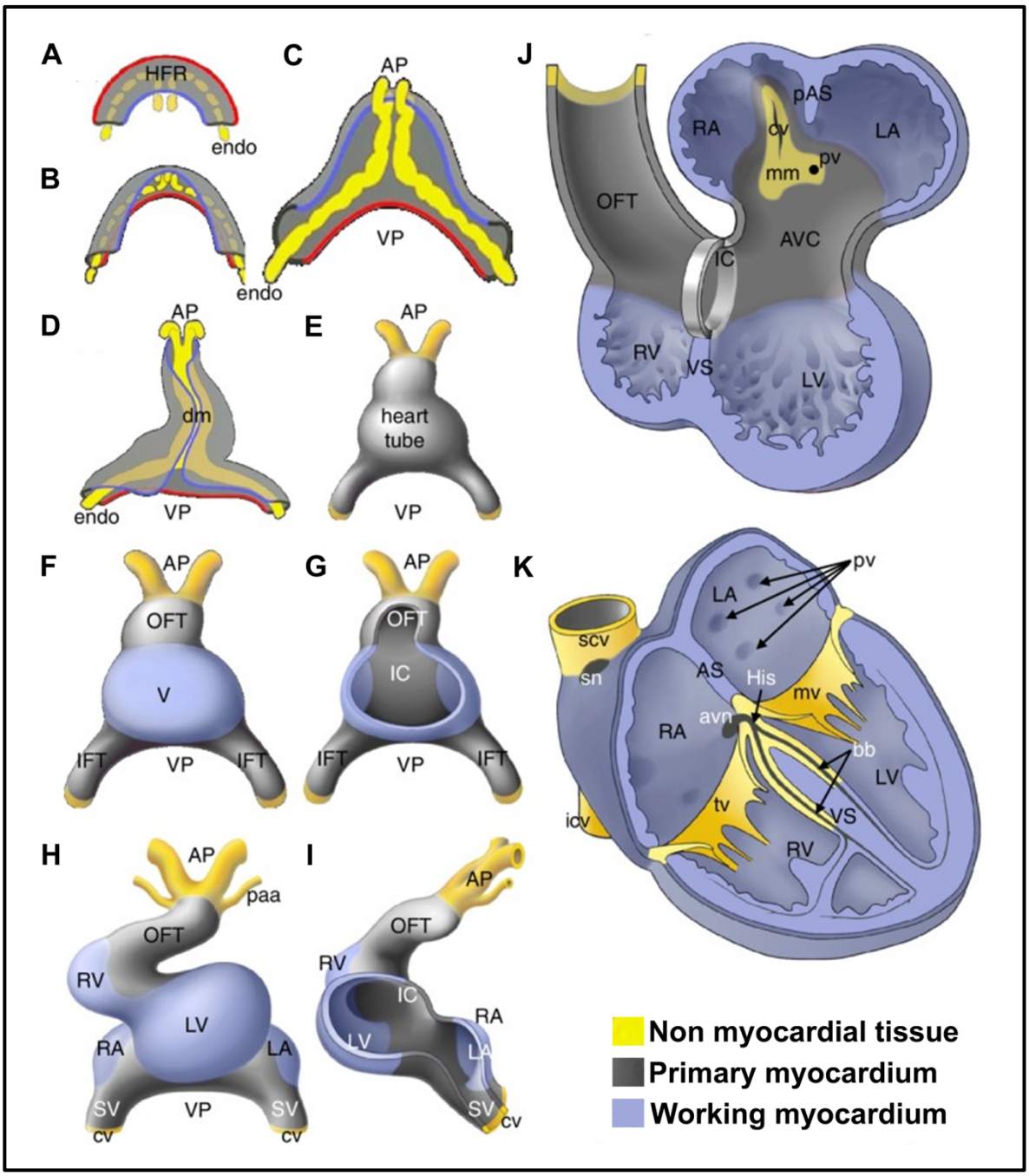

Figure 2. Formation of the adult heart. **A–D,** Diagrams showing a dorsal perspective of heart development. The red line indicates the lateral edge of the heart forming region (HFR), whereas the

blue line represents its medial limit. As embryonic folding advances, the HFR shifts to a position ventral to the foregut (see Figure 1). Where the lateral edges of the HFR meet, the straight heart tube becomes anchored to the body wall via the dorsal mesocardium (dm). **E–H,** Ventral view showing the transformation of the linear heart tube into a four-chambered structure. **F,** Ventral differentiation initiating within the embryonic ventricle (V). **G,** The dorsal portion of the heart tube preserves the primary myocardium, referred to as the inner curvature (IC), which also remains present in the inflow tract (IFT) and outflow tract (OFT) regions. **H,** As looping proceeds, the heart tube bends rightward and chamber formation becomes apparent. The right ventricle (RV) begins to form from primary myocardium in the OFT, while the left atrium (LA) and right atrium (RA) originate from the IFT region. As the heart elongates, newly formed cardiomyocytes are incorporated into the myocardium of the sinus venosus (SV). Venous inflow at the venous pole (VP) is facilitated by the left and right cardinal veins (cv), while outflow at the arterial pole (AP) occurs through the pharyngeal arch arteries (paa)**. I,** Schematic diagram of the ballooning heart, illustrating initial chamber formation. **J,** Representation of the 5-week-old human heart showing enlarged atria and ventricles. Residual primary myocardium is retained in regions like the IFT, AVC (atrioventricular canal), IC, and OFT. The developing primary atrial septum (pAS) and ventricular septum (VS) are also visible. In the left atrium (LA), the mediastinal mesenchyme (mm) connects the heart to the body wall, providing an entry point for the cardinal vein (cv) and the future pulmonary vein (pv). **K,** As the heart matures, the primary myocardium in the atrioventricular canal (AVC) and inflow tract (IFT) differentiates into key elements of the cardiac conduction system, including the sinoatrial node (sn), His bundle, atrioventricular node (avn), and bundle branches (bb). The right atrium receives blood from the superior (scv) and inferior vena cava (icv), while the pulmonary veins (pv) drain into the left atrium. The tricuspid (tv) and mitral (mv) valves develop around the heart chambers. (*Adopted from Buijtendijk et al., 2020*)

Furthermore, endocardial Notch1 also induces myocardial Bmp10 expression, maintaining cardiomyocyte proliferation during trabeculation (Grego-Bessa et al., 2007). Throughout trabeculation, new cardiomyocytes continually add at the base rather than the apex of trabeculae, extending their length. By CS22, marking the eighth week of human development, trabeculations become compact, gradually turning thicker and shorter.

1.1.4.1 Atrial Chamber Formation

The atrial chambers develop symmetrically on the dorso-lateral sides of the heart tube. Myocardium differentiation leads to the creation of working myocardium, which then proliferates to form two pouches known as future atrial appendages. The shape of these appendages is regulated by left-right signaling and influenced by the transcription factor Paired-like homeodomain transcription factor 2c (Pitx2c). Precocious expression of Pitx2c on the left side results in the development of two structurally identical right atria (right atrial isomerism), and the opposite scenario occurs as well (Mommersteeg et al., 2007). Developing atrial myocardium expresses ANF and Cx40, and is bordered by the primary myocardium of the atrioventricular canal (AVC) and the sinus venosus (Christoffels et al., 2000). The AVC distinguishes the atria from the ventricles regarding blood flow, whereas the sinus venosus differentiates the systemic veins from the atria. The atrial myocardium that is formed at the

beginning persists as trabeculated atrial appendages (Christoffels et al., 2000). As development progresses, the atria receive an addition of smooth-walled myocardium.

1.1.4.2 Ventricular Chamber Formation

At CS10, the third week of human development, the ventricles start to develop at the outer edge of the heart tube due to increased cell proliferation and gene expression involved in chamber formation (Moorman & Christoffels, 2003). This process begins with the formation of trabecular myocardium, which expands by incorporating cells at the base instead of the lumen, leading to the external ballooning of the developing ventricles. While the mechanism behind the distinct morphologies of the two ventricles remains unclear, research indicates variations in gene expression patterns between the two ventricles as a plausible cause. For instance, Franco et al. demonstrated using reporter mice that the Myosin light chain 1, ventricular (Mlc1v) is found in the right ventricular myocardium, while Fast Myosin light chain 3 (Mlc3f) is present in the left ventricular myocardium (Franco et al., 2006). The transcription factors heart and neural crest derivatives expressed 1 (Hand1) and heart and neural crest derivatives expressed 2 (Hand2) also play different roles in ventricle formation, with Hand1 directing the formation of the left ventricle and Hand2 guiding the right ventricle's development (Vincentz et al., 2011). By CS14, around 6-7 weeks of gestation, the compact layer of the ventricles arises from the trabecular structure due to interactions between epicardial-derived fibroblasts and trabecular myocardium, leading to enhanced proliferation and differentiation (Ieda et al., 2009). Compaction is driven by thickening of the myocardium located on the epicardial surface of the ventricular walls, while proliferation in the trabeculations of the ventricles ceases. During this phase, the expression of ANF and Cx40 is confined to the initial trabeculated myocardial region and absent in the dense ventricular layer (Sizarov et al., 2011).

Collectively, these processes indicate that the chambers form through ballooning, which occurs due to the proliferation and differentiation of the heart tube. The expanded atrial chambers give rise to the trabeculated myocardium seen in the atrial appendages, while the smooth-walled regions of the atria originate from myocardium associated with the connecting veins. The ventricles develop at the heart tube's outer curvature by forming trabeculated myocardium; with proliferation halting on the luminal side, it instead increases on the pericardial side to create the compact myocardium. Throughout these processes, cardiomyocytes are crucial in various roles such as contraction, conduction, and automaticity, with T-box transcription factors being essential in all three functions.

1.1.4.3 T-Box (Tbx) transcription factors play a crucial role in determining the fate of cardiomyocytes.

The Tbx transcription factor family plays a critical role in regulating the identity of cardiomyocytes during cardiac development (Figure 3). This set of transcription regulators are expressed in various regions of the forming heart, and they influence the heart's electrical organization. While Tbx1 is predominantly expressed in the OFT, Tbx2 is active in the inflow tract (IFT), atrial floor (AF), AVC, inner curvature (IC) and OFT. Tbx3 is primarily expressed in the AF, IC, and AVC. Tbx5, on the contrary, is mainly expressed in IFT, atrial roof (AR), AVC, AF, left ventricle (LV) and IC, and is absent in right ventricle (RV) and OFT. Tbx2 and Tbx3 serve as inhibitors of the gene program responsible for the working myocardium, preserving the primary status of the myocardium of IFT, AVC, and OFT, which allows these areas to take on a different developmental path. Tbx18 is expressed only in IFT (venous pole). Tbx20 is one such transcription factor that is expressed in most parts of the heart (IFT, OFT, AR, AF, LV, RV, AVC and IC) (Sylva et al., 2014).

1.1.5 Development of the Conduction System

During CS9-CS10, which signifies the onset of week three of embryonic development, the peristaltic contraction waves move from the venous end to the arterial end, guaranteeing a unidirectional flow of blood. The Electrocardiograph (ECG) tracing at this point of development exhibits a sinusoidal shape (Christoffels et al., 2010). The polarity of these contractions is due to the presence of the pacemaker channel gene hyperpolarization activated cyclic nucleotide gated potassium channel 4 (Hcn4) located in the cardiomyocytes positioned at the venous pole of heart tube (Mommersteeg et al., 2007). At CS10, developing chamber myocardium transmits depolarizing waves more swiftly than the primary myocardium that flanks the chambers at the venous end, AVC canal and OFT. The presence of differentiating sarcomeres and sarcoplasmic reticulum within the forming chambers also contributes to faster contractions. This variation in contraction speed between the chamber myocardium and primary myocardium helps prevent blood from flowing backwards, thereby ensuring a smooth flow of blood in the absence of valves. The ECG at this stage closely resembles that of an adult ECG, primarily due to the organization of cardiac regions with distinct types of cardiomyocytes, even though a conduction system or differentiated nodes have not yet formed.

1.1.5.1 The Sinus Node

From the early heart tube to the mature heart, electrical impulses consistently travel from

the venous to the arterial pole, positioning the pacemaker activity primarily at the venous pole. The sinus node forms in the myocardium that gets added to the venous pole, where this myocardium does not express Nkx2.5 but does express Tbx18 (Wiese et al., 2009). Lineage tracing studies have indicated that the entire sinus myocardium originates from Tbx18-positive cells (Mommersteeg et al., 2010). The expression of Nkx2.5 is under the control of short stature homeobox 2 (Shox2) (Espinoza-Lewis et al., 2009) (Figure 3).

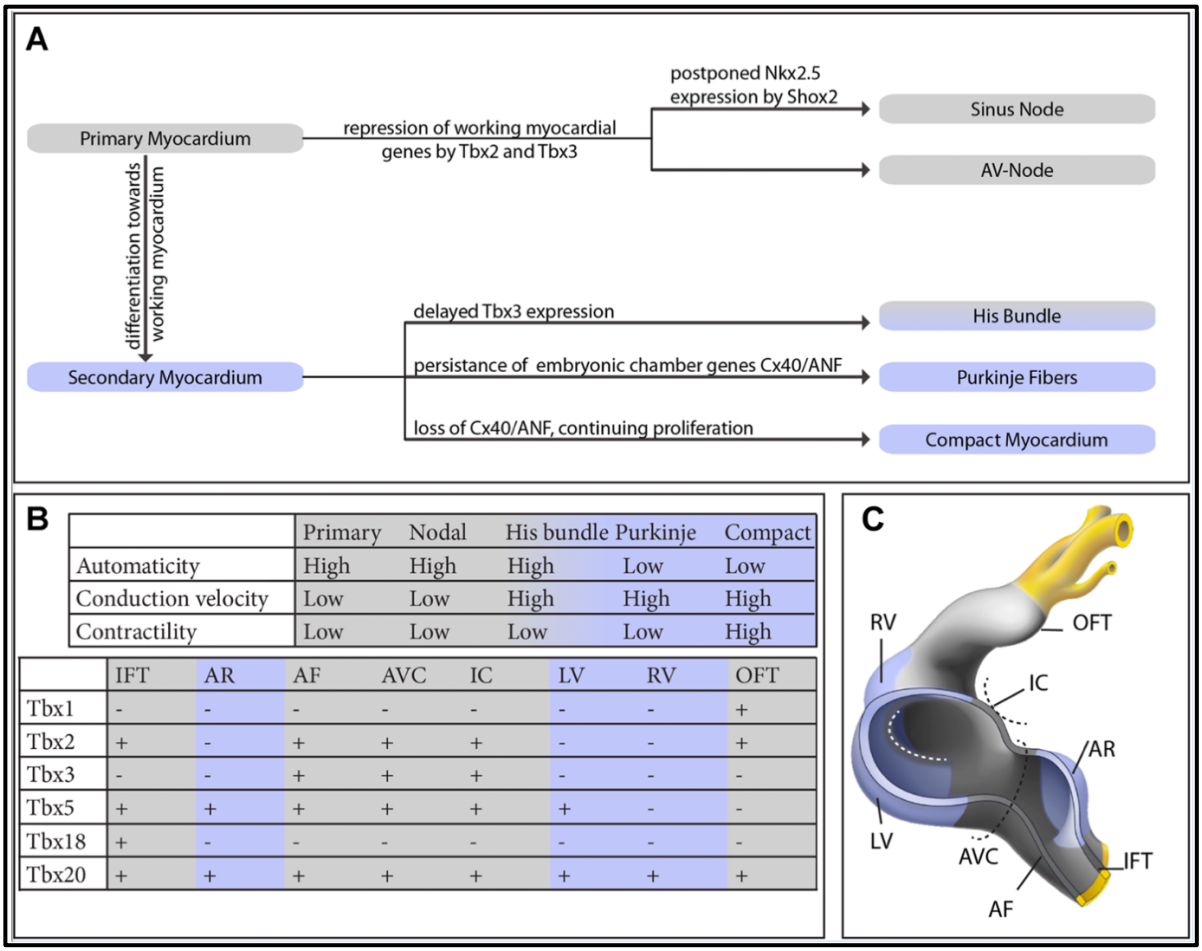

	Primary	Nodal	His bundle	Purkinje	Compact
Automaticity	High	High	High	Low	Low
Conduction velocity	Low	Low	High	High	High
Contractility	Low	Low	Low	Low	High

	IFT	AR	AF	AVC	IC	LV	RV	OFT
Tbx1	-	-	-	-	-	-	-	+
Tbx2	+	-	+	+	+	-	-	+
Tbx3	-	-	+	+	+	-	-	-
Tbx5	+	+	+	+	+	+	-	-
Tbx18	+	-	-	-	-	-	-	-
Tbx20	+	+	+	+	+	+	+	+

Figure 3. Development of the primary myocardium. A, Flowchart depicting the differentiation of the primary myocardium and secondary myocardium and the transcriptional regulation of different factors in determining the development of different types of adult myocardium. **B**, The upper table summarizes the features of various types of myocardium with respect to their electrophysiological behaviour (automaticity and conduction velocity) and contractibility. The lower table outlines the expression pattern of T-box transcription factors in distinct regions of the heart. **C,** Schematic illustration of ballooning heart. Abbreviation: IFT, inflow tract; AR, atrial roof; AF, atrial floor; AVC, atrioventricular canal; IC, inner curvature; LV, left ventricle; RV, right ventricle; OFT, outflow tract. (*Adopted from Sylva et al., 2014)*

Another transcription factor, Tbx3, is exclusively found on the right side of the sinus myocardium. It has been demonstrated that Tbx3 inhibits chamber-specific (working myocardium) gene programs, which prevents the formation of chambers. Pitx2c also regulates

sinus node formation on the right side since the expression of Pitx2c is only present on the left side of the sinus myocardium, and there it inhibits the development of the right-sided sinus node.

1.1.5.2 Atrioventricular node and bundle branches

The atrioventricular (AV) node and the bundle branches form within the AVC myocardium. The transcription factors Tbx2 and Tbx3 preserve the primary identity of the AVC by inhibiting the expression of chamber-specific (working myocardium) genes within the AVC myocardium (Aanhaanen et al., 2011; Stefanovic et al., 2014). The expression of Tbx2 and Tbx3, in turn, is regulated by Bone morphogenetic protein 2 (Bmp2) via a mechanism involving Tbx20 (Singh et al., 2009). In addition, Nkx2.5 and Notch1 signaling also play an important role in maintaining the phenotype of AVC myocardium (Rentschler et al., 2011). Atrioventricular (His) bundle are formed from the differentiation of a group of cells present on top of the forming ventricular septum (Keith & Flack, 2004; Wessels et al., 1992).

1.1.5.3 Peripheral ventricular conduction system

The Purkinje fibers facilitate the transmission of electrical signals from the bundle branches to the heart muscle cells (Figure 3). The gap junctions within the ventricular conduction system have a high concentration of Cx40 and Cx43, which contributes to their rapid conduction capability. In the early stages of development, in the absence of Purkinje fibers, the trabeculated myocardium that expresses connexins serves as both conducting and working myocardium. However, as development progresses, the growth of trabeculae ceases relative to the growth of the compact layer (de Boer et al., 2012). This generates trabeculations as tiny structures that express conducting connexins on the endocardial surface of the heart, and research has demonstrated that they ultimately develop into the Purkinje fibers within the heart (Miquerol et al., 2010).

1.1.6 Septation

Septation is a complicated process that physically separates the initial bloodstream into systemic and pulmonary circulations (Figure 4). The process of septation initiates with the formation of ECM or cardiac jelly between the endocardial and myocardial layers in AVC and OFT. The cardiac jelly deposition becomes sculpted into four major cushions: the posterior and anterior AVC cushions, along with the parietal and septal cushions of the OFT, which are collectively known as ridges.

1.1.6.1 Atrial septation

Atrial septation initiates at CS12 with the formation of a crescent-shaped primary atrial septum due to the proliferation of atrial cells. The front edge of the septum is overlaid by a mesenchymal cap. Anteriorly, the mesenchymal cap is positioned adjacent to the anterior AVC cushion, whereas posteriorly, it connects with the dorsal mesocardial protrusion (DMP) and the posterior AVC cushions (Snarr et al., 2008; Wessels et al., 2000). DMP formation is controlled by Bmp, Sonic Hedgehog (Shh), and Wnt/β-catenin signaling (Briggs et al., 2013, 2016). At CS16, the components of the mesenchymal complex fuse, leading to the closure of atrial foramen. Before the primary atrial foramen closes at CS15, the merging of the apoptosis-mediated small openings in the primary atrial septum leads to the creation of the secondary foramen or ostium secundum. From CS17 onwards, the right atrial muscular walls fold inward to give rise to the secondary atrial septum.

1.1.6.2 Ventricular septation

The interventricular septum is composed of a muscular (myocardial) portion and a membranous portion. As the primary heart tube gives rise to the right and left ventricles, cells located between them contribute to the formation of the upper part of the ventricular septum. The ventricular septum grows by apposition, a process where cells are added to the base of the septum (Sizarov et al., 2011). Aberrant apposition results in the formation of holes in the ventricular septum. The space between the apex of the interventricular septum and the inner curvature is referred to as the ventricular foramen. Before septation, the bloodstream is laminar, and it is separated into right and left-sided circulation (Hogers et al., 1995). Through the ventricular foramen, blood from the right atrium passes to the right ventricle during diastole, and blood from the left ventricle connects to future aorta during systole. The ventricular foramen never closes, and by the end of CS18, it becomes divided by the membranous septum.

1.1.6.3 Septation of the Outflow Tract (OFT)

The myocardial OFT travels from the forming ventricles to the aortic sac, which is located within the pharyngeal arches and linked to the arch arteries. By CS18, continued development results in the division of the OFT by the OFT cushions, giving rise to separate pulmonary and aortic channels (Sizarov et al., 2012). At the beginning, the OFT lengthens by the incorporation of differentiated cardiomyocytes from the SHF at distal extremities (Sizarov et al., 2012; Webb et al., 2003). Starting from CS14, marking the fifth week of human gestation, the OFT gradually shortens as the proximal portion integrates into the right ventricle. In adults,

the OFT features a non-myocardial segment at the mid-point between its distal myocardial edge and pericardial cavity borderline, which ultimately forms the intrapericardial sections of the pulmonary artery and the aorta (Rana et al., 2007; Sizarov et al., 2012). Cells forming the non-myocardial region of the OFT originate from SHF and cardiac neural crest (Cai et al., 2003; Z. Zhou et al., 2017). At CS16, which represents the sixth week of development, the separation of the OFT initiates from the distal end and progresses towards the proximal end, concluding within a week's time by CS18 (Sizarov et al., 2012). The cushions located in the OFT are organized in a spiral manner, ultimately resulting in a 180º twist between the pulmonary and aortic arteries (Sizarov et al., 2012; Ya et al., 1998). At the beginning of the fusion of OFT cushions, cells derived from the endocardium and neural crest invade the proximal region, with the latter occurring at the distal edge. The incomplete fusion of the OFT leads to a condition known as truncus arteriosus.

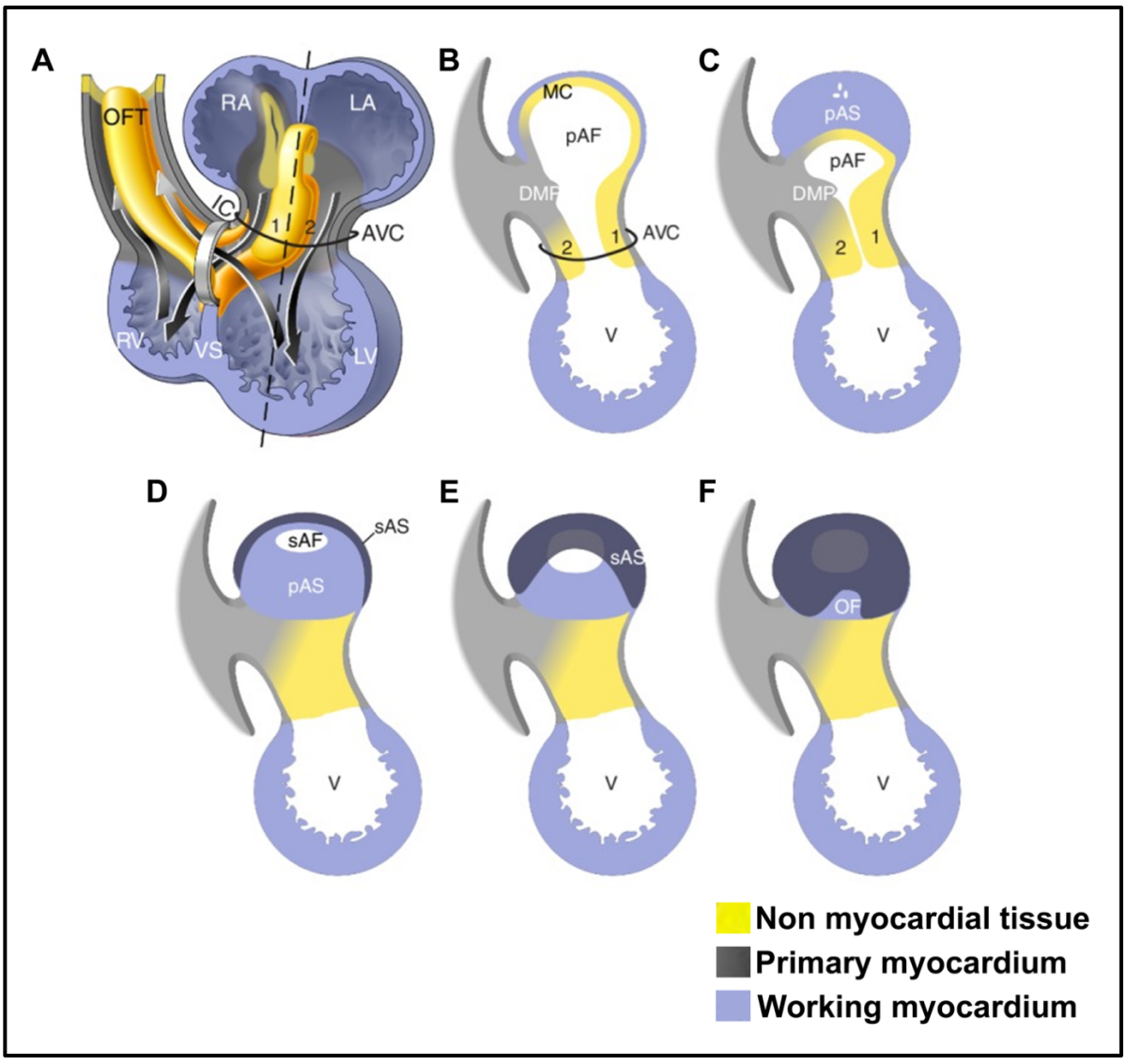

Figure 4. Septation of the heart. A, Illustrative diagram of the developing heart chambers, showing the presence of cushions in the outflow tract (OFT) and atrioventricular canal (AVC). The arrow depicts the flow of blood. The arrows pointing upwards towards the OFT represent the blood flow during systole, whereas the two downward arrows moving through the atrioventricular canal in the ventricle indicate blood flow during diastole. The ventricular foramen marks the junction between the distal end of the ventricular septum (VS) and the inner curvature (IC), serving as a critical pathway for blood flow from the right atrium (RA) to the right ventricle (RV), and from the left ventricle to the outflow tract (OFT). Panels **B–F,** Sagittal sections illustrating atrial septation, corresponding to the dashed line in panel A. The mesenchymal complex composed of the anterior (1) and posterior (2) atrioventricular cushions, the anterior cushion's extension across the atrial roof (MC), and the extracardiac dorsal mesenchymal protrusion (DMP) encircles the connection between the left atrium (LA) and right atrium (RA), the secondary atrial septum (sAS) extends from the atrial wall into the lumen, partially overlapping the primary atrial septum (pAS) and entirely covering the pAF. The portion of the pAS that remains visible is known as the oval fossa (OF). Abbreviations: LA, left atrium; V, ventricle. (*Adopted from Buijtendijk et al., 2020*)

1.1.7 The Cardiac Connective Tissues

Although cardiomyocytes account for approximately 90% of the adult heart's volume, they represent only 50% of the total cell number (Litvinukova et al., 2020). The non-myocyte population of the heart consists of fibroblasts, endothelial cells, smooth muscle cells, hematopoietic-derived cells and immune cells. The cardiac connective tissue arises from four main sources: endocardium, the DMP, cardiac neural crest and epicardium. In addition to that, the heart is also populated by bone-marrow derived cells.

1.1.7.1 Development of Cardiac Vasculature

The coronary veins develop from the expansion of the sinus venosus and ultimately encircle the heart through the enlargement of the associated vessels, a process known as angiogenesis or sprouting. The endothelium of the coronary veins originates from the sinus venosus. The creation of the coronary arteries is a more intricate process. Coronary arteries develop within the sub-epicardial mesenchyme between CS16 and CS18. A coronary plexus arises in this mesenchyme, which later undergoes remodeling to create the coronary artery system. The smooth muscle cells lining of arteries are derived from epicardial cells. The formation of the coronary arteries involves vasculogenesis, which is the development of new vessels that subsequently integrate into the circulatory system. It remains unclear whether the endothelial cells of the coronary arteries originate from the sprouting veins or a separate precursor population present in the sub-epicardial mesenchyme (Katz et al., 2012). After the coronary arteries and veins have developed, they establish a connection to the aorta. The specific signaling mechanisms that promote the growth of coronary arteries towards the aorta and facilitate their entry into the aortic wall to connect with the systemic circulation are still not fully understood. Alterations in OFT development such as those caused by Tbx1 deficiency

disrupts the connection between the coronary arteries and the cardiac outflow tracts, highlighting the close relationship between OFT formation and coronary artery development (Theveniau-Ruissy et al., 2008).

1.1.8 Development of the valves

Heart valves maintain unidirectional blood flow. The arterial valves stop blood from flowing back into the ventricles during diastole, whereas the atrioventricular valves prevent blood from returning to the atria during systole. In the initial heart tube, where blood flow is unidirectional, the backflow of blood is halted by the closure of the cardiac lumen during contraction, a process supported by the cardiac jelly positioned between the endocardium and the myocardium. As heart development progresses, the chambers begin to form. These chambers do not contain cardiac jelly, and the myocardium of the heart undergoes changes in its contractile characteristics. The cardiac jelly found in the venous pole, AVC, and OFT myocardium transforms to form cushions and ridges. These cushions and ridges then develop into the valves (Moorman et al., 2007) (Figure 5).

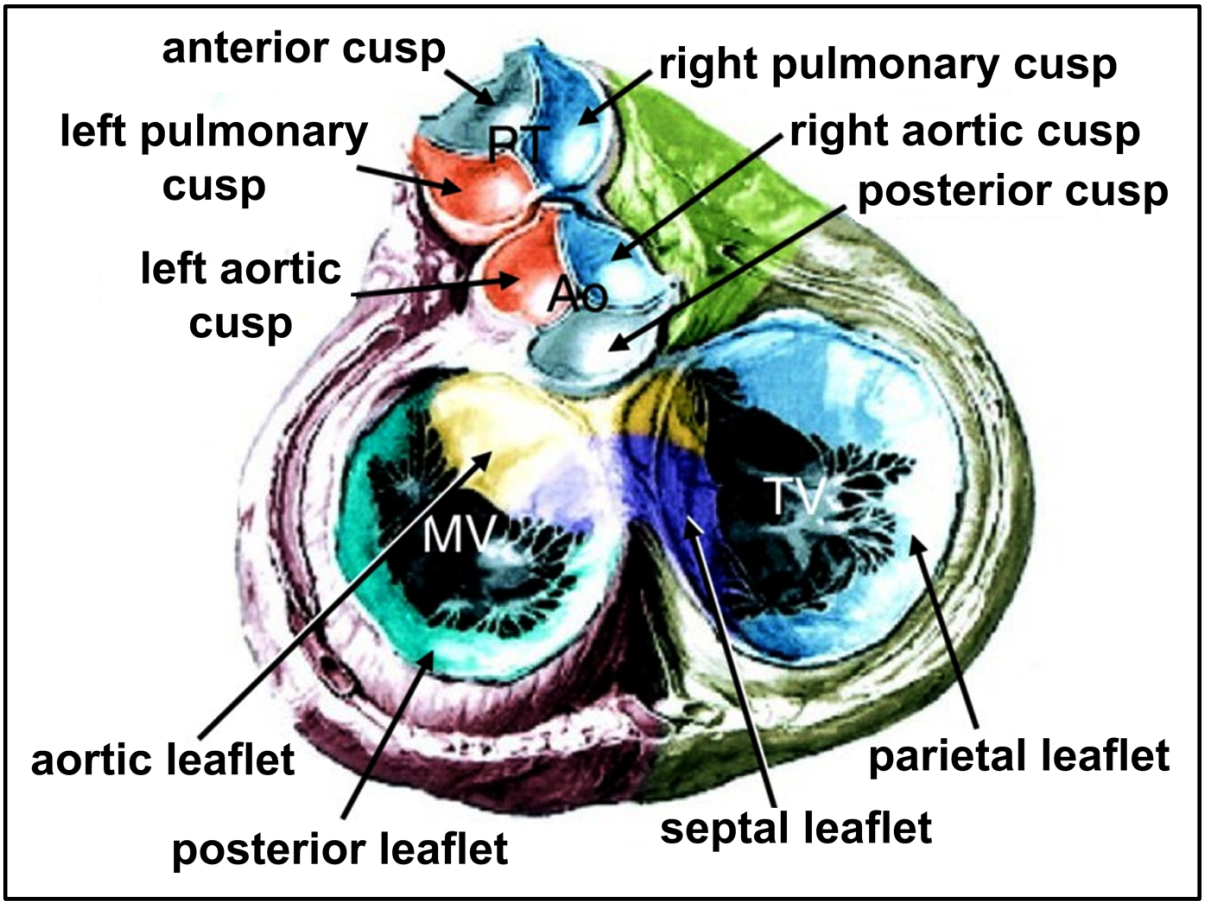

Figure 5. Contributing tissues in the development of atrioventricular (AV) and outflow tract (OFT) valves. Diagram illustrating the tissue origins involved in the development of the mitral valve (MV), tricuspid valve (TV), and semilunar valves. The left pulmonary and left aortic cusps are derived

from the septal outflow tract (OFT) cushion (orange), while the right pulmonary and right aortic cusps originate from the parietal OFT cushion (blue). The anterior cusp of the pulmonary trunk (PT) forms from the right intercalated disc (gray), and the posterior aortic cusp is derived from the left intercalated disc (gray). In the MV, the aortic (anterior) leaflet develops from the ventral atrioventricular (AV) cushion (yellow), and the posterior leaflet forms from the left lateral AV cushion (green). For the TV, the septal leaflet arises from the fused dorsal AV cushion (violet), and the parietal leaflet is derived from the right lateral AV cushion (light blue). The MV's aortic leaflet and the TV's septal leaflet originate from endocardial cells, whereas the MV's posterior leaflet and TV's parietal leaflet are derived from epicardial cells. (*Adopted from Buijtendijk et al., 2020*)

1.2 Difference in cardiovascular development between humans and mice

The cardiovascular development in human and mouse fetuses follows almost similar sequential events with few minor differences. In humans, the superior vena cava is singular and located on the right side, while in mice, it is bilateral. The AV septum of humans is thin and fibrous, whereas in mice, they are thick. Mice lack a difference in trabeculation of the right and left ventricles. In mice, the moderator band is absent. Humans generally have multiple pulmonary venous orifices, whereas in mice, they only have a single orifice. In mice, the atrial appendages are notably more pronounced than those in humans. In humans, the atrial appendages are small. The concurrent phases of cardiovascular development in human and mice is listed in Table 1.

Table 1: Concurrent phases of cardiovascular development in both humans and mice (Oostra et al., 2007; O'Rahilly & Muller, 2010)**.**

Human (Days post coitum)	Mouse (Days post coitum)	Human Carnegie Stage	Developmental events
17-19	7	CS8	Formation of cardiac crescent
19-21	7.5	CS9	The embryo begins to fold, the pericardiac cavity reaches its final location, a groove of myocardium develops, the endocardial plexus is established, and cardiac jelly is produced.
22-23	8	CS10	The heart begins to beat, the endocardial tubes come together and fuses, the mesocardium develops perforations, looping begins, and the ventricle starts to balloon.
23-26	8.5	CS11	The atria balloons, while the pro-epicardium develops.
26-30	9.5	CS12	The septum primum begins to develop, the right venous valve forms, cells appear

			within the cardiac jelly, and the growth of the epicardium commences.
28-30	10.5	CS13	The AV cushion develops, left venous valve forms, the pulmonary vein connects with the atrium, epicardial mesenchyme forms.
31-35	11.5	CS14	The atrioventricular cushions move closer together, OFT ridges start to emerge, capillaries develop within the epicardial mesenchyme.
35-38	12	CS15	The AV cushions face each other, the secondary foramen develops, the distal OFT becomes septated, the OFT ridges extend to the primary foramen.
37-42	12.5	CS16	The primary atrial septum completes its closure, the OFT ridges move towards the interventricular septum. The whole heart becomes enveloped in epicardium.
42-44	13.5	CS17	The secondary atrial septum becomes evident, allowing the sinus node to be discernable, the connections between the left and right atrioventricular areas become distinct, the proximal OFT undergoes septation, and the semilunar valves begin to form.
44-48	14.5	CS18	The formation of AV valves commences
48-51	15	CS19	The left venous valve merges with the secondary septum, and the mural leaflets of both the mitral and tricuspid valves are released.
53-54	16	CS21	Coronary artery branches becomes evident.
54-56	16.5	CS22	Formation of chorda tendinae
56-60	17.5	CS23	Delamination of leaflet of tricuspid valve.

1.3 The major cell types of the heart

The heart tissue is composed of multiple cell types. There are mainly two populations of cardiac cells: myocytes and non-myocytes. The myocytes consist of cardiomyocytes, whereas the non-myocytes are composed of fibroblasts, endothelial cells, smooth muscle cells, pericytes, adipocytes, immune cells and neuronal cells (Figure 6).

1.3.1 Cardiomyocytes

The cardiomyocytes make up most of the heart's volume due to their large size and are responsible for cardiac contraction and relaxation, which are essential for pumping blood throughout the body. The cytoplasm of cardiomyocytes is rich in sarcomeres (necessary for contraction and relaxation) and mitochondria (needed for the cross-bridge cycle during

contraction and relaxation). There is a difference in transcriptional regulation between atrial and ventricular cardiomyocytes. Cardiomyocytes are mechanically and electrically coupled to each other, and they interact with one another and with other cell types (for circulation and structural support) through direct physical contact via gap junctions, desmosomes, and adhesion junctions, or through paracrine and autocrine signaling (Totland et al., 2020). In post-natal hearts, cardiomyocytes undergo structural alterations, with cell cycle arrest, and eventually become binucleated, growing by hypertrophy to meet the physiological requirements of the growing heart (Hirai et al., 2016). They also undergo alteration in metabolic and energy requirements as they shift from glycolysis to fatty acid oxidation, since fatty acid oxidation produces the highest yield of Adenosine Triphosphate (ATP).

1.3.2 Cardiac Fibroblasts

Fibroblasts are the most prevalent cell type (non-cardiomyocyte) found in the heart. Cardiac fibroblasts are spindle-shaped cells that are localised in the myocardial interstitium and in close proximity to blood vessels and capillaries, and display huge levels of phenotypic plasticity. Cardiac fibroblasts are derived from the epicardium via EMT as they express epicardial markers Wt1 and Transcription factor 21(Tcf21) (Acharya et al., 2012; Wessels et al., 2012). In addition to this, mesoangioblasts also adds to the population of fibroblasts (Cossu & Bianco, 2003). In the developing heart, fibroblast aids in cardiomyocyte proliferation via fibronectin/β1–integrin-mediated signaling (Ieda et al., 2009). They play an important role in providing structural and mechanical support to the heart by coordinating the synthesis and remodelling ECM and collagen fibres to ensure proper rhythm and conduction throughout the heart. Cardiac fibroblasts have a significant membrane resistance, enabling them to conduct effectively. In response to injury, the cardiac fibroblasts are activated primarily by TGFβ (Stempien-Otero et al., 2016). TGFβ binding results in heterodimerization of TGFβR1 and TGFβR2, which causes phosphorylation of transcription factor Smad2/3. Smad2/3 then translocates to the nucleus, where it forms a complex with Smad4 and augments the transcription of fibroblast differentiation-specific genes (Derynck & Zhang, 2003). Other signaling pathways like Wnt/β-catenin, p38 MAPK, GPCR, and Hippo signaling also induce the activation of fibroblasts upon myocardial injury (Duan et al., 2012; Molkentin et al., 2017; Woodall et al., 2016; Xiang et al., 2017; Xiao et al., 2019). Activated fibroblasts release pro-inflammatory cytokines and chemokines like IL-1, TNFα, and Chemokine (C-C) motif ligand 2 (CCL2) that in turn, contribute to the recruitment of leukocytes. Activated fibroblasts also release MMPs that promote ECM degradation. At first, all of these alterations are essential for

the reparative process of wound healing; however, as time progresses, these modifications can become detrimental, resulting in fibrosis and impaired cardiac function.

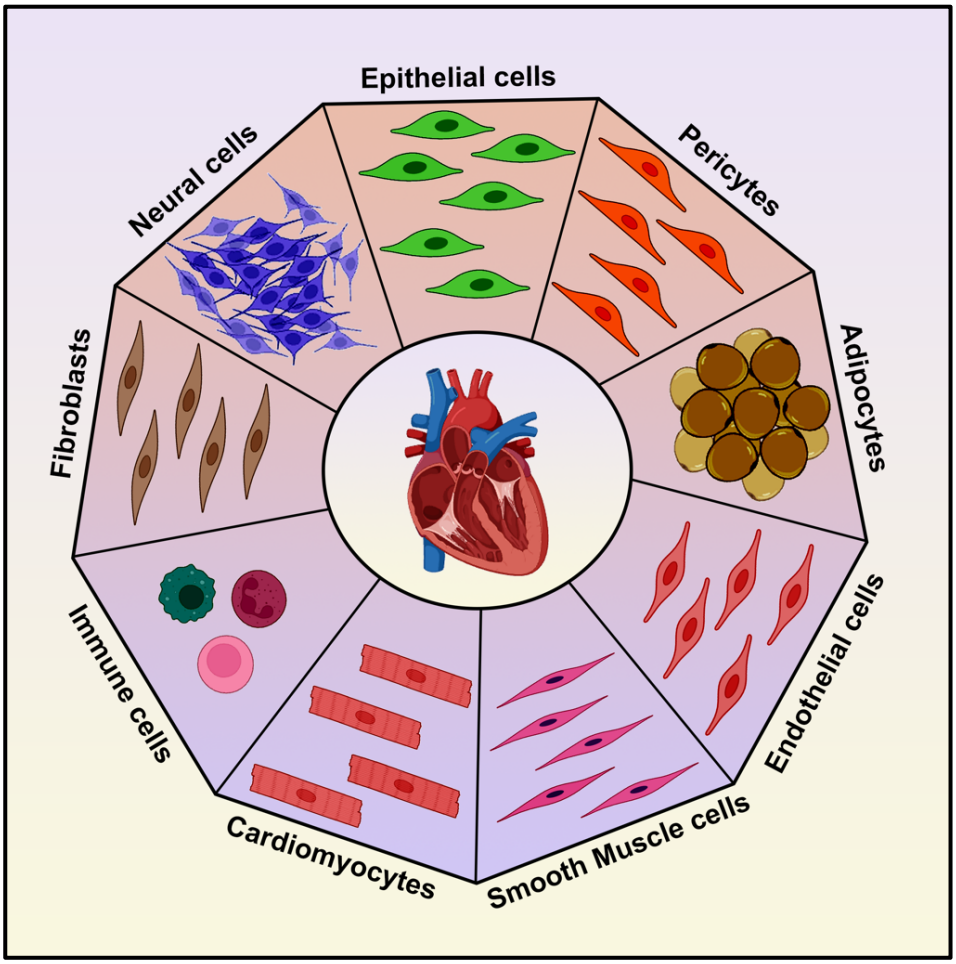

Figure 6. Cell types of the heart. Schematic representation of different cell types of the heart.

1.3.3 Endothelial Cells

Endothelial Cells (ECs), which line the interior of blood vessels and lymphatics, are metabolically active and play vital roles in regulating blood flow, vasomotor function, nutrient and gas exchange, angiogenesis, and inflammatory responses (Aird, 2007, 2012). The endothelium can keep blood in a liquid state, which helps to restrict the formation of clots. ECs produce various anti-coagulant factors, including tissue factor pathway inhibitor, heparan, thrombomodulin, endothelial protein C receptor, prostacyclin, and nitric oxide. In contrast, ECs can also synthesize procoagulant factors such as tissue factor, plasminogen activator inhibitor-1, von Willebrand factor, and protease-activated receptors (Aird, 2001). The endothelium can be classified into two types: continuous and discontinuous. Continuous endothelium can further be classified into two types: fenestrated and non-fenestrated. Continuous endothelium is defined by ECs that are closely linked to one another and are enclosed by an uninterrupted

basement membrane. Non-fenestrated continuous endothelium exists in the arteries, veins, and capillaries of the brain, skin, heart, and lungs (Aird, 2007). The connections between endothelial cells in arteries are more closely bound than those seen in veins. Capillaries feature flattened ECs along with sporadic pericytes and an ECM (Aird, 2007). The heart contains various compartments that contain ECs, such as endocardium, coronary arteries, and capillaries. The higher presence of gap junctions, including connexins, in the endocardium versus myocardial capillary ECs arises from the greater number of intercellular clefts, gap junctions, and fewer vesicles in the endocardium (Aird, 2007). The ECs lining the coronary arteries share structural and functional similarities with ECs found in other body arteries; in contrast, the capillaries within the heart feature a continuous endothelium. Like the endocardium, the endothelial cells in myocardial capillaries participate in reciprocal signaling with cardiomyocytes (Aird, 2007). Within the endocardium, the levels of von Willebrand factor and nitric oxide synthase are significantly higher compared to those in myocardial microvessels, and in the endocardium. EC dysfunction results in different pathophysiological conditions like atherosclerosis, hypertension, valvular degeneration, thrombosis and sepsis.

1.3.4 Smooth Muscle Cells

Smooth Muscle Cells (SMCs) are found in the tunica media of blood vessels, where they are responsible for vascular contraction and the production of ECM (Zhuge et al., 2020). These cells are also crucial for the vessel's compliance and ability to rebound elastically in response to changes in hemodynamic conditions. However, under pathological or stressed conditions, SMCs can undergo a phenotypic shift from a contractile to a synthetic state or even transform into different cell types, which can either positively or negatively influence the progression of disease (Zhuge et al., 2020). Contractile SMCs express integrins α1β1 and α7β1. The lack of these integrins transforms the constricted and spindle-shaped contractile SMCs to a synthetic epithelioid form. In contrast, synthetic SMCs express serum integrins α2β1, α5β1, and αvβ3, which support collagen and fibronectin deposition and prevent Ox-LDL-mediated apoptosis in SMCs, thereby contributing to plaque stability (Finney et al., 2017). Research indicates that smooth muscle cell (SMC) proliferation and migration into the intima play a role in forming early atherosclerotic plaques, whereas in later stages, they contribute to fibrous cap formation that stabilizes vulnerable plaques. SMCs also recruit macrophages at the site of atherosclerotic plaques, thereby increasing the inflammatory response in the plaque area (Basatemur et al., 2019). SMCs are also involved in the pathogenesis of hypertension due to phenotypic switching and their plasticity. The contraction and relaxation of SMCs promptly influence the diameter

of blood vessels, consequently impacting blood flow velocity and altering the pressure exerted on the walls of the blood vessels. The overproduction of proteases by SMCs and the phenotypic switching changes in SMCs all play a role in the development of aneurysms (Chen et al., 2020; Kim & Weintraub, 2016).

1.3.5 Pericytes

Cardiac pericytes originate from the heart's epicardial layer. As the heart develops, there is a transition from epicardial cells to mesenchymal cells via EMT. These mesenchymal cells then differentiate into mural cells or pericytes and fibroblasts within the heart (Murray et al., 2017). Endothelial cells, along with the mesothelium, also act as progenitor cells for pericytes. Endothelial to mesenchymal transition (Endo-MT) leads to an increase in mesenchymal cells, which further aids in the formation of pericytes. Pericytes' secretome is crucial for the repair and regeneration of tissue. At basal levels, various proinflammatory cytokines and chemokines, including Interleukin 6 (IL-6), IL-8, TNFα, and interferon gamma-induced protein 10, have been detected in pericytes, which in turn play an important role in T-cell activity (Guijarro-Munoz et al., 2014). Under stress stimulation, pericytes secrete Eotaxin and Rantes, further exacerbating the damage response (Nehme & Edelman, 2008). Pericytes additionally release anti-inflammatory agents such as leukemia inhibitory factor, heme oxygenase-1 and cyclooxygenase-2 in response to inflammation (Ghannam et al., 2010). Pericytes also secrete various ECM proteins and factors like acidic and cysteine-rich (SPARC) that facilitate ECM production and angiogenesis (Avolio et al., 2021).

In addition to these, the adult heart also expresses other cell types like immune cells, adipocytes and neuronal cells that play an essential role in cardiac development and maintaining cardiac homeostasis.

1.4 Cross-talk between Cardiomyocytes and Cardiac Fibroblasts

Cardiomyocytes and cardiac fibroblasts are interspersed throughout the myocardium, with nearly every cardiomyocyte in close proximity to one or more fibroblasts. Communication between them can occur through direct communication between cells and indirect communication via the ECM and paracrine signaling (Zhang & Mende, 2012). The interplay between these cell types is crucial for determining the structural, mechanical, and electrical properties of both healthy and remodeled myocardium (Figure 7). Direct communication includes gap junctions and adhesion molecule-mediated mechanical force transmission. Gap junctions (made of connexons) allow for the rapid transfer of small molecules and metabolites

between cells, influencing the electrophysiological activity and contractile function of cardiomyocytes. When associated with cardiomyocytes, fibroblasts can function as sources and/or sinks of current, influencing the properties of action potentials and the speed of conduction in cardiomyocytes. *In vitro* studies have shown that electrical coupling occurs between cardiomyocytes and cardiac fibroblasts through Cx43 (Banerjee et al., 2006; Kohl, 2003). Additionally, fibroblast-myocyte coupling has been observed via Cx45 in the sinoatrial node (Banerjee et al., 2006; Kohl, 2003). Studies have also indicated functional coupling of cardiac fibroblasts through Cx40 and Cx43 (Louault et al., 2008). These findings imply that cardiac fibroblasts may serve as connections that link distinct areas of myocytes that are typically electrically separated by connective tissue. The interaction of cardiac fibroblasts plays a role in the depolarization of cardiomyocytes. Furthermore, *in vitro* cell-cell interaction experiments have indicated that cardiac fibroblasts and myocytes communicate by forming tight cell–cell junctions (Baudino et al., 2008). By mediating mechanical force and signal transduction between cells, adhesion molecules (adherens junctions and cadherin/catenin complex) regulate the morphology and function of cardiomyocytes. Adherens junctions among cardiomyocytes and fibroblasts are crucial for coordinating myofibrillogenesis and for the development and maintenance of a functional cardiac phenotype. In fibroblasts, the formation of adherens junctions occurs during their transition to myofibroblasts and is vital for synchronizing periodic calcium oscillations. TGFβ-activated myofibroblasts can apply sustained contractile forces on cardiomyocytes and disrupt electric conduction due to heightened activation of mechanosensitive channels. Membrane nanotubes are a newly identified method of communication between cells that allows for interaction over greater distances, permitting the transfer of organelles, plasma membrane elements, and cytoplasmic substances between cardiomyocytes and fibroblasts, either internally or along their surfaces. Indirect communication takes place via the release of growth factors, cytokines, chemokines and soluble factors from cardiac fibroblasts, which influence the biological activities of cardiomyocytes and vice versa. Fibroblasts can stimulate cardiomyocyte hypertrophy by activating protein kinase A (PKA)/protein kinase G (PKG) and TGFβ signaling. Connective Tissue Growth Factor (CTGF), which is stimulated by TGFβ and found in both cardiomyocytes and cardiac fibroblasts, acts as a mediator for the proliferation, migration, and ECM deposition of fibroblasts. The paracrine secretion of CTGF from cardiomyocytes and the resulting intercellular signaling with fibroblasts have been associated with the progression of cardiac fibrosis. IL-33 (a member of the IL-1 family primarily synthesized by fibroblasts) reduces cardiomyocyte hypertrophy and apoptosis *in vitro*. IL-6 stimulates cell growth, shields cells

from apoptosis, encourages the turnover of the ECM, and leads to cardiac hypertrophy. Fibroblast-specific fibronectin, collagen and growth factors promote cardiomyocyte proliferation via β1-integrin on cardiomyocytes (Ieda et al., 2009). The pacing of collagen expression in HL-1 atrial cardiomyocytes induced by cardiac fibroblasts is mediated through a mechanism involving the paracrine secretion of Angiotensin II (Ang II) and Reactive Oxygen Species (ROS) by cardiomyocytes. These factors activate connective tissue growth factor and procollagen α1 in co-cultured mouse atrial cardiac fibroblasts through TGFβ1 (Tsai et al., 2011). Therefore, crosstalk between cardiomyocytes and cardiac fibroblasts is crucial for both the maintenance of homeostasis as well as disease progression.

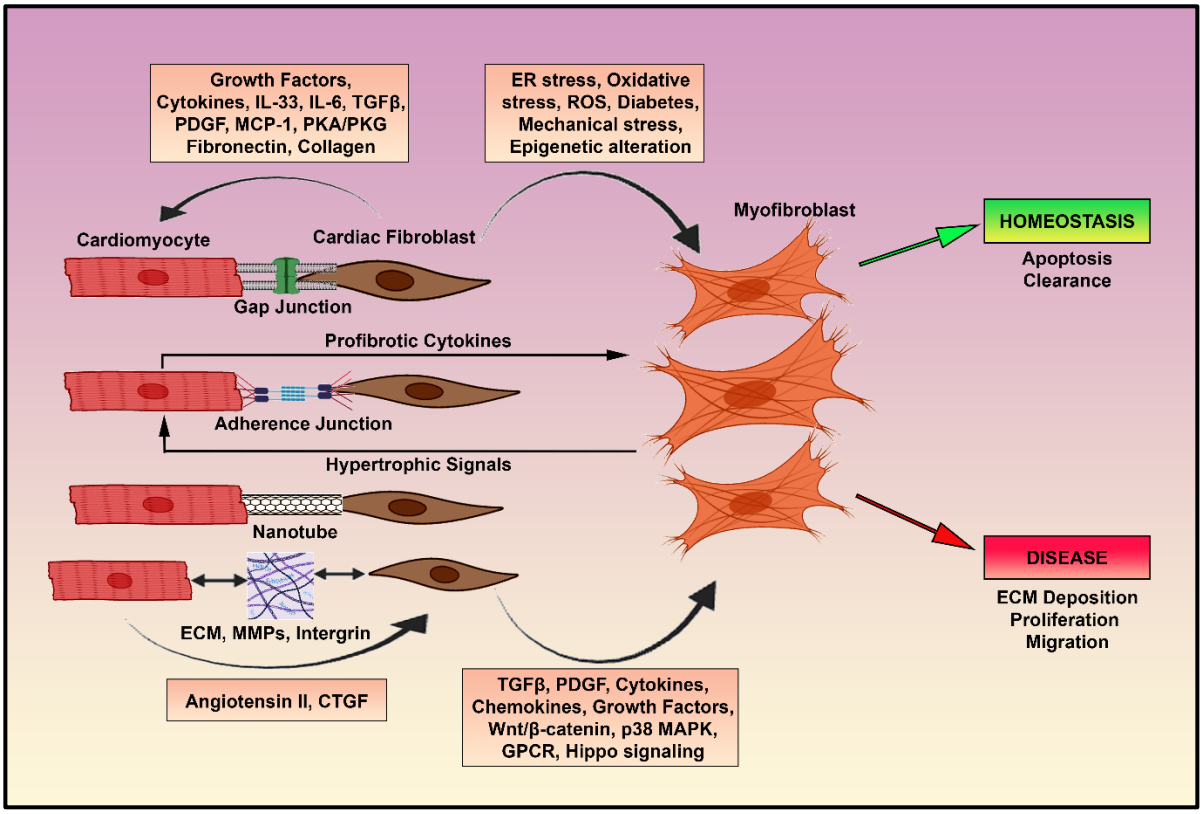

Figure 7. Cross-talk between cardiomyocytes and cardiac fibroblasts. A schematic representation depicting the possible interaction mechanism between cardiomyocytes and cardiac fibroblasts, as well as the remodeling alterations that occur in the diseased heart.

1.5 Cardiac regeneration: from old dogma to new understandings

As per the old dogma, it was believed that in mammals, adult cardiomyocytes are post-mitotic as they undergo irreversible cell cycle arrest and molecular switching to hypertrophic growth. Before birth, during embryogenesis, the cardiomyocyte proliferates and differentiates, and the heart grows by hyperplasia. In the developing heart, the cardiomyocytes proliferate primarily via the Neuregulin/Erythroblastic leukemia viral oncogene (ErbB)/Extracellular

signal-regulated kinase (ERK) pathway. Following midgestation, the Insulin-like Growth Factor (IGF)/Phosphatidylinositol 3-kinase (PI3K) pathway and Bmp signaling control the hyperplastic growth of the cardiomyocytes. During development and after birth, cardiomyocyte proliferation is regulated by the Hippo-Yes-associated protein (Yap) signaling. Cardiomyocyte differentiation and proliferation during development and after birth are regulated by several factors like Tbx, Nkx2.5, GATA, Myocyte enhancer factor 2 (Mef2) and Hand family genes (Yutzey, 2017). The neonatal hearts possess regenerative capacity upto one week after birth; however, upon encountering any stress or injury, the hearts undergo scarring (Porrello et al., 2011). Using Myocardial Infarction (MI) and Ventricular Resection models, Porello et al. showed regeneration of lost tissue within 3 weeks (Porrello et al., 2011). Multiple studies have shown robust neonatal cardiomyocyte proliferation during ventricular resection, MI, cryo-infarction and clamping (Bryant et al., 2015; Haubner et al., 2012; Porrello et al., 2011; Strungs et al., 2013). In adult hearts, stress or injury results in a huge loss of cardiomyocytes and since the adult cardiomyocytes do not possess proliferative or regenerative capacity, they are unable to make up for the overwhelming loss and are eventually replaced by fibrotic tissues.

However, this old dogma was revoked when multiple studies showed that activating the cardiogenic transcription factors or reinitiating the proliferative pathways can result in dedifferentiation and proliferation of adult cardiomyocytes. Overexpression of the Tbx20 pathway in transgenic mice, as well as stress-induced upregulation of Tbx20, promotes cardiomyocyte proliferation (Chakraborty et al., 2013; Das et al., 2023). Injection of Nrg1 was also promotes cardiomyocyte regeneration post-MI (Bersell et al., 2009). Jagged1, a protein of Notch signaling, also promotes cardiomyocyte proliferation via Notch activation (Collesi et al., 2008). Activating GATA4 upregulates cardiomyocyte proliferation by directly increasing the transcription of Cyclin D2 and CDK4 (Rojas et al., 2008). Recombinant or adenoviral-mediated delivery of different cyclins (Cyclin D1, Cyclin B1, Cyclin A2) and CDKs (CDK1, CDK4) also enhances myocardial regeneration post-ischemia and MI. On the contrary, depletion of Meis1, Glycogen synthase kinase 3 beta (GSK-3β) and Dystroglycan 1 promotes myocyte proliferation post-myocardial injury by promoting cell cycle entry and removing the inhibitory effect from Yap (Mahmoud et al., 2013; Morikawa et al., 2017).

Adult stem cells also differentiate into cardiomyocytes. Bone marrow cells (BMCs)+c-kit differentiates into myocytes in the infarcted region of mice with Left Anterior Descending (LAD) Coronary Artery Ligation (Orlic et al., 2001). c-kit + BMC cells also differentiates into myocytes and endothelial cells post-ischemia (Jackson et al., 2001). Hematopoietic and

mesenchymal stem cells have the potential to differentiate into cardiomyocytes (Michler, 2018). Adult stem cells secrete several paracrine, autocrine and endocrine growth factors like Vascular Endothelial Growth Factor (VEGF), TGFβ, IGF-1 and Hepatocyte Growth Factor (HGF) that induce regeneration and repair in the heart post-myocardial injury (Sid-Otmane et al., 2020). Transplantation of exosomes derived from MSCs augments cardiac proliferation and promotes cardiac repair following ischemic injury (Ju et al., 2018).

Human Embryonic stem cell-derived cardiomyocytes (hESC-CMs) and human induced pluripotent stem cell-derived cardiomyocytes (hiPSC-CMs) transplantation also promotes cardiac repair as they exhibit markers, subcellular structures and form tissues with striated cardiomyocytes. Intramyocardial injection of hiPSC-CM in mice with LAD ligation reinstates cardiac function by expressing cardiac markers, enhancing angiogenesis and improving myocardial remodelling (Jiang et al., 2020; Rojas et al., 2017). Similarly, hESC-CM and hiPSC-CM injection in rats with ischemia/reperfusion (I/R) injury and LAD ligation reduced ventricular dilation, preserved contractile functions and remuscularize myocardial infarcts partially (Laflamme et al., 2007). In guinea pigs, hESC-CM injection induces cardiac gene expression and enhances grafts with improved structural and functional properties post-cryo-injury (Dhahri et al., 2022).

Therefore, the field of cardiac regeneration is expanding but remains largely in its early stages. Thus, the discovery of new molecular and signaling regulations that will reinstate cardiomyocyte proliferation will be invaluable for the development of newer therapeutic interventions.

1.6 Cardiovascular diseases (CVDs)

CVDs refer to the category of diseases that affect the heart and blood vessels. They are the primary cause of death around the globe, resulting in nearly 17.9 million fatalities each year. Various factors contribute to CVDs, including high blood pressure, stress, obesity, diabetes, unhealthy habits (smoking and alcohol), and pollution, among others. There are several categories of heart diseases (Figure 8):

1.6.1 Coronary Heart Disease: It is also known as **ischemic heart disease** or **coronary artery disease**, and happens due to insufficient bloodflow to the heart due to arterial plaque formation (atherosclerosis) in the coronary arteries. Coronary heart disease includes conditions such as stable angina, acute coronary syndrome, and silent myocardial ischemia. The primary cause of mortality related to coronary heart disease is coronary artery disease. Acute coronary

syndrome generally presents with symptoms and comprises issues like unstable angina and myocardial infarction. **Atherosclerotic plaque** formation initiates with the formation of a 'fatty streak' resulting from the deposition of lipid-rich macrophages in the subendothelial layer, referred to as '**foam cells**'. When a vascular injury occurs, the intimal layer is compromised, allowing monocytes to enter the subendothelial space, where they transform into macrophages. These macrophages absorb oxidized LDL particles, leading to the formation of foam cells. There is increased activation of T cells and cytokines, resulting in increased inflammatory response. Growth factors stimulate smooth muscle cells, which also take in oxidized LDL particles and collagen, alongside activated macrophages, leading to an increase in foam cell numbers. As a result, subendothelial plaque gradually forms. The plaque can either expand or stabilize over time if no further endothelial damage occurs. If the plaque stabilizes, a **fibrous cap** develops, and the lesion may **calcify** over time. As time progresses, the lesion may reach a level where it becomes hemodynamically significant. If the lumen is obstructed by at least 70%, myocardial tissue perfusion may prove inadequate, resulting in angina symptoms during periods of increased demand (such as exercise). These symptoms typically subside at rest when oxygen needs diminish. In cases where the coronary artery is 90% stenosed, angina can occur even at rest. Certain plaques may rupture and expose tissue factor, leading to thrombosis that can cause complete lumen occlusion. Severe acute blockage usually manifests as **acute coronary syndrome**.

1.6.2 Myocardial Infarction (MI): It happens when there is insufficient blood flow to the heart because of obstructions in the arteries (such as blood clots or atherosclerotic plaques), leading to a reduced oxygen supply to the heart muscle, which in turn causes tissue death in the cardiac muscles. MI is pathologically characterized by the death of myocardial cells resulting from extended ischemia. The initial ultrastructural changes, which include reduced cellular glycogen levels, relaxed myofibrils, and disruptions in the sarcolemma, can be observed as soon as 10 to 15 mins after ischemia begins (Jennings & Ganote, 1974). In humans, myocyte necrosis may take hours to be identifiable through post-mortem analysis; this differs from animal studies, where biochemical signs of myocardial cell death due to apoptosis can be detected within 10 mins of triggered myocardial ischemia, along with evidence of myocyte death (Ooi et al.,2000). In experimental settings, the necrosis advances from the inner layer of the heart (subendocardium) to the outer layer (subepicardium) over several hours. The two well-identified biomarkers of MI are cardiac troponin I (cTnI) and cardiac troponin T (cTnT). Whereas elevation in the levels of cTnI is exclusive to cardiac tissue, the expression of cTnT

is also increased in injured skeletal muscles. Acute MI is characterized by myocardial injury with a rising and/or falling trend of cTn values with at least one measurement exceeding the 99th percentile upper reference limit (URL) and resulting from myocardial ischemia. MI is divided into two categories based on symptoms. Patients with discomfort in the chest with new ST-segment elevation in two adjacent leads or new bundle branch blocks along with ischemic repolarization patterns are classified as ST elevation MI (**STEMI**). On the contrary, patients without ST segment elevation are characterized as non–ST elevation MI (**NSTEMI**). Besides these categories, MI can also be divided into several types based on variations in pathology, clinical presentation, prognosis, and different therapeutic interventions. **Type 1 MI** is characterized by atherothrombotic coronary artery disease (CAD), typically triggered by the erosion or rupture of atherosclerotic plaques. The extent of atherosclerosis and thrombosis in the lesion responsible varies significantly, and the shifting thrombotic elements can result in embolization downstream of the coronary artery, causing necrosis of cardiomyocytes. In addition to intraluminal thrombosis, plaque rupture may also be further complicated by hemorrhage into the plaque from the torn surface (Thygesen et al., 2018). **Type 2 MI** is characterized by ischemic myocardial injury due to a difference between oxygen demand and supply. The oxygen demand and supply imbalance can occur due to several factors like coronary atherosclerosis, vasospasm, coronary microvascular dysfunction, coronary embolism, prolonged tachyarrhythmia, severe anemia, severe bradyarrhythmia, severe hypertension with or without left ventricular hypertrophy, coronary artery dissection with or without intramural hematoma, and respiratory distress (Thygesen et al., 2018). **Type 3 MI** is characterized by myocardial ischemia along with ischemic ECG alterations or ventricular fibrillation without any alteration of cardiac biomarkers (Thygesen et al., 2018). **Type 4a MI** (Myocardial infarction associated with percutaneous coronary intervention) is characterized by a rise in cTn values exceeding 5 times the 99th percentile URL in patients who have normal baseline levels. In patients with increased preprocedure cTn levels that remain stable (≤20% variation) or decline, the postprocedure cTn must increase by more than 20%. Nevertheless, the absolute postprocedural value must still be at least 5 times the 99th percentile URL (Thygesen et al., 2018). **Type 4b MI** (Stent/scaffold thrombosis associated with percutaneous coronary intervention) is characterized by stent/scaffold thrombosis. The severity of Type 4b MI is indicated by time of thrombosis in relation to the intervention procedure: Acute, 0 to 24 hours; Subacute, 24hours to 30 days; Late, >30 days to 1 year; Very late, >1 year after implantation (Thygesen et al., 2018). **Type 5 MI** (Myocardial infarction associated with coronary artery bypass grafting) is characterized by a rise in cTn values exceeding 10 times the 99th percentile

URL in patients who have normal baseline levels. In patients with increased preprocedure cTn levels that remain stable (≤20% variation) or decline, the postprocedure cTn must increase by more than 20% (Thygesen et al., 2018).

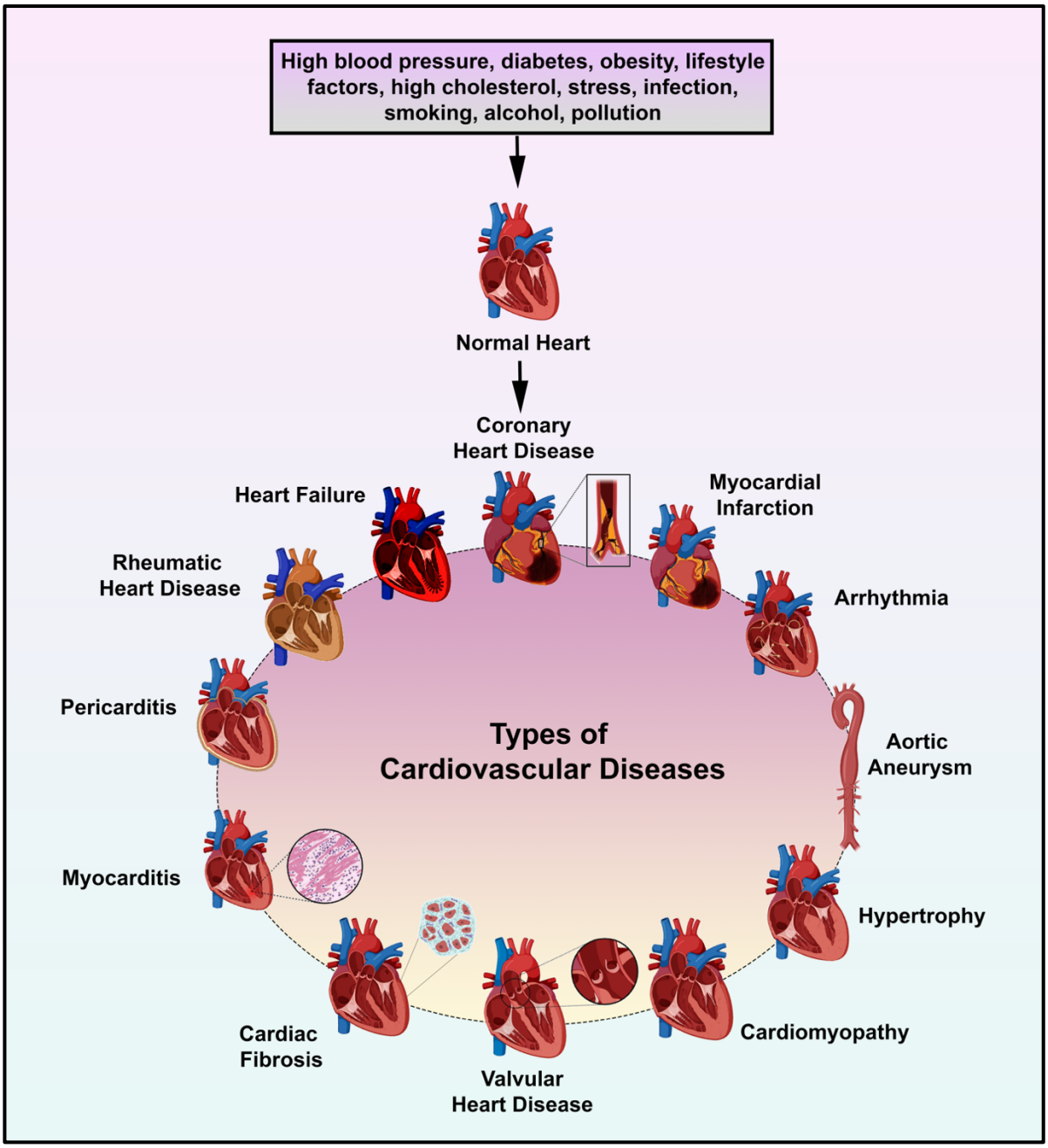

Figure 8. Types of Cardiovascular Diseases (CVDs). Schematic representation showing different types of CVDs caused due to diverse stressors affecting a normal healthy heart.

1.6.3 Arrhythmia: It occurs due to irregular heart rate or rhythm, due to erratic electrical impulses in the heart. There are different types of arrhythmias, namely **bradycardia**, **tachycardia**, **atrial fibrillation**, **ventricular fibrillation**, **atrial flutter**, **conduction disorders** and **premature contraction**. **Bradycardia** is defined as a resting heart rate < 60

beats per minute in adults, with a few exceptions, like the resting heart rate during sleep and the resting heart rate of physically active adults. There are different causes of bradycardia, like defects in the sinoatrial node, defects in conduction pathways of the heart, hypothyroidism, congenital heart defects, myocarditis, etc. **Tachycardia** is defined as a resting heart rate > 100 beats per minute in adults. Tachycardia is further classified into **Supraventricular Tachycardia (SVT)/ Paroxysmal Supraventricular Tachycardia (PSVT)**, **Ventricular Tachycardia** and **Sinus Tachycardia**. **SVT** is defined as a heart rate > 100 beats per minute starting from the atria. Electrical signals become irregular and increase the heart rate, resulting in improper filling of chambers during contractions. **PSVT** is defined as a sudden and occasional increase in heart rate. **Ventricular tachycardia** is defined as a heart rate > 100 beats per minute originating from the ventricles due to electric impulses firing abnormally in the ventricles. These impulses interfere with the impulses from the sinus node, resulting in a faster heart rate that interferes with complete filling of the chambers. **Sinus tachycardia** occurs due to increased heart rate, originating from abnormal electrical signals from the sinus node. **Atrial fibrillation** is defined as irregular or abnormal beating of the atrial chambers of the heart. Atrial fibrillation often causes blood clots due to retention of blood in the atrium, which can further lead to heart failure or stroke. **Ventricular fibrillation** is one of the most serious arrhythmias, and it results from abnormal heart rhythm due to altered electrical impulses in the ventricles, thereby causing them to quiver instead of proper contraction. This can cause instant collapse due to cardiac arrest. **Atrial flutter** is also caused by to faster beating of the atrium (250 to 350 times per minute). However, atrial flutter is less common compared to atrial fibrillation. **Conduction disorders** can also cause arrhythmias, and they are divided into **bundle branch block** (occurs when one ventricle contracts more slowly than the other due to blockage in the bundle branches, thereby resulting in generation of abnormal electrical impulses), **heart block** (occurs due to delay in electrical impulses travelling from atria to ventricles as a result of heart blockage), and **Long QT Syndrome** (occurs when the ventricles takes too long to contract and relax resulting in improper electrical impulses). **Premature contractions** can originate in the atria or ventricles, causing an 'extra beat' that results in a pause, thereby causing the next normal heartbeat to be more reinforced (Schmidt et al., 1987).

1.6.4 Aortic Aneurysm: It occurs due to ballooning or bulging of the aorta due to trauma or a genetic condition, resulting in weakening of its walls. The aorta is composed of three layers: intima, media and adventitia. There are mainly two types of aortic aneurysms, namely the **Thoracic aortic aneurysm** and the **Abdominal aortic aneurysm**. **Thoracic aortic aneurysm**

occurs when there is an expansion of the upper section of the aorta situated above the diaphragm. **Abdominal aortic aneurysm** occurs due to ballooning in the segment of the aorta situated within the abdominal cavity. It is a more prevalent form of aneurysm, and it happens due to several reasons. Elastin, a protein present in the walls of the aorta, is reduced in the abdominal area. Another cause is abdominal aorta lacks vasa vasorum, blood vessels that supply nutrients within the aorta. Aortic aneurysm can cause **rupture** (hole in the ballooned area causing blood to burst out in the body) or **dissection** (surging of blood forcefully through the aorta, causing a separation of the layers within the artery wall, thereby resulting in a persistent accumulation of blood leaking into the area that further separates the artery wall) (Calero & Illig, 2016).

1.6.5 Hypertrophy: Hypertrophy of the heart is defined as the enlargement of the heart muscle. This can occur as a normal physiological adaptation to increased demands, such as in athletes, or as a disease state like hypertrophic cardiomyopathy (HCM). Hypertrophy can further be classified as **Concentric hypertrophy** (**pathological hypertrophy**), where there is thickening of heart muscles without any alteration of the size of chambers. Concentric hypertrophy occurs as a consequence of 'pressure-overload' due to different stressors like hypertension, valvular defects, congenital heart defects and defects in the myocardium. Concentric hypertrophy occurs due to the addition of new sarcomeres in parallel to existing sarcomeres, resulting in increased thickness of the myocardium without subsequent expansion of ventricle size. This form of hypertrophy is maladaptive due to insufficient proliferation of blood vessels supplying the myocardium, thereby resulting in ischemia. This response can serve as a temporary compensation and enhance cardiac function when faced with stressors. However, this form of hypertrophy can lead to dilation of the ventricle that struggles to pump blood effectively, resulting in heart failure (Carabello, 2002). **Eccentric hypertrophy** (**physiological hypertrophy**) is another form of hypertrophy that occurs due to the stretching of heart muscles with a subsequent increase in the size of the chambers. Eccentric hypertrophy occurs due to the addition of new sarcomeres in series to existing sarcomeres, thereby enabling contraction with greater reinforcement. Eccentric hypertrophy is typically considered a healthy form of hypertrophy, often referred to as "athlete's heart." It occurs as a natural reaction to regular exercise or during pregnancy, leading to a rise in the myocyte mass and pumping efficiency of the heart. This adaptation is triggered by 'volume-overload,' whether due to increased regurgitation of blood to the heart during physical activity or as a result of an increase in total blood volume during pregnancy (Carabello, 2002). However, this form of hypertrophy

can also sometimes result in conduction dysfunction and cardiac arrest due to the increased weight of the left ventricles.

1.6.6 Cardiomyopathy: It is the disease of the myocardium (heart muscle) resulting in enlargement, thickening and stiffening of the heart, making it difficult to pump blood effectively. Cardiomyopathy can be classified as **Hypertrophic cardiomyopathy (HCM)**, **Dilated cardiomyopathy (DCM)**, **Restrictive cardiomyopathy (RCM)**, **Arrhythmogenic cardiomyopathy (ACM)**, and **Left Ventricular Non-compaction (LVNC)**. **HCM** is a heart muscle disease that can be familial or acquired and is characterized by the thickening of the muscle (hypertrophy). This thickening usually occurs in the left ventricle. The heart muscle may thicken at the septum (the muscular wall dividing the left and right sides of the heart), the posterior wall (the outer wall of the left ventricle), the apex (the bottom portion of the heart), or throughout the entire left ventricle. When the muscle thickens, it can hinder the efficient flow of blood into and out of the heart, particularly during physical activity. In certain instances, the muscle thickening can obstruct blood flow from the left ventricle to the aorta. **DCM** is characterized by thinning of the myocytes and enlargement or dilation of the left ventricle, resulting in the inability of the heart to pump efficiently, thereby reducing the amount of blood pumped to the body. DCM can be familial or acquired due to myocarditis, metabolic diseases or exposure to chemotherapy. **RCM** is characterized by stiffness of the myocytes, preventing them from relaxing and filling with blood. While the heart's contraction ability may remain normal, its relaxation process is impaired. When the left ventricle cannot expand and receive blood, it leads to increased pressure that can result in irregular heart rhythms and heart failure symptoms. RCM can be familial or it can happen due to different conditions like amyloidosis in cardiomyocytes, hemochromatosis, sarcoidosis or other inherited diseases like Fabry disease. **ACM** is characterized by the replacement of the cardiomyocytes of the right ventricle by fibrous or fat tissue. In ACM, the right ventricles become enlarged, resulting in impairment of contraction with abnormal heart rhythms, causing sudden cardiac arrest. **LVNC** is characterized by the extension of trabeculations into the heart chambers. In normal development, these trabeculations compact, resulting in the transformation of the spongy myocytes to a smooth and solid structure. However, in LVNC, this compaction is absent (Schaufelberger, 2019).

1.6.7 Valvular Heart Disease: It is a condition in which one or more valves (tricuspid valve, bicuspid valve or mitral valve, and semilunar valves) do not function properly. It can occur due to **Valvular stenosis** (narrowing of valve opening), **Valvular atresia** (improper development

of valves), **Regurgitation** (incomplete closure of the valves) and **Valvular prolapse** (bulging of the valve flaps into the heart chamber). **Valvular stenosis** is further classified into **Tricuspid valve stenosis** (narrowing of the tricuspid valve results in incomplete flow of blood from the right atrium to the right ventricle, resulting in atrium enlargement, which can further cause irregularity of bloodflow to surrounding chambers and veins, or it can also result in the right ventricle becoming smaller), **Pulmonary valve stenosis** (narrowing of pulmonary valve causes restricted flow of blood from right ventricle to the lungs through pulmonary arteries), **Mitral valve stenosis** (narrowing of mitral valve restricts the bloodflow from the left atrium to the left ventricles causing left atrium enlargement and fluid buildup in lungs) and **Aortic valve stenosis** (narrowing of aortic valve restricts bloodflow from aorta to rest of the body which further leads to thickening of the left ventricle). **Valvular atresia** is further classified into **Aortic atresia** (improper formation or opening of the aortic valve), **Mitral atresia** (improper development of the mitral valve), **Tricuspid atresia** (absence of the tricuspid valve between the right atrium and the right ventricle) and **Pulmonary atresia** (absence of the pulmonary valve between the right ventricle and the pulmonary artery). **Regurgitation** is further classified into **Tricuspid valve regurgitation** (improper closure of the tricuspid valve resulting in regurgitation of blood pumped from the right ventricle to the lungs back to the right atrium, resulting in atrium enlargement), **Pulmonary valve regurgitation** (improper closure of the pulmonary valve resulting in regurgitation of the blood from the lungs into the heart), **Mitral valve regurgitation** (improper closure of the mitral valve resulting in regurgitation of the blood into the left atrium causing increase in blood volume and pressure in the left atrium), **Aortic valve regurgitation** (improper closure of the aortic valve resulting in regurgitation of blood from the aorta to the left ventricle which can lead to ventricular hypertrophy). **Valvular prolapse** is further classified into **Mitral valve prolapse** (the mitral valve does not close properly as a result when the two ventricles contract, part or the entire mitral valve bulges upward into the atrium). This may permit a small volume of blood to regurgitate through the valve. Mitral valve prolapse is also referred to as click-murmur syndrome, Barlow's syndrome, or floppy valve syndrome and **Tricuspid, pulmonary and aortic valve prolapse** (the leaflets of these valves fail to close properly; however, these forms of prolapse are rare) (Lipton & Coulden, 1999).

1.6.8 Cardiac Fibrosis: Cardiac fibrosis refers to the scarring process that occurs in the heart muscle, marked by an increase in Type I collagen deposition, along with the activation of cardiac fibroblasts and their transformation into myofibroblasts. These pathological alterations result in heightened matrix stiffness, which disrupts normal cardiac function. Cardiac fibrosis

is classified into three types, namely, **Reactive interstitial fibrosis** (arises from pressure overload and cardiomyopathies due to the excessive deposition of extracellular matrix without significant loss of cardiomyocytes), **Infiltrative interstitial fibrosis** (arises due to accumulation of glycolipids in various heart cells, a condition observed in patients with Fabry disease) and **Replacement fibrosis** (occurs following cardiac injury, such as MI, where cardiomyocytes sustain damage). In this case, damaged cardiomyocytes are substituted with fibroblasts, resulting in the formation of a scar enriched with collagen. The fibrotic scars form four different types of structures: compact, diffuse, interstitial and patchy (Disertori et al., 2017).

1.6.9 Myocarditis: It occurs due to inflammation of the myocardium (middle layer of the heart) due to several causes like viral infection, bacterial infection (Streptococcus or Staphylococcus), fungal infection (Candida), autoimmune disorders, medications, toxicity, etc. Myocarditis results in ventricular remodeling and cardiac dysfunction.

1.6.10 Pericarditis: It occurs due to inflammation of the pericardium (double-layered sac surrounding the heart) due to viral infection, autoimmune diseases, etc. Pericarditis can be classified into **Acute pericarditis** (defined by symptoms lasting less than four to six weeks), **Incessant pericarditis** (defined by symptoms lasting more than four to six weeks but less than three months), **Chronic pericarditis** (defined by symptoms lasting more than three months) and **Recurrent pericarditis** (defined by relapse of pericarditis without any symptoms for at least four weeks).

1.6.11 Rheumatic Heart Disease: It is a life-threatening heart condition that arises from the damage inflicted on heart valves and heart muscles due to one or more episodes of rheumatic fever, which is an autoimmune inflammatory response triggered by an infection with Streptococcal bacteria (such as Streptococcal pharyngitis). The bacteria known as *Streptococcus pyogenes* (group A streptococcus) can easily spread from person to person, similar to how other upper respiratory infections are transmitted. These infections predominantly occur in children.

1.6.12 Heart Failure: It is a chronic condition in which the heart muscle cannot pump sufficient blood to meet the body's oxygen and nutritional needs. Heart failure can occur when the heart struggles to contract effectively, known as systolic heart failure, or heart failure with a reduced ejection fraction (HFrEF). It can also occur when the heart muscle becomes rigid and has difficulty filling with blood, despite normal pumping ability; this condition is referred to as diastolic heart failure, or heart failure with a preserved ejection fraction (HFpEF).

Our study mainly focuses on Endoplasmic Reticulum (ER) stress and diabetes induced cardiomyopathy. Recently, there has been overwhelming evidence that has shown the involvement of ER stress in inducing CVDs, and ER stress is also involved in the pathogenesis of diabetes, which in turn causes cardiomyopathy. Therefore, we sought to decipher the molecular mechanisms involved in ER stress/diabetes induced cardiomyopathy.

1.7 Endoplasmic Reticulum (ER) stress: a new player in cardiomyopathy

The Endoplasmic Reticulum (ER) is an organelle responsible for coordinating the synthesis and correct assembly of numerous secretory and membrane-associated proteins. ER also plays a pivotal role in multiple processes, including calcium homeostasis, protein biosynthesis and secretion, biosynthesis of lipid and steroid hormones, and carbohydrate metabolism, to name a few (Pizzo & Pozzan, 2007). Factors such as internal environment or external stimuli that disrupt the proper functioning of the ER often result in the generation of ER stress (Sanderson et al., 2015).

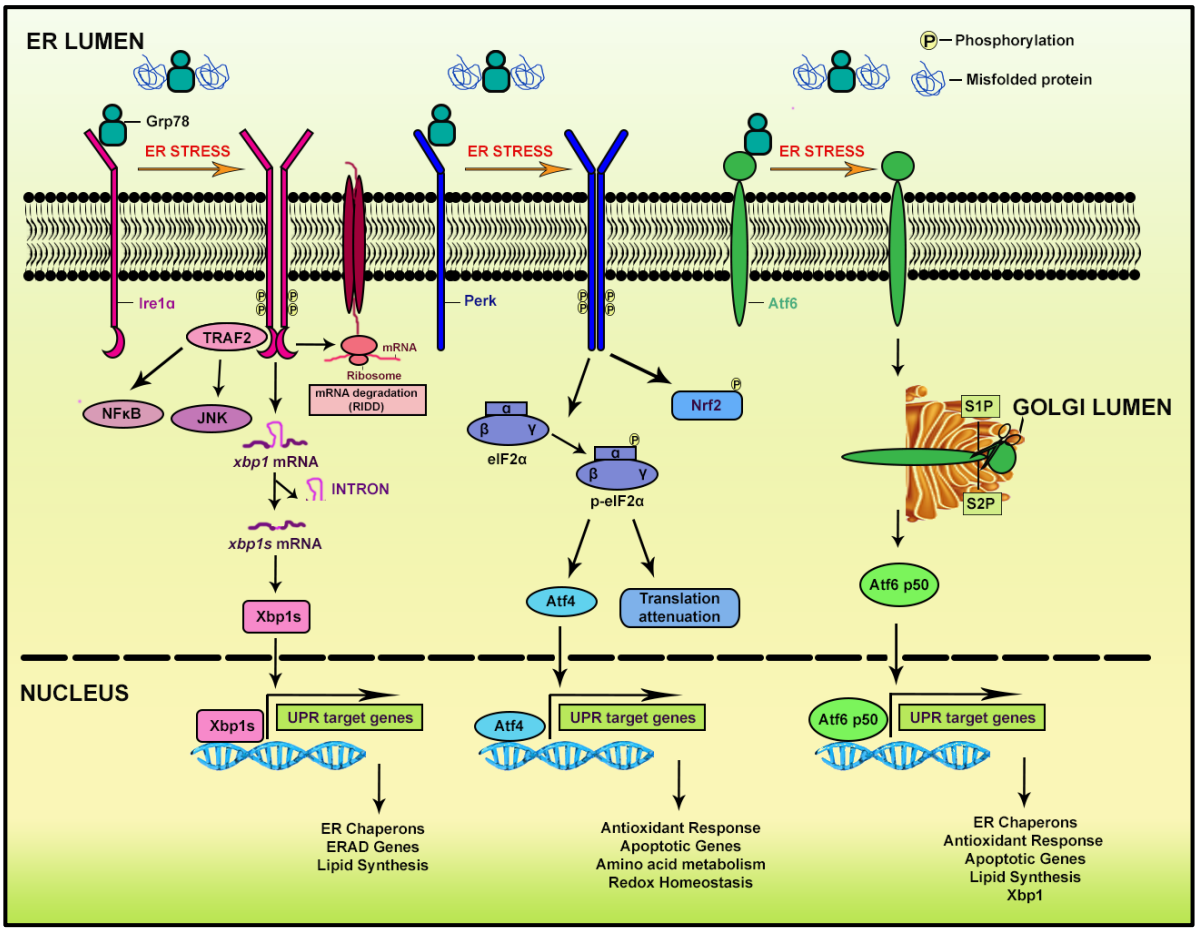

Figure 9. The Unfolded Protein Response (UPR) signaling pathway. The build-up of misfolded or unfolded proteins within the ER lumen is detected by the chaperone glucose-regulatory protein 78 (Grp78). Upon ER stress, Grp78 dissociates from the three UPR stress sensors: inositol-requiring

protein 1α (Ire1α), protein kinase RNA-like endoplasmic reticulum (ER) kinase (Perk), and activating transcription factor 6 (Atf6). The dimerization of Ire1α, followed by autophosphorylation, activates its endoRNase activity, which processes the mRNA that encodes unspliced X box-binding protein 1 (Xbp1) into its functional transcription factor version, spliced Xbp1 (Xbp1s). Xbp1s moves to the nucleus to regulate the transcription of genes that code for ER chaperones, as well as genes related to the Endoplasmic reticulum-associated protein degradation (ERAD) pathway and lipid synthesis. Additionally, Ire1α facilitates the breakdown of various mRNAs via the regulated Ire1-dependent decay (RIDD) pathway. Ire1α interacts with the adapter protein TNF receptor-associated factor 2 (TRAF2) to activate stress pathways mediated by c-Jun-N-terminal kinase (JNK) and nuclear factor-κB (NF-κB). Activated Perk phosphorylates the initiation factor eukaryotic translation initiator factor 2α (eIF2α), which reduces the overall protein synthesis machinery. Perk also phosphorylates nuclear factor erythroid 2-related factor 2 (Nrf2), a transcription factor that plays a role in redox metabolism. The phosphorylation of eIF2α allows for the translation of *atf4* mRNA, which encodes the transcription factor that regulates the transcription of genes associated with apoptosis, antioxidant responses, and amino acid metabolism. Atf6 is transported to the Golgi apparatus, where site 1 proteases S1P and S2P process it, resulting in the release of the active transcription factor Atf6-p50. Atf6-p50 regulates the expression of genes involved in the ERAD pathway, apoptosis, antioxidant responses, lipid synthesis, and Xbp1. (*Adopted from Das et al., 2021)*

The ER stress is initially beneficial as it often results in the restoration of homeostasis by upregulation of the Unfolded Protein Response (UPR); however, a prolonged ER stress drives the cells toward programmed cell death (Das et al., 2021) (Figure 9). The UPR consists of three pathways, namely Inositol-requiring protein 1α (Ire1α), Protein kinase RNA-like ER kinase (Perk), and Activating transcription factor 6 (Atf6). A very fine balance exists between ER stress-induced cell survival and cell death (Das et al., 2021) (Figure 10). The three arms of the UPR signaling play a pivotal role in this delicate balance between survival and cell death. ER stress has been identified as a contributing factor in the initiation and progression of CVDs. During ischemic heart disease, ER stress molecules Glucose regulated protein 78 (Grp78), Activating transcription factor 4 (Atf4) and C/EBP homologous protein (Chop) are elevated. Chop is a pro-apoptotic transcription factor that further stimulates the expression of Bim, whereas it inhibits the expression of Bcl-2 (K. Liu et al., 2014). Chop also activates growth arrest and increases the expression of DNA damage-inducible protein 34 (GADD34), causing increased translation of apoptotic genes (Li et al., 2014). Xin et al. showed that during ER stress, there is increased phosphorylation of eIF2α with a subsequent increase of Atf4 due to activation of the Perk pathway. During heart failure, the expression of ER stress markers Grp78, Chop, caspase 12, and c-Jun-N-terminal kinase (JNK) elevates significantly (W. Xin, Li, et al., 2011).

In another study, Ohoka et al. showed that prolonging ER stress results in elevated Tribbles3 expression, which in turn induces cell death, leading to heart failure (Ohoka et al., 2005). Increased ER stress during heart failure upregulates the expression of Sarcoplasmic/Endoplasmic Reticulum Calcium ATPase 3f (Serca3f), which leads to increased

expression of Grp78 and increased splicing of X-box binding protein 1 (Xbp1) (Safiedeen et al., 2017). Activation of Perk/Atf4 signaling during ER stress downregulates the expression of Neurite outgrowth inhibitor β (Nogo-β), a protein involved in maintaining ER structure that further causes increased myocardial hypertrophy (Li et al., 2018). ER stress is often accompanied by increased Ca^{2+} release, which triggers the apoptosis pathway, leading to cardiac arrhythmia (Safiedeen et al., 2017). Liu et al. showed that ER stress in cardiomyocytes results in ventricular arrhythmia. Atherosclerosis is also triggered by ER stress (Z. Liu et al., 2014).

Therefore, ER stress is a critical factor in inducing cardiovascular diseases, and targeting ER stress can serve as an effective therapeutic approach in reducing the burden of CVDs. Therefore, identifying cardiac genes or cardiac molecular regulators that can aid in reducing the load of ER stress is pivotal in reducing the incidence of CVDs.

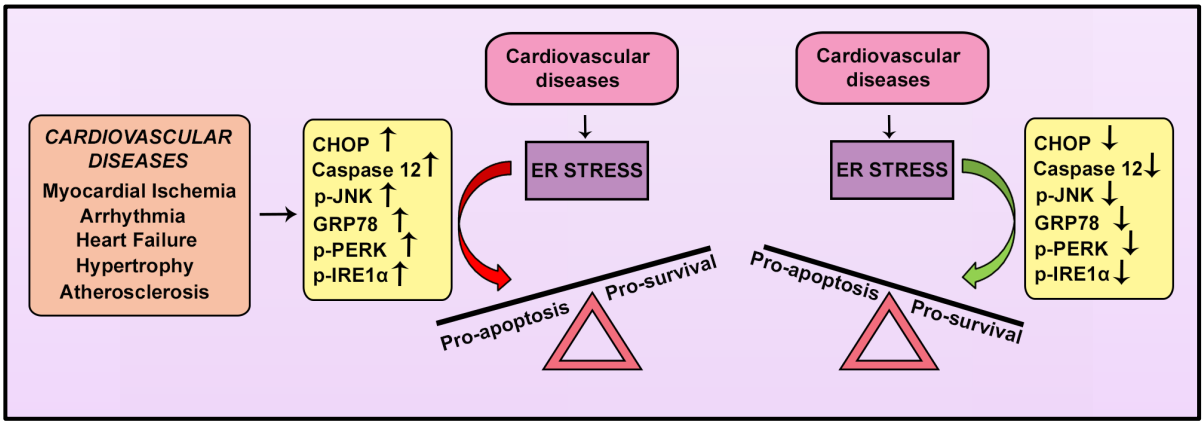

Figure 10. Triggers of ER stress during cardiovascular diseases and the existence of a fine balance between ER stress-induced pro-survival and pro-apoptosis. (*Adopted from Das et al., 2021)*

1.7.1 Ire1α and Perk: the cardiomyopathy inducers of UPR signaling

Ire1α is a serine/threonine kinase and endoribonuclease domain-containing transmembrane protein (Groenendyk et al., 2010). Under normal physiological conditions, it remains associated with Grp78. However, upon ER stress, it dissociates from Grp78 and dimerizes. Following dimerization, Ire1α autophosphorylates, resulting in the formation of activated Ire1α. Activated Ire1α further removes 26 nucleotide intron from Xbp1, resulting in the formation of a transcriptionally active spliced variant of Xbp1 (sXbp1), which translocates to the nucleus and transcribes the expression of other ER stress genes.

Multiple studies have shown that the upregulation of the Ire1α pathway often results in detrimental consequences, thereby aggravating CVDs. During ER stress, it binds to TNF

receptor-associated factor 2 (TRAF2), which further activates apoptosis signal-regulating kinase 1 (ASK1), which further accelerates JNK and p38, thereby inducing cardiomyocyte apoptosis (Nishitoh et al., 2002). Eliminating ASK1 restores cardiac function and reduces cellular apoptosis in pressure overload-induced hypertrophy. Ire1α/JNK signaling pathway promotes autophagic death of cardiac cells under hypercholesterolemic conditions (Sozen et al., 2020). Ire1α/TRAF2 upregulates the Nuclear Factor kappa B (NFκB), which further induces the inflammatory response in cardiac cells (Janssens et al., 2014). Prolonged ER stress augments the Ire1α-dependent decay of mRNA (RIDD) that enhances the degradation of survival genes, thereby increasing cardiac cell apoptosis (Maurel et al., 2013).

Perk is a Type 1 transmembrane serine/threonine kinase domain-containing protein that, under physiological conditions, remains associated with Grp78. Upon ER stress, it dissociates from Grp78, dimerizes and autophosphorylates. Phosphorated Perk inactivates eukaryotic initiation factor 2 alpha (eIF2α) by phosphorylating it, thereby resulting in global translational attenuation (Cui et al., 2011). Activated Perk, however, augments the translation of genes having positively acting short upstream Open reading frames (ORFs) in their 5' untranslated region (5'UTR). One such gene is Atf4, which further accelerates the expression of downstream targets like Chop. I/R induction also activates Perk, which subsequently increases the phosphorylation of eIF2α. Activated Atf4 induces Chop, which further increases oxidative stress and programmed cell death (Marciniak et al., 2004). Activation of Perk also increases NF-κB mediated cardiomyocyte apoptosis by reducing the translation of NF-κB inhibitor I-kappa B (IκB) (Janssens et al., 2014).

Therefore, both these pathways of UPR signaling are involved in the pathogenesis of. ER stress-induced CVDs.

1.7.2 Atf6: the cardioprotective molecule of UPR signaling

Atf6 is a transcription factor of 670 amino acids. It is a Type II transmembrane protein bearing a CREB/ATF bZIP domain in its N-terminal. Its N-terminus is oriented toward the cytosol, while the C-terminus is positioned towards the ER lumen (Cao & Kaufman, 2014). Under the normal scenario, Atf6 remains as oligomers via disulfide bonds and is associated with Grp78; however, upon ER stress, the disulfide bond is reduced, thus forming Atf6 monomers. The monomers then translocate to the Golgi apparatus, where two enzymes, S1P and S2P, cleave them to produce an active N-terminal fragment of around 400 amino acids (Atf6-p50), which further moves into the nucleus to trigger the transcription of multiple genes.

Among the three pathways of UPR signaling, Atf6 is the one that has primarily been shown to promote survival by reducing the severity of ER stress. I/R induction in transgenic mice overexpressing Atf6 demonstrates increased expression of the ER chaperones Grp 78 and Grp 94 (Martindale et al., 2006). These transgenic mice also exhibit improved cardiac function, as indicated by increased left ventricular developed pressure (LVDP), alongside a decrease in the expression of necrotic and apoptotic markers and a reduction in the size of the infarct (Blackwood et al., 2019; Martindale et al., 2006). Other studies revealed that Atf6 conditional knockout mice are more susceptible to I/R damage and display increased hypertrophic response (Blackwood et al., 2019). *In vitro*, the knockdown of Atf6 followed by I/R leads to reduced cellular viability and lower expression of Grp78 (Jin et al., 2017). Dominant negative mutation of Atf6 decreases cell survival rates following myocardial infarction (MI) (Toko et al., 2010). In another study, constitutive expression of Atf6 in response to cardiac stress led to the upregulation of Serca2a, which in turn restores normal cardiac function and reduces the expression of apoptotic genes (W. Xin, Li, et al., 2011). Atf6 also conveys its cardioprotective effects due to its antioxidant properties. I/R induction scavenges reactive oxygen species (ROS) generation due to the heightened expression of Atf6. Transcriptomic analysis demonstrated that Atf6 overexpression correlates with increased expression of antioxidant genes such as catalase, peroxiredoxin 5, and VCP-interacting membrane protein, which are known to scavenge ROS production (Jin et al., 2017).

Very few studies have highlighted Atf6 to be an inducing factor for cardiomyopathy. In one such study, increased expression of Atf6 led to dilated cardiomyopathy and ischemic study in patients with heart failure (Ortega et al., 2014). The active form of Atf6 (Atf6-p50) elevates the expression of C-reactive protein, which further increases the expression of Monocyte Chemoattractant Protein-1 (MCP-1), which in turn causes an increase in cardiac inflammation (Ridker, 2014). Another protein, Peroxisomal enzyme fatty acyl-CoA reductase 1 (FAR1), augments cardiomyocyte apoptosis during I/R in an Atf6-dependent manner (Marsh et al., 2021).

Since most of the studies done so far have shown the cardioprotective effect of Atf6, therefore deciphering the molecular regulation between Atf6 and cardiac transcription factors will be interesting in lowering the burden of ER stress to ameliorate the progression of CVDs.

1.8 Diabetic cardiomyopathy

Rubler et al. first identified a new form of cardiomyopathy in patients with diabetic glomerulosclerosis, where the patients' hearts exhibited ventricular hypertrophy, myofibrillar

hypertrophy, thickening of the walls of coronary arterioles, and altered myocardial metabolism (Rubler et al., 1972). Since then, multiple studies have demonstrated the role of diabetes in the pathophysiology of the myocardium in the absence of coronary artery disease or hypertension. According to the World Health Organization (WHO), in 2021, diabetes led to 1.6 million deaths worldwide, with 47% of those occurring before the age of 70 (Antar et al., 2023). Thus, diabetes represents a major health concern and frequently results in the development of cardiovascular diseases (CVDs) (Hayat et al., 2004).

Multiple studies have shown that diabetes is associated with structural changes in the heart initiated by left ventricular hypertrophy (LVH), resulting in increased ventricular mass and thickness of ventricular walls (Aneja et al., 2008). Changes in the myocardial geometry during diabetes result from long-term alterations due to factors like obesity and hyperglycemia, where obesity during diabetes, especially, is a pivotal factor promoting LVH (Eguchi et al., 2008). Studies have shown that obesity promotes LVH due to increased cytokines (leptin and resistin) release from adipose tissue, causing an increase in ROS generation and upregulation of Insulin Receptor Substrate 1 (IRS-1) and Mitogen-Activated Protein Kinase (MAPK) (Xu et al., 2004). LVH due to diabetes occurs due to insulin resistance and hyperinsulinemia, which eventually leads to heart failure. Diabetes also causes diastolic and systolic dysfunction, which eventually leads to contractile dysfunction (Van den Bergh et al., 2008). Diabetes-associated obesity results in myocardial lipotoxicity. The first evidence of lipotoxicity was reported in 1977 when the authors showed the presence of lipofuscin deposits in LV biopsies of Type 2 Diabetes patients (Regan et al., 1977). These patients also exhibited elevated levels of triglycerides and cholesterol (Regan et al., 1977). In Type 2 Diabetes patients, myocardial steatosis causes diastolic dysfunction (Rijzewijk et al., 2008). In diabetes patients, lipid accumulation and an increase in mitochondrial fatty acid oxidation in cardiac cells generate oxidative stress, which in turn leads to the pathogenesis of diabetic cardiomyopathy (Boudina et al., 2007). Increased apoptosis and necrosis of myocardium during diabetes result in diabetic cardiomyopathy (Boudina et al., 2007). Diabetes patients harbour increased apoptosis and necrosis, which is further aggravated upon induction of I/R (Chowdhry et al., 2007). The hearts of ob/ob and db/db mice also exhibit increased apoptosis of cardiomyocytes. Upon deciphering the mechanism for this increase, it was shown that leptin deficiency, along with hyperglycemia, induces Ras-related C3 botulinum toxin substrate 1 (RAC1) induced nicotinamide adenine dinucleotide phosphate (NADPH), and ROS (Shen et al., 2009). Activation of the renin-angiotensin (RAS) during diabetes also causes apoptosis and necrosis of cardiomyocytes and

endothelial cells. Hyperglycemia induces the expression of several pro-inflammatory cytokines like IL-6, IL-1β, IL-18, TNFα, and NLRP3 inflammasomes, which were eventually shown to increase cardiomyocyte apoptosis (Zhang & Dhalla, 2024). In another study, authors have shown that high glucose results in increased expression of caspase 8 and caspase 9, which eventually increases the expression of caspase 3, thereby causing cardiomyocyte apoptosis (Wei et al., 2022). Hyperglycemia also facilitates the production of TGFβ, resulting in the activation of fibroblasts to myofibroblasts (Liu et al., 2021). Diabetic patients exhibit increased interstitial fibrosis with increased collagen deposition in the myofibers. Diabetic myocardium also shows increased expression of Connective tissue growth factor (CTGF) and protein kinase C β2 (PKCβ2) (Way et al., 2002). All these factors cause an increase in cardiac fibrosis during diabetes, resulting in the pathogenesis of diabetic cardiomyopathy. In addition to these, miRNAs also induce diabetic cardiomyopathy (Guo & Nair, 2017). Several studies have shown that miRNAs are key modulators that induce diabetic cardiomyopathy via alteration of cardiac gene expression, which eventually leads to increased ROS generation, inflammatory response, apoptosis, Ca^{2+} perturbation, fibrosis, mitochondrial dysfunction and altered epigenetic regulation.

Therefore, diabetic cardiomyopathy is a serious health concern, and the identification of cardiac genes that can ameliorate the pathogenesis of diabetic cardiomyopathy and their molecular regulation is critical in developing therapeutics for the detection and cure of cardiomyopathy.

1.9 ER stress in the pathogenesis of diabetic cardiomyopathy

The first evidence of the involvement of ER stress in the development of diabetic cardiomyopathy was reported in 1985 when the hearts of diabetic patients were reported to harbour swollen ER (Bhimji et al., 1986; Jackson et al., 1985). In 2007, ER stress was shown to induce apoptosis of myocardium in an STZ-induced Type 1 Diabetic rat model (Li et al., 2007). In diabetic hearts, the expression of ER stress markers Grp78, Chop and caspase-12 is found to be elevated, and since apoptosis plays a pivotal role in the pathogenesis of diabetic cardiomyopathy, it was concluded that ER stress-induced apoptosis leads to diabetic cardiomyopathy (Kaur et al., 2020). The role of ER stress in the pathogenesis of diabetic cardiomyopathy was further established by the administration of metallothionein, an antioxidant that was previously shown to prevent diabetes-induced cardiomyocyte apoptosis. In diabetic mice, the expression of Endoplasmic Reticulum Stress Response (ERSR) genes is elevated. Ang II and Homocystein (Hcy) are also involved in the induction of diabetic

cardiomyopathy (Wei et al., 2010). Administration of Ang II and Hcy increases the expression of ER stress pathway genes (Sukumaran et al., 2011; Wei et al., 2010). All these studies thus prove that ER is critical in the development of diabetic cardiomyopathy.

ER stress can also induce diabetic cardiomyopathy by increasing the inflammatory response and cardiac fibrosis. ER stress triggers the expression of TNFα, IL-1β and IL-6, which in turn augments the progression of cardiac hypertrophy (Tan et al., 2020). Activation of the UPR signaling activates NLRP3 inflammasomes, which eventually interact with various immune and apoptotic pathways, resulting in myocyte apoptosis, which was further confirmed by blocking the IRE1α pathway (Menu et al., 2012). Upregulation of the pro-inflammatory pathways recruits neutrophils, which infiltrate the cardiac tissues, resulting in NETosis, a form of cell death where nuclear constituents and granular components form structures known as Neutrophil Extracellular Traps (NET) (Islam & Takeyama, 2023). The Perk pathway augments the expression of Atf4, which eventually leads to increased cardiomyocyte apoptosis via upregulating CHOP during diabetes.

Collectively, these studies highlight the pivotal role of ER stress in the development of diabetic cardiomyopathy. Therefore, targeting the molecules and the pathways involved in the progression of ER stress can eventually lead to a decrease in the incidence of diabetic cardiomyopathy. In our study, in addition to ER stress alone, we have also looked into the expression of our target genes during diabetic cardiomyopathy. Since ER stress has been implicated in the pathogenesis of diabetic cardiomyopathy, therefore, to corroborate our findings in an actual disease model we have also used diabetic cardiomyopathy as our model system.

1.10 T-box transcription factor 20 (Tbx20): Its role in cardiac development and homeostasis

T-box (Tbx) family genes are a group of transcription factors that play an indispensable role in cardiac development (Naiche et al., 2005). They aid in proper embryonic development and organogenesis (Naiche et al., 2005). The *T* gene, or *brachyury*, is the earliest member of its gene family and is crucial for mesoderm formation. *T* gene loss-of-function impairs the specification and differentiation of mesodermal cells (Herrmann et al., 1990; Papaioannou, 2001). T-box transcription factor 20 (Tbx20) belongs to the Tbx1 subfamily and consists of at least four isoforms, Tbx20a-d (Figure 11). Tbx20a isoform encodes a full-length protein of 445 amino acids, and it consists of a central T-box DNA binding domain, which is flanked by N-

terminal (102 amino acids) and C-terminal (158 amino acids) domains. The C-terminal contains the transactivation and transrepression domains. Tbx20b (~300 amino acids) and Tbx20c (~300 amino acids) are alternatively spliced variants that contain the T-box DNA binding domain but lack the C-terminal domain. Tbx20d, the shortest isoform at 281 amino acids, features a truncated T-box DNA-binding domain (Hammer et al., 2008; Stennard et al., 2003). Tbx20 is expressed in cardiac lineages throughout evolution, from nematodes to vertebrates.

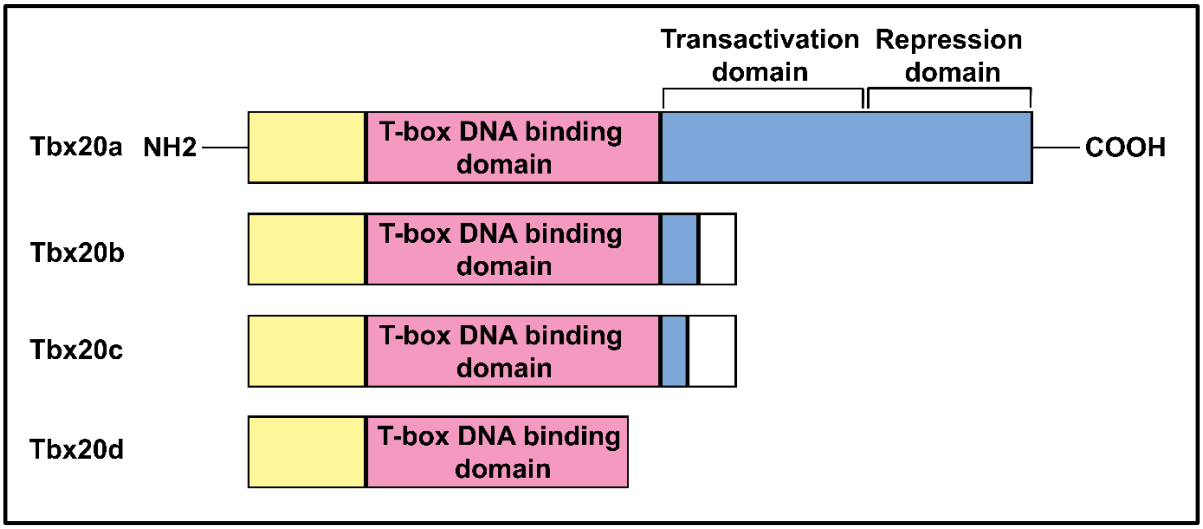

Figure 11. Different isoforms of Tbx20. Tbx20a isoform consists of the T-box DNA binding domain, the transactivation and repression domains. Tbx20b and Tbx20c are alternatively spliced variants that contain the T-box DNA binding domain but lack the transactivation and repression domain. Tbx20d isoform is the shortest, and it contains a truncated T-box DNA binding domain.

1.10.1 Tbx20 is a crucial regulator of embryonic, fetal and adult heart development and homeostasis.

Tbx20 expression is evident throughout heart development. At E7.5, it appears in the cardiac mesoderm progenitor region and progressively moves to the cardiac crescent and heart tube by E8.0-8.5. By E9.5, it is additionally expressed in all four developing heart chambers (Kraus et al., 2001). Following this, Tbx20 expression transitions from the cardiac mesoderm to the lateral plate mesoderm. During heart development, Tbx20 is strongly expressed in the myocardium and endocardium of the cardiac crescent (Kraus et al., 2001) and is crucial for defining the anterior heart field (AHF). Its expression rises significantly later in the endocardial cushion of the cardiac outflow tract (OFT), atrioventricular canal (AVC), and interatrial septum primum, aiding in the formation of cardiac valves and the atrioventricular septum (Stennard et al., 2003). Studies have emphasized Tbx20's critical role in cardiac looping, chamber differentiation, and in directing gene specification essential for cardiomyocyte proliferation

(Cai et al., 2005; Stennard et al., 2005). Complete knockout of Tbx20 leads to death by E10.5 owing to hemodynamic failure (Cai et al., 2005; Singh et al., 2005), and Tbx20 null mice display a severely hypoplastic heart, with failures in dorsoventral patterning, myocardium development, cardiac looping, and chamber formation (Takeuchi et al., 2005). During heart development, Tbx20 specifically regulates N-myc proto-oncogene protein 1 (Nmyc1) expression by repressing Tbx2, thereby enhancing Nmyc1 levels, which promotes cardiomyocyte proliferation (Cai et al., 2005). Additionally, Tbx20 collaborates with the homeodomain transcription factor Nkx2.5 and the zinc-finger transcription factors GATA4 and GATA5 to activate key cardiac genes involved in endocardial differentiation and heart development (Stennard et al., 2003). Intriguingly, Tbx20 can dose-dependently influence the expression of other transcription factors vital for cardiac development. Studies utilizing RNA interference to induce graded loss of Tbx20 in mouse embryos demonstrated that while complete Tbx20 knockout results in a severely hypoplastic heart and defects in cardiac morphogenesis, an intermediate loss (about 60%) leads to phenotypes reminiscent of congenital heart defects (Takeuchi et al., 2005). Although the heart's overall morphology remains unchanged, it results in right ventricular hypoplasia, OFT septation defects, and impaired valve formation. Additionally, numerous studies indicate that gain-of-function mutations in Tbx20 can result in defective ventricular walls and various congenital heart disorders, including bicuspid aortic valve, thoracic aortic aneurysms, patent foramen ovale, congenital atrial septal defects, valve disorders, double outlet right ventricle, and familial tetralogy of fallot (Huang et al., 2017; Luyckx et al., 2019; Pan et al., 2015; Posch et al., 2010; Zhang et al., 2011). Beyond its role in embryonic and fetal cardiac development, Tbx20 is crucial for cardiac homeostasis in adults as well. Conditional knockout of Tbx20 in mouse myocardium leads to cardiac chamber dilation and results in lethality within 5-16 days (Shen et al., 2011). Tbx20 ablation is also associated with dilated cardiomyopathy, resulting in altered cardiac function, arrhythmias, and heart failure (Shen et al., 2011). Moreover, Tbx20 overexpression fosters adult cardiomyocyte proliferation following MI by repressing cell cycle inhibitors such as $p21^{WAF1/Cip1}$, Meis1, and Btg2 (Xiang et al., 2016). Cardiomyocyte-specific gain-of-function studies revealed that Tbx20 enhances cardiomyocyte proliferation by upregulating the PI3K/AKT/GSK3β/β-catenin and Bmp2-pSmad1/5/8 signaling pathways (Chakraborty et al., 2013).

1.10.2 Tbx20 is a key regulator of cardiac transcription factor expression spatiotemporally

Several studies have reported the importance of Tbx20 in regulating the expression of multiple genes during development and proliferation in different compartments and cell types of the heart (Figure 12).

1.10.2.1 Cardiac Outflow Tract (OFT) formation

Tbx20 is critical for the proper development of the cardiac outflow tract (OFT) (Figure 12). It facilitates OFT formation by enhancing the expression of Nkx2.5 and Myocyte Enhancer Factor 2c (Mef2c). In Tbx20-deficient embryos, the expression of Nkx2.5, Bmp4, Mef2c, and Pitx2 genes essential for OFT development is significantly reduced (Delot et al., 2003; Kioussi et al., 2002; Lin et al., 1997; Liu et al., 2004; Takeuchi et al., 2005). Tbx20 operates synergistically with Isl1 and GATA4 to promote the expression of Nkx2.5 and Mef2c, essential for the formation of the anterior heart field (AHF) (Cai et al., 2003). Within the OFT, Tbx2 interacts with Nmyc1 to inhibit its expression, and both Tbx2 and Nmyc1 are under the regulation of Tbx20. Studies suggest that Tbx2's regulation of Nmyc1 is affected by its spatial expression pattern. Although Tbx20 can induce Nmyc1 expression in the OFT, the repression by Tbx2 outweighs this, leading to reduced proliferation rates in the OFT (Cai et al., 2005). Moreover, chromatin immunoprecipitation (ChIP) assays in the OFT demonstrate that Tbx20 inhibits the expression of Second Heart Field (SHF) genes, such as Isl1, FGF10, and HOP homeobox (Hopx). This indicates that Tbx20 plays a greater role in the differentiation and maturation of cardiomyocytes in the OFT rather than in their proliferation (Boogerd et al., 2018).

1.10.2.2 Cardiac Atrium formation

Tbx20 conditional knockout mutants harbour defects in atrial chamber formation. In the cardiac atrium, Tbx20 directly augments the expression of genes that are required for the establishment of atrial identity (Chen et al., 2021) (Figure 12). Tbx20 ChIP-Seq data, followed by functional analysis, showed that Tbx20 directly binds to and increases the expression of chicken ovalbumin upstream promoter transcription factor 2 (COUP-TFII). COUP-TFII, in turn, partners with nuclear receptor subfamily 2, group F, member 2 (Nr2f2) to promote the expression of atrial-specific genes while suppressing ventricular gene expression, such as ventricular myosin light chain-2 (Mlc2v) (Boogerd et al., 2018; Cai et al., 2003; Wu et al., 2013). Tbx20 also elevates the levels of the Hairy/Enhancer-of-split-related YRPW motif

protein 1 (Hey1) gene, which is pivotal for proper atrium formation (Boogerd et al., 2018). Additionally, Tbx20 inhibits the expression of the ventricular genes Bmp2 and Bmp10 in atrial cardiomyocytes (Boogerd et al., 2018). In the atrium, Tbx20 downregulates ANF expression. ANF contains binding sites for both Tbx5 and Tbx20, where Tbx5 activates ANF expression while Tbx20 suppresses it (Plageman & Yutzey, 2004). Consequently, the ANF expression level depends on the localization and relative amounts of Tbx5 and Tbx20, with both competing for transcriptional regulation of ANF in the atrial tissue.

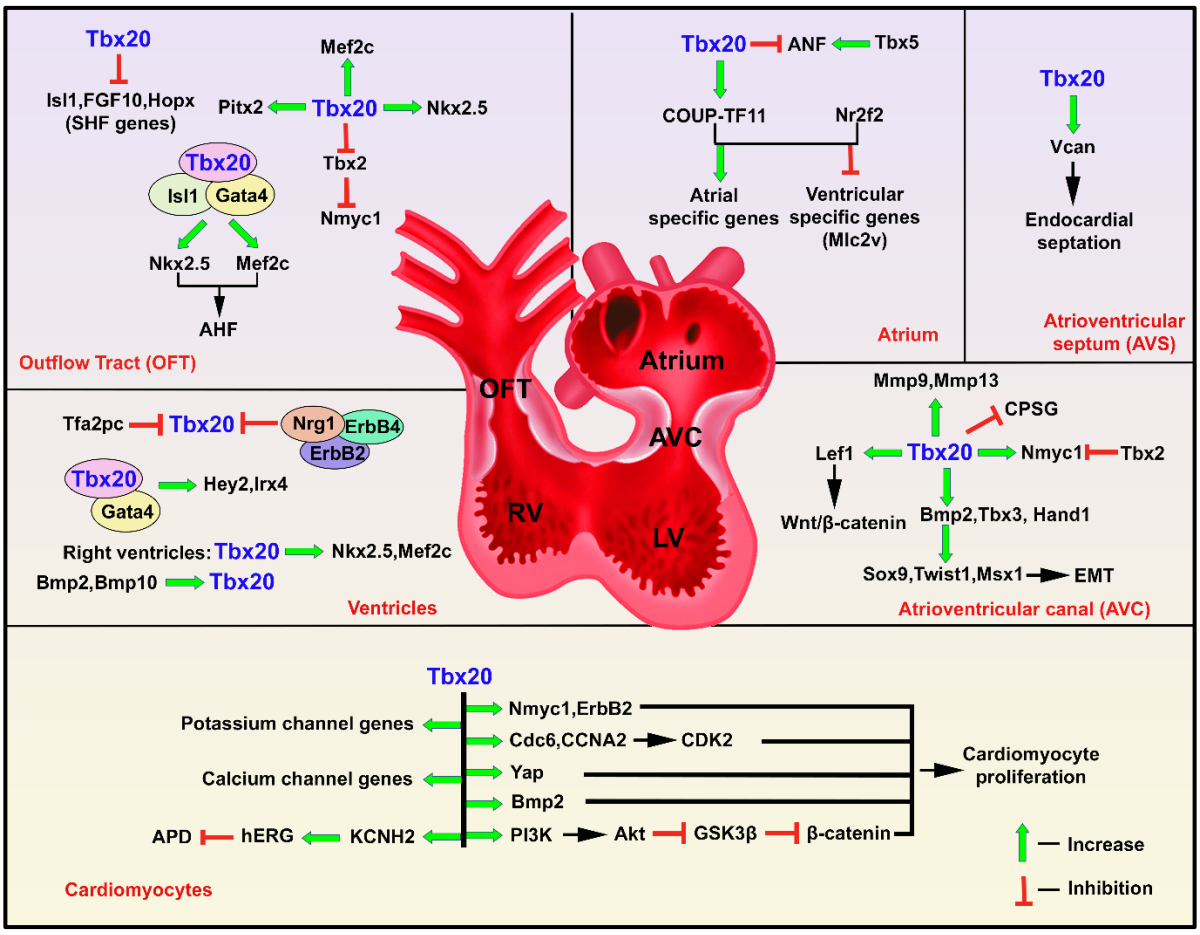

Figure 12. Schematic illustration of the transcriptional regulation mediated by Tbx20 during cardiovascular development. Tbx20 is spatiotemporally expressed in different compartments of the heart, and it is involved in multiple cardiogenic mechanisms through its interactions with multiple transcriptional networks in embryonic, fetal and adult hearts.

1.10.2.3 Atrioventricular canal (AVC) and atrioventricular septum (AVS) formation

Tbx20 has been demonstrated to have a crucial function in the formation of cardiac valves, which originate from structures known as endocardial cushions (Figure 12). Tbx20 gain of function in the endocardial cushions increases the expression of matrix metalloproteinases (MMPs) such as MMP9 and MMP13, while simultaneously decreasing levels of Chondroitin

Sulfate Proteoglycans (CSPGs), including Versican (Vcan) and Aggrecan (Shelton & Yutzey, 2007). In contrast, Tbx20 loss of function results in elevated CSPG expression and reduced MMP levels, underscoring its critical role in promoting epithelial-mesenchymal transition (EMT) (Shelton & Yutzey, 2007). Tbx20 also enhances the growth of cells in mesenchymal valve precursors derived from the endocardial cushions. It does this by competing with Tbx2 for binding sites on the Nmyc1 promoter/enhancer, which boosts its expression and subsequently promotes the proliferation of cells in the AVC, crucial for chamber formation (Cai et al., 2005). Within the AVC, Tbx20 modulates and boosts the expression of Bmp2, Tbx3, and Hand1. Bmp2 then triggers EMT by elevating the expression of Sox9, Twist1, and Msh homeobox 1 (Msx1) in the ventricular cushions (Cai et al., 2011; Ma et al., 2005). Beyond EMT, Tbx20 also enhances Wnt/β-catenin signaling by promoting the expression of Lymphoid Enhancer-Binding Factor 1 (Lef1), which contributes to valve elongation and the maturation of endocardial cushions (Cai et al., 2013). Tbx20 is essential for the process of endocardial septation by regulating the expression of Vcan (Boogerd et al., 2016).

1.10.2.4 Ventricle formation

Tbx20 also plays a pivotal role in regulating the gene expression program during ventricle formation (Figure 12). Tbx20, along with GATA proteins, controls and induces the expression of Hey2, a basic helix-loop-helix transcription factor that plays a pivotal role in ventricular myocyte differentiation and ventricular wall formation (Ihara et al., 2020). Tbx20 regulates the expression of Hey2 through a distal enhancer conserved in humans and mice. Tbx20 establishes ventricular identity by regulating the expression of the ventricle-specifying gene Iroquois homeobox 4 (Irx4) (Boogerd et al., 2018). Nrg1, an epidermal growth factor family gene, is expressed in the endocardium and myocardium and is important for ventricular trabeculation (Lai et al., 2010). In late ventricular myocardium, Nrg1, along with Erb-B2 Receptor Tyrosine Kinase 2 (ErbB2) and Erb-B2 Receptor Tyrosine Kinase 4 (ErbB4), suppresses the expression of Tbx20, thereby highlighting that Tbx20 is not essential for differentiation of late ventricular wall (Bersell et al., 2009). Tbx20, in turn, is inhibited by AP-2 gamma (Tfap2c) in the ventricular myocardium (Hammer et al., 2008). In the ventricular myocardium, Tbx20 is also regulated by Bmp family genes. Using chicken embryo explants, it was shown that Bmp2 induces the expression of Tbx20 in the ventricular myocardium (Plageman & Yutzey, 2004). Tbx20 is also regulated by Bmp10 as it contains a Smad binding site in the proximal promoter region. By binding to Tbx20, Bmp10 induces its expression,

which in turn aids in ventricular wall maturation and development. In the right ventricles, Tbx20 induces the expression of ventricular genes Nkx2.5 and Mef2c (Takeuchi et al., 2005).

1.10.2.5 Cardiomyocyte proliferation

Several studies have shown the importance of Tbx20 in driving cardiomyocyte proliferation during development as well as disease (Figure 12). Tbx20 upregulates the expression of Cell division cycle 6 (Cdc6) and Cyclin A2 (CCNA2) to induce cardiomyocyte proliferation (Boogerd et al., 2018). Cdc6 and CCNA2, in turn, activate Cyclin-dependent kinase 2 (CDK2), which is required for the G1 to S phase transition (Uranbileg et al., 2012). Conditional knockout of Tbx20 in cardiomyocytes causes a decrease in cell cycle progression due to decreased expression of Cdc6 and CCNA2. Tbx20 also induces cardiomyocyte proliferation via inducing the expression of Nmyc1. Tbx20 does so by removing the repression of Tbx2 on Nmyc1 (Boogerd et al., 2018). Tbx20 conditional knockout myocytes attenuate the expression of ErbB2, which is required for cardiomyocyte proliferation (Chen et al., 2021). Overexpression of Tbx20 in adult cardiomyocytes was shown to augment cardiomyocyte proliferation via the PI3K/AKT/GSK3β/β-catenin signaling axis. Tbx20 overexpression upregulates cardiomyocyte proliferation in the adult heart via augmenting the PI3K/AKT, Yes-associated protein (Yap) and transcriptional coactivator with PDZ-binding motif (TAZ) and Bmp signaling pathway and repressing cell cycle inhibitors p21, Meis1 and Btg2 (Chakraborty et al., 2013; Xiang et al., 2016). Tbx20 overexpression facilitates the regeneration of cardiomyocytes following MI (Xiang et al., 2016). Apart from this, Tbx20 also regulates various calcium channel and potassium channel genes. In cardiomyocytes, Tbx20 controls the expression of the potassium voltage-gated channel subfamily H member 2 (KCNH2) gene by enhancing its transcription, which encodes the Kv11.1 (hERG) channel, that is the channel generating ventricular repolarizing currents, resulting in shortening of action potential duration (APD) (Caballero et al., 2017). Mutations in Tbx20 or KCNH2 causes Long QT syndrome (LQTS). Therefore, taken together, Tbx20 plays a central role in cardiac development, proliferation and regeneration.

The lack of proliferation of the adult cardiomyocytes and their subsequent replacement with fibrotic tissue under the influence of stress or disease makes it essential for the re-initiation of the regulatory pathways that initiate cardiomyocyte proliferation. Thus, to re-initiate adult cardiomyocyte proliferation during stress stimulus, we investigated the role of Tbx20 in a pathophysiological model of ER stress and diabetes induced cardiomyopathy. We found that in cardiomyocytes during stress, Activating transcription factor 6 (Atf6) induced upregulation

of Tbx20 drives cardiomyocyte proliferation via Bmp2-pSmad/1/5/8 signaling (Data shown in Chapter 4; Das et al., 2023). Our study also showed the importance of Tbx20 in maintaining proper cardiac function during ER stress-induced cardiomyopathy. We also showed that Tbx20 negatively regulates the senescence response in cardiomyocytes during ER stress and diabetes (Data shown in Chapter 5). Thus, our findings shed light on the novel and unexplored function of Tbx20 during ER stress and diabetes-induced cardiomyopathy, and this can be extrapolated further by cardiomyocyte-specific overexpression studies to persistently upregulate Tbx20 even during prolonged stresses to reinstate homeostasis.

1.11 Bone morphogenetic protein 2 (Bmp2): Its role in cardiac development and homeostasis

Bone morphogenetic protein 2 (Bmp2) is part of the transforming growth factor beta superfamily (TGFβ) and is crucial for cardiac development (Halloran et al., 2020). Bmp2 guides cardiac progenitor cells in the formation of the endocardial cushions (EC) (Rivera-Feliciano & Tabin, 2006). The development of heart valves begins with swelling, which is followed by the deposition of ECM in that region. The myocardium in the area of the heart valve sends signals to the endocardium beneath it, causing it to detach, migrate into the extracellular space between the endocardium and myocardium, and give rise to EC via epithelial-mesenchymal transition (EMT). The myocardium within the heart valve region expresses Bmp2, which is essential for the formation of the EC. Embryos lacking Bmp2 do not survive past E8.5, prior to the formation of the EC (Zhang & Bradley, 1996). Bmp2 is critical for initiating endocardial cushion expansion and the development of valve mesenchyme. In Bmp2 conditional knockout models, EC formation and atrioventricular constriction are absent, with development halting prior to matrix deposition, ultimately preventing endocardial swelling (Rivera-Feliciano & Tabin, 2006). Bmp2 also initiates EMT of AVC for the production of invasive mesenchyme (Prados et al., 2018; Von Gise & Pu, 2012). Bmp2 conditional knockout explants fail to produce mesenchymal cells; however, the addition of recombinant Bmp2 protein was shown to rescue EMT in these explants, resulting in the formation of invasive mesenchymal cells (Rivera-Feliciano & Tabin, 2006). Here, the authors showed the formation of invasive mesenchymal cells by co-expressing PECAM1 and α-SMA. These two markers are co-expressed only in activated endothelial cells and invasive mesenchymal cells, and it is indicative of EMT (Camenisch et al., 2002; Sugi et al., 2004). Though Bmp2 conditional knockout explants lack this co-expression, the addition of Bmp2 protein to these explants co-expresses both the markers, thus potentiating the necessity of

Bmp2 in driving EMT for the formation of EC cells. The authors also showed that Bmp2 is required for the specification of segments during the patterning of the heart (Rivera-Feliciano & Tabin, 2006). In normal cardiac development, when Bmp2 is present, ANP, a chamber myocardium-specific marker, is expressed in the outer curvature of the atrial and ventricular compartments. On the contrary, it is absent in the IC, IFT, OFT and AVC (Christoffels et al., 2000). In Bmp2 knockout mutants, ANP expression extends into the inner curvature, inflow tract (IFT), and atrioventricular canal (AVC), indicating that the absence of Bmp2 leads inner curvature myocardium to acquire features typical of differentiated outer curvature myocardium. ANP is also present in AVC in the absence of Bmp2, thereby showing that in the absence of Bmp2, AVC acquires the identity of chamber myocardium (Rivera-Feliciano & Tabin, 2006). The importance of Bmp2 in cardiac development is also highlighted as they are essential for atrial specification. In Bmp2 knockout mutants, Mlc2v (a ventricular and AVC-specific marker) is ectopically expressed in the atrial appendages (Franco et al., 1999; Rivera-Feliciano & Tabin, 2006). The expansion of ventricular and AVC markers to other regions of the developing heart in the absence of Bmp2 thus proves that Bmp2 is required for the specification of cardiac valve-forming regions. Bmp2 also maintains cardiac endothelium competence by regulating the expression of GATA4, Inhibitor of DNA binding 1 (Id1) and Notch1 (Rivera-Feliciano & Tabin, 2006).

Therefore, Bmp2 is a prerequisite for the specification of AVC, myocardial patterning and EMT induction for the formation of endocardial cushions.

1.12 Bmp2 and its role in inducing cardiac inflammation

Though Bmp2 plays a pivotal role in cardiac development, multiple studies have shown the involvement of Bmp2 in inducing inflammatory responses in cardiac cells. Studies have shown that the expression of Bmp2 is increased post-MI (Pulkkinen et al., 2023; Sanders et al., 2016). In the MI hearts, Bmp2 augments pro-inflammatory response in endothelial cells, resulting in increased expression of adhesion molecules and infiltrating inflammatory cells (Al-Shabrawey et al., 2021; Csiszar et al., 2006). Bmp2 works in synergy with TNFα to amplify the inflammatory response in endothelial cells, while its inhibitor, Gremlin 2 (Grem2), mitigates inflammatory cell infiltration following MI (Sanders et al., 2016). Using Grem2 gain and loss functional mutants, it was shown that Grem2 restricts the inflammatory response in the peri-infarct ventricular tissue by inhibiting the expression of Bmp2 and thereby improving the cardiac function. Bmp2 also induces pro-inflammatory response during atherosclerosis (Wu & Hatzopoulos, 2019). Increased Bmp2 induces monocyte infiltration into endothelial

cells (Csiszar et al., 2006). Bmp2 is also elevated in the epicardial tissue of coronary artery disease patients, and its increase correlates with the increase of calcified plaque formation (Zhang et al., 2015). In another study, in a porcine heart, Bmp2 gene transfer caused pathological pericardial effusion (Pulkkinen et al., 2023). Transfer of the Bmp2 gene triggers an inflammatory response in porcine myocardium affected by ischemia. In Type 2 Diabetes patients, elevated levels of Bmp2 correlate with atherosclerotic burden and calcification of coronary arteries (Zhang et al., 2015).

Therefore, though Bmp2 is essential for cardiac development and homeostasis, its increased expression can also lead to an increase in the inflammatory response in the heart. We showed that Bmp2 could be considered a putative biomarker for the early detection of CVDs. In our study, we showed that during different stresses like ER stress, Diabetes, Type 2 Myocardial Infarction and High-Fat diet model, the expression of Bmp2 is increased initially during a short duration of stress in cardiomyocytes. This increase in Bmp2 resulted in an increase in cardiomyocyte proliferation via the Smad1/5/8 pathway, thereby restoring cardiac homeostasis and cardiomyocyte survival (Data shown in Chapter 4). Extended stress exposure led to a sustained and marked increase in Bmp2 expression within cardiac fibroblasts (Data shown in Chapter 5). Increased Bmp2 was shown to augment the expression of inflammatory markers TNFα and IL-6 in cardiac fibroblasts, thereby aggravating the severity of CVDs. The persistent upregulation of Bmp2 throughout the progression of stress response in the heart makes it a potential candidate biomarker and warrants further investigation.

1.13 MicroRNAs

MicroRNAs (miRNAs) belong to a group of non-coding RNA molecules. They consist of small (21-25 nucleotides), endogenous, single-stranded RNAs that originate from long primary miRNAs (pri-miRNAs) containing one or more hairpin structures. In 1993, the Ambros and Ruvkun laboratories discovered the first microRNA, *lin-4*, in *Caenorhabditis elegans* (Lee et al., 1993; Wightman et al., 1993). They demonstrated that *lin4* has a complementary sequence to the 3' untranslated region (3'UTR) of *lin14*, which leads to the post-transcriptional repression of *lin14* by its 3'UTR. miRNAs are highly conserved among different species, and their discovery has significantly transformed research in this emerging field (Friedlander et al., 2014; Li et al., 2010). Though most of the miRNA hairpins are derived from introns and non-coding RNAs, recently, studies have shown that they can also be transcribed from protein-coding regions. A single microRNA is capable of regulating numerous messenger RNAs (mRNAs). They function by post-transcriptionally binding to the

target gene via a "seed sequence", which is a 6-8 nucleotide stretch of complementary sequence. In addition to the seed sequence, recently it was shown that in some cases, additional pairing to 3'sequences also determines target specificity. Besides the 3'UTR, miRNAs can also bind to promoters, 5'UTRs, and coding sequences (Broughton et al., 2016). They reside in extracellular microvesicles and shuttle between cellular compartments for cell-cell communication and are often present in biological fluids, making them a potent candidate biomarker (Boon & Vickers, 2013). Though miRNAs are involved in various biological processes, their aberrant expression pattern often leads to the development of disease conditions.

1.13.1 Biogenesis of miRNAs

The biogenesis of miRNAs takes place by both canonical and non-canonical pathways. The canonical pathway involves two RNase III enzymes, Drosha and Dicer (Figure 13). On the contrary, the non-canonical pathway may be Dicer-independent or Drosha-independent (Figure 14).

1.13.1.1 Canonical pathway of miRNA biogenesis

Most miRNAs are intragenic in origin, mainly derived from introns and, less frequently, from exons of protein-coding genes. However, certain miRNAs are intergenic and undergo processing independently of any host gene (de Rie et al., 2017). Some of the miRNAs are also transcribed as clusters having identical seed sequences (Tanzer & Stadler, 2004). miRNA biogenesis begins in the nucleus with the transcription of primary miRNAs (pri-miRNAs) from their respective genes by RNA polymerase II or III. The pri-miRNA is a hairpin stem-loop structure. The pri-miRNAs that are transcribed by RNA polymerase II are post-transcriptionally modified and contain a 5' cap structure and 3'polyadenylation (Lee et al., 2004). The Microprocessor complex, which includes the RNase III enzyme Drosha and the RNA-binding protein DGCR8 (DiGeorge Syndrome Critical Region 8), cleaves pri-miRNA to generate precursor miRNA (pre-miRNA) (Denli et al., 2004). In mammals, methyltransferase-like 3 (METTL3) methylates pri-miRNA at the N6 position of adenosine for its recognition by DGCR8 (Alarcon et al., 2015). DGCR8 aids in the functioning of Drosha by recognizing the N(6)-methyladenosine mark and recruiting Drosha to the site (Alarcon et al., 2015). Drosha, in turn, cleaves the pri-miRNA at the base of the hairpin structure, resulting in the formation of pre-miRNA, which is about 55-70 nucleotides in length. Cleavage by Drosha creates 2 nucleotide overhangs at each 3'end on pre-miRNA. The Exportin-5/Ran-GTP complex transports the pre-miRNA to the cytoplasm, where it undergoes further processing by the

RNase III enzyme Dicer. Dicer, along with TRBP, cleaves the pre-miRNA to miRNA duplex (Zhang et al., 2004). The N-terminal domain of Dicer, which has helicase activity, recognizes the terminal loop of pre-miRNA, whereas the C-terminal domain containing the tandem RNase III domain forms the catalytic centre for proper cleavage. The name of the mature miRNA duplex is determined by its directionality, where '5p' denotes the 5'end of the pre-miRNA and '3p' denotes the 3'end of the pre-miRNA. Strand selection from the miRNA duplex for Argonaute (Ago) loading is influenced by the thermodynamic stability at the 5' end and the presence of a uracil at the first nucleotide position.

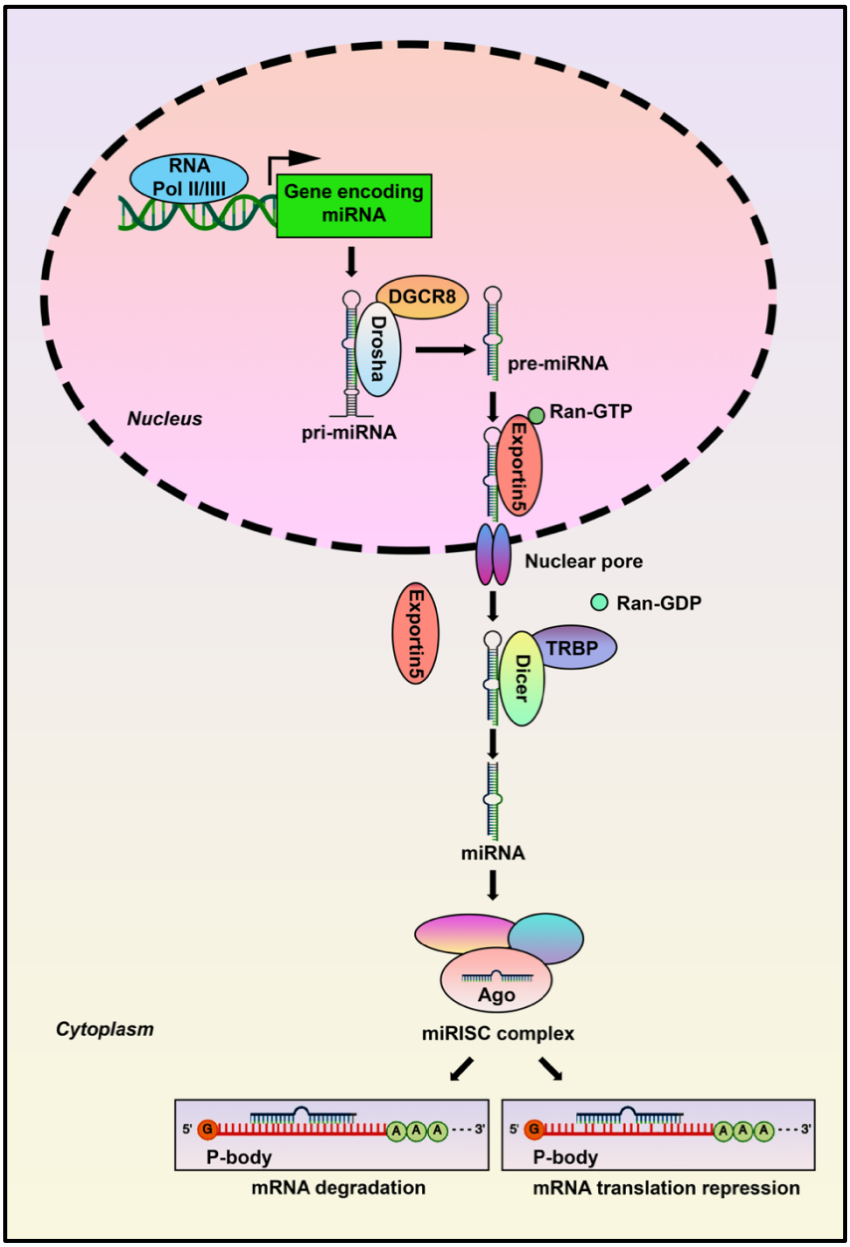

Figure 13. Canonical pathway of miRNA biogenesis. The canonical miRNA pathway starts in the nucleus with the transcription of primary miRNA (pri-miRNA) from designated genes. The pri-miRNA

is subsequently processed by the Microprocessor complex, made up of Drosha and DGCR8, into a precursor miRNA (pre-miRNA). Exportin-5, in conjunction with Ran-GTP, transports the pre-miRNA to the cytoplasm, where it is further cleaved by the Dicer/TRBP complex to produce a mature miRNA duplex. Either the 5p or 3p strand of this duplex is then incorporated into the Argonaute (Ago) protein, forming the miRNA-induced silencing complex (miRISC). miRISC can further bind to the target mRNAs, resulting in their degradation (full complementarity) or their translational attenuation (absence of complete complementarity).

The strand with lesser 5'end thermodynamic stability or 5'uracil is loaded onto the Ago protein and is known as the 'guide strand'. The other strand is known as the 'passenger strand'; it is unwound from the guide strand and is degraded by cellular degradation machinery (Meijer et al., 2014). The single-stranded miRNA directs the Argonaute (Ago) protein complex to complementary RNA, which is further targeted for degradation.

1.13.1.2 Non-canonical pathway of miRNA biogenesis

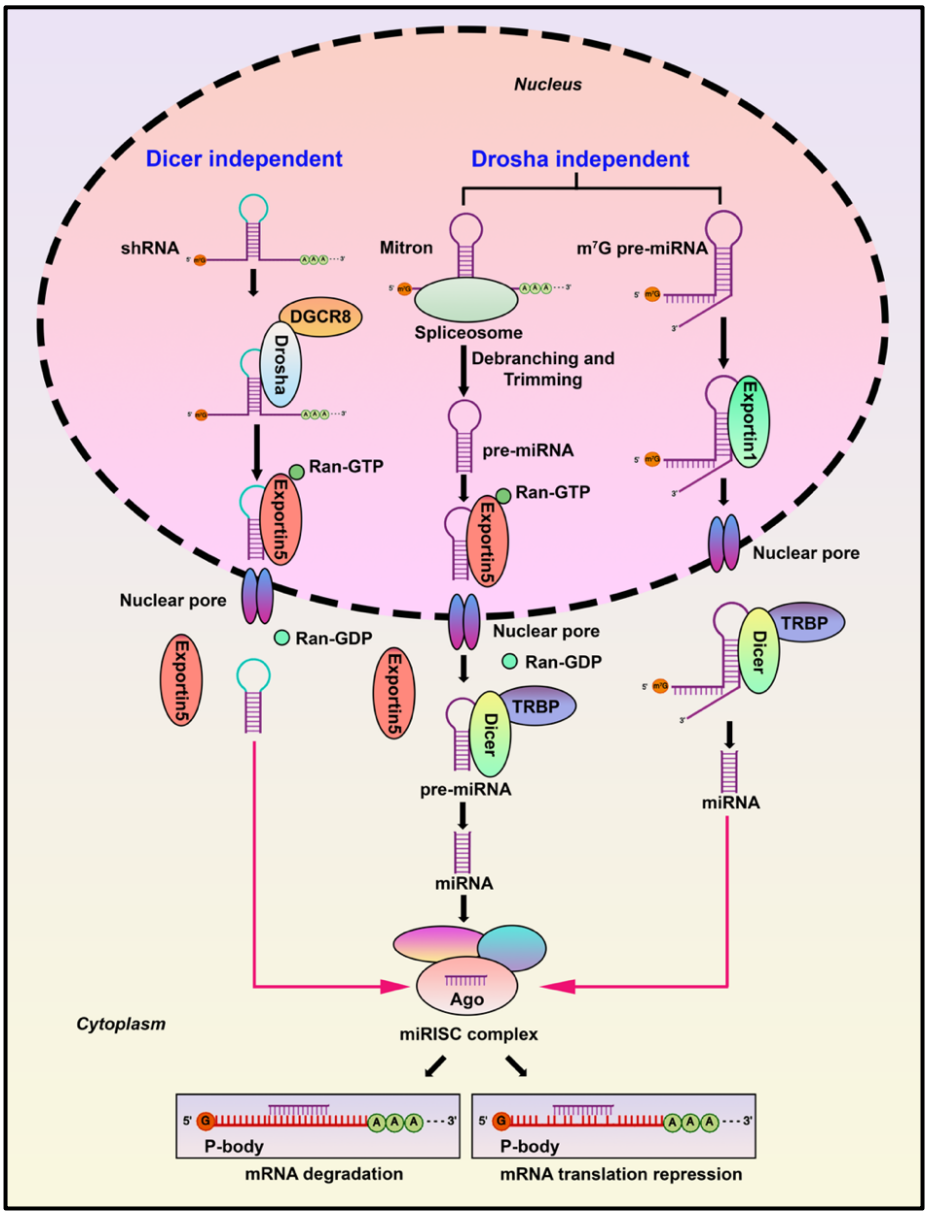

Figure 14. Non-canonical pathway of miRNA biogenesis. The non-canonical pathway of miRNA biogenesis consists of Dicer-independent and Drosha-independent pathways. In the Dicer independent pathway, small hairpin RNA (shRNA) are processed by the Drosha/DGCR8 complex in the nucleus and is exported to the cytoplasm through the Exportin5/Ran-GTP complex. In the cytoplasm, it is processed by the Ago protein and loaded into the miRISC complex for mRNA degradation or translational attenuation. In the Drosha independent pathway, mitrons are spliced and trimmed by the spliceosome complex and the debranching enzyme to form the pre-miRNA. The pre-miRNA is exported to the cytoplasm via the Exportin5/Ran-GTP complex and further processed by the Dicer/TRBP complex to form the mature miRNA. 7-methylguanosine (m^7G) capped pre-miRNAs are also processed by the Drosha independent pathway. They are transported to the cytoplasm from the nucleus via Exportin1. In the cytoplasm, they are processed by the Dicer/TRBP complex to form mature miRNA. Both these pathways leads to Ago-dependent miRISC loading followed by degradation or translational attenuation of target mRNAs.

1.13.1.2.1 Dicer independent pathway

The Dicer-independent pathway utilizes short hairpin RNA (shRNA) transcripts, which are processed by the Drosha/DGCR8 complex (Yang et al., 2010) (Figure 14). They are later exported to the cytoplasm via Exportin5/Ran-GTP complex, where in the cytoplasm they are processed by the Ago2 protein complex as the lengths of these shRNA are too short to be substrates for Dicer. Ago2 facilitates pre-miRNA maturation by cleaving the 3p strand and trimming the 5p strand, leveraging its endoribonuclease function.

1.13.1.2.2 Drosha/DGCR8 (Microprocessor)-independent pathway

In the Microprocessors-independent pathway, the newly formed pre-miRNA is transported from the nucleus to the cytoplasm without requiring cleavage by Drosha/DGCR8. One example is mitrons, which resemble pre-miRNAs and are processed through splicing and intron debranching enzymes (Ruby et al., 2007) (Figure 14). Mitrons are carried to the cytoplasm through the Exportin-5/Ran-GTP transport system. Another Drosha-independent pathway includes 7-methylguanosine (m7G)-capped pre-miRNAs, which are generated by RNA polymerase II (Figure 13). The m7G pre-miRNAs are transported to the cytoplasm through Exportin1, and the presence of the m7G cap aids in the loading of the 3p strand onto the Ago protein while inhibiting the loading of the 5p strand (Xie et al., 2013).

1.13.1.3 miRNA-induced silencing complex (miRISC) mediated gene silencing

The miRISC complex comprises the Ago protein and the guide strand (Kawamata & Tomari, 2010). The Ago protein contains four characteristic domains, namely the N-terminal domain, the PAZ domain, the MID domain and the C-terminal PIWI domain (Wu et al., 2020). The PAZ domain sequence independently recognizes the guide strand, whereas the Mid domain and PIWI domain containing the 5'-phosphate pocket anchors the 5'-monophosphate of the

guide strand (Nakanishi, 2022). miRISC targets specific mRNAs by recognizing complementary sequences called miRNA response elements (MREs) within the target RNA.

Ago2-mediated target mRNA degradation or RISC-mediated translational attenuation is determined by the degree of MRE complementarity. A full complementarity between miRNA and MRE results in Ago2 endonuclease activity, resulting in target cleavage; whereas, the absence of complete complementarity results in translational attenuation. The RISC complex can also induce target mRNA poly(A)-deadenylation by recruiting effector protein complex (PAN2-PAN3 and CCR4-NOT) and can also decay the 5'cap of the target mRNA by decapping protein 2 (Dcp2) and other related proteins (Christie et al., 2013). Following decapping, the target mRNA is degraded by exoribonuclease 1 (Xrn1) (Braun et al., 2012).

1.13.2 miRNA and its role in cardiovascular diseases (CVDs)

Since their discovery, miRNAs have played a major role in the pathophysiology of CVDs. Upon encountering stress stimuli or during adverse external conditions, miRNAs are aberrantly expressed, resulting in the pathogenesis of cardiac pathological conditions like hypertrophy, arrhythmia, myocardial infarction, cardiac fibrosis, cardiomyopathies, and heart failure (Figure 15). The human genome encodes approximately 2500 miRNAs, and out of them, about one-third or more miRNAs are involved in both pathophysiology and well as maintenance of cardiac homeostasis.

1.13.22.1 miRNAs and Hypertrophy

Cardiomyocyte hypertrophy occurs when cardiomyocytes increase in size without a rise in cell count (Ahmad et al., 2005). Initially, this is a compensatory and adaptive mechanism to maintain cardiac homeostasis; however, if sustained for too long, hypertrophy can lead to negative physiological effects (Berk et al., 2007; Hill & Olson, 2008). It can be triggered by physiological conditions (such as exercise or pregnancy) or pathological conditions, leading to cardiomyopathy. miRNAs are crucial in both promoting and mitigating cardiac hypertrophy.

The miR-212/132 family is elevated in response to hypertrophic stimuli like phenylephrine, fetal calf serum, angiotensin II, and insulin-like growth factor 1 (Ucar et al., 2012). *In vivo* experiments showed that transverse aortic constriction (TAC) also increases the expression of miR-212/132. This miRNA family induces hypertrophy by targeting the Forkhead box O3 (FoxO3) transcription factor, which activates the Calcineurin/Nuclear factor of activated T cell (NFAT) pathway (Ucar et al., 2012). Another significant miRNA is miR-22, which promotes cardiac hypertrophy. Overexpressing miR-22 in neonatal rats increases the

levels of hypertrophic markers ANP, Brain natriuretic peptide (BNP), and β-Myosin heavy chain (β-MHC). Conversely, reduced function of miR-22 correlates with a diminished hypertrophic response under various stress stimuli (phenylephrine, isoproterenol, or angiotensin II) (Huang et al., 2013). MiR-495 has also been linked to inducing cardiac hypertrophy, as it inhibits Phosphatase and TENsin homolog deleted on chromosome 10 (PTEN) and activates the PI3K/AKT signaling pathway in a rat model of pulmonary arterial hypertension (PAH) (Clark et al., 2016; Fu et al., 2018). MiR-199b promotes hypertrophy by targeting dual-specificity tyrosine-regulated kinase 1A (Dyrk1a). Additionally, Yap mediated upregulation of miR-206 increases the hypertrophic effect in cultured cardiomyocytes by targeting Forkhead box protein P1 (FOXP1) (Yang et al., 2015). Additional miRNAs involved in promoting hypertrophy include miR-23a, miR-410, miR-208a, miR-27a, and miR-154 (Bernardo et al., 2016; Callis et al., 2009; Clark et al., 2016; Nishi et al., 2011).

miR-1 and miR-133 are two miRNAs associated with reduced cardiac hypertrophy. In pressure-overload models, miR-1 levels drop, which is linked to an increased hypertrophic response (Sayed et al., 2007). miR-1 targets twinfilin-1; thus, when miR-1 levels decrease, twinfilin-1 levels rise, contributing to greater hypertrophy (Li et al., 2010). miR-1 also inhibits hypertrophy by affecting calcium–calmodulin signaling through the calcineurin/NFAT pathway and by suppressing Mef2a and GATA4 expression (Ikeda et al., 2009). Lastly, treatment with Ang II during hyperthyroidism increases hypertrophy due to the downregulation of miR-133, resulting in the upregulation of Serca2a and Calcineurin (Chen et al., 2017).

1.13.2.2 miRNAs and Arrhythmia

Anomalies in the heart rate or rhythm can result in cardiac arrhythmia (Antzelevitch & Burashnikov, 2011). Changes in the intracellular calcium (Ca^{2+}) cycle in the sarcoplasmic reticulum cause arrhythmias. Phosphorylation of phospholamban, ryanodine receptor (RyR2), and the L-type Ca^{2+} channel (Bers, 2002) keeps the Ca^{2+} cycling process going. Arrhythmia also happens due to abnormalities in gap junctions (Delmar & Liang, 2012).

Overexpression of miR-1 causes cardiac arrhythmia due to aberrant Ca^{2+} cycling and targeting Protein phosphatase 2A (PP2A) regulatory subunit b56α and upregulating the phosphorylation of L-type Ca^{2+} channel and RyR2 channel (Terentyev et al., 2009). Another miRNA, miR-17-92 cluster, targets gap junction alpha-1 and PTEN to induce cardiac arrhythmia and lethal hypertrophic cardiomyopathy (Danielson et al., 2013). In another study, miR-206 overexpression in adult mouse hearts targets gap Cx43 in cardiomyocytes to induce

cardiac arrhythmia (Delmar & Liang, 2012). Several other miRNAs are involved in the progression of arrhythmia.

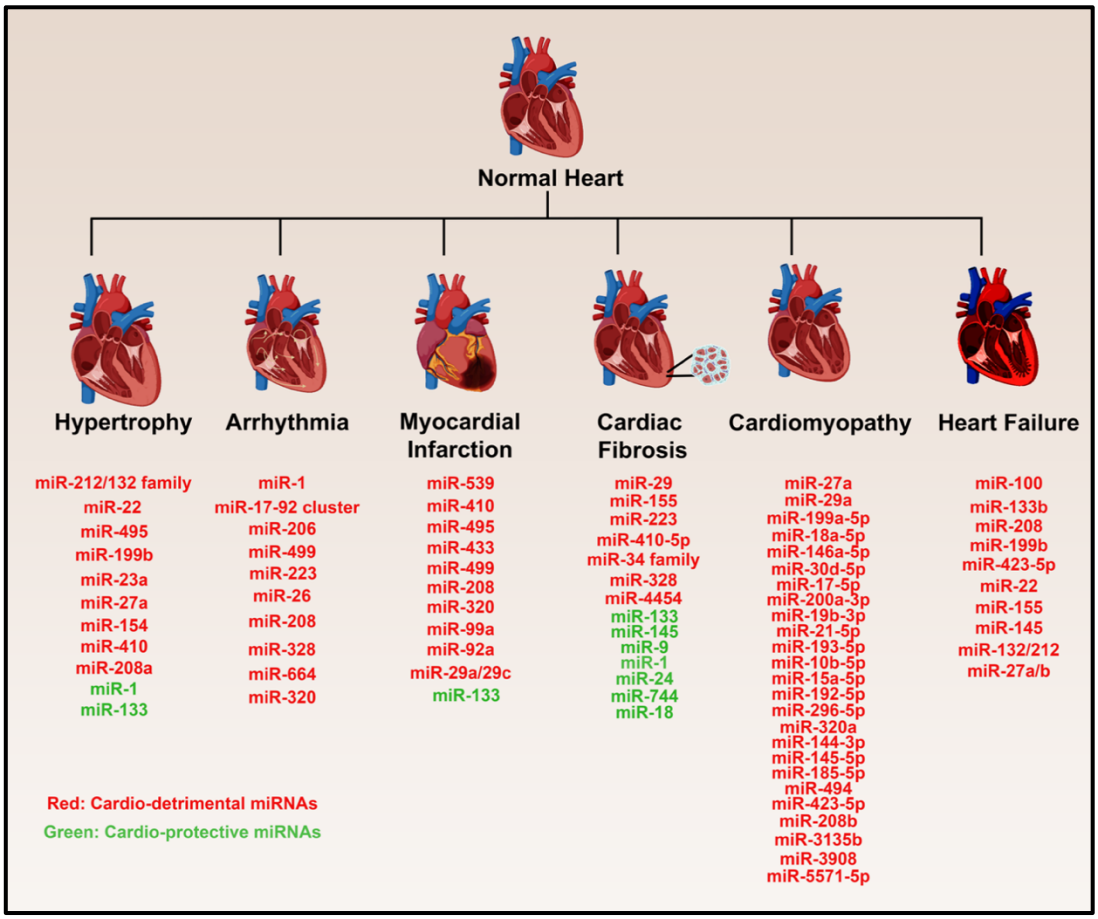

Figure 15. Regulation of miRNAs during cardiovascular diseases. Schematic illustration showing the different miRNAs that are differentially regulated during cardiovascular diseases like hypertrophy, arrhythmia, myocardial infarction, cardiac fibrosis, cardiomyopathy and heart failure. The miRNAs written in red are cardio-detrimental, and the miRNAs written in green are cardio-protective.

1.13.2.3 miRNAs and Myocardial Infarction (MI)

Myocardial infarction results from diminished blood flow to the heart caused by plaque build-up within the artery walls (atherosclerosis), leading to insufficient oxygen delivery to the cardiomyocytes (Lu et al., 2015).

The imprinted Delta-like homolog 1 (Dlk1)- type III iodothyronine deiodinase (Dio3) locus derived from a polycistron harbours multiple non-coding RNA clusters like fifty miRNAs, three long non-coding (lncRNAs) and one small nucleolar RNA (snoRNA), and it regulates different biological processes in the heart (Dill & Naya, 2018; Janssen et al., 2013). In the mouse model of MI, multiple miRNAs of this locus are elevated. During MI, miR-539 targets O-GlcNAcase (Oga), thereby resulting in an altered cardiac response (Ferron et al., 2019; Muthusamy et al., 2014). Another study showed two other miRNAs of the locus miR-

410 and miR-495 are elevated during MI, hypertrophy and dystrophy, and their inhibition results in attenuation of cardiac hypertrophy (Clark et al., 2016). miR-433 targets Antizyme inhibitor 1 (Azin1) and JNK, thereby activating the TGFβ pathway and the mitogen-activated protein kinase 1 (MAPK1), leading to altered cardiac function and fibrosis in an animal experimental model of MI (Tao et al., 2016).

Though multiple miRNAs were shown to aggravate CVD, a few of them also impart their protective function by improving the cardiac function post-MI. Overexpression of miR-133 during MI targets zinc finger transcription factor Snail1, resulting in improvement of cardiac function, decrease of inflammatory response and reduction of infarct size (Chen et al., 2017). Elevated levels of miR-133 by β-blocker carvedilol in cardiomyocytes improve cardiac function and decrease apoptosis upon induction of oxidative stress (Julien & Wells, 2017). Upregulation of miR-133 by anthraquinone aloe-emodin (AE) in mice prevents MI upon treatment with hydrogen peroxide (Yu et al., 2019).

1.13.2.4 miRNAs and Cardiac Fibrosis

Cardiac fibrosis is a cardiac remodelling phenomenon resulting from the accumulation of collagen and other ECM proteins caused by cardiac diseases like cardiomyopathy, MI, and heart failure. It is often associated with the upregulation of multiple miRNAs.

miR-29 induces cardiac fibrosis by regulating the Extracellular signal-regulated kinase 1/2 (ERK)-mitogen-activated protein kinase (MAPK) signaling during I/R and heart failure (van Rooij et al., 2008). miR-155 contributes to cardiac fibrosis when stress is induced by Ang II (Wei et al., 2017). miR-223 induces cardiac fibrosis post-MI by targeting RAS p21 protein activator 1 (RASA1) (Liu et al., 2018). miR-410-5p is another miRNA that upregulates cardiac remodelling upon administration of a high-fat diet (Zou et al., 2018). Aberrant overexpression of miR-433 promotes cardiac fibrosis by targeting Azin1 and JNK, leading to the activation of TGFβ1 and ERK pathways, respectively (Tao et al., 2016). miR-34 family (34a/b/c) induces cardiac fibrosis, as attenuation of miR-34 family members results in restoration and improvement of cardiac function (Bernardo et al., 2012). miR-328 is a potent fibrotic inducer, and it activates TGFβ1 signaling by targeting TGFβRIII (Du et al., 2016). miR-4454 elevates ventricular fibrosis during hypertrophic cardiomyopathy and is a novel biomarker candidate (Thottakara et al., 2021).

Other miRNAs were shown to attenuate cardiac fibrosis. miR-9 reduces collagen accumulation in fibroblasts by targeting TGFBR2 during high-glucose administration. miR-1

attenuates fibroblast proliferation by targeting Cyclin D2 and CDK6 (Valkov et al., 2019). miR-24 is another miRNA that reduces cardiac fibrosis by regulating the Furin-TGFβ signaling pathway (Wang et al., 2012). Decreased levels of miR-744 in plasma indicates cardiac fibrosis and heart failure (Wang et al., 2018). There are other miRNAs like miR-133, 145, and 18, that also reduces cardiac fibrosis (Chen et al., 2014; Geng & Guan, 2017; Huang & Wang, 2014; Liu et al., 2023).

1.13.2.5 miRNAs and Cardiomyopathy

Cardiomyopathy is a disorder that impacts the heart muscle, known as the myocardium. Several miRNAs are involved in the pathogenesis of cardiomyopathy.

HCM is characterized by dilation of the left ventricle (Marian & Braunwald, 2017). MiR-27a, miR-29a, and miR-199a-5p are elevated in patients with HCM as compared to controls, and they correlate with cardiac hypertrophy (Roncarati et al., 2014). miR-29a is also elevated in HCM patients with fibrosis. In another study, 14 miRNAs (miR-18a-5p, 146a-5p, 30d-5p, 17-5p, 200a-3p, 19b-3p, 21-5p, 193-5p, 10b-5p, 15a-5p, 192-5p, 296-5p, 29a-3p, and 133a-3p) were upregulated in HCM patients with diffused myocardial fibrosis (Fang et al., 2015). ACM is a rare inherited cardiomyopathy characterized by the replacement of myocardium with fibrous and fatty tissue (Saguner, 2014; Sen-Chowdhry et al., 2008). Elevated plasma concentrations of miR-320a are associated with an increased occurrence of ACM (Sommariva et al., 2017). ACM patients also display higher serum levels of circulating miR-144-3p, 145-5p, 185-5p, and 494 (Yamada et al., 2018). miR-130a induces ACM by targeting desmocollin-2 (DSC2) (Mazurek et al., 2017). Another miRNA, miR-29b-3p, is involved in the pathogenesis of ACM in cardiac stromal cells (Rainer et al., 2018). Other miRNAs that contribute to the progression of ACM in humans are miR-122-5p, miR-182-5p, and miR-183-5p (Bueno Marinas et al., 2020). DCM involves hypertrophy of the left ventricular walls, enlargement of cardiac chambers, and diminished systolic function (Japp et al., 2016). miR-423-5p is upregulated in heart failure patients with DCM (Fan et al., 2013). MiR-3135b, 3908, and 5571-5p are also elevated and reported as novel biomarkers for DCM (Wang et al., 2017). A study reported elevated levels of miR-24-3p, 100-5p, 28-5p, 103-3p, 214-3p, let-7b-5p, 125b-5p and let-7c-5p in patients with both ischemic and idiopathic DCM (Onrat et al., 2018). In the diabetic DCM group, the levels of miR-34b, 34c, 199b, and 210 are elevated (Greco et al., 2012). miR-208b is another miRNA upregulated in DCM patients with severe heart failure, and inhibition of miR-208b results in improvement of cardiac function (Q. Zhou et al., 2017).

1.13.2.6 miRNA and Heart Failure

Heart failure is a condition that arises when the heart cannot supply sufficient blood to meet the body's requirements, caused by either the rigidity or weakness of the heart muscles.

Several miRNAs play a role in the development of heart failure. During heart failure, miR-100 shows increased levels, and blocking it can stop the reduction of adult gene expression associated with the fetal gene program mediated by β-adrenoceptors (β-AR) (Sucharov et al., 2008). An increase in miR-133b suppresses β-AR, which consequently raises the likelihood of developing heart failure (Sucharov et al., 2008). Ablation of miR-208 during thyroid signaling and hemodynamic overload also reduces cardiac hypertrophy (van Rooij et al., 2007). miR-199b is another miRNA that targets Dyrk1a, resulting in increased NFAT signaling, which in turn increases hypertrophy and fibrosis in an animal model of heart failure (da Costa Martins et al., 2010). In another study, miRNA-423-5p acts as a putative biomarker in patients suffering from heart failure (Tijsen et al., 2010).

1.13.3 miRNAs: biomarkers and therapeutics for CVDs

The presence of aberrant levels of miRNAs in cardiac tissues as well as biological fluids like serum and plasma makes them efficient targets for the development of biomarkers. In biological fluids, miRNAs possess great stability as they reside in P-bodies, exosomes, cytoplasmic granules and multivesicular bodies, making them secure from any RNase-mediated degradation (O'Brien et al., 2018). CVD is the leading cause of death worldwide, with 17.9 million deaths every year. Therefore, identification of CVD during its early stages can save millions of lives, and that warrants the development of early biomarkers. Early detection of CVD will ensure early therapeutic intervention that will help in ameliorating the severity and curing the disease.

miRNA therapeutics involve using antisense inhibitor oligonucleotides (AMO) that have complete sequence complementarity to the target miRNA (Lima et al., 2018). Antagomirs are another class of therapeutics that can efficiently degrade target miRNA by disrupting the binding between miRNA and its target mRNA (Stenvang et al., 2012). These therapeutics are generally modified using viral vectors like Adeno-associated virus (AAV), lipoplexes, neutral liposome, Poly(lactide-co-glycolide) (PGLA), polyethyleneimine (PEI), EnGeneIC Delivery Vehicle nanocells, N-acetyl-D-galactosamine (GalNAc) and locked-nucleic-acid-modified oligonucleotides for cellular internalization and precise delivery to designated receptors or tissues (Cai et al., 2017; Dai & Zhang, 2019; Nicoletti et al., 2022; Obernosterer et al., 2007;

Pagoni et al., 2023; Wang et al., 2018; Yamamoto et al., 2021). miRNA sponges and miRNA erasers can also be effectively used to attenuate a specific or a group of miRNAs (Ebert & Sharp, 2010). miRNA sponges are constructed as multiple tandem repeats of the target miRNA binding site and are generally expressed under a strong promoter inside the cells. In contrast to miRNA sponges, miRNA erasers contain two antisense binding sites specific to the target miRNA and are introduced into cells using recombinant adenovirus vectors.

1.13.4 Role of miR-101-3p during different diseases

This field is relatively promising and holds great opportunities for developing biomarkers and therapeutic interventions. In our study, we found upregulation of miR-101-3p during prolonged cardiomyopathy (ER stress/ Diabetes). miR-101-3p has been studied extensively in cancer growth and progression. It acts as a tumor suppressor and inhibits cancer cell progression and metastasis by targeting Ubiquitin-specific protease 47 (USP47) induced deubiquitination of ribosomal protein L11 (RPL11) and EZH2, which is the catalytic subunit of the polycomb repressive complex 2 (PRC2) (Park et al., 2022). It was shown to inhibit invasion and metastasis in different types of cancer like hepatocellular carcinoma, lung cancer, oral cancer, breast cancer, and cervical squamous cell carcinoma (Lammerhirt et al., 2024; Talvan et al., 2024; Wang et al., 2021; Zhang et al., 2017; Zhu et al., 2025). However, the role of miR-101-3p in CVDs is relatively unexplored. In one study, it was shown that inhibition of miR-101-3p protects against myocardial injury inflicted due to sepsis (Xin et al., 2021). Suppressing miR-101-3p has also been found to reduce calcification of interstitial cells in the human aortic valve (Chen et al., 2023). Except for these few studies, the role of miR-101-3p in regulating the expression of cardiogenic genes during CVDs is relatively unexplored. We showed that miR-101-3p targets important cardiogenic genes Tbx20 and Bmp2 during prolonged stresses to induce senescence and inflammation, resulting in the aggravation of cardiomyopathy.

Our findings not only shed light on this unexplored function of miR-101-3p but also provide overwhelming evidence for establishing miR-101-3p as a putative biomarker for the detection of cardiomyopathy.

1.14 Senescence: Its role in inducing cardiac diseases

Cellular senescence is a stable state of cell cycle arrest where the cells continue constant metabolic activities. Senescence can arise from different endogenous factors and exogenous stresses. Cellular senescence that occurs naturally with age, also known as replicative

senescence, was first observed by Hayflick and Moorhead. They found that human diploid fibroblasts have a limited capacity for division due to the shortening of telomeres (Hayflick & Moorhead, 1961). However, when senescence occurs due to stress or injury, it is termed as premature senescence, and it can be telomere length independent (Luan et al., 2024). Different stresses, such as DNA damage response, oxidative stress, ER stress, hypoxia, activation of oncogenes and mitochondrial dysfunction within the cardiovascular system, can cause senescence (Evangelou et al., 2023; Pluquet et al., 2015). Senescent cells are characterized by a flattened, enlarged shape and a reduction in nuclear lamin B1 expression (Figure 16). Other characteristics of senescent cells are telomere attrition and DNA damage response. Senescent cells are also marked by a permanent arrest of the cell cycle. Increasing evidence indicates cardiovascular cell senescence, including endothelial cells, vascular smooth muscle cells, fibroblasts, cardiomyocytes, and T cells, which accumulate in lesions and play roles that can both promote and hinder the progression and outcomes of CVDs.

Cellular stresses often result in DNA damage, which upregulates the cascade involving different kinases like Ataxia-Telangiectasia Mutated (ATM), Ataxia-Telangiectasia and Rad3-related (ATR), and downstream kinases Checkpoint Kinase 1 (CHK1) and Checkpoint Kinase 2 (CHK2). CHK1/CHK2, in turn, activate the tumor suppressor gene p53. Studies have shown the involvement of p53 in exacerbating senescence response, resulting in CVDs. p53 can further accentuate the senescence response by upregulating the expression of cyclin-dependent kinase inhibitor $p21^{WAF1/CIP1}$ (encoded by the *cdkn1α* gene). $p21^{WAF1/CIP1}$, in turn results in cell cycle arrest at G1 phase by inhibiting the expression of CDK2 (Stein et al., 1999). Another cyclin-dependent kinase inhibitor that plays an essential role in inducing cellular senescence is $p16^{INK4A}$ (encoded by the *cdkn2α* gene). p16 acts as an inhibitor of the retinoblastoma (pRb)/E2F signaling pathway. Under normal conditions with low $p16^{INK4A}$ expression, CDK4 and CDK6 hyperphosphorylate pRb, leading to the release of E2F, which in turn promotes the transcription of cell cycle genes and drives the transition from G1 to S phase. However, during senescence, increased levels of $p16^{INK4A}$ inhibit CDK4 and CDK6, which causes pRb to remain in a hypophosphorylated state, and it remains bound to E2F. The absence of E2F leads to arrest in the transition from G1 to S phase in senescent cells (Stein et al., 1999) (Figure 16). Senescent cells are also characterized by the presence of senescence-associated heterochromatin foci (SAHF) (Figure 16). SAHF are distinct areas of facultative heterochromatin that contribute to the silencing of genes that encourage proliferation (such as E2F target genes) in senescent cells. Senescent cells secrete the senescence-associated secretory phenotype (SASP), a

collection of cytokines and chemokines. The SASP activates the inflammatory response, thereby destroying their own cells (autocrine signaling) and neighbouring healthy cells (paracrine signaling) (Figure 16).

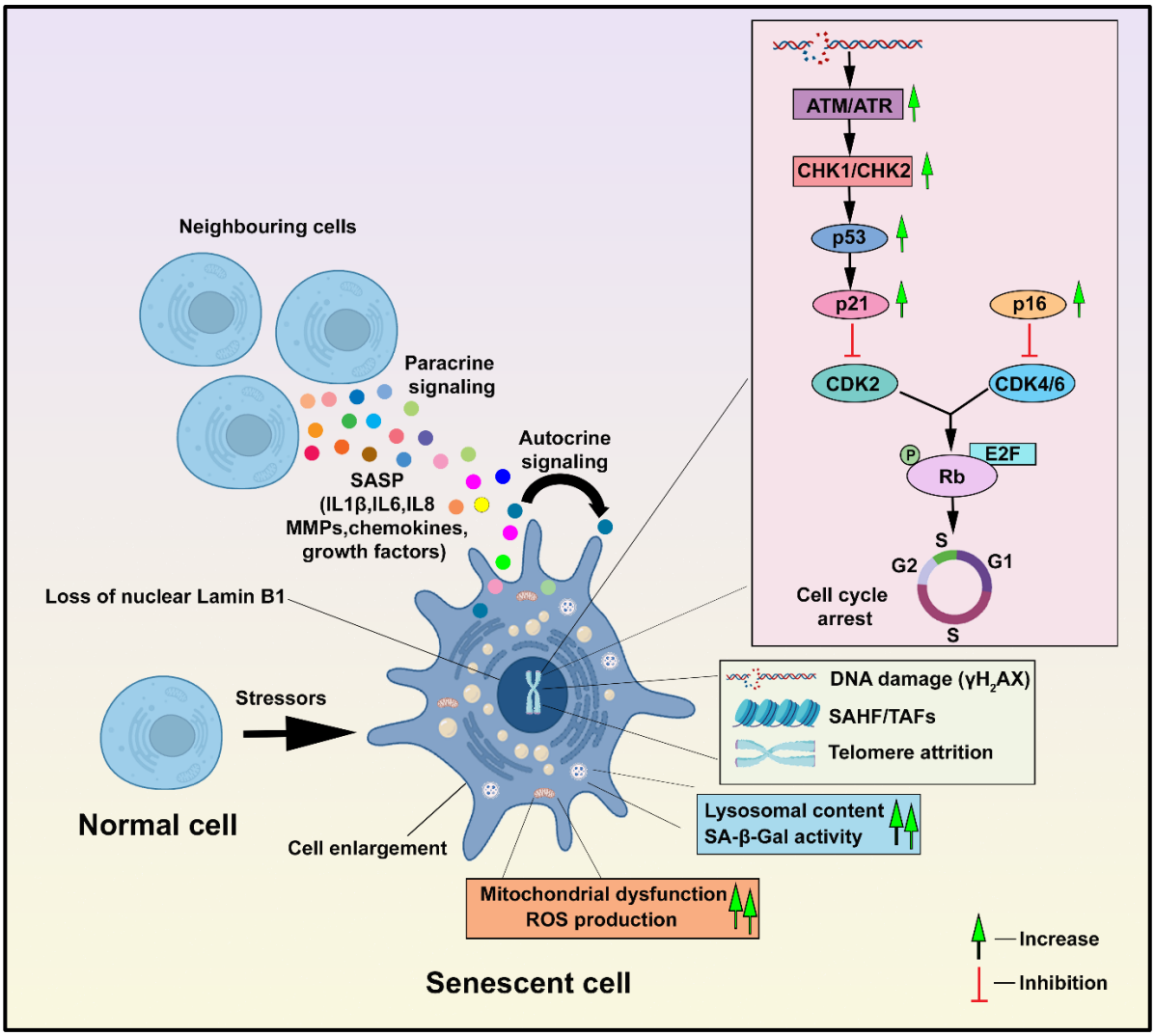

Figure 16. Characteristics of senescent cells. In the presence of different stressors, the normal cells are transformed into senescent cells. The senescent cells are enlarged, lack nuclear lamin B1, display mitochondrial dysfunction and increased reactive oxygen species (ROS) generation, and display increased lysosomal content with elevation of SA-β-Gal activity. The senescent cells also show telomere attrition, increased DNA damage and presence of senescence-associated heterochromatin foci (SAHF). They also show cell cycle arrest due to the elevation of p53 and p16-mediated DNA damage response. Senescent cells release factors collectively known as the senescence-associated secretory phenotype (SASP). SASP further accentuates the detrimental inflammatory response in the senescent cells via autocrine signaling or in the neighbouring healthy cells via paracrine signaling.

Though senescence is beneficial during early development as it aids in organogenesis, embryonic development, angiogenesis and regeneration, however, senescence has been shown to play an important role in the pathogenesis of CVDs. Senescence can result in cardiac hypertrophy, ER stress, mitochondrial dysfunction, and subsequent ROS generation, leading

to cardiomyocyte senescence. Senescent cardiomyocytes produce SASPs like TGFβ2, endothelin 3 (Edn3) and Growth/differentiation factor-15 (GDF-15) that cause pathological cardiomyocyte hypertrophy, cardiac fibrosis and endothelial dysfunction (Hu et al., 2022). Increased SASP-mediated inflammatory response often results in adverse cardiac remodelling, thereby leading to MI. In adults, senescence response impairs the proliferation of cardiomyocytes post-injury, thus exacerbating the progression of cardiomyopathy. IGF-1 signaling has also been shown to increase senescence response in cardiomyocytes. In cardiac fibroblasts, increased expression of SASPs like IL-6, TNFα, IL-1β , as well as different MMPs, has been shown to induce fibrosis (Hu et al., 2022). In addition, the Renin angiotensin aldosterone system (RAAS) activation has been implicated in upregulation of senescence response resulting in heart failure. Senescence markers were also shown to be elevated in patients with atrial fibrillation and atherosclerosis. Therefore, senescence plays a crucial role in the development of CVDs. Their elimination is a prerequisite for restoring homeostasis and re-entering cardiomyocytes towards proliferation post-injury.

1.15 Working model for the study

Based on all the background studies and literature reviews, we have worked on the following study design to establish our hypothesis and objectives.

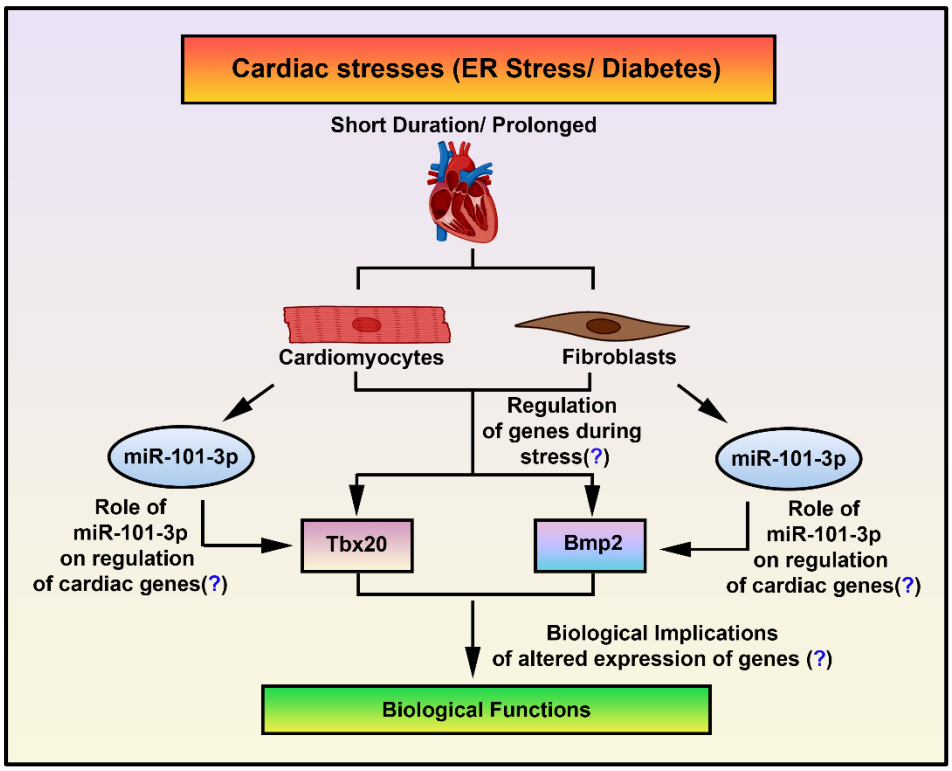

Figure 17. Working model for the study. Schematic illustration of the working model for the study.

Chapter 2

Hypothesis & Objectives

2.1 Hypothesis:

The cross-talk between cardiac developmental factors T-box transcription factor 20 (Tbx20), Bone morphogenetic protein 2 (Bmp2), and miR-101-3p regulates cardiac homeostasis in the rodent cardiomyopathy model.

2.2 Objectives:

The subsequent objectives were addressed to substantiate our hypothesis.

Objective 1: To understand whether ER stress-induced upregulation of Tbx20 activity is beneficial and necessary for cardiomyocyte viability and maintenance of cardiomyocyte homeostasis by regulating proliferation and apoptosis *in vivo* and *in vitro*.

Objective 2: To determine the expression of Tbx20 and Bmp2 during different models of cardiomyopathy (ER stress, Diabetes, Type 2 Myocardial Infarction and High-Fat Diet).

Objective 3: To investigate the role of miR-101-3p in regulating the expression of Tbx20 and Bmp2 during ER stress/diabetes *in vivo* and *in vitro*.

Objective 4: To examine the role of Tbx20 in attenuating senescence response in cardiomyocytes and Bmp2 in augmenting inflammatory response in cardiac fibroblasts during ER stress/diabetes *in vivo* and *in vitro*.

Chapter 3

Materials & Methods

3.1 Animal treatments and tissue collection

3.1.1 Induction of Endoplasmic Reticulum (ER) stress *in vivo*

For ER stress induction, male Swiss albino mice and male Wistar rats were administered with an intraperitoneal injection of Tunicamycin (catalog no: T7765; Sigma–Aldrich) at a final concentration of 1 mg/kg body weight diluted in 150 nM dextrose (Crider et al., 2018; Cybulsky et al., 2002). The control animals were given an intraperitoneal injection of equal volumes of 150 nM dextrose supplemented with 1% dimethyl sulfoxide. The heart tissue was collected after 8 hours (short-term) and 2 days (prolonged) by euthanization with carbon dioxide, followed by cervical dislocation. All the animals were housed as per the guidelines of the Control and Supervision of Experiments on Laboratory Animals (CPCSEA) with 12 hours of light/dark cycles in controlled temperature and humidity conditions. The animals were fed normal chow and water *ad libitum*. The Institutional Animal Ethics Committee (IAEC) of Jadavpur University approved all animal studies (Ref no.: AEC/PHARM/1701/05/2017 dated November 12, 2020).

3.1.2 Induction of Diabetes *in vivo*

For Diabetes induction, male Swiss albino mice were administered an intraperitoneal injection of Alloxan monohydrate (catalog no: 2244-11-3; LOBA Chemie) at a final concentration of 150 mg/kg body weight diluted in 0.9% saline (Du et al., 2016). The control animals were given an intraperitoneal injection of an equivalent volume of 0.9% saline. The mice with blood glucose levels > 200 mg/dl were maintained for 1 month (short-term) and 4 months (prolonged), and the heart tissue was collected for experimental purposes by euthanization with carbon dioxide, followed by cervical dislocation (Li et al., 2019; Mondal et al., 2022). All the animals were housed as per the guidelines of the Control and Supervision of Experiments on Laboratory Animals (CPCSEA) with 12 hours of light/dark cycles in controlled temperature and humidity conditions. The animals were fed normal chow and water *ad libitum*. The experimental procedures were approved by the Institutional Ethical Committee, Presidency University (Registration PU/IAEC/SC/39), registered under “Committee for the purpose of CPCSEA, Ministry of Environment and Forests, Govt. of India”.

3.1.3 Induction of Type 2 Myocardial Infarction (T2MI) *in vivo*

For T2MI induction, male Swiss albino mice were administered an intraperitoneal injection of Isoproterenol hydrochloride (catalog no: I6504; Sigma-Aldrich) at a final concentration of 160 mg/kg body weight dissolved in Phosphate buffered saline (PBS) (Forte

et al., 2021). The control mice were administered with an equivalent volume of PBS. The heart tissues were collected at 2 days (short-term) and 14 days (prolonged) by euthanization with carbon dioxide, followed by cervical dislocation. All the animals were housed as per the guidelines of the Control and Supervision of Experiments on Laboratory Animals (CPCSEA) with 12 hours of light/dark cycles in controlled temperature and humidity conditions. The animals were fed normal chow and water *ad libitum*.

3.1.4 Induction of High-Fat induced obesity *in vivo*

For High-Fat diet administration, male Swiss albino mice were fed with a High-Fat diet (60% fat by calories) (Speakman, 2019). The control mice group was fed with normal chow (10% fat by calories). The heart tissues were collected after 1 month (short-term) and 3 months (prolonged) by euthanization with carbon dioxide, followed by cervical dislocation (Lepczynski et al., 2021). All the animals were housed as per the guidelines of the Control and Supervision of Experiments on Laboratory Animals (CPCSEA) with 12 hours of light/dark cycles in controlled temperature and humidity conditions. The animals were fed normal chow and water *ad libitum*.

3.2 Electrocardiograph (ECG) recording in anaesthetized rats

Male Wistar rats were treated with 1 mg/kg body weight of Tun, and the heart tissue was harvested after 8 hours and 2 days. The cardiac function after Tun treatment was assessed by ECG recording. Before harvesting, the rats were anaesthetized using 60 mg/kg body weight ketamine and 10 mg/kg body weight xylazine as mentioned previously (Hatzopoulos et al., 2002). ECG was recorded for 10 mins using standard lead II (metal ECG leads). The ECG signals were then analyzed by BIOPAC MP36. The QT and the RR intervals were measured. The QT interval was measured from the beginning of the QRS signal to the completion of the T wave. The RR interval was measured as the time elapsed between two successive R waves of the QRS signal.

3.3 Determination of Heart weight/Body weight (HW/BW) ratio

After treating the rodents with 1 mg/kg body weight Tun, the heart tissue was harvested from them after 8 hours and 2 days by euthanization with carbon dioxide, followed by cervical dislocation. The weights of the harvested whole hearts were measured. Prior to euthanization, the BW of the rodents were measured. The HW normalised to BW was measured in milligrams/gram units.

3.4 Determination of cardiomyocyte cell size by Wheat Germ Agglutinin (WGA) staining

Wheat Germ Agglutinin (WGA) is a lectin that binds to the glycoprotein of the cell membrane (Yoshida et al., 1984). The effect of Tun treatment on the induction of cardiac hypertrophy was determined by WGA staining.

After treating the male Swiss-Albino mice with 1 mg/kg body weight of Tun, the heart tissue was harvested from them after 8 hours and 2 days. The heart tissue was fixed with 4% paraformaldehyde (PFA), dehydrated and embedded in paraffin. Then, 5 µm tissue sections were cut using a microtome and embedded on glass slides. For WGA staining, the glass slide containing the tissue section was placed on a 60 ^{o}C hot plate to melt the paraffin, and thereafter the slides were kept in xylene for 7 mins. After paraffin melting, sections were rehydrated in graded ethanol (100%, 90%, 70%, 50% and lastly distilled water). Following rehydration, the sections were subjected to antigen retrieval with citrate buffer (10mM citric acid, 0.05% Tween-20, pH 6.0) in a microwave oven for 10 mins. The tissue sections were then stained with FITC-labelled WGA (catalog no: L4895; Sigma–Aldrich) and incubated for 1 hour at room temperature. After incubation, the sections were washed with 1X PBS for 5 mins. The step was repeated 3 times. The nucleus was counterstained with nuclear stain 4', 6-diamidino-2-phenylindole (DAPI, catalog no: D9542; Sigma–Aldrich) and incubated at room temperature for 10 mins. The sections were washed with 1X PBS for 3 times and mounted with mounting media. The images were taken by Leica DM2000 across multiple fields. Cell size was quantified using ImageJ (National Institutes of Health) software.

3.5 Determination of fibrosis by Masson's Trichrome Staining

Masson's Trichrome staining is a tricolour staining method that is used to determine collagen fibre deposition in tissues. In this staining procedure, the collagen fibres are stained blue, the cytoplasm and muscle fibres are stained pink or red, whereas the nucleus is stained black (Ryota, 2023). The effect of Tun treatment on the induction of cardiac fibrosis was determined by Masson's Trichrome staining. Increased cardiac fibrosis is proportional to the amount of collagen fibres deposited in the tissue.

After treating the male Swiss-Albino mice with 1mg/kg body weight of Tun, the heart tissue was harvested from them after 8 hours and 2 days. The heart tissue was fixed with 4% PFA, dehydrated and embedded in paraffin. Then, 5 µm tissue sections were cut using a microtome and embedded on glass slides. For Masson's Trichrome staining, the glass slide containing the tissue section was placed on a 60 ^{o}C hot plate to melt the paraffin, and thereafter

the slides were placed in xylene for 7 mins. After paraffin melting, the sections were rehydrated in graded ethanol (100%, 90%, 70%, 50% and lastly distilled water). Following rehydration, the slides were placed in Bouin's solution (mordant) and boiled in a microwave oven for 10 mins. After cooling, the tissue sections were stained with Weigert's haematoxylin (staining the nucleus) for 10 mins. The sections were then placed in Biebrich Scarlet solution (stains the cytoplasm and muscle tissue) for 3 mins and thereafter rinsed with distilled water. Following washing, phosphotungstic acid was added to the tissue sections for 10 mins, and the sections were incubated overnight in Aniline blue solution (stains collagen fibres). The sections were rinsed with distilled water to wash off excess stains. The tissue section was then dehydrated with ethanol upgradation (50%, 70%, 90%, 100% and lastly xylene). The slides were dried and mounted with mounting media. The images were taken by Leica DM2000 across multiple fields. The collagen deposition was quantified using ImageJ (National Institutes of Health) software.

3.6 Cell culture

3.6.1 H9c2 culture

H9c2 cells were purchased from the National Centre for Cell Science (NCCS), Pune. The cells were maintained in Dulbecco's Modified Eagle's Media (DMEM) (catalog no: 12100046; Gibco) in the presence of 10% Fetal Bovine Serum (FBS) (catalog no: RM1112; Himedia), 100 units/ml penicillin G sodium, and 100 µg/ml streptomycin sulfate (catalog no: 15140122; Gibco) in a humidified CO_2 incubator at 37^{o}C in presence of 5% CO_2 (Das et al., 2023). Upon reaching 60-70% confluency, the cells were treated for different experimental procedures.

3.6.2 Cardiac fibroblasts culture

Cardiac fibroblasts were cultured as described previously (Almazloum & Khalil, 2023). Briefly, after the isolation of hearts from adult male Wistar rats, they were rinsed with ice-cold 1X PBS. After rinsing, the hearts were perfused with ice-cold perfusion buffer. Following perfusion, the hearts were minced thoroughly with sterilized microscissors. The minced heart tissue was then digested with Type II collagenase (80 units/ml DMEM; catalog no: C6885, Sigma-Aldrich). It was incubated for 30 mins at 37 ^{o}C with gentle shaking. Complete digestion of the heart tissue was ensured by manually triturating 10-15 times with a serological pipette. After allowing the tissue to settle down, the supernatant was strained through a 40 µm cell strainer into a Falcon tube. This was repeated for 2 more times. The strained supernatant was then centrifuged at 3000 rpm for 5 mins at 4 ^{o}C. The supernatant was discarded, and the pellet

was resuspended in DMEM in the presence of 20% FBS, 100 units/ml penicillin G sodium, and 100 µg/ml streptomycin sulfate and maintained in a humidified CO_2 incubator at 37 ºC in the presence of 5% CO_2. Upon reaching 60-70% confluency, the cells were treated for different experimental procedures (Figure 1).

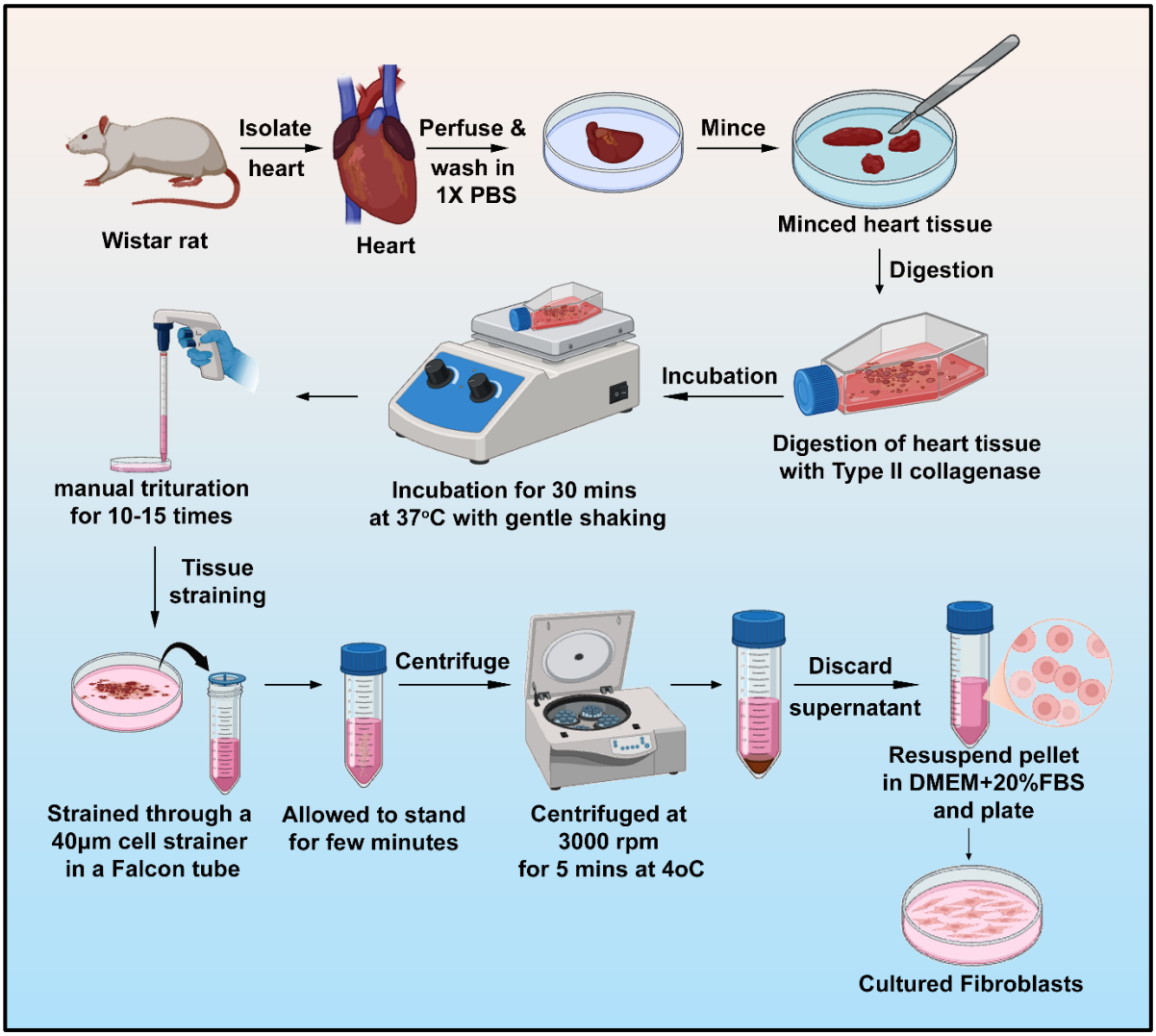

Figure 1. Isolation of cardiac fibroblasts from Wistar rats. Schematic illustration of cardiac fibroblast isolation from Wistar rats.

3.7 Cell treatments and RNA interference

3.7.1 Induction of ER stress

3.7.1.1 Tunicamycin (Tun)

For ER stress induction *in vitro* by Tun, H9c2 cardiomyocytes or cardiac fibroblasts were serum-starved for 6 hours after reaching 60-70% confluency. Following starvation, the cells were treated with different concentrations (2, 5, 10, 20, 50, and 100 µg/ml) of Tun to induce

ER stress (Abdullahi et al., 2017; Das et al., 2023; Guha et al., 2017). The cells were incubated for 24 hours and harvested for different experimental procedures.

3.7.1.2 Thapsigargin (Tg)

For ER stress induction *in vitro* by Tg, H9c2 cardiomyocytes were serum-starved for 6 hours after reaching 60-70% confluency. Following starvation, H9c2 cardiomyocytes were treated with different concentrations (1.5, 2, 6, and 10 μM) of Tg (catalog no: T9033; Sigma–Aldrich) to induce ER stress (Z. Li et al., 2020). The cells were incubated for 24 hours and harvested for different experimental procedures.

3.7.1.3 Dithiothreitol (DTT)

For ER stress induction *in vitro* by DTT, H9c2 cardiomyocytes were serum-starved for 6 hours after reaching 60-70% confluency. Following starvation, H9c2 cardiomyocytes were treated with different concentrations (1, 3, 5, and 10 mM) of DTT (catalog no: D9779; Sigma–Aldrich) to induce ER stress (X.-Y. Xiang et al., 2016). The cells were incubated for 24 hours and harvested for different experimental procedures.

3.7.2 Induction of Hyperglycemia

For hyperglycemia induction *in vitro*, H9c2 cardiomyocytes or cardiac fibroblasts were starved overnight in serum-free and glucose-free media after reaching 60-70% confluency. Following starvation, cells were treated with 5 mM glucose and 25 mM glucose-containing media, serving as control and hyperglycemia conditions, respectively (Das et al., 2023). The culture media was changed every alternate day with the respective media. The cells were harvested at 2 days and 5 days for different experimental procedures.

3.7.3 ER stress induction followed by treatment with Recombinant Bmp2 protein

H9c2 cardiomyocytes or cardiac fibroblasts were serum-starved for 6 hours after reaching 60-70% confluency. Following starvation, cells were treated with 50 μg/ml Tun for 24 hours. After Tun treatment, the cells were treated with 200 ng/ml Recombinant Bmp2 protein (RecBmp2; catalog no: 355-BM; R&D Systems) for another 24 hours (Chakraborty et al., 2013). The control cells were treated with 0.1% Bovine Serum Albumin (BSA) in 1X PBS. After incubation, the cells were harvested for different experimental procedures.

3.7.4 Treatment of Recombinant Noggin protein followed by ER stress induction

H9c2 cardiomyocytes were serum-starved for 6 hours after reaching 60-70% confluency.

Following starvation, the cells were treated with 200 ng/ml Noggin protein (Nog; catalog no: 719-NG; R&D Systems) for 24 hours (Chakraborty et al., 2013). The control cells were treated with 1X PBS. After Nog treatment, cells were treated with 10 µg/ml Tun for another 24 hours. After incubation, the cells were harvested for different experimental procedures.

3.7.5 4-(2-Aminoethyl)benzene sulfonyl fluoride hydrochloride (AEBSF) treatment followed by ER stress induction

H9c2 cardiomyocytes were serum-starved for 6 hours after reaching 60-70% confluency. Following starvation, the cells were treated with 300 µM of water-soluble serine protease inhibitor (AEBSF) (catalog no: A8456; Sigma–Aldrich) for 6 hours (T. Okada et al., 2003). After AEBSF treatment, cells were treated with 20 µg/ml Tun for 24 hours. After incubation, the cells were harvested for different experimental procedures.

3.7.6 siRNA mediated knockdown of Tbx20 followed by ER stress induction

For siRNA-mediated knockdown of Tbx20, H9c2 cardiomyocytes were serum-starved overnight after reaching 60-70% confluency. Following starvation, cells were treated with 100 nM Tbx20 siRNA (titrated for maximal downregulation) (Assay ID: s164031; Ambion) targeting the coding region of Tbx20 using Lipofectamine RNAiMAX (catalog no: 13778-075; Invitrogen) reagent according to the manufacturer's instructions. The concentration was chosen after titrating for maximum downregulation of Tbx20. The cells were maintained in the transfection mix for 6 hours at 37 ºC in a 5% CO_2 humidified incubator. After 6 hours, the media was replenished with DMEM containing 10% FBS and incubated for 24 hours. After 24 hours of siRNA transfection, the cells were treated with 20 µg/ml Tun and incubated for an additional 24 hours (Das et al., 2023). After incubation, the cells were harvested for different experimental procedures.

3.7.7 miR-101-3p treatment

3.7.7.1 Overexpression of miR-101-3p followed by ER stress induction

For overexpression of miR-101-3p, H9c2 cardiomyocytes or cardiac fibroblasts were serum-starved overnight after reaching 60-70% confluency. Following starvation, cells were treated with 100 nM miR-101-3p mimic (Assay ID: MC11414; Ambion) using Lipofectamine RNAiMAX reagent according to the manufacturer's instructions. The concentration was chosen after titrating for maximum upregulation of miR-101-3p. The cells were maintained in the transfection mix for 6 hours at 37 ºC in a 5% CO_2 humidified incubator. After 6 hours, the media was replenished with DMEM containing 10% FBS and incubated for 24 hours. After 24

hours of transfection, the cells were treated with 20 µg/ml Tun and incubated for an additional 24 hours and harvested for different experimental procedures.

3.7.7.2 Inhibition of miR-101-3p followed by ER stress induction

For inhibition of miR-101-3p, H9c2 cardiomyocytes or cardiac fibroblasts were serum-starved overnight after reaching 60-70% confluency. Following starvation, cells were treated with 200 nM miR-101-3p mimic (Assay ID: MH11414; Ambion) using Lipofectamine RNAiMAX reagent according to the manufacturer's instructions. The concentration was chosen after titrating for maximum downregulation of miR-101-3p. The cells were maintained in the transfection mix for 6 hours at 37 ^{o}C in a 5% CO_2 humidified incubator. After 6 hours, the media was replenished with DMEM containing 10% FBS and incubated for 24 hours. After 24 hours of transfection, the cells were treated with 50 µg/ml Tun and incubated for an additional 24 hours. After incubation, the cells were harvested for different experimental procedures.

3.8 3-[4,5-Dimethylthiazol-2-yl]-2,5 diphenyl tetrazolium bromide cell viability assay

The cell viability upon treatment of Tun was measured using 3-[4,5-Dimethylthiazol-2-yl]-2,5 diphenyl tetrazolium bromide (MTT) cell viability assay. For this assay, the H9c2 cells were seeded in a 96-well plate before treatment with Tun. The cells were treated with increasing concentrations of Tun (2, 5, 10, 20, and 50 µg/ml) for 24 hours. A 5 mg/ml MTT (catalog no: MB186; Himedia) stock solution was prepared, which was further diluted in a ratio of 1:10 in 1X PBS. About 40 µl of diluted MTT reagent was added to each well containing the cells and incubated for 3 hours at 37 ^{o}C in a 5% CO_2 humidified incubator. After 3 hours of incubation, the MTT reagent was discarded, and the cells were extracted in an extraction buffer. The absorbance was measured at 570 nm.

3.9 Reactive Oxygen Species (ROS) estimation

Tunicamycin treatment results in ROS generation. To measure the amount of intracellular ROS generated due to increasing concentration of Tun, the H9c2 cells were treated with different concentrations of Tun (2, 5, 10, 20, and 50 µg/ml) and incubated for 24 hours. 24 hours post incubation, the cells were washed with an ice-cold Hank's balanced salt solution. After washing, the cells were treated with 100 µM 2',7'-dichlorofluorescin diacetate (catalog no: D6883; Sigma–Aldrich), which upon reaction with intracellular ROS results in the formation of green fluorescent compound dichlorofluorescein and incubated for 30 mins at 37 ^{o}C in a 5% CO_2 humidified incubator. For positive control, the cells were treated with 1% H_2O_2

for 6 hours (Das et al., 2023). After incubation, the cells were lysed with an alkaline solution, and the fluorescence intensity was measured with excitation of 485 nm and emission at 520 nm (Hitachi).

3.10 Senescence Associated-β-galactosidase (SA-β-Gal) assay

Senescence Associated-β-galactosidase (SA-β-Gal) assay is used to detect the presence of senescent cells. In this assay, at pH 6.0, the lysosomal β-Galactosidase (β-Gal) enzyme cleaves the substrate 5-bromo-4-chloro-3-indoyl-β-d-galactopyranoside (X-gal). X-gal is a colourless substrate that possesses a galactose moiety linked to an indole. Upon hydrolysis by lysosomal β-Gal, the X-gal forms a blue-coloured insoluble product. This assay is distinct in senescent cells because non-senescent cells exhibit acidic β-Gal activity, which is detected at pH 4.0.

For the SA-β-Gal assay (catalog no: 9860, Cell Signaling Technology), cultured H9c2 cardiomyocytes and cardiac fibroblasts were seeded in a 35 mm dish for different treatment conditions. The growth media were discarded after cellular treatments, and the cells were rinsed with 1X PBS. After washing, 1X Fixative solution was added to the cells and they were allowed to fix for 15 mins at room temperature. After incubation, the cells were rinsed with 1X PBS for 2 times. Following rinsing, β-Galactosidase Staining solution was added to the cells and they were incubated at 37 ^{o}C overnight in a dry incubator. The cells were then visualized under a microscope for the development of blue colour.

3.11 RNA Isolation

3.11.1 From Heart Tissue

Total RNA was isolated from rodent heart tissue using TRIzol Reagent (catalog no: 15596026; Thermo Fisher Scientific) as per the manufacturer's protocol. For heart tissue samples, an appropriate amount of TRIzol reagent was used, and the tissue was homogenized using a handheld homogenizer. Following homogenization, the mixture was incubated for 5 mins to allow maximum lysis. After lysis, chloroform was added (for 1 ml TRIzol reagent, 0.2 ml chloroform was used) and the mixture was vortexed vigorously and incubated for 2 mins at room temperature. It was then centrifuged at 12000 g for 15 mins at 4 ^{o}C for phase separation. Following centrifugation, the upper aqueous phase was transferred to a fresh RNase-free microcentrifuge tube, and to it was added 0.5 ml ice-cold isopropanol and incubated at -20^{o}C overnight. The mixture was then centrifuged at 12000 g for 10 mins at 4 ^{o}C to precipitate the RNA. The precipitated RNA was then washed with 0.5 ml 75% ice-cold ethanol and

centrifuged at 7500 g for 5 mins at 4 ºC. The supernatant was discarded, and the pellet was dissolved in nuclease-free water based on the size of the pellet and stored at -80 ºC until further use. The RNA concentration was quantified using a Qubit4 Fluorometer (Thermo Fisher Scientific).

3.11.2 From Cells

Total RNA was isolated from H9c2 cardiomyocytes or cardiac fibroblasts using TRIzol Reagent as per the manufacturer's protocol. Following the addition of TRIzol reagent, the cells were scraped and pipetted several times to allow adequate cell lysis, and it was incubated for 5 mins at room temperature. After lysis, chloroform was added (for 1 ml TRIzol reagent, 0.2 ml chloroform was used) and the mixture was vortexed vigorously and incubated for 2 mins at room temperature. It was then centrifuged at 12000 g for 15 mins at 4 ºC for phase separation. Following centrifugation, the upper aqueous phase was transferred to a fresh RNase-free microcentrifuge tube, followed by the addition of 0.5 ml ice-cold isopropanol and incubation at -20 ºC overnight. The mixture was then centrifuged at 12000 g for 10 mins at 4 ºC to precipitate the RNA. The precipitated RNA was then washed with 0.5 ml 75% ice-cold ethanol and centrifuged at 7500 g for 5 mins at 4 ºC. The supernatant was discarded, and the pellet was dissolved in nuclease-free water based on the size of the pellet and stored at -80 ºC until further use. The RNA concentration was quantified using a Qubit4 Fluorometer (Thermo Fischer Scientific).

3.12 Reverse Transcription

The total RNA isolated from different treatment conditions were used to synthesize the complementary DNA (cDNA) using an iScript cDNA synthesis kit (catalog no: 170889; BioRad). For a 20 µl reaction volume, 1 µg of RNA template was used. A reaction mixture of RNA along with 4 µl 1X iScript Reaction Mix, 1 µl iScript Reverse Transcriptase and Nuclease-free water was run in a thermal cycler (catalog no: T100 Thermal Cycler; Biorad) using the protocol: Priming at 25 ºC for 5 mins, Reverse Transcription at 46 ºC for 20 mins, Reverse transcriptase inactivation at 95 ºC for 1 min. The synthesized cDNA was further used for polymerase chain reaction (PCR).

3.13 Polymerase Chain Reaction (PCR)

PCR was performed using either GoTaq Flexi DNA Polymerase (catalog no: M8291; Promega) for Chromatin Immunoprecipitation (ChIP) or high-fidelity LA Taq DNA Polymerase (catalog no: RR002A; Takara) for cloning. For the ChIP assay, PCR master mix

(1X) was prepared by setting up a 25 µl reaction mix containing 1X GoTaq Flexi Buffer, 4 mM $MgCl_2$, 0.2 mM each dNTP, 1 µM primer mix, 1.25 U GoTaq DNA Polymerase, 200 ng DNA isolated after ChIP and Nuclease-free water. The reaction mix was run in a thermal cycler according to the following conditions: initial denaturation at 95 ºC for 2 mins followed by 35 cycles of denaturation at 95 ºC for 1 min, annealing at 60 ºC for 1 min and extension at 72 ºC for 1 min. This was followed by a final extension at 72 ºC for 5 mins. The primers used for the ChIP assay are enlisted in Table 10. The PCR product was analyzed in a 2% agarose gel using a 100 bp DNA ladder (catalog no: MBT049; Himedia).

For cloning, PCR master mix (1X) was prepared by setting up a 50 µl reaction mix containing 1X LA PCR Buffer II, 2.5 mM $MgCl_2$, 2.5 mM each dNTP, 2 µM primer mix, 2.5 U Takara LA Taq DNA Polymerase, 500 ng genomic DNA or 1 ng plasmid DNA and Nuclease-free water. The reaction mix was run in a thermal cycler according to the following conditions: initial denaturation at 94 ºC for 1 min, followed by 30 cycles of denaturation at 98 ºC for 10 secs, annealing at 55 ºC-60 ºC (depending on the primers) for 5 mins. This was followed by a final extension at 72 ºC for 10 mins. The primers used for cloning are listed in Table 2, 3, 4, 5, 6, and 7. The PCR product was analyzed in a 2% agarose gel using a 100 bp DNA ladder or a 1 kb DNA ladder (catalog no: MBT051; Himedia).

3.14 Quantitative Real-Time Polymerase Chain Reaction (qRT-PCR)

qRT-PCR relies on fluorescence from SYBR Green (intercalating dye) for the generation of real-time data after PCR amplification. SYBR Green binds to double-stranded DNA in a non-specific manner, thereby emitting fluorescence. With the increase in amplification, the amount of double-stranded DNA increases, thereby allowing more SYBR Green dye to intercalate into it and fluoresce. Therefore, this technology allows the measurement of PCR products in a real-time manner as the number of SYBR Green molecules incorporated in DNA is proportional to the amount of product amplified.

qRT-PCR was performed using iTaq Universal SYBR Green Supermix (catalog no: 1725121; Bio-Rad). For qRT-PCR, a PCR master mix (1X) was prepared by setting up a 10 µl reaction mix containing 1X iTaq Universal SYBR Green Supermix, 500 nM each primer, 100 ng cDNA and Nuclease-free water. The reaction mix was run in a 7500 real-time PCR system (Applied Biosystems) according to the following conditions: initial holding at 95 ºC for 10 mins followed by 40 cycles of 95 ºC for 15 secs and 60 ºC for 1 min and a dissociation stage of 95 ºC for 15 secs, 60 ºC for 1 min, and then 95 ºC for 30 secs. Expression of β-actin mRNA

was used as an endogenous control. The amount of RNA was quantified using the comparative CT method (ΔΔCt). The primers used for qRT-PCR are listed in Table 1.

Table 1: List of primers for qRT-PCR

Primer Name		**Primer Sequence (5' ⟶3')**	**Accession number**
Rattus norvegicus			
atf6	Forward	GTACTGAGGAGACAGCAGCG	NM_001107196.1
	Reverse	GCCTCTGGTTCTCTGACACC	
grp78	Forward	TCAGCCCACCGTAACAAT	NM_013083.2
	Reverse	CAAACTTCTCGGCGTCAT	
tbx20	Forward	AGGAGCTCTGGGACAAATTCC	NM_001401090.1
	Reverse	GAACATCCTCCTGCCAGACTTG	
bmp2	Forward	AAGAAGCCATCGAGGAACTTCCAG	NM_017178.2
	Reverse	CCTGAGACCAGCTGTGTTCATCTT	
bnp	Forward	AGTCCTAGCCAGTCTCCAGA	NM_031545.1
	Reverse	GTCTCTCCTGGATCCGGAAG	
β-mhc	Forward	CCAGTCCCGAGGTGTACTTT	NM_017240.2
	Reverse	TCCTCCTTCATGTTGGCCAT	
serca2	Forward	GCTCCATCTGCTTGTCCATG	NM_001110823
	Reverse	CAGGCAGGGAGATTTTCAGC	
nog	Forward	TCTGAACGAGACGCTGCTG	NM_017178.2
	Reverse	CTTTGATCTCGCTCGGCATG	
tnfα	Forward	ACTCCCAGAAAAGCAAGCAA	NM_012675.3
	Reverse	CGAGCAGGAATGAGAAGAGG	
il6	Forward	TCACAGAGGATACCACCCACAA	NM_012589.2

	Reverse	CTGACAGTGCATCATCGCTGTT	
β-actin	Forward	TCTTCCAGCCTTCCTTCCTG	NM_031144.3
	Reverse	CACACAGAGTACTTGCGCTC	
Mus musculus			
atf6	Forward	GAAGTGGAAAGGACCAAATCTAGAAG	NM_001081304.1
	Reverse	CTCACTCCCAGAATTCCTACTGATG	
grp78	Forward	TGCAGCAGGACATCAAGTTC	NM_022310.3
	Reverse	TACGCCTCAGCAGTCTCCTT	
chop	Forward	CTGCCTTTCACCTTGGAGAC	NM_007837.4
	Reverse	CGTTTCCTGGGGATGAGATA	
tbx20	Forward	AAACCCCTGGAACAATTTGTGG	NM_194263.3
	Reverse	CATCTCTTCGCTGGGGATGAT	
bmp2	Forward	TGCACCAAGATGAACACAGC	NM_007553.3
	Reverse	GTGCCACGATCCAGTCATTC	
bnp	Forward	AAGTCCTAGCCAGTCTCCAGA	NM_008726.6
	Reverse	GAGCTGTCTCTGGGCCATTTC	
β-mhc	Forward	ACGGATGCCATACAGAGGAC	NM_080728.3
	Reverse	CCTCATAGGCGTTCTTGAGC	
serca2	Forward	GGGCGAGCCATCTACAACAA	NM_001110140.3
	Reverse	TGTCACCAGATTGACCCAGAGT	
tnfα	Forward	CCCTCACACTCAGATCATCTTCT	NM_013693.3
	Reverse	GCTACGACGTGGGCTACAG	
il6	Forward	TACCACTTCACAAGTCGGAGGC	NM_031168.2
	Reverse	CTGCAAGTGCATCATCGTTGTTC	

β-actin	Forward	CCTCTATGCCAACACAGTGC	NM_007393.5
	Reverse	CCTGCTTGCTGATCCACATC	

3.15 Taqman assay for analysis of expression of miR-101-3p

Taqman assay is a more specific and sensitive method of qRT-PCR as it involves the hydrolysis of specific Taqman probes. In this assay, target-specific oligonucleotides called Taqman probes are used, which contain a 5'fluorescent reporter dye and 3' quencher dye. The Taqman probe binds to the cDNA template of a specific gene of interest or microRNA (miRNA) with the complementary sequence. During PCR with a specific set of primers, the Taq polymerase extends the probe binding region, and as it encounters the Taqman probe, it degrades the probe due to its 5'-3' exonuclease activity. As a result, the fluorophore is released from the quenching effect, and it fluoresces, which is detected and is proportional to the amount of template present in the reaction mix. So in our study, we have used the Taqman assay for analysis of miRNA expression in both heart tissue and cells.

For the Taqman assay, total RNA was isolated from heart tissue, H9c2 cardiomyocytes or cardiac fibroblasts after different treatment conditions using the miRVana RNA Isolation kit (catalog no: AM1560, Ambion). After RNA isolation, 50 ng of the total RNA was reverse transcribed using specific RT primers for miR-101-3p (Assay ID: 002253; Applied Biosystems) and U6 snRNA (Assay ID: 001973; Applied Biosystems) with the Taqman MicroRNA Reverse Transcription kit (catalog no: 4366596; Applied Biosystems) using the following thermal cycling condition: Reverse transcription at 16 ^{o}C for 30 mins and 42 ^{o}C for 30 mins, followed by stop reaction at 85 ^{o}C for 5 mins and an infinite hold at 4 ^{o}C. The expression of miR-101-3p was determined using a specific Taqman probe and Taqman Universal PCR Master Mix (catalog no: 4304437, Applied Biosystems) in a 7500 real-time PCR system (Applied Biosystems) according to the following thermal conditions: initial denaturation at 95 ^{o}C for 10 mins, followed by 40 cycles of denaturation at 95 ^{o}C for 15 secs. This was followed by annealing and extension at 60 ^{o}C for 1 min. The levels of miR-101-3p were normalised using the U6 snRNA expression level. The amount of miR-101-3p was normalised relative to the expression of U6 snRNA. The amount of RNA was quantified using the comparative CT method ($\Delta\Delta$Ct).

3.16 Reporter Plasmid Construction for Dual-Luciferase Reporter Assay

Since miRNAs bind to the 3'untranslated region (3'UTR) of any gene to exert its inhibitory effect, therefore, to corroborate the direct binding of miR-101-3p to the 3'UTR of *tbx20* and *nog* gene, luciferase reporter plasmid was constructed.

3.16.1 T-box transcription factor 20 (Tbx20) reporter plasmid construction

Rat *tbx20* (NM_001401090.1) 3'UTR 881-nt fragment containing miR-101-3p binding site (5'-ACTGTAA-3') was amplified from rat genomic DNA using high fidelity LA Taq with the following primer pairs (Table 2).

Table 2: List of primers used for cloning the 881-nt fragment of Tbx20 3'UTR containing miR-101-3p seed sequence

Primer	Sequence
Forward primer	5'-AAACGAGCTCGCTAGCTTACTATTCTGTAGCTGTTATAAAA-3'
Reverse primer	5'-ATGCCTGCAGGTCGACTTCTGTACAATTTGGGATAAT-3'

The amplified region was further cloned in pmirGLO Dual-Luciferase miRNA Target Expression Vector (catalog no: E1330, Promega) downstream of the firefly luciferase gene using *Nhe1* and *Sal1* restriction sites to generate the *tbx20* 'wild-type' reporter construct.

The mutant form of *tbx20* 3'UTR was generated by introducing two point mutations in the seed sequence of miR-101-3p (5'-ACTACAA-3') using GeneArt™ Site-Directed Mutagenesis System (catalog no: A13282, Thermo Fisher Scientific) with the following primer pairs to generate the *tbx20* 'mutant' reporter construct (Table 3).

Table 3: List of primers used for introduction of point mutations in the 881-nt fragment of Tbx20 3'UTR

Primer	Sequence
Forward primer	5'-AGTCACTACAATGCAGTGTGCGGGGTG-3'
Reverse primer	5'-TGCATTGTAGTGACTTTTCCACGCAAATTG-3'

To further corroborate the direct binding of miR-101-3p to the 3'UTR of the *tbx20* gene, a rat *tbx20* 3'UTR 493-nt fragment that does not contain a miR-101-3p binding site was amplified from rat genomic DNA using high-fidelity LA Taq using the following primer pairs (Table 4).

Table 4: List of primers used for cloning the 493-nt fragment of Tbx20 3'UTR not containing miR-101-3p seed sequence

Primer	Sequence
Forward primer	5'-TATAGCTAGCAGGAGAAAATGGAAGCCAGTAGC-3'
Reverse primer	5'-ATATGTCGACTTAATATGCAAAAGGCCTCCTGACG-3'

The amplified region was further cloned in pmirGLO Dual-Luciferase miRNA Target Expression Vector downstream of the firefly luciferase gene using *Nhe1* and *Sal1* restriction sites to generate the *tbx20* 'negative-control' reporter construct.

3.16.2 Noggin (Nog) reporter plasmid construction

Rat *nog* (NM_012990.1) 3'UTR 439-nt fragment containing miR-101-3p binding site (5'- TACTGTA-3') was amplified from rat genomic DNA using high fidelity LA Taq with the following primer pairs (Table 5).

Table 5: List of primers used for cloning the 439-nt fragment of Nog 3'UTR containing miR-101-3p seed sequence

Primer	Sequence
Forward primer	5'-ATATGCTAGCCTCTAGCGAGGGTTTTCAATGAA-3'
Reverse primer	5'-TATAGTCGACACTCTATAACTTCTTCGAGGTCTAAGG-3'

The amplified region was further cloned in pmirGLO Dual-Luciferase miRNA Target Expression Vector downstream of the firefly luciferase gene using *Nhe1* and *Sal1* restriction sites to generate the *nog* 'wild-type' reporter construct.

The mutant form of the *nog* 3'UTR was generated by introducing two point mutations in the seed sequence of miR-101-3p (5'-TA<u>AG</u>GTA-3') using GeneArt™ Site-Directed Mutagenesis System with the following primer pairs to generate the *nog* 'mutant' reporter construct (Table 6).

Table 6: List of primers used for introduction of point mutations in the 439-nt fragment of Nog 3'UTR

Primer	Sequence
Forward primer	5'-GCTTCTAAGGTATTTAAAAAAAATAAGCAAGCAAAGT-3'
Reverse primer	5'-TTAAATACCTTAGAAGCCGGGTAACTTTTGAC-3'

To corroborate the direct binding of miR-101-3p to the 3'UTR of the *nog* gene, a rat *nog* 3'UTR 243-nt fragment that does not contain a miR-101-3p binding site was amplified from rat genomic DNA using high-fidelity LA Taq using the following primer pairs (Table 7).

Table 7: List of primers used for cloning the 243-nt fragment of Nog 3'UTR not containing miR-101-3p seed sequence

Primer	Sequence
Forward primer	5'-ATATGCTAGCGCGCCTAGACACTTGATG-3'
Reverse primer	5'-TATAGTCGACGCCGGGTAACTTTTGACGTAT-3'

The amplified region was further cloned in pmirGLO Dual-Luciferase miRNA Target Expression Vector downstream of the firefly luciferase gene using *Nhe1* and *Sal1* restriction sites to generate the *nog* 'negative-control' reporter construct.

All the reporter constructs generated were used for the Dual-Luciferase Reporter Assay (Figure 2).

3.17 Dual-Luciferase Reporter Assay

For Dual-Luciferase Reporter Assay, HEK-293T cells were seeded at $2x10^5$ in a 35 mm dish 24 hours before transfection. For test samples, the HEK-293T cells were cotransfected with 150 ng reporter plasmid ("wild-type" or "mutant" or "negative control") using Lipofectamine LTX (catalog no: A12621; Thermo Fischer Scientific) and 100 nM miR-101-3p mimic (Assay ID: MC11414; Ambion) using Lipofectamine RNAiMAX (catalog no: 13778075; Thermo Fischer Scientific). For control samples, HEK-293T cells were cotransfected with 150 ng reporter plasmid ("wild-type" or "mutant" or "negative control") using Lipofectamine LTX, and 100 nM scrambled mimic (Assay ID: MC11414; Ambion) using Lipofectamine RNAiMAX. The cells were incubated in the transfection mix for 24 hours to measure luciferase activity by Dual-Luciferase Reporter Assay System (catalog no: E1910, Promega). After incubation, the growth media were discarded, and the cells were washed with 1X PBS. The PBS was discarded, and 1X Passive Lysis Buffer (PLB) was added to the cells. The cells were scraped from the culture dish in the presence of 1X PLB to make a homogenous lysate. The lysate was stored in a microcentrifuge tube for further use. Next, 100 µl of Luciferase Assay Reagent II (LAR II) was predispensed in 96-well black plates. To the LAR II reagent, 20 µl of cell lysate was added and mixed by pipetting 2-3 times. The luciferase activity was then measured. This measurement gives the value of 'Firefly' luciferase (FL)

activity. Next, 100 µl of Stop and Glo Reagent was added to the reaction mix and the luciferase activity was measured. This measurement gives the value of 'Renilla' luciferase (RL) activity. The luminescence emitted from both FL and RL was measured by an Agilent Biotek Synergy H1 Plate Reader (Agilent Technologies Inc., USA). The relative luciferase activity was then measured by normalizing Firefly luciferase activity to Renilla luciferase activity. Relative fold change was measured by taking the activity of the control sample as 100%.

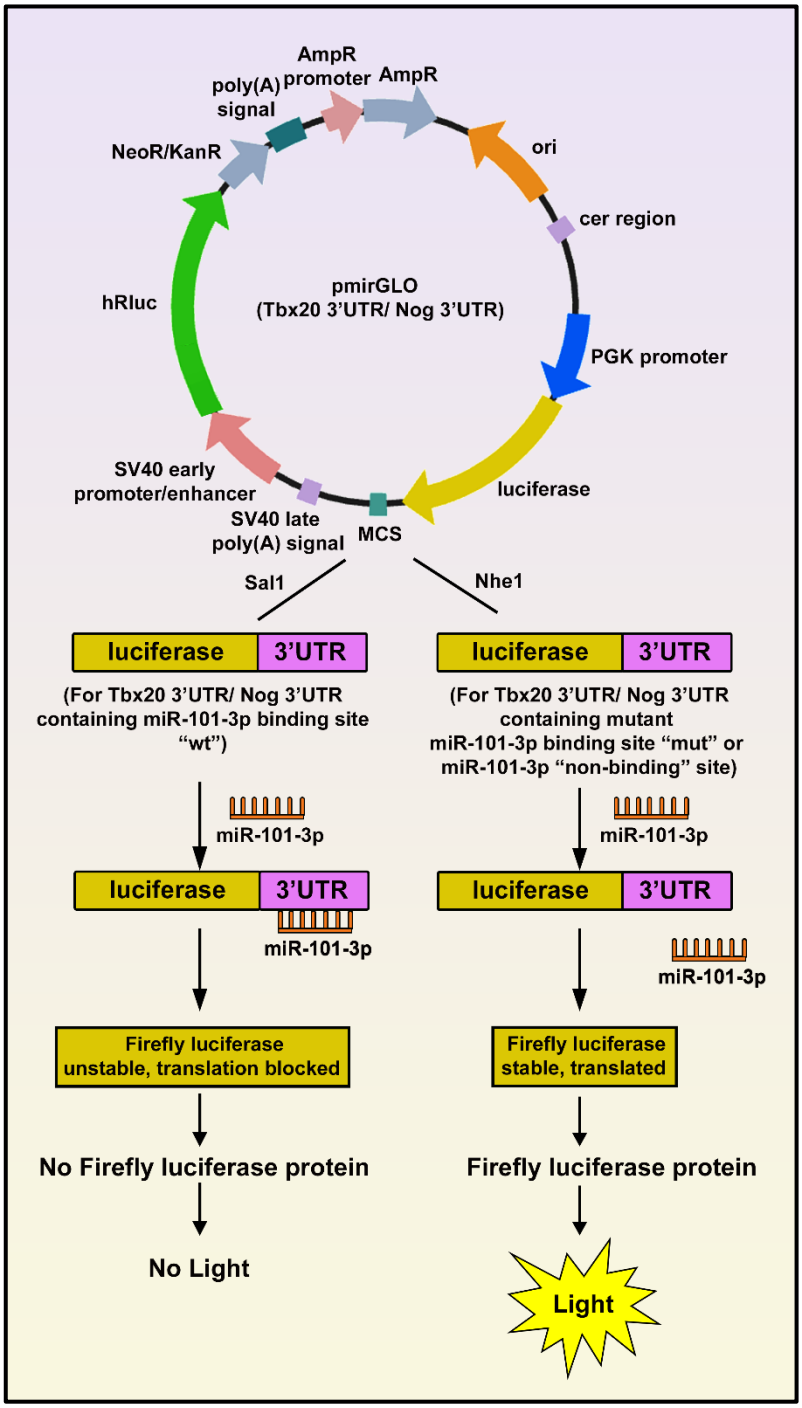

Figure 2. Dual-Luciferase Reporter Assay. Schematic representation of the reporter construct and the miRNA interaction with the 3'UTR of the luciferase gene during Dual-Luciferase Reporter Assay.

3.18 Protein Isolation

3.18.1 From Tissue

For total protein isolation from heart tissue after different treatment conditions, the tissue pieces were weighed, and an adequate volume of protein lysis buffer was added to them. The protein lysis buffer consists of 20 mM Tris-HCl pH 7.5, 150 mM NaCl, 1 mM EDTA, 1 mM EGTA, 1% Nonidet P-40, 1% glycerol, 1 mM DTT, 100 mM NaF, 1 mM Na_3VO_4 and 0.2 mM PMSF along with protease inhibitor cocktail (catalog no: GX-2811AR; Puregene) and phosphatase inhibitor cocktail (catalog no: GX-1211AR; Puregene). The tissue in the lysis buffer was homogenized using a handheld homogenizer and incubated on ice for 10 mins. After incubation, the mixture was centrifuged at 14000 g for 10 mins at 4 ^oC. Following the centrifugation, the supernatant containing the total protein was transferred into a fresh microcentrifuge tube and stored at -80 ^oC until further use.

3.18.2 From Cells

For total protein isolation from H9c2 cardiomyocytes and cardiac fibroblasts after different treatment conditions, protein lysis buffer (20 mM Tris-HCl pH 7.5, 150 mM NaCl, 1 mM EDTA, 1 mM EGTA, 1% Nonidet P-40, 1% glycerol, 1 mM DTT, 100 mM NaF, 1 mM Na_3VO_4 and 0.2 mM PMSF along with protease inhibitor cocktail and phosphatase inhibitor cocktail) was added to the cells. The cells were scraped in lysis buffer to make a homogenous solution and incubated on ice for 10 mins. After incubation, the mixture was centrifuged at 14000 g for 10 mins at 4 ^oC. Following centrifugation, the supernatant containing the total protein was transferred into a fresh microcentrifuge tube and stored at -80 ^oC until further use.

3.19 Protein Estimation

Total protein isolated from heart tissue, H9c2 cardiomyocytes or cardiac fibroblasts was estimated using Bradford Reagent (catalog no: ML106; Himedia). Bradford protein assay works on the principle of complex formation between Coomassie Brilliant Blue G-250 and the protein samples to form a blue solution that is measured at 595 nm.

For total protein estimation, a serial dilution of 1 mg/ml stock Bovine Serum Albumin (BSA) was prepared to make a standard curve. For unknown samples (tissue or cells), suitable dilutions were prepared. Next, Bradford Reagent was added to standard and unknown samples and incubated for 10 mins at room temperature for colour development. Post incubation, the absorbance was measured at 595 nm. Next, with the absorbance of the known concentrations of BSA standard samples, a standard curve was plotted, and the concentration of the unknown

samples was calculated from the curve. The concentration of the protein obtained from the standard curve was used for western blotting analysis.

3.20 Western Blotting

For Western Blotting analysis, 60-100 µg of protein lysates from heart tissue, H9c2 cardiomyocytes and cardiac fibroblasts under different treatment conditions were fractionated under reducing conditions in 10-12% SDS-PAGE. Following resolution, the samples were transferred onto a polyvinylidene difluoride (PVDF) membrane (catalog no: IPVH00010; Merck Millipore). Following the transfer, the PVDF membrane was blocked with 5% skimmed milk in Tris-buffered saline with Tween-20 (TBS-T) for 1 hour at room temperature. After blocking, the membranes were incubated with respective primary antibodies diluted in skimmed milk or BSA according to the manufacturer's instructions at 4 ^{o}C overnight with constant shaking. The next day, after washing the blots two times with TBS-T for 5 mins each, the immunoblots were incubated with respective secondary antibodies for 1 hour. After incubation, the immunoblots were washed two times with TBS-T for 7 mins each, and the immunoblots were developed using Clarity ECL substrate (catalog no: 1610182; Bio-rad). The antibodies for Western Blotting, along with their dilution ratio, are listed in Table 8.

Table 8: List of antibodies used for Western Blotting analysis

Antibody name	Make	Dilutions Used	Catalog Number
Atf6	Santa Cruz Biotechnology	1:500	sc-166659
Bax	Cell Signaling Technology	1:1000	2772S
Bcl_{XL}	Cell Signaling Technology	1:1000	2764S
Bmp2	Thermo Fisher Scientific	1:1000	PA5-85956
Chop	Cell Signaling Technology	1:1000	2895S
Col I	Thermo Fisher Scientific	1:1000	PA5-95137
Col III	Thermo Fisher Scientific	1:1000	PA5-95595
Grp78	Cell Signaling Technology	1:1000	3177T
GAPDH	Bio Bharti Life Science	1:2000	AB0060
pJNK	Cell Signaling Technology	1:1000	9251S
JNK	Cell Signaling Technology	1:1000	9252S
Nog	Abclonal	1:1000	A8305

p16	Thermo Fisher Scientific	1:500	PA5-20379
p21	Thermo Fisher Scientific	1:500	14-6715-81
Periostin	Abcam	1:1000	ab14041
RUNX2	Novus Biologicals	1:500	NBP2-67777
pSmad 1/5/9	Cell Signaling Technology	1:1000	13820S
Smad1	Cell Signaling Technology	1:1000	9743S
Tbx20	Thermo Fisher Scientific	1:500	PA5-40669
TNFα	Thermo Fisher Scientific	1:1000	PA5-19810
Anti-rabbit IgG, HRP-linked Antibody	Cell Signaling Technology	1:1000	7074S
Anti-mouse IgG, HRP-linked Antibody	Cell Signaling Technology	1:1000	7076S

3.21 Immunostaining

3.21.1 For Tissue

After treating the male Swiss-Albino mice with different treatment conditions, the heart tissue was harvested and fixed with 4% Paraformaldehyde (PFA) (catalog no: GRM3660, Himedia), dehydrated and embedded in paraffin. Then, 5 µm tissue sections were cut using a microtome and embedded on glass slides. For immunostaining of tissue sections, the glass slide containing the tissue section was placed on a 60 ºC hot plate to melt the paraffin, and thereafter the slides were kept in xylene for 7 mins. After paraffin melting, sections were rehydrated in graded ethanol (100%, 90%, 70%, 50% and lastly distilled water). Following rehydration, the sections were subjected to antigen retrieval with citrate buffer (10 mM citric acid, 0.05% Tween-20, pH 6.0) in a microwave oven for 10 mins. The tissue sections were then blocked with blocking buffer (2% BSA, 0.1% Tween-20 in 1× PBS) for 1 hour at room temperature. After blocking, the tissue sections were incubated with respective primary antibodies overnight at 4 ºC with constant shaking. After incubation, the sections were washed three times with 1X PBS for 5 mins each. Following washing, the sections were incubated with respective secondary antibodies for 1 hour at room temperature. Post incubation, the tissue sections were washed three times with 1X PBS for 7 mins each. The nucleus was counterstained with DAPI and incubated at room temperature for 10 mins. The sections were washed with 1X PBS for 3

times and mounted with mounting media. The images were taken by Leica DM2000 across multiple fields. Cell size was quantified using ImageJ (National Institutes of Health) software (Sengupta et al., 2011).

3.21.2 For Cells

For immunostaining of H9c2 cardiomyocytes or cardiac fibroblasts, the cells treated with different treatment conditions were fixed with 4% PFA. After fixation, the cells were blocked with blocking buffer (2% BSA, 0.1% Tween-20 in 1× PBS) for 1 hour at room temperature. Following blocking, respective primary antibodies were added to the cells and incubated overnight at 4 ºC with constant shaking. The cells were then washed three times with 1X PBS for 5 mins each. After washing, the cells were incubated with respective secondary antibodies and incubated for 1 hour at room temperature. The cells were then washed three times with 1X PBS for 5 mins each. The nucleus was counterstained with DAPI and incubated at room temperature for 10 mins. The cells were washed with 1X PBS for 3 times and mounted with mounting media. The images were taken by Leica DM2000 across multiple fields. The antibodies used for immunostaining, along with their dilution ratio, are listed in Table 9.

Table 9: List of antibodies used for Immunostaining analysis

Antibody name	Make	Dilutions Used	Catalog Number
Atf6	Santa Cruz Biotechnology	1:250	sc-166659
Bax	Cell Signaling Technology	1:200	2772S
Bcl_{XL}	Cell Signaling Technology	1:200	2764S
Bmp2	Thermo Fisher Scientific	1:200	PA5-85956
Chop	Cell Signaling Technology	1:500	2895S
Ki67	Cell Signaling Technology	1:250	9252S
Mf20	Developmental Studies Hybridoma Bank	1:200	
Nog	Abclonal	1:250	A8305
p16	Thermo Fisher Scientific	1:250	PA5-20379
p21	Thermo Fisher Scientific	1:250	14-6715-81
α-SMA	Thermo Fisher Scientific	1:250	14-9760-82
pSmad 1/5/9	Cell Signaling Technology	1:500	13820S

Tbx20	Thermo Fisher Scientific	1:100	PA5-40669
TNFα	Thermo Fisher Scientific	1:250	PA5-19810
γH₂AX	Thermo Fisher Scientific	1:250	MA1-2022
Vim	Abclonal	1:250	A19607
Goat Anti-Rabbit IgG H&L (Alexa Fluor 488)	Abcam	1:1000	ab150077
Goat Anti-Mouse IgG H&L (Texas Red)	Abcam	1:1000	ab6787

3.22 Chromatin Immunoprecipitation (ChIP) assay

For the ChIP assay, approximately $4x10^6$ cells are required for one DNA-protein complex preparation. The chromatin complexes were prepared from H9c2 cardiomyocytes treated with 20 µg/ml Tun. The ChIP assay was performed according to the following protocol (Sengupta et al., 2011):

3.22.1 Chromatin Crosslinking and Lysis

For chromatin crosslinking, 10 ml of complete growth media (DMEM+10%FBS) containing 1% formaldehyde was added to culture dishes and incubated for 10 mins. After incubation, the unused formaldehyde was neutralized with 2 ml of 10X glycine solution. The cells were then washed with ice-cold 1X PBS containing protease inhibitor cocktail. After washing, the cells were scraped in 2 ml of 1X PBS supplemented with a protease inhibitor cocktail. The cells were centrifuged at 700 g for 5 mins at 4 °C to pellet cells. The supernatant was discarded, and the pellet was resuspended in 1 ml of SDS Lysis buffer supplemented with protease inhibitor cocktail.

3.22.2 Sonication to Shear DNA

The lysed cell lysate was sonicated ten times for 30 secs each with 1 min of refractory period on ice. After sonication, the cell lysate was centrifuged at 10000 g for 10 mins at 4 °C to remove insoluble materials. The supernatant was transferred to a fresh microcentrifuge tube in 100 µl aliquots.

3.22.3 Immunoprecipitation of chromatin

To 100 µl of chromatin (approximately 10 µg), 900µl Dilution buffer was added. Then

to the diluted chromatin, 60 µl of Protein AG Plus Agarose beads (catalog no: BB-PAG001PB, BioBharati) was added and incubated for 1 hour at 4 ºC with constant rotation ("preclear" of chromatin). The agarose beads were pelleted at 3000 g for 1 min. 2% of the supernatant was removed for Input. The remaining supernatant was dispensed into 1 ml aliquots. For immunoprecipitation, to each 1 ml aliquot was added 5 µg of the respective antibodies (Atf6 or Tbx20). For negative control, immunoprecipitation was done with rabbit IgG. The chromatin-antibody complexes were incubated overnight at 4 ºC with constant rotation. After incubation, to each complex, 60 µl of Protein AG Plus Agarose beads was added and incubated for 1 hour at 4 ºC with constant rotation. The AG Agarose beads were pelleted at 3000 g for 1 min, and the supernatant was discarded. The Protein AG Plus Agarose beads-antibody/ chromatin complex was resuspended in 1 ml of cold Low Salt Immune Complex buffer and incubated for 5 mins at 4 ºC with rotation. After incubation, the beads were pelleted at 3000 g for 1 min, and the supernatant was discarded. Next, the pellet containing Protein AG Plus Agarose beads-antibody/ chromatin complex was resuspended in 1 ml of cold High Salt Immune Complex buffer and incubated for 5 mins at 4 ºC with rotation. After incubation, the beads were pelleted at 3000 g for 1 min, and the supernatant was discarded. Next, the pellet containing Protein AG Plus Agarose beads-antibody/ chromatin complex was resuspended in 1 ml of cold LiCl Immune Complex buffer and incubated for 5 mins at 4 ºC with rotation. After incubation, the beads were pelleted at 3000 g for 1 min, and the supernatant was discarded. Lastly, the pellet containing Protein AG Plus Agarose beads-antibody/ chromatin complex was resuspended in 1 ml of cold TE buffer and incubated for 5 mins at 4 ºC with rotation. After incubation, the beads were pelleted at 3000 g for 1 min, and the supernatant was discarded. The washing step with TE was repeated another time.

3.22.4 Elution of DNA/Protein Complexes

To each immunoprecipitated complex and input samples, 200 µl Elution buffer (10 µl 20% SDS, 20 µl 1M $NaHCO_3$ and 170 µl distilled water) was added. It was incubated for 15 mins at room temperature. The agarose was pelleted at 3000 g for 1 min, and the supernatant was collected in fresh microcentrifuge tubes.

3.22.5 Reverse crosslinking of DNA/ Protein complexes

To each immunoprecipitated complex and input samples, 8 µl of 5 M NaCl was added and incubated for 5 hours at 65 ºC to reverse crosslink the DNA/Protein complexes. Then, to all the tubes was added 4 µl 0.5 M EDTA, 8 µl 1 M Tris-HCl and 1 µl Proteinase K and

incubated for 1 hour at 45 ºC to degrade the protein. The DNA was purified using the phenol-chloroform method. The purified DNA was analyzed by qRT-PCR as well as semi-quantitative PCR using *tbx20* specific promoter (designed around the consensus Atf6 binding site), and *atf6* specific promoter (designed around the consensus Tbx20 binding site). Fold enrichment relative to IgG (negative control) was calculated from three independent experiments (n=3) using the comparative CT method (ΔΔCt). The list of primers used for the ChIP assay is listed in Table 10.

Table 10: List of primers used across the Atf6 binding site and Tbx20 binding site before the transcription start site (TSS) within the *tbx20* promoter and *atf6* promoter, respectively

Binding site	**Primer sequence**		**Promoter position**
Atf6	*rattbx20* Fwd	5'- GGAAGCAGTGACGTGAGAC-3'	466 bp upstream of TSS of *tbx20*
	rattbx20 Rev	5'- GCGACCTAAACTGTGCCT-3'	
Tbx20	*ratatf6* Fwd	5'- TCCAGTCTAACGTGTGATGCA-3'	4257 bp upstream of TSS of *atf6*
	ratatf6 Rev	5'- AAGAGTTAGGCTTCCCACCC-3'	

3.23 Bioinformatic analysis

To predict the miR-101-3p binding on *tbx20* and *nog* gene, TargetScan, miRPathDB, miRTarBase, and the Aging atlas database software were used.

3.24 Statistical analysis

All the data obtained were calculated as mean±SD of at least three independent experiments. The statistical analysis between different experimental groups was performed using Student's *t*-test for two experimental groups and one-way ANOVA for multiple experimental groups using GraphPad Prism 9 Software (GraphPad Software, Inc.). For all experimental groups, results with $p < 0.05$ were considered statistically significant for the mean values.

Chapter 4

*ER stress induces upregulation of transcription factor Tbx20 and downstream Bmp2 signaling to promote cardiomyocyte survival**

***Results from this section have been published in the *Journal of Biological Chemistry* (2023), 299(4), 103031**

4.1 Background and Significance of the Study

Cardiovascular diseases (CVDs) represent a significant danger to humanity, as indicated by the World Health Organization (WHO), which reports that they are the primary cause of death globally (17.9 million fatalities occurred in 2019) (Antar et al., 2023). This constitutes 32% of all deaths worldwide, emphasizing the necessity for the creation of early biomarkers and therapies for the prevention and treatment of CVDs.

The neonatal mammalian heart is highly proliferative; however, the proliferative capacity ceases in the adult heart as the cardiomyocyte exits the cell cycle and primarily grows by hypertrophy (Li et al., 1996; Pasumarthi & Field, 2002; Porrello et al., 2011; Siedner et al., 2003). However, this notion was recently revoked by growing studies showing that adult cardiomyocytes can re-enter the cell cycle post-injury by modulating the regulation of key regulatory signaling pathways (Zhu et al., 2021). Therefore, identification of novel signaling pathways that can switch the adult cardiomyocytes towards proliferation post-injury will open newer avenues for the treatment of CVDs.

ER stress has been implicated in the pathogenesis of cardiomyopathy (Park et al., 2017; Safiedeen et al., 2017; W. Xin, Li, et al., 2011; W. Xin, Lu, et al., 2011; Zhang et al., 2017). The Unfolded Protein Response (UPR) during ER stress resides on a very fine balance where it is initially beneficial as it restores homeostasis; however, a prolonged ER stress in due course leads to cell death via apoptosis (Das et al., 2021). Therefore, tilting the balance of UPR towards pro-survival during ER stress-induced diseases is essential for the maintenance of cellular survivability. Thus, targeting the ER stress by delineating novel pathways that can shift the balance of the UPR towards pro-survival can serve as a therapeutic approach for the prevention of CVDs.

Tbx20, a component of the Tbx1 subfamily of T-box genes, plays an indispensable role in proper heart development (Huang et al., 2017; Luyckx et al., 2019; Naiche et al., 2005; Pan et al., 2015; Posch et al., 2010). In addition, Tbx20 also plays an important role in cardiac remodelling and maintenance of homeostasis following injury (Xiang et al., 2016). Therefore, Tbx20 plays a pivotal role in cardiac development and disease. However, no studies have been done so far to delineate the role of Tbx20 during ER stress-induced cardiomyopathy. This prompted us to look into the role of Tbx20 during ER stress.

Therefore, our study, for the first time, will unravel the novel function of Tbx20 signaling during ER stress-induced cardiomyopathy, and we will decipher whether Tbx20 can shift the

balance of the UPR towards pro-survival to serve as a novel signaling mechanism in ameliorating cardiomyopathy.

4.2 Results

4.2.1 The expression of Tbx20 and Bmp2 is increased upon ER stress induction in H9c2 cardiomyocytes *in vitro*

The role of Tbx20 and Bmp2 signaling during ER stress remains unexplored. To elucidate their functions, we treated H9c2 cardiomyocytes with increasing concentrations (2, 5, 10, 20, and 50 μg/ml) of the ER stress inducer Tunicamycin (Tun) at various time points (8 hours, 12 hours, and 24 hours). Both 8 hours and 12 hours treatments led to a gradual increase in the expression of Tbx20 and Bmp2, as confirmed by Western blotting (Figure 1A, 1B). Notably, 24 hours treatment produced the highest expression levels of Tbx20 and Bmp2, and thus, the 24 hours time point was selected for subsequent experiments. We assessed cell viability after ER stress induction using the MTT assay over 24 hours (Figure 1C). The assay revealed no significant change in cell viability among control, 2 μg/ml Tun, and 5 μg/ml Tun-treated cells. However, the difference in viability between control and 10 μg/ml Tun-treated cells was significant, while no substantial change was observed in cell survival between the 10 μg/ml and 20 μg/ml Tun treatments. Consequently, 10 μg/ml and 20 μg/ml Tun concentrations were chosen for further studies. The 50 μg/ml Tun treatment resulted in a viability of 45.6%, approaching the IC50 value. We included this concentration in our experiments to better understand the pathophysiological effects of high ER stress levels. We validated the establishment of ER stress via qRT-PCR for ER stress markers *grp78* and *atf6,* along with Western blotting for cleaved Atf6 (Atf6-p50) (Figure 1D, 1E, 1F). Both mRNA and protein levels of Tbx20 and Bmp2 exhibited a gradual increase with rising Tun concentrations up to 20 μg/ml (Figure 1D, 1E, 1F). However, the expression of Tbx20 and Bmp2 significantly decreased at 50 μg/ml compared to the 20 μg/ml treatment. This upward trend in Tbx20 and Bmp2 expression was correlated with Atf6-p50 levels. Our data indicate that Tbx20 and Bmp2 levels increase in response to ER stress until a certain concentration, reflecting both the viable and physiological status of the cells during ER stress. With increasing ER stress, the Bmp2 signaling cascade was also activated. Western blotting showed increased levels of pSmad1/5/8 upon increasing ER stress up to a concentration of 20 μg/ml Tun. However, increasing the concentration to 50 μg/ml Tun resulted in a significant decrease in the expression of pSmad/1/5/8 (Figure 1E, 1F). The data was further corroborated by immunofluorescence

staining of cells (Figure 1G, 1H, 1I, 1J, 1K). Thus, our results showed upregulation of Bmp2-pSmad1/5/8 signaling cascade upon induction of ER stress.

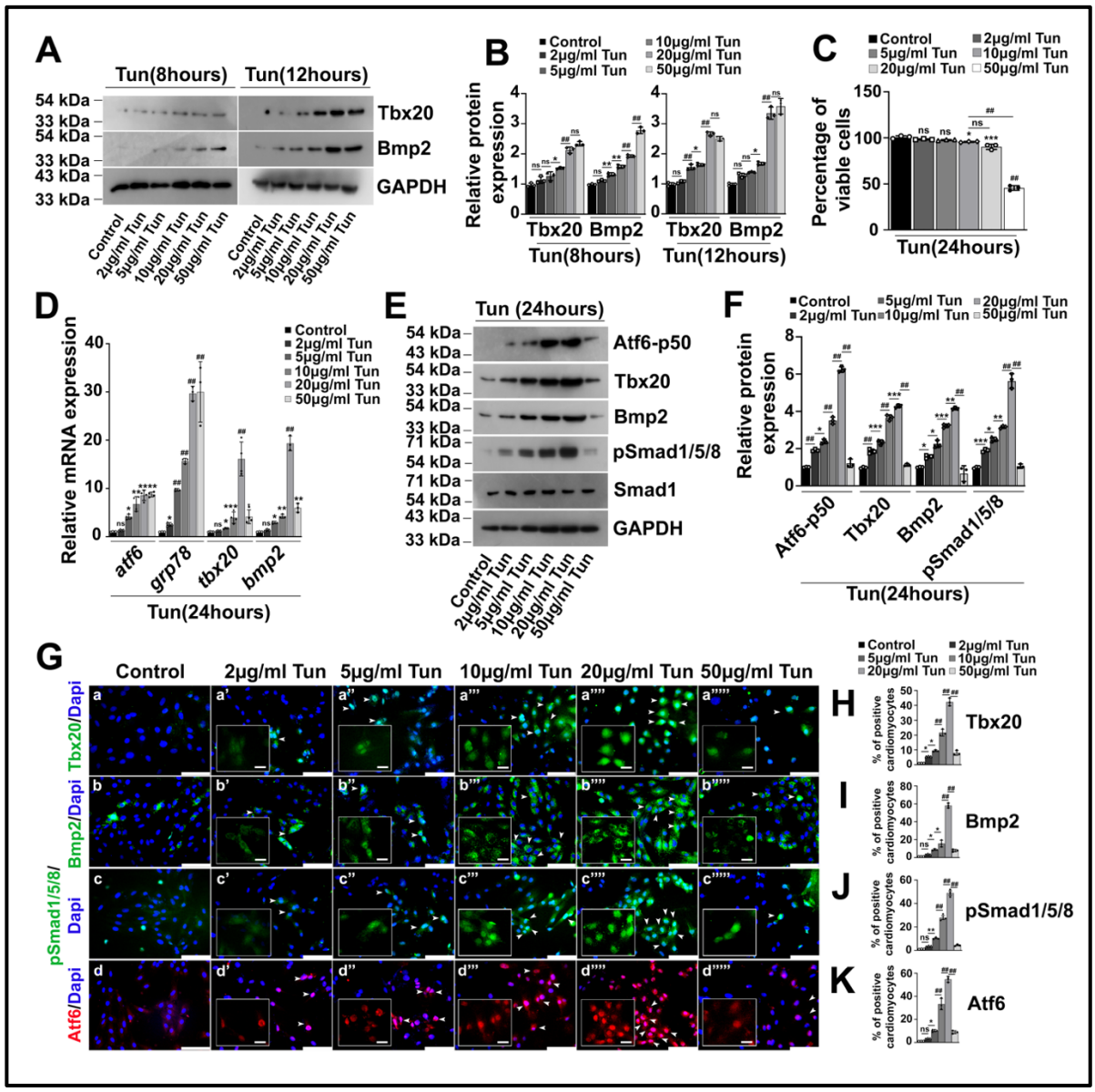

Figure 1. The expression of T-box transcription factor 20 (Tbx20) and bone morphogenetic protein 2 (Bmp2) is increased upon Endoplasmic Reticulum (ER) stress induction *in vitro*. A, Western blot analysis showing a gradual increase in the expression of Tbx20 and Bmp2 upon ER stress induction with tunicamycin (Tun) for 8 hours and 12 hours. **B,** Quantitative representation by ImageJ software of the proteins from A. **C,** H9c2 cells were treated with different concentration (2 µg/ml, 5 µg/ml 10 µg/ml, 20 µg/ml, 50 µg/ml and 100 µg/ml) of Tun for 24 hours and cell viability was assessed by 3-[4,5-Dimethylthiazol-2-yl]-2,5 diphenyl tetrazolium bromide (MTT) assay. **D,** The expression of ER stress markers *atf6* and *grp78* is increased upon Tunicamycin (Tun) treatment in H9c2 cells as determined by quantitative real-time PCR (qRT–PCR). **E,** Western blot analysis showing a gradual increase in the expression of Activating transcription factor 6 (Atf6)-p50 with increasing concentration of Tun. However, its expression decreased in 50 µg/ml Tun-treated cells. The expression of Tbx20, Bmp2, and its downstream cascade molecule pSmad1/5/8 increased gradually up to a concentration of 20 µg/ml Tun. Increasing the concentration of Tun to 50 µg/ml resulted in a significant decrease in the expression of Tbx20, Bmp2, and pSmad1/5/8. **F,** Quantitative representation by ImageJ software of the

proteins from E. **G,** Immunostaining analysis showing an increase in the expression of Tbx20, Bmp2, pSmad1/5/8, and Atf6 proteins upon increasing ER stress induction (a', a'', a''', and a''''), (b', b'', b''', and b''''), (c', c'', c''', and c''''), and (d', d'', d''', and d'''') as compared with control (a, b, c, and d), respectively. Increasing the intensity of ER stress by treatment with 50 µg/ml Tun, however, resulted in a decrease in expression of Tbx20 (a'''''), Bmp2 (b'''''), pSmad1/5/8 (c'''''), and Atf6 (d'''''). Insets in G show single-channel cropped images of indicated areas (white arrows). Scale bar of the main images represents 50 µm. Scale bar of the inset represents 20 µm. **H-K,** Quantitative representation of G. Statistical significance was calculated by one-way ANOVA. Error bars represent SD from at least three biological replicates. ns, p: nonsignificant, ∗p < 0.05, ∗∗p < 0.005, ∗∗∗p < 0.0005, ##p < 0.0001; (n≥3) independent experiments.

4.2.2 ER stress induction with other stress inducers (Thapsigargin or Dithiothreitol) results in elevated levels of Tbx20 and Bmp2 in H9c2 cardiomyocytes *in vitro*

To further validate the increase in Tbx20 and Bmp2 signaling during ER stress, we employed two additional ER stress inducers, Thapsigargin (Tg) and Dithiothreitol (DTT), to provoke ER stress in H9c2 cardiomyocytes.

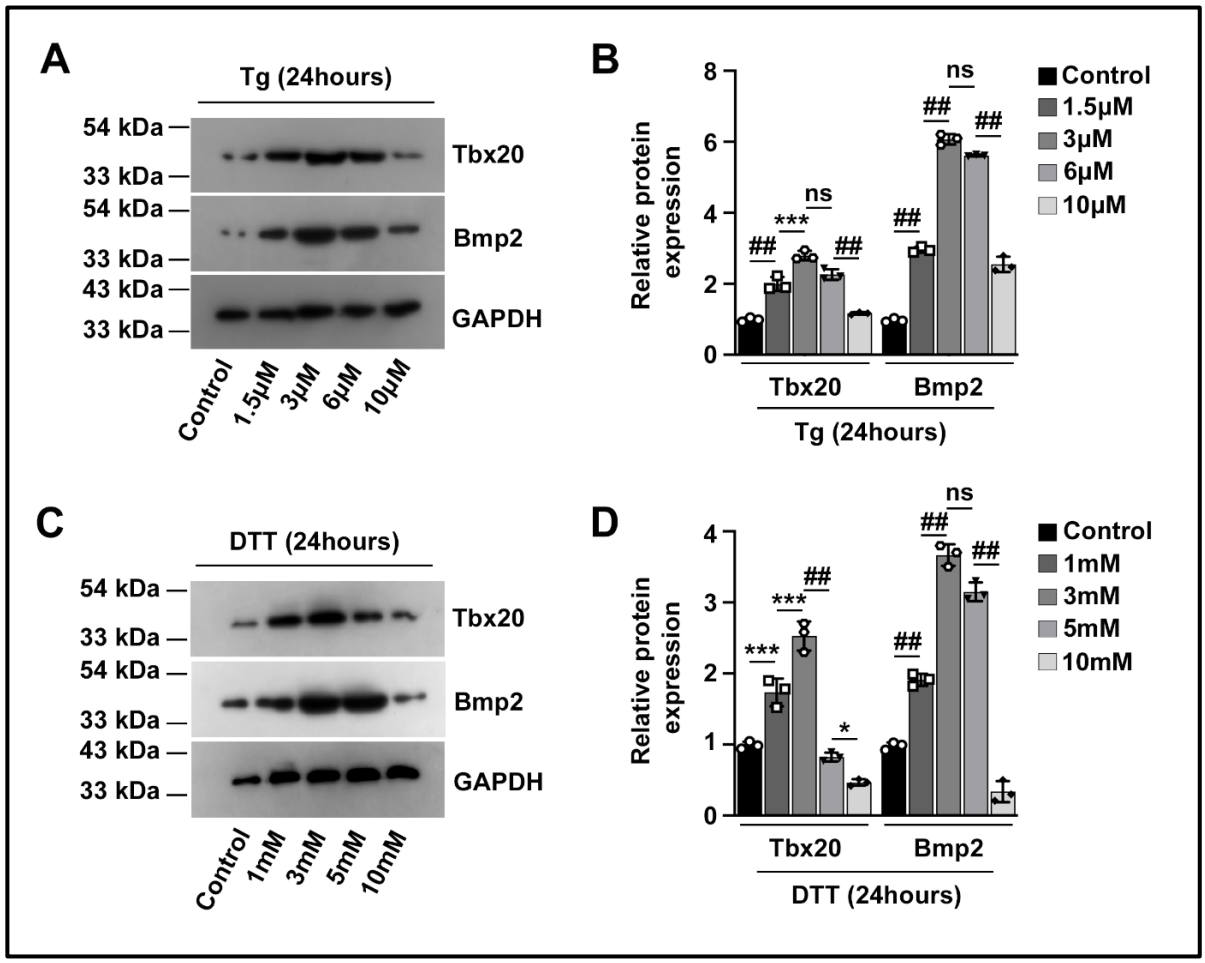

Figure 2. Endoplasmic reticulum (ER) stress inducers Thapsigargin (T_g) and Dithiothreitol (DTT) cause upregulation of Tbx20 and Bmp2 in H9c2 cardiomyocytes *in vitro*. A, Western blot analysis showing that ER stress induction with Tg caused an increase in the expression of Tbx20 and Bmp2 upto 6 µM concentration of Tg. The expression of Tbx20 and Bmp2 decreased significantly at a Tg

concentration of 10 μM. **B,** Quantitative representation by ImageJ software of the proteins from A. **C,** Western blot analysis showing that ER stress induction with DTT increased the expression of Tbx20 and Bmp2 upto 3 mM DTT concentration. The expression of Tbx20 decreased significantly at 5 mM DTT concentration, whereas the expression of Bmp2 decreased significantly at 10 mM DTT concentration. **D,** Quantitative representation by ImageJ software of the proteins from C. Statistical significance was calculated by one-way ANOVA. Error bars represent S.D. from three independent biological replicates (n=3). ns, p: nonsignificant, *, $p<0.05$, **, $p<0.005$, ***, $p<0.0005$, ##, $p<0.0001$.

H9c2 cells were treated with Tg at concentrations of 1.5, 3, 6, and 10 μM for 24 hours to induce ER stress. The induction of ER stress with Tg resulted in a progressive rise in Tbx20 and Bmp2 levels up to the 10 μM concentration. However, when the concentration was increased beyond 10 μM, there was a notable decrease in the expression of both Tbx20 and Bmp2 (Figure 2A, 2B). Treatment with DTT caused a gradual increase in Tbx20 levels, reaching 2.5 ± 0.2-fold at 3 mM DTT compared to control cells. Nonetheless, its expression decreased in cells treated with 5 mM DTT (0.82 ± 0.06-fold) and further dropped to 0.46 ± 0.04-fold in the 10 mM DTT-treated cells (Figure 2C, 2D). The expression of Bmp2 showed a similar increase up to 3 mM in DTT-treated cells. However, it later decreased significantly in the 10 mM DTT-treated cells (Figure 2C, 2D). Taken together, the induction of ER stress with all three inducers (Tun, $T_{g,}$ and DTT) led to an increase in Tbx20 and Bmp2 up to a certain threshold. However, exceeding that threshold resulted in reduced levels of Tbx20 and Bmp2. Taken together, these results show that in addition to Tun, Tg and DTT induced ER stress also results in increased expression of Tbx20 and Bmp2, thus reinforcing that ER stress induction in cardiomyocytes is associated with elevation of Tbx20 and Bmp2.

4.2.3 The increased expression of Tbx20 during ER stress is mediated by the Atf6 arm of the UPR

The upregulation of Tbx20 during ER stress prompted us to look into the mechanism that drives the expression of Tbx20. Since in our study, we showed a similar expression pattern of Atf6-p50 and Tbx20 during ER stress and with a decrease in the expression of Atf6-p50 in 50 μg/ml Tun treated cells the expression of Tbx20 also decreased; therefore, we speculated that the upregulation of Tbx20 during ER stress is driven by Atf6 arm of UPR signaling. Atf6, a basic leucine zipper family of transcription factors was shown to bind to the canonical Unfolded Protein Response element (UPRE) TGACGTGG/A of different genes to transcribe them (Wang et al., 2000). Atf6 was shown to impart its cardioprotective effect in the direction of pro-survival by ameliorating the extent of ER stress, and it also has a role in compensatory myocyte growth. It was also shown to confer global protection of cardiomyocytes from ischemia/reperfusion injury by reprogramming cellular proteostasis (Blackwood et al., 2019).

Atf6 was also shown to play a vital role in maintaining homeostasis of cardiomyocytes under both pathological and physiological states. In one study, chromatin immunoprecipitation (ChIP)-Seq analysis was performed to identify the putative targets of Atf6 (Ramdas Nair et al., 2022). This study identified Tbx20 as one of the possible targets of Atf6. Hence, *tbx20* genomic sequences were examined for the Atf6 binding consensus sequence.

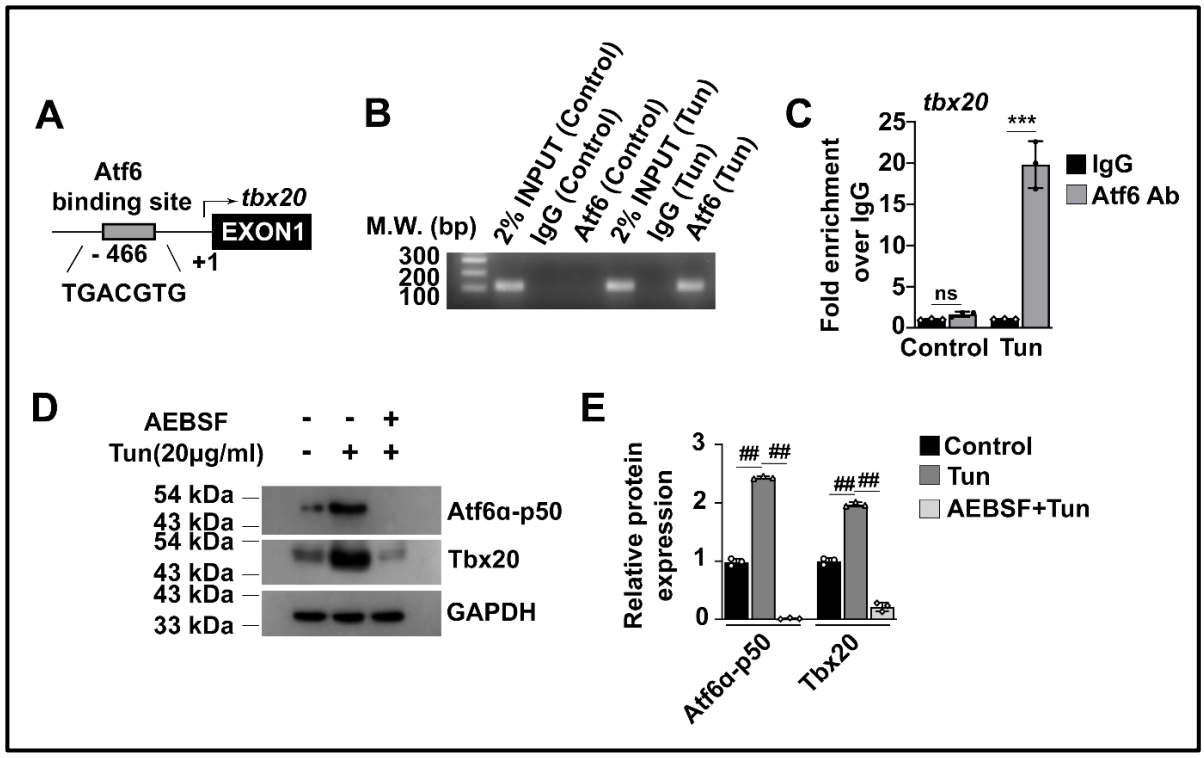

Figure 3. During Endoplasmic Reticulum (ER) stress, Activating transcription factor 6 (Atf6) mediates the upregulation of T-box transcription factor 20 (Tbx20). A. The rat *tbx20* gene contains a conserved canonical Atf6 DNA-binding sequence TGACGTG in its promoter region. **B,** Chromatin immunoprecipitation (ChIP) analysis showed direct binding of Atf6 in the *tbx20* promoter region. **C,** ChIP assay followed by quantitative RT–PCR (qRT–PCR) showed ~19-fold enrichment of Atf6 binding to the *tbx20* promoter region during ER stress induction. **D,** Western blot analysis revealed that pretreatment of H9c2 cardiomyocytes with 300 µM AEBSF, followed by ER stress induction, resulted in a significant decrease in the expression of Atf6-p50. Inhibition of nuclear translocation of Atf6 was accompanied by a concomitant decrease in the expression of Tbx20. **E**, Quantitative representation by ImageJ software of the proteins from D. Statistical significance was calculated by one-way ANOVA. Error bars represent S.D. from three independent biological replicates (n=3). ns, p: nonsignificant, *, $p<0.05$, **, $p<0.005$, ***, $p<0.0005$, $^{\#\#}$, $p<0.0001$.

In silico analysis showed the presence of canonical UPRE TGACGTGG/A in the promoter of the rat *tbx20* gene (Figure 3A). To further corroborate the direct binding of Atf6 to the promoter of the *tbx20* gene, H9c2 cardiomyocytes were treated with 20 µg/ml Tun, and the DNA binding ability of Atf6 was confirmed by Chromatin immunoprecipitation (ChIP) assay. ChIP assay revealed direct binding of Atf6 to the promoter of *tbx20*, which was further corroborated by qRT-PCR, which showed Atf6 binds with 19.85 ± 2.8-fold enrichment over

immunoglobulin G (IgG) controls to the tbx20 promoter (Figure 3B, 3C). To further validate our findings, we treated H9c2 cells with Atf6-specific inhibitor 4-(2-aminoethyl) benzenesulfonyl fluoride hydrochloride (AEBSF), followed by treatment with 20 μg/ml Tun. AEBSF works by blocking the cleavage of Golgi membrane-bound Atf6, thereby hindering its nuclear translocation. Western blotting showed that AEBSF treatment followed by ER stress induction, resulted in decreased expression (0.01 ± 0.01-fold) of Atf6-p50 as compared to Tun treatment alone (2.43 ± 0.02-fold; Figure 3D, 3E). AEBSF treatment followed by ER stress induction caused a significant decrease in the expression of Tbx20 (0.21 ± 0.07-fold) as compared to ER stress induction alone (Figure 3D, 3E). Therefore, our data unravelled a novel regulatory pathway where increased expression of Tbx20 during ER stress is mediated by the Atf6 arm of UPR signaling.

4.2.4 Elevated levels of Tbx20 causes augmentation of cardiomyocyte proliferation and limits cardiomyocyte apoptosis post-ER stress

To delineate the effects of elevated Tbx20 during ER stress, we investigated the expression of proliferation and apoptosis markers, given that Tbx20 has been shown to enhance fetal cardiomyocyte proliferation (Chakraborty et al., 2013). Immunofluorescence analysis revealed a steady rise in the proliferative marker Ki67, reaching 12.4 ± 2.4% in 5 μg/ml Tun (Figure 4, Aa'' and B), 34.3 ± 5.5% in 10 μg/ml Tun (Figure 4, Aa''' and B), and 60.43 ± 4.04% in 20 μg/ml Tun-treated cells (Figure 4, Aa'''' and B), compared to the control (Figure 4, Aa and B). However, Ki67 expression declined in cells treated with 50 μg/ml Tun (Figure 4, Aa''''' and B). The Ki67 levels corresponded with the expression patterns of Tbx20 and Bmp2 signaling. We also examined Ki67 expression in response to another ER stress inducer, Tg. At 3 μM Tg (Figure 4, Fa' and G), we observed increased cardiomyocyte proliferation accompanied by elevated levels of Tbx20 and Bmp2 (Figure 2, A and B) compared to the control, although the levels decreased at 10 μM Tg concentration (Figure 4, Fa'' and G). Thus, Tbx20 enhances cardiomyocyte proliferation during ER stress.

We then investigated apoptosis markers in response to increasing ER stress. The transcription factor C/EBP homologous protein (Chop), which induces apoptosis during ER stress, was notably upregulated in cells treated with 50 μg/ml Tun (59.13 ± 4.8%; Figure 4, Ab''''' and C) relative to those treated with 20 μg/ml Tun (15.17 ± 2.8%; Figure 4, Ab'''' and C). Previous studies indicated that Chop promotes apoptosis by increasing Bax expression and decreasing Bcl_{XL} levels (Allagnat et al., 2012). An increase in Chop resulted in a corresponding rise in the pro-apoptosis marker Bax in 50 μg/ml Tun-treated cells (33.23 ± 3.2%; Figure 4,

Ac’’’’’ and D) compared to 20 µg/ml Tun-treated cells (7.03 ± 2.9%; Figure 4, Ac’’’’ and D), 10 µg/ml Tun (5.2 ± 0.8%; Figure 4, Ac’’’ and D), and 5 µg/ml Tun (2.9 ± 0.37%; Figure 4, Ac’’ and D), 2 µg/ml Tun (1.9 ± 0.85%; Figure 4, Ac’ and D), and control (1.7 ± 0.62%; Figure 4, Ac and D) cells. Conversely, the anti-apoptotic marker Bcl_{XL} decreased in the 50 µg/ml Tun-treated group (18.67 ± 6.5%; Figure 4, Ad’’’’’ and E) versus the 20 µg/ml Tun group (55.83 ± 5.1%; Figure 4, Ad’’’’ and E). Immunostaining and Western blot analysis of Chop with another ER stress inducer, Tg also demonstrated a significant increase at 10 µM Tg compared to control and 3 µM Tg-treated cells (Figure 4, F, G, H and I), where Tbx20 and Bmp2 expression decreased (Figure 2, A and B). Collectively, our findings indicate that ER stress-induced increases in Tbx20 facilitate cardiomyocyte proliferation by activating the Bmp2-pSmad1/5/8 signaling pathway. In contrast, when ER stress reaches a threshold, Tbx20 loses its protective function, leading to increased cardiomyocyte apoptosis.

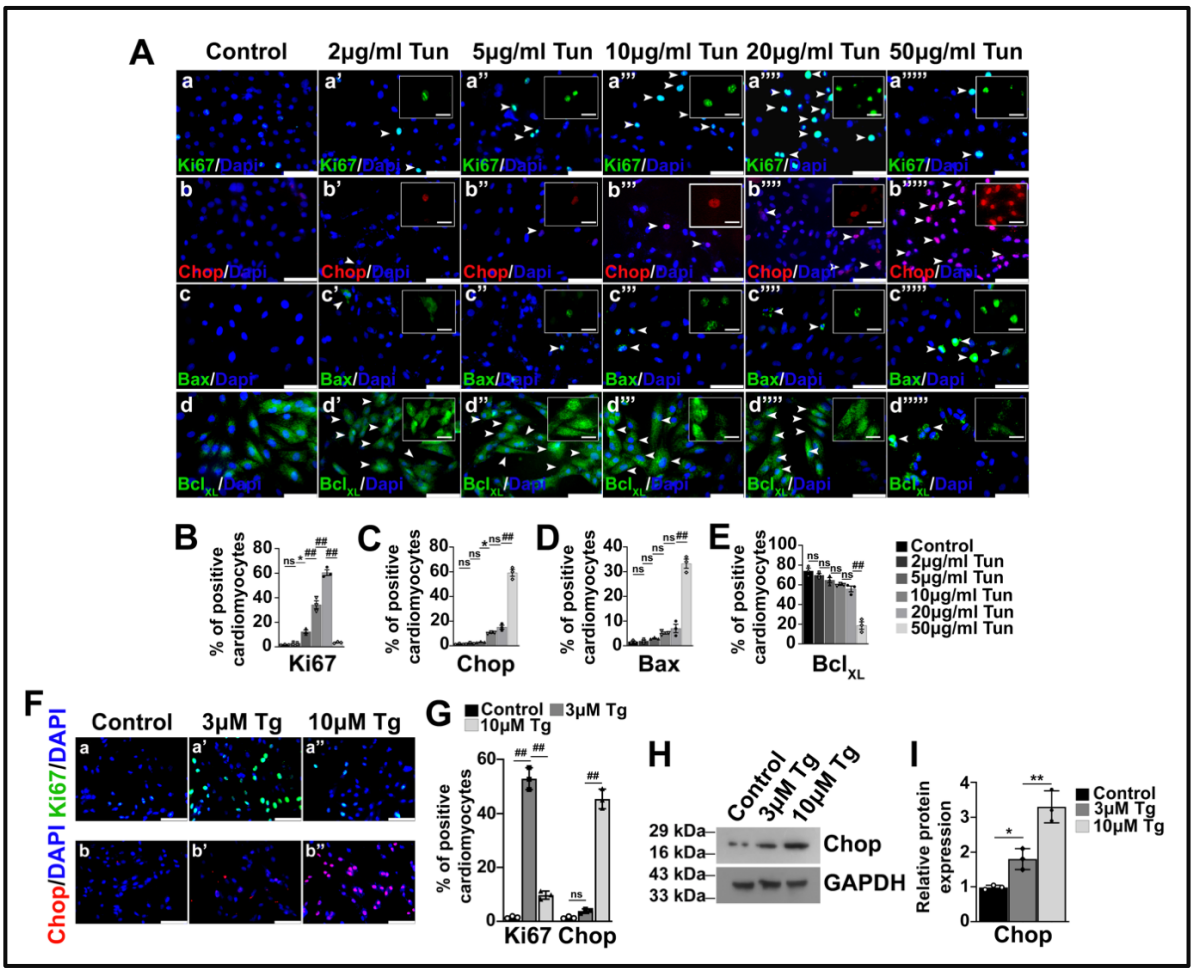

Figure 4. Endoplasmic reticulum (ER) stress induced elevation of T-box transcription factor 20 (Tbx20) augments cardiomyocyte proliferation and limits cardiomyocyte apoptosis. A. Immunofluorescence staining revealed that increase in expression of Tbx20 during ER stress is accompanied with increased expression of proliferative marker Ki67 (a’’, a’’’, and a’’’’) as compared with control (a). However, a Tun concentration of 50 µg/ml resulted in a decrease in cardiomyocyte

proliferation marked by decreased expression of Ki67 (a’’’’’). A decrease in the expression of Tbx20 is accompanied by increased cardiomyocyte apoptosis. The expression of apoptosis inducer Chop and proapoptotic marker Bax is increased upon 50 µg/ml Tun treatment (b’’’’’ and c’’’’’) in comparison to lower concentrations of Tun (b’, b’’, b’’’, and b’’’’) and (c’, c’’, c’’’, and c’’’’) respectively. The expression of antiapoptotic marker Bcl_{XL} is decreased during 50 µg/ml Tun treatment (d’’’’’) in comparison to lower concentrations of Tun (d’, d’’, d’’’, and d’’’’). Insets in A show single-channel cropped images of indicated areas (white arrows). Scale bar of the main images represents 50 µm. Scale bar of the inset represents 20 µm**. B-E**, Quantitative representation of A. **F**. Immunofluorescence staining revealed an increase in the expression of proliferative marker Ki67 in 3 µM Tg-treated cells (a’) as compared to control (a). However, in the 10 µM Tg-treated cells, the expression of Ki67 is decreased (a’’). On the contrary, the expression of apoptotic marker Chop is increased in 10 µM Tg-treated cells (b’’) as compared to control (b) and 3 µM Tg-treated cells (b’). Scale bar represents 50 µm. **G.** Quantitative representation of panel F. **H,** Western blot showing an increase in the expression of apoptotic marker Chop in 10 µM Tg-treated cells as compared to 3 µM Tg-treated and control cells. **I,** Quantitative representation by ImageJ software of the proteins from H. Statistical significance was calculated by one-way ANOVA. Error bars represent SD from (n=3) independent biological replicates. ns, p: nonsignificant, ∗p < 0.05, ∗∗p < 0.005, ∗∗∗p < 0.0005, ##p < 0.0001.

4.2.5 Elevated levels of Tbx20 suppress Reactive Oxygen Species (ROS) generation during ER stress/hyperglycemia

ER stress induced by Tun inhibits N-linked glycosylation of proteins, leading to improper maturation and stress generation (Guha et al., 2017). This increased ER stress subsequently results in ROS generation due to disrupted disulfide bonds (Bhandary et al., 2012). We observed a gradual rise in ROS production with increasing ER stress. Notably, at a Tun concentration of 50 µg/ml, where Tbx20 expression dropped significantly, ROS generation surged (Figure 5A). Prior research indicates that Tbx20 overexpression can alleviate oxidative stress (Bhattarai et al., 2021). To confirm the role of Tbx20 in reducing ROS during ER stress, we examined ROS levels after siRNA-mediated knockdown of Tbx20, followed by ER stress induction (20 µg/ml Tun). Surprisingly, knocking down Tbx20 along with inducing ER stress resulted in a significant increase in ROS levels compared to ER stress alone (Figure 5B).

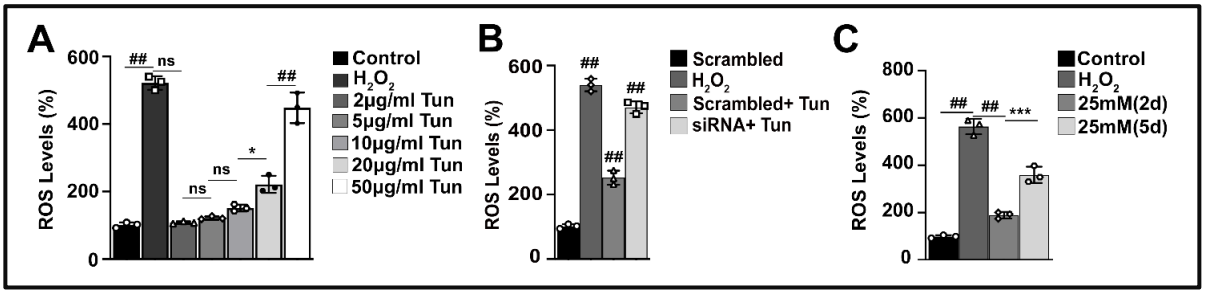

Figure 5. Increased expression of T-box transcription factor 20 (Tbx20) suppresses reactive oxygen species (ROS) generation during Endoplasmic reticulum (ER) stress/hyperglycemia. A. ER stress showed a gradual increase in the level of ROS production by the 2′,7′-dichlorofluorescin diacetate (DCFDA) method. A decrease in the expression of Tbx20 in 50 µg/ml Tun-treated cells was accompanied by a significant rise in ROS levels as compared with 20 µg/ml Tun-treated cells. **B,**

Measurement of ROS levels showed a significant increase upon knockdown of Tbx20, followed by ER stress induction. **C,** ROS levels were increased upon prolonging the hyperglycemic stress for 5 days (25 mM 5d) as compared with 2 days (25 mM 2d) and control cells. Statistical significance was calculated by one-way ANOVA. Error bars represent SD from (n=3) independent biological replicates. ns, p: nonsignificant, ∗p < 0.05, ∗∗p < 0.005, ∗∗∗p < 0.0005, ##p < 0.0001.

Additionally, Tbx20 was also shown to reduce ROS during hyperglycemic stress. A short duration of hyperglycemia (25mM 2d) did not lead to a significant rise in ROS when Tbx20 expression was high. However, prolonged hyperglycemic stress (25mM 5d) caused a notable increase in ROS generation when Tbx20 levels dropped (Figure 5C). Thus, our study demonstrates that Tbx20 plays a protective role during ER stress and hyperglycemia by suppressing ROS generation.

4.2.6 Tbx20 works upstream of Bmp2-pSmad 1/5/8 signaling and is necessary for imparting protection to cardiomyocytes during ER stress

We showed that Tbx20 accelerates cardiomyocyte proliferation via Bmp2-pSmad1/5/8 signaling. Therefore, to delineate the molecular hierarchy between Tbx20-Bmp2-pSmad1/5/8 signaling, we knocked down Tbx20 in H9c2 cardiomyocytes by Tbx20 siRNA followed by ER stress induction (20 μg/ml Tun). Western blotting revealed significant downregulation of Tbx20 upon pre-treatment with Tbx20 siRNA followed by ER stress induction. Western blot analysis showed that pre-treatment of H9c2 cells with Tbx20-specific siRNA followed by ER stress induction, resulted in a significant decrease in the expression of Tbx20 (0.18 ± 0.02-fold) as compared with Tun treatment alone (1.84 ± 0.15-fold; Figure 6, A and D). A decrease in Tbx20 followed by ER stress induction resulted in concomitant downregulation of Bmp2 (0.4 ±0.03-fold) and downstream pSmad1/5/8 (0.33 ± 0.03-fold) compared to ER stress induction alone (Figure 6, A and D). Immunostaining study showed that knockdown of Tbx20 followed by 20 μg/ml Tun treatment resulted in decreased expression of Bmp2 (4.8 ± 1.0%; Figure 6, Ea'' and F) as compared with 20 μg/ml Tun treatment alone (61.27 ± 3.0%; Figure 6, Ea' and F). Taken together, our data revealed that Tbx20 works upstream of Bmp2-pSmad1/5/8 signaling to protect cardiomyocytes during ER stress.

To substantiate the necessity of Tbx20 in imparting protection to cardiomyocytes by upregulating proliferation and limiting apoptosis, we looked into the expression of proliferative marker Ki67 and apoptosis markers Chop, Bax, Bcl_{XL} and pJNK upon knockdown of Tbx20. Knockdown of Tbx20 followed by ER stress induction resulted in a significant increase in the expression of Chop (2.67 ± 0.19-fold) as compared with ER stress treatment alone (1.4 ± 0.08-fold; Figure 6, B and D). Pre-treatment of Tbx20 siRNA followed by ER stress induction

resulted in significant upregulation of pro-apoptotic markers pJNK (9.4 ± 0.56-fold; Figure 6, B and D) and Bax (2 ± 0.24-fold; Figure 6, B and D) in comparison to ER stress induction alone (2.4 ± 0.22-fold) and (1.18 ± 0.09-fold) respectively. On the contrary, the expression of anti-apoptotic marker Bcl_{XL} decreased significantly (0.4 ± 0.09-fold; Figure 6, B and D) upon knockdown of Tbx20 followed by ER stress induction compared to ER stress induction alone and control cells. Immunostaining showed significant ablation of proliferative marker Ki67 (8.03 ± 1.0%; Figure 6, Eb'' and F) upon knockdown of Tbx20 followed by ER stress induction in comparison to ER stress induction alone (54.33 ± 4.0%; Figure 6, Eb' and F). However, the expression of apoptotic marker Chop increased up to (72 ± 4.0%; Figure 6, Ec'' and F) upon silencing Tbx20 followed by ER stress induction as compared with 20 µg/ml Tun treatment alone (8.14 ± 3.1%; Figure 6, Ec' and F).

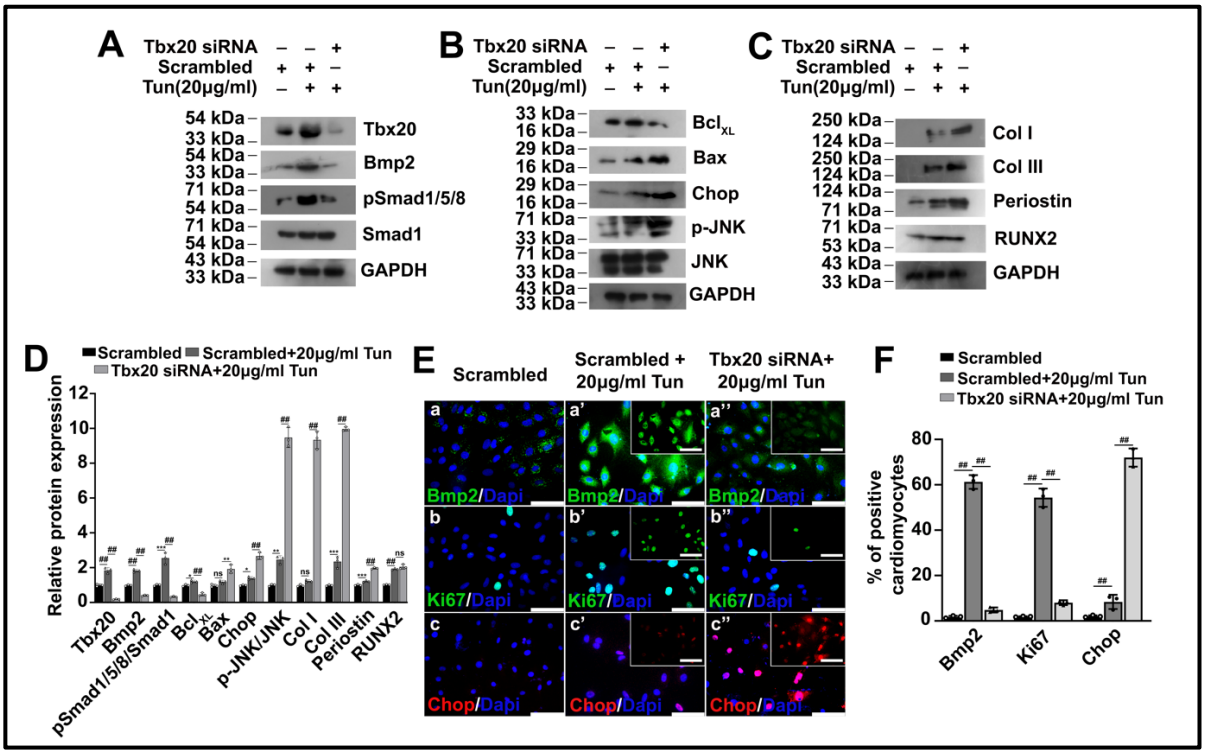

Figure 6. T-box transcription factor 20 (Tbx20) works upstream of Bmp2-pSmad 1/5/8 signaling in protecting cultured H9c2 cardiomyocytes against Endoplasmic Reticulum (ER) stress. A, Western blot analysis showing a decrease in the expression of Tbx20 upon knockdown with Tbx20 siRNA followed by ER stress induction as compared with ER stress induction alone. Knockdown of Tbx20 followed by ER stress induction resulted in a significant decrease in the expression of Bmp2 and its downstream signal transducer pSmad1/5/8. **B,** Knockdown of Tbx20 followed by ER stress induction resulted in increased cardiomyocyte apoptosis as marked by increased expression of Bax, Chop, p-JNK, and decreased expression of Bcl_{XL} as compared with Tun treatment alone. **C,** Knockdown of Tbx20 followed by ER stress induction also resulted in increased expression of fibrotic genes Collagen I (Col I), Collagen III (Col III), and Periostin. The expression of calcification marker (RUNX2) increased significantly from the control group; however, its expression between the knockdown group and the ER stress induction alone group remained unchanged. **D,** Quantitative representation by ImageJ software of the proteins from A-C. **E,** Immunofluorescence staining showing siRNA-mediated knockdown of

Tbx20 followed by ER stress induction (20 μg/ml Tun) resulted in decreased expression of Bmp2 (a'') as compared with 20 μg/ml Tun treatment alone (a') and control (a) cellsn. Knockdown of Tbx20 followed by Tun treatment is accompanied by decreased cardiomyocyte proliferation marked by decreased expression of Ki67 (b'') and increased apoptosis marked by increased expression of Chop (c'') as compared with Tun treatment alone (b' and c') and control cells (b and c), respectively. Insets in E show single-channel images of the respective makers. Scale bar of main images and insets represents 50 μm. **F**, Quantitative representation of E. Statistical significance was calculated by one-way ANOVA. Error bars represent SD from three independent biological replicates (n=3). ns, p: nonsignificant, ∗p < 0.05, ∗∗p < 0.005, ∗∗∗p < 0.0005, ##p < 0.0001.

Next, we also looked into the expression of fibrosis markers Collagen I (Col I), Collagen III (Col III) and Periostin since previously ER stress was shown to cause fibrosis (Burman et al., 2018; Lawson et al., 2011; Tanjore et al., 2013). Silencing of Tbx20 followed by ER stress induction (20 μg/ml Tun) resulted in significant abrogation in the expression of fibrosis markers Col I, Col III and Periostin (Figure 6, C and D).

Together, these data suggest that Tbx20 is located upstream of Bmp2-pSmad1/5/8 signaling axis, and it is necessary in imparting protection against ER stress by increasing cardiomyocyte proliferation and decreasing cardiomyocyte apoptosis and fibrosis, which together result in restoration of cardiomyocyte homeostasis.

4.2.7 Tbx20-Bmp2 signaling acts in a feed-forward loop mechanism in protecting cardiomyocytes against Tun-induced ER stress

We next sought to decipher the regulatory relationship between Tbx20 and Bmp2. For that, we chose a concentration of Tun (50 μg/ml) where the expression of Tbx20 and Bmp2 decreased. We treated H9c2 cells with 50 μg/ml Tun followed by ectopic overexpression of Recombinant Bmp2 (RecBmp2) protein (200 ng/ml RecBmp2). It resulted in a significant augmentation of Bmp2 protein (12.49 ± 1.4-fold) in comparison to treatment with 50 μg/ml Tun (2.1 ± 0.21-fold; Figure 7, A and B). To our surprise, RecBmp2 treatment followed by ER stress induction caused significant upregulation of Tbx20 (2.3 ± 0.23-fold) as compared to ER stress induction alone (1.2 ± 0.12-fold; Figure 7, A and B). Heightened levels of Tbx20 resulted in decreased expression of the apoptotic marker Chop upon treatment with RecBmp2 followed by ER stress induction (Figure 7, A and B). Immunofluorescence study showed that the expression of Bmp2 was increased significantly (51.83 ± 3.5%; Figure 7, Ca'' and D) in RecBmp2 and Tun group as compared with Tun treatment alone (11.07 ± 1.8%; Figure 7, Ca' and D). The expression of Tbx20 was significantly elevated by approximately 29.80 ± 2.6% (Figure 7, Cb'' and D) upon RecBmp2 and Tun treatment relative to Tun treatment alone (12.33 ± 1.6%; Figure 7, Cb' and D). Ki67 immunoreactivity, which is indicative of cardiac

proliferation, also increased by approximately 31.57 ± 2.5% (Figure 7, Cc'' and D) upon RecBmp2 and Tun treatment as compared with Tun treatment alone (2.8 ± 0.3%; Figure 7, Cc' and D). However, RecBmp2 and Tun treatment resulted in a significant decrease in the expression of apoptosis inducer Chop by approximately 24.03 ± 2.1% (Figure 7, Cd'' and D) as compared with only Tun treatment (61.37 ± 2.5%; Figure 7, Cd' and D).

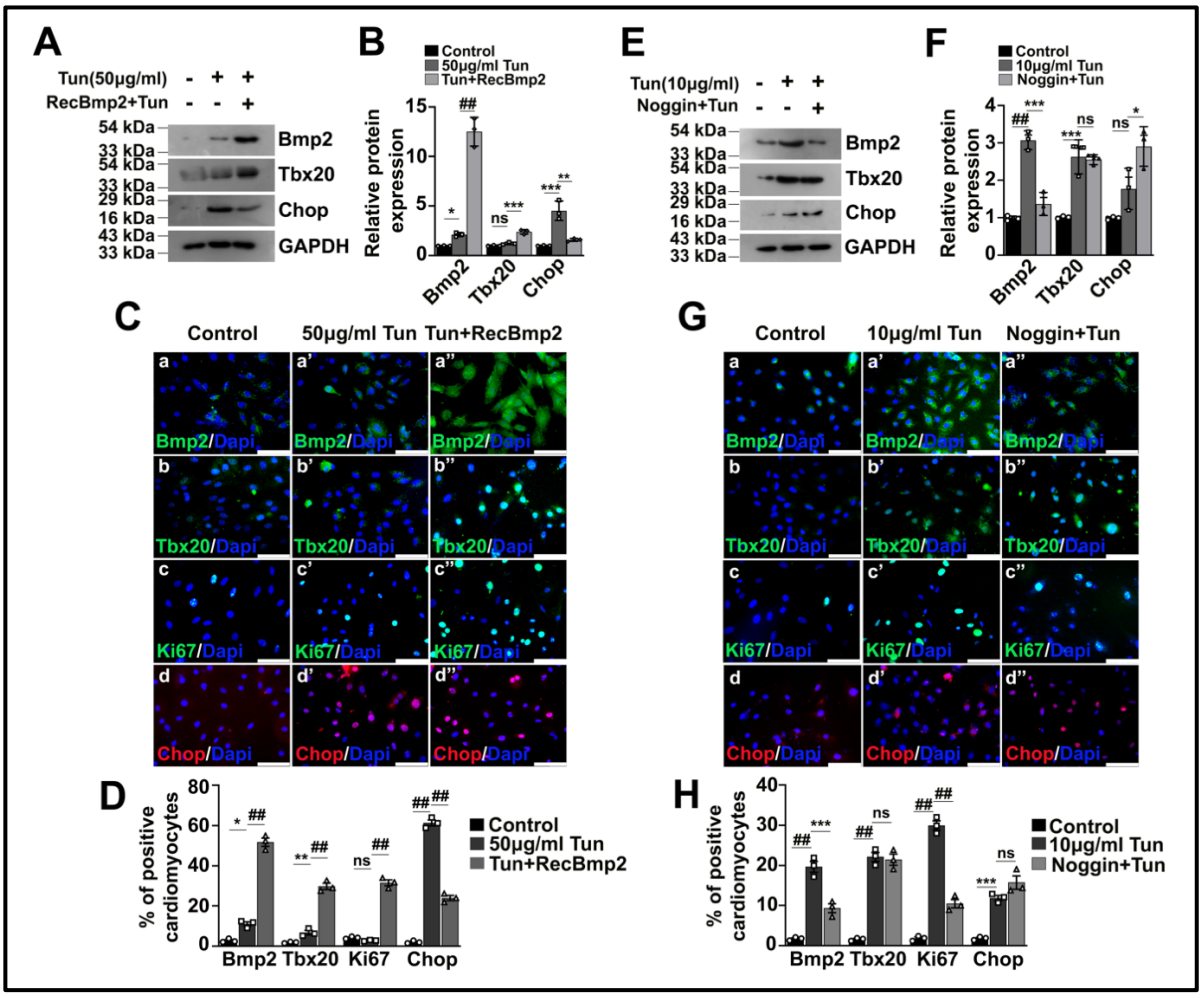

Figure 7. Tbx20-Bmp2 signaling acts in a feed-forward loop mechanism to protect cultured H9c2 cardiomyocytes against Endoplasmic Reticulum (ER) stress. A, Western blot analysis of H9c2 cells treated with 50 µg/ml Tun followed by administration of Recombinant Bmp2 (RecBmp2), showing a significant increase in the expression of Bmp2 even during increased ER stress. Administration of RecBmp2 protein following ER stress induction resulted in a significant increase in the expression of Tbx20 as compared to the 50 µg/ml Tun-treated group. Treatment of the ER stressed cells with RecBmp2 resulted in a decrease in the expression of the apoptotic marker Chop. **B,** Quantitative representation by ImageJ software of the proteins from A. **C,** Immunofluorescence staining showing that RecBmp2 treatment following ER stress induction (50 µg/ml Tun) increased the expression of Bmp2 (a'') and Tbx20 (b'') in comparison to 50 µg/ml Tun treatment alone (a' and b') and control cells (a and b), respectively. Increase in Bmp2 expression is accompanied by increased expression of Ki67 (c'') and decreased expression of Chop (d'') as compared with 50 µg/ml Tun treatment alone (c' and d') and control cells (c and d), respectively. **D,** Quantitative representation of panels in C. **E,** Western blot analysis of H9c2 cells treated with Bmp2 inhibitor Noggin followed by ER stress induction (10 µg/ml Tun), caused a significant decrease in the expression of Bmp2 as compared with the ER stress

induction group alone. Treatment with Noggin followed by ER stress induction, however, caused no significant change in the expression of Tbx20 from the ER stress induction alone group. **F,** Quantitative representation by ImageJ software of the proteins from E. **G,** Immunostaining of H9c2 cells treated with Bmp2 inhibitor Noggin followed by Tun treatment (10 μg/ml Tun) showing ia decrease in the expression of Bmp2 (a'') with reference to 10 μg/ml Tun treatment alone (a') and control cells (a). Noggin treatment followed by ER stress induction caused no significant change in the expression of Tbx20 (b'') as compared with ER stress induction alone (b'). Noggin administration followed by Tun treatment resulted in a significant decrease in the expression of proliferative marker Ki67 (c'') as compared with the Tun treatment alone group (c'). The expression of apoptosis inducer Chop, however, remained unchanged between the Noggin administered group (d'') as compared with the Tun treatment alone (d'). **H,** Quantitative representation of panels in G. Scale bar represents 50 μm. Statistical significance was calculated by one-way ANOVA. Error bars represent SD from three independent biological replicates (n=3); ns, p: nonsignificant, $*p < 0.05$, $**p < 0.005$, $***p < 0.0005$, $##p < 0.0001$.

To further corroborate the feed-forward relationship between Tbx20 and Bmp2, we treated H9c2 cells with Bmp2 inhibitor Noggin protein, followed by ER stress induction with 10 μg/ml Tun. Interestingly, though the concentration of Bmp2 decreased upon treatment with Noggin followed by ER stress induction (Figure 7, E, F, G and H), the levels of Tbx20 remained unaltered as evidenced by both Western blotting and Immunofluorescence staining thus substantiating that Tbx20 functions upstream of Bmp2 during ER stress (Figure 7, E, F, G and H). The study also shows the existence of a feed-forward loop between Tbx20 and Bmp2, wherein overexpressing Bmp2 can augment the expression of Tbx20 during ER stress. The expression of proliferative marker Ki67 decreased significantly upon inhibition of Bmp2 by Noggin, thus corroborating the fact that Bmp2 drives cardiomyocyte proliferation during ER stress (Figure 7, G and H). Western blotting and immunofluorescence staining showed unaltered expression of apoptotic marker Chop upon treatment with Noggin followed by ER stress induction (Figure 7, E, F, G and H), thus further strengthening our findings that Tbx20 negatively regulates apoptotic response during ER stress.

These results are consistent with our previous observation (Figure 6) that Tbx20 is located upstream of Bmp2 in imparting protection against ER stress by increasing cardiomyocyte proliferation. These data also indicate the fact that exogenous administration of Bmp2 can impart protection during increased ER stress by increasing cardiomyocyte proliferation by a positive feed-forward mechanism.

4.2.8 Tbx20 upregulates Atf6 arm of UPR via a feedback loop mechanism

The simultaneous decrease of Tbx20 and Atf6-p50 during increasing ER stress (50 μg/ml Tun) intrigued us to look into the regulatory relationship between the two. Previously, we showed that Tbx20 is upregulated during ER stress by the Atf6 arm of UPR signaling. However, to our surprise, knockdown of Tbx20 followed by ER stress induction (20 μg/ml

Tun) also resulted in significant downregulation of Atf-p50 as evidenced by both Western blotting (Figure 8, A and B) and Immunofluorescence staining (Figure 8, C and D). *In silico* analysis revealed the presence of a Tbx20 binding site in the promoter of the *atf6* gene (Figure 8E). ChIP assay followed by qRT-PCR showed Tbx20 binds to the *atf6* promoter with 7.3 ± 1.2-fold enrichment over IgG controls (Figure 8, F and G). Therefore, our study showed that Tbx20 helps in maintaining the pool of Atf6 during ER stress via a feedback loop mechanism by directly binding and upregulating its expression.

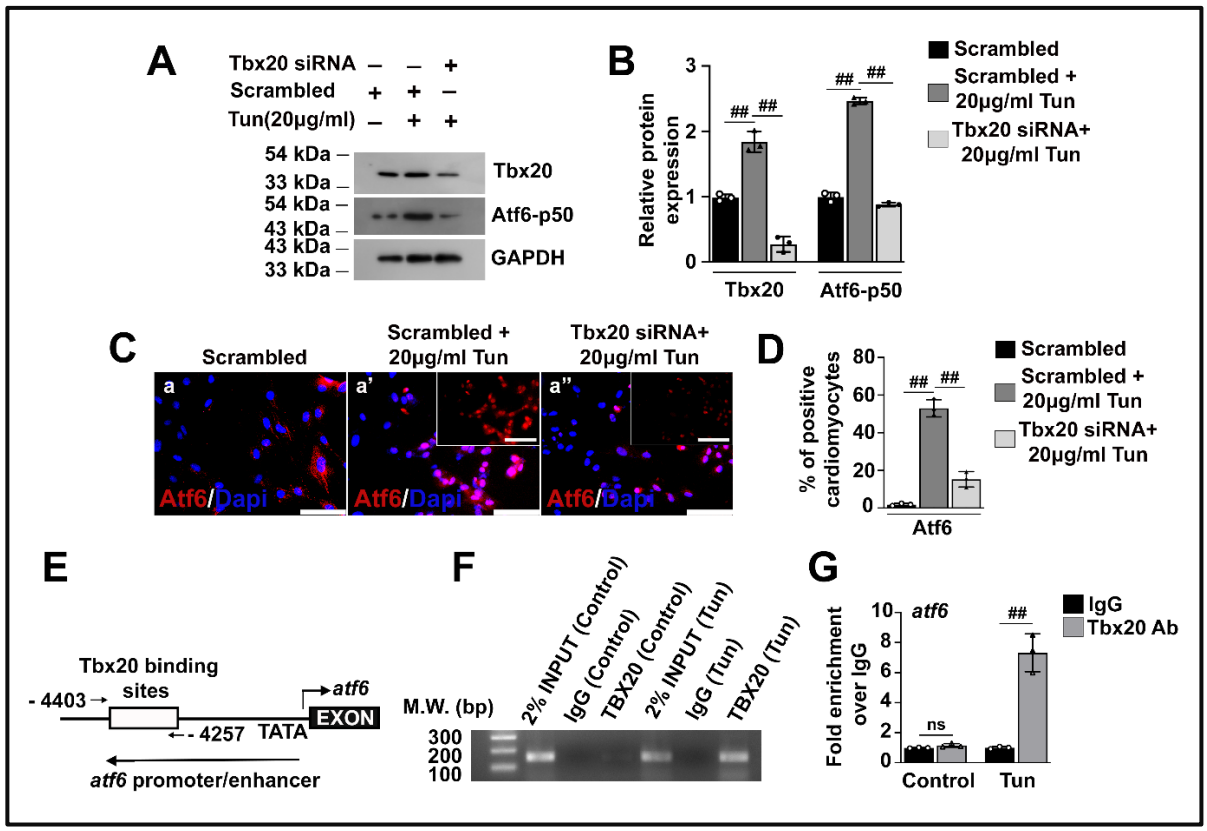

Figure 8. T-box transcription factor 20 (Tbx20) upregulates Activating transcription factor 6 (Atf6) arm of Unfolded Protein Response (UPR) via a feedback loop mechanism. A, Western blot analysis showing a decrease in the expression of Tbx20 upon knockdown with Tbx20 siRNA followed by ER stress induction as compared with ER stress induction alone. Knockdown of Tbx20 followed by ER stress induction, resulted in a significant decrease in the expression of Atf6. **B,** Quantitative representation by ImageJ software of the proteins from A. **C,** Immunofluorescence staining showed that knockdown of Tbx20 followed by Tun treatment resulted in decreased expression of Atf6 (a'') as compared with Tun treatment alone (a') and control cells (a). Insets in E show single channel images of the respective makers. Scale bar of main images and insets represents 50 µm. **D,** Quantitative representation of panels in C. **E,** Bioinformatics analysis revealed the presence of a canonical binding sequence for Tbx20 in the promoter of rat *atf6* gene **F,** Chromatin immunoprecipitation (ChIP) assay followed by PCR analysis revealed that Tbx20 binds to *atf6* promoter and induces its activity during ER stress induced by Tun. **G,** Tbx20 binds to the promoter of *atf6* with 7.3±1.2-fold enrichment over IgG controls during ER stress induced by Tun.. Statistical significance was calculated by one-way ANOVA. Error bars represent SD from three independent biological replicates (n=3); ns, p: nonsignificant, ∗p < 0.05, ∗∗p < 0.005, ∗∗∗p < 0.0005, ##p < 0.0001.

4.2.9 ER stress results in upregulation of Tbx20 and Bmp2 in rodent heart *in vivo*

Next, we wanted to look into the expression profile and role of Tbx20 and Bmp2 during ER stress in rodent hearts *in vivo*. For ER stress induction, we treated the animals (both mice and rats) with 1 mg/kg body weight of Tun. We harvested the heart tissue at 8 hours (short duration) and 2 days (prolonged) to corroborate the *in vitro* results.

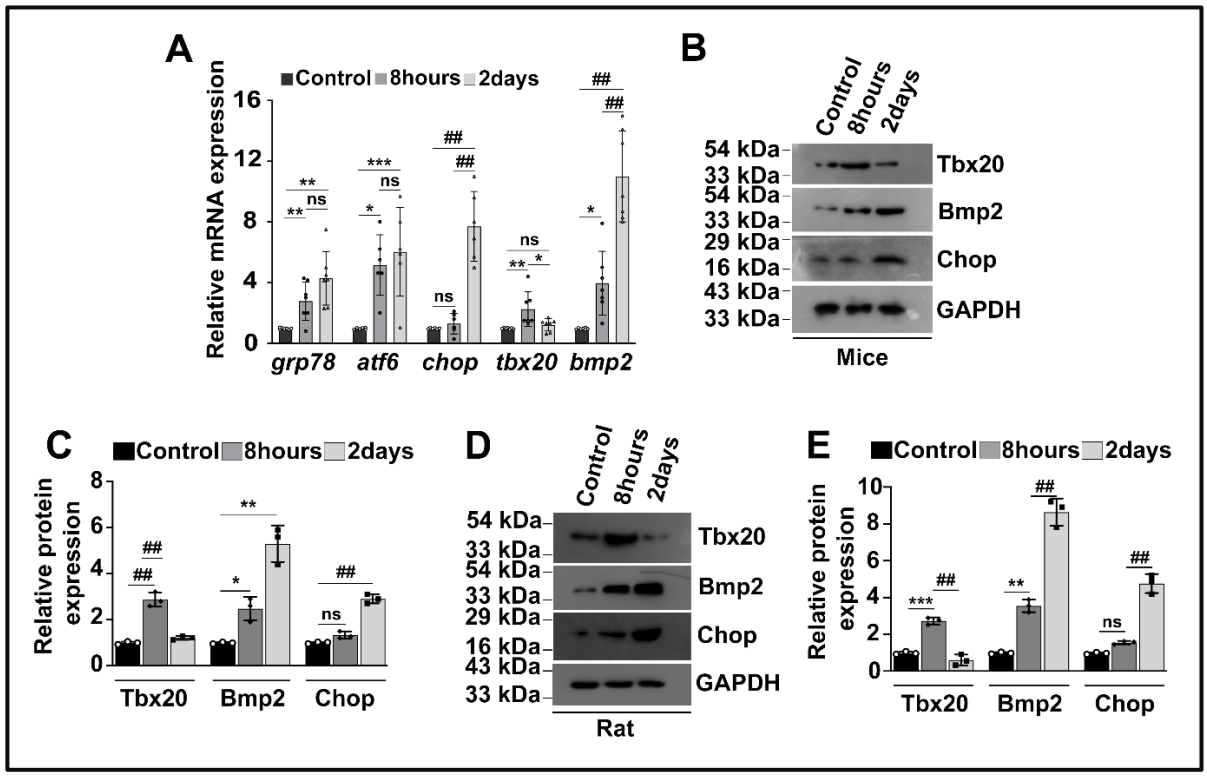

Figure 9. Endoplasmic reticulum (ER) stress causes upregulation of T-box transcription factor 20 (Tbx20) and Bone morphogenetic protein 2 (Bmp2) in the rodent heart *in vivo*. A, ER stress induction for short duration (8hours) and prolonged (2days) resulted in an increase in the expression of ER stress markers *grp78* and *atf6* compared with the control group as determined by qRT–PCR. The expression of apoptosis inducer *chop* increased significantly in the prolonged ER stress (2 days) group as compared with 8 hours and control groups. The change in expression of *chop* between 8 hours and the control group was non-significant. The expression of *tbx20* and *bmp2* increased during ER stress induction for a short duration (8 hours) as compared with control; however, the expression of *bmp2* increased significantly in the 2 days ER stress-induced group. **B,** Western blot analysis of Tbx20 in mice showed a significant increase in its expression in 8 hours Tun-treated group as compared with the control group. The expression of Tbx20 later decreased significantly in the 2 days group. The expression of Bmp2 increased significantly during 2 days as compared with 8 hours Tun-treated group. The expression of apoptotic marker Chop increased significantly in the 2 days group as compared with 8 hours and control groups. **C,** Quantitative representation by ImageJ software of the proteins from B. **D,** Western blot analysis showing a decrease in the expression of Tbx20 in rats upon prolonged ER stress (2 days) as compared to ER stress induction for 8 hours. The expression of Bmp2, however, increased significantly between 8 hours and 2 days group. **E,** Quantitative representation by ImageJ software of the proteins from D. Error bars represent SD from at least three independent biological replicates. Statistical significance was calculated by one-way ANOVA. ns, p: nonsignificant, $*p < 0.05$, $**p < 0.005$, $***p < 0.0005$, $\#\#p < 0.0001$; $n \geq 3$ independent experiments.

The establishment of ER stress was checked by qRT-PCR of ER stress markers *grp78* and *atf6*. The expression of *tbx20* was increased at mRNA level in the 8 hours group in comparison to the control. However, prolonging the ER stress to 2 days resulted in significant downregulation of *tbx20*. The expression of *bmp2* also increased significantly in 8 hours group, however, *bmp2* showed a drastic increase in the 2 days group (Figure 9A).

Western blotting in both mice and rats showed a significant upregulation of Tbx20 during 8 hours; however, its expression later decreased in the 2 days group (Figure 9, B, C, D, E). Similarly, Bmp2 at the protein level corroborated with the mRNA results. Bmp2 increased significantly during the 8 hours ER stress induction group, and its expression increased robustly in the 2 days group (Figure 9, B, C, D and E). Therefore, our study showed increased expression of Tbx20 *in vivo* during ER stress induced for a short duration (8 hours). However, prolonging the ER stress (2 days) resulted in decreased activity of Tbx20. Bmp2, on the contrary, showed a gradual increase throughout ER stress induction *in vivo.*

These results are consistent with the *in vitro* results. ER stress induction for a shorter interval leads to the upregulation of Tbx20 and the protective ER stress component Atf6. Prolonging the ER stress eventually leads to a decrease in the expression of Tbx20. A non-significant increase in the expression of Atf6 in the prolonged ER stress group might be attributed to the fact that the heart is composed of a heterogeneous population of cells as compared with a pure cardiomyocyte population of H9c2 cells; hence, the expression of Atf6 might be regulated by factors other than Tbx20 in murine heart. The drastic increase of Bmp2 in the prolonged ER stress group may also be due to the heterogeneity of the adult rodent heart.

4.2.10 ER stress-induced upregulation of Tbx20 and Bmp2 maintains cardiac homeostasis by regulating cardiomyocyte proliferation and apoptosis *in vivo*

To decipher the role of increased Tbx20 and Bmp2 during ER stress in cardiomyocytes, we looked into the expression of proliferative and apoptotic markers. Colocalization of Tbx20 and $Mf20^{+}$ (cardiomyocyte-specific marker) showed significant elevation of Tbx20 in cardiomyocytes upon ER stress induction for 8 hours (32 ± 6.6%; Figure 10, Aa' and B) compared to control (5.02 ± 2.2%; Figure 10, Aa and B). However, prolonged ER stress (2 days) resulted in the downregulation of Tbx20 (13.64 ± 3.2%; Figure 10, Aa'' and B) in cardiomyocytes in comparison to 8 hours. An increase in Tbx20 resulted in a simultaneous increase in the downstream molecule Bmp2 in cardiomyocytes during short-term ER stress

generation (Figure 10, Ac' and D) compared to control (Figure 10, Ac and D). Its expression later decreased during prolonged ER stress in cardiomyocytes (Figure 10, Ac'' and D).

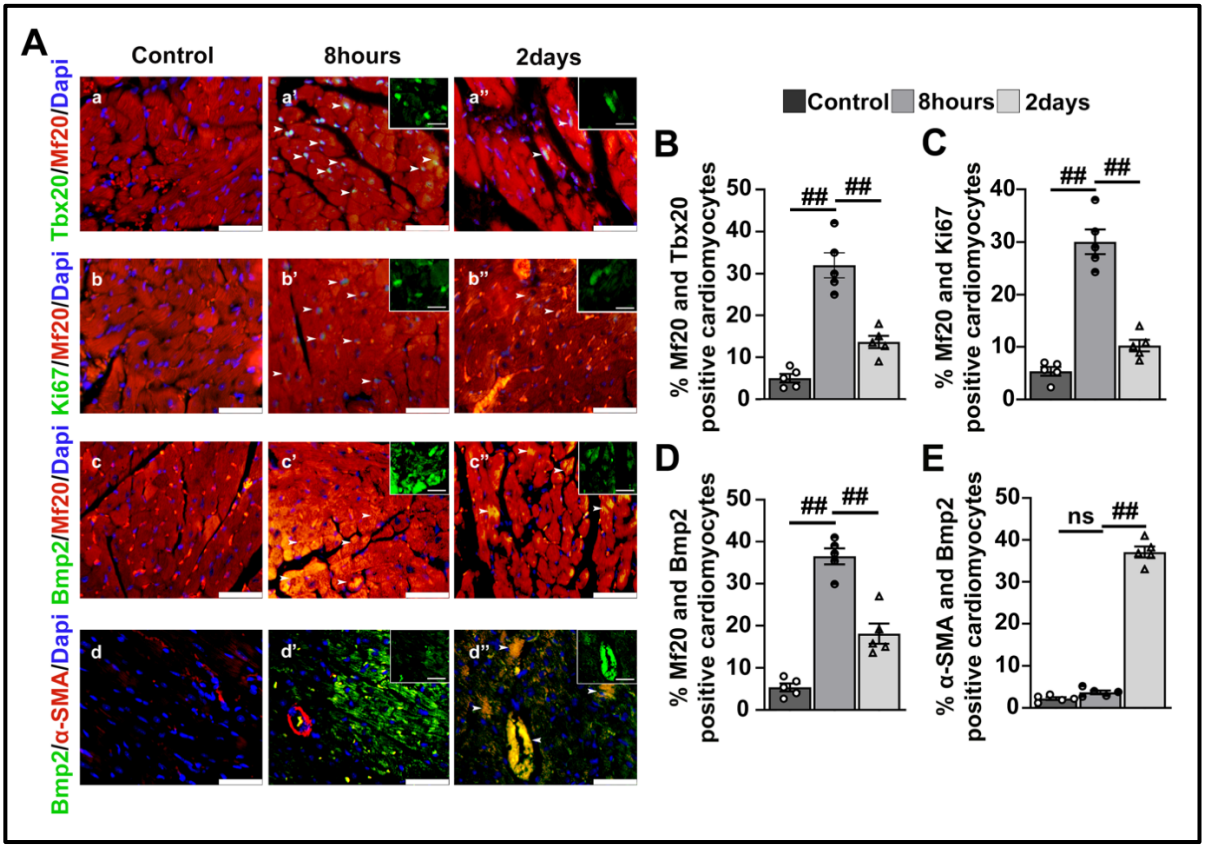

Figure 10. Endoplasmic reticulum (ER) stress–mediated upregulation of Tbx20-Bmp2 signaling results in increased cardiomyocyte proliferation and limits cardiomyocyte apoptosis in adult murine hearts. A, ER stress induction for short duration (8 hours) resulted in cardiomyocyte-specific increase in the expression of Tbx20 (a') marked by Tbx20-positive nuclei (green) co-labelled with cardiomyocyte-specific Mf20 (red) compared with control (a). However, a prolonged ER stress resulted in a decrease in the expression of Tbx20 (a''). The expression of proliferation marker Ki67 increased significantly, as marked by increased Ki67-positive nuclei (b'; green) co-labelled with cardiomyocyte-specific Mf20 (red) during 8 hours of ER stress induction compared with control (b). Prolonged ER stress (2 days) resulted in decreased expression of Ki67 (b'') compared with 8 hours ER stress induction group. Cardiomyocyte-specific expression of Bmp2 was increased in 8 hours of ER stress (c') as compared with control (c). However, its expression later decreased during 2 days ER stress (c'') induction group. Bmp2 was shown to colocalize with α-SMA with increased expression during prolonged ER stress (d'') condition as compared with 8 hours ER stress (d') and control (d) groups. **B-E,** Quantitative representation of panels in A. Scale bar of the main images represents 50 μm. Scale bar of the inset represents 20 μm. Statistical significance was calculated by one-way ANOVA. Error bars represent SD from at least three independent biological replicates (n≥3); ns, p: nonsignificant, ∗p < 0.05, ∗∗p < 0.005, ∗∗∗p < 0.0005, ##p < 0.0001.

Elevated levels of Tbx20 and Bmp2 during 8 hours of ER stress resulted in a concomitant increase of cardiomyocyte proliferation as evidenced by increased activity of Ki67 (30.06 ± 5.2%; Figure 10, Ab' and C) compared to control (5.36 ± 1.8%; Figure 10, Ab and C). The Ki67 activity later decreased during prolonged ER stress (10.24 ± 2.4%; Figure 10, Ab'' and

C), which is suggestive of decreased proliferation because of the decrease in Tbx20. Therefore, in accordance with the *in vitro* results, the expression of Tbx20 and Bmp2 increased during ER stress induced for a short duration (8 hours) with a concomitant increase of cardiomyocyte proliferation *in vivo*. However, prolonging the ER stress (2 days) caused suppression of Tbx20 and Bmp2 activity in cardiomyocytes with a simultaneous decrease in cardiomyocyte proliferation. Thus, upregulation of Tbx20-Bmp2 signaling drives cardiomyocyte proliferation of adult murine hearts post-ER stress.

The heart tissue is composed of a myriad of cell types, and according to our data, the increase of Bmp2 in cardiomyocytes during ER stress is mediated by Tbx20. Therefore, we speculated that the drastic elevation of Bmp2 during the 2 days ER stress group, both at the mRNA level and protein level, is due to other cell types and not cardiomyocytes. Colocalization of Bmp2 and α-SMA (myofibroblast-specific marker) showed increased expression of Bmp2 in fibroblasts during prolonged ER stress (37.08 ± 2.9%; Figure 10, Ad'' and E) as compared to 8 hours ER stress group (3.7 ± 0.9%; Figure 10, Ad' and E). Therefore, these observations imply that the increase in Bmp2 is attributed to cell types other than cardiomyocytes, and the cause and consequence of this increase will be discussed in subsequent chapters.

Taken together, these observations further strengthen our hypothesis that there is a fine balance between ER stress-induced survival and death. ER stress induction for a short interval leads to upregulation of Tbx20, which eventually causes increased cardiomyocyte proliferation because of increased expression of Bmp2 and limits cardiomyocyte apoptosis. However, a prolonged ER stress abrogates the expression of Tbx20, resulting in decreased proliferation and increased cardiomyocyte apoptosis, which leads to disruption of the homeostasis, eventually leading to cardiomyocyte death.

4.2.11 Tbx20 is necessary to suppress hypertrophy and fibrosis during ER stress *in vivo*

Prolonged ER stress induction (2 days) resulted in significant morphological abnormalities like hypertrophy (increased cardiomyocyte size) and fibrosis (increased collagen deposition) compared to 8 hours and the control group. 2 days of ER stress resulted in a significant increase in heart weight (HW)/body weight (BW) ratio (6.27 ± 0.36 mg/g) compared to 8 hours (4.92 ± 0.55 mg/g) and control (4.42 ± 0.45 mg/g) group (Figure 11A). Similar to murine heart, ER stress induction in rats resulted in a significant increase in the HW/BW ratio upon prolonging the stress response as compared to short duration of ER stress and control groups (Figure 11B). Prolonged ER stress caused increased cardiomyocyte cell size as

evidenced by Wheat Germ Agglutinin (WGA) staining. The cardiomyocyte cell size increased up to 363.3 ± 35.74 μm^2 in the 2 days ER stress group (Figure 11C) compared to 8 hours (211.3 ± 36.89 μm^2; Figure 11C) and control group (165 ± 14.93 μm^2; Figure 11C). The change in cell size between 8 hours and the control group was non-significant. Next, we looked into the fibrosis level in the heart upon ER stress induction. Masson's Trichrome staining showed increased collagen deposition (an indicator of fibrosis) in the hearts of the 2 days ER stress group compared to the 8 hours and control group (Figure 11D).

Therefore, a decreased level of Tbx20 during prolonged ER stress is accompanied by increased cell size and collagen deposition in the heart *in vivo*.

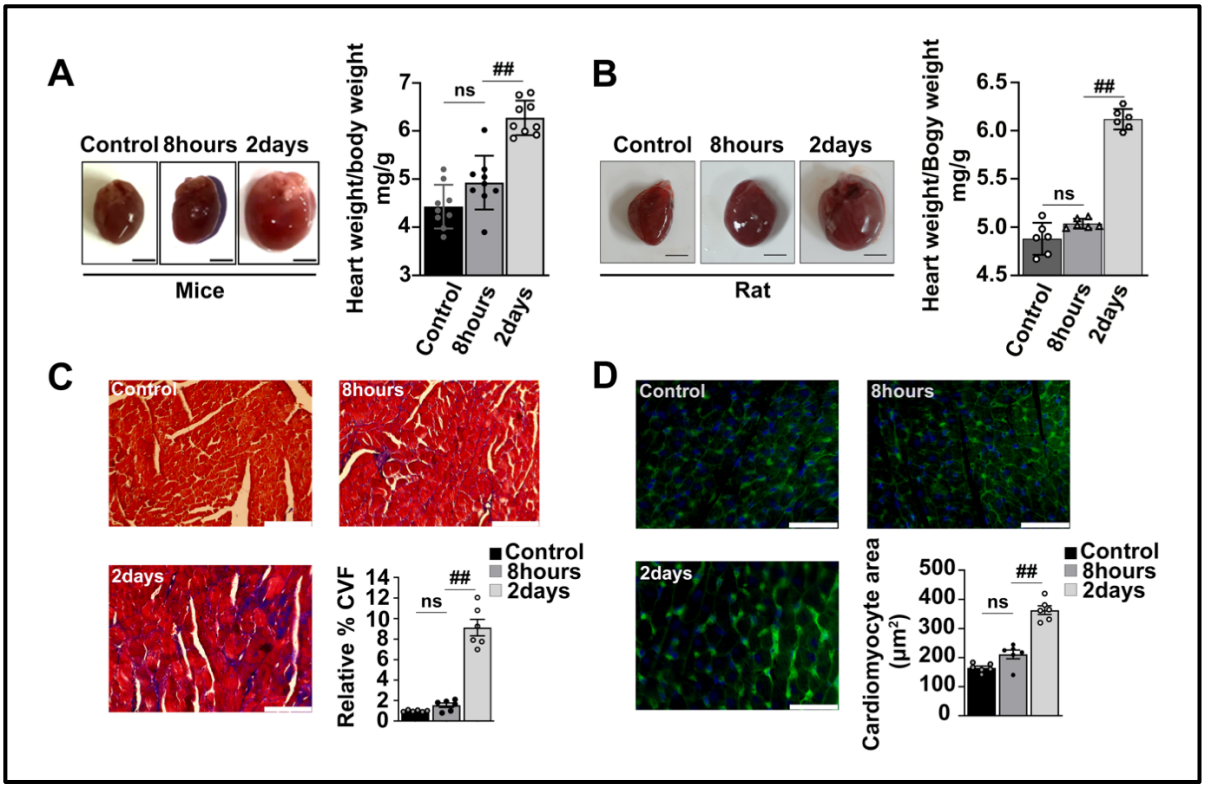

Figure 11. T-box transcription factor 20 (Tbx20) suppresses hypertrophy and fibrosis during ER stress *in vivo*. A, The heart weight to body weight ratios indicative of cardiac hypertrophy are increased significantly during prolonged (2 days) ER stress as compared with ER stress induction for short duration (8 hours) and the control group in murine hearts. The change in heart weight to body weight ratio between 8 hours of ER stress and the control group was non-significant (n=9). Scale bar represents 20 μm. **B,** Prolonged ER stress induction (2 days) in rats results in a significant increase in heart weight/body weight ratio as compared to ER stress induction for short duration (8 hours) and the control group. Scale bar represents 20 μm. **C,** Prolonged (2 days) ER stress results in increased collagen deposition indicative of cardiac fibrosis, as shown in Masson's trichrome-stained adult heart sections as compared with 8 hours ER stress group and control group (n = 6). **D,** During prolonged (2 days) ER stress induced adult mice, cardiomyocyte cell size is increased, marked by wheat-germ agglutinin (WGA) staining (green) in comparison to 8 hours ER stress group and control group, respectively (n=6). Scale bar represents 50 μm. Error bars represent SD from at least three independent biological replicates. Statistical significance was calculated by one-way ANOVA. ns, p: nonsignificant, ∗p < 0.05, ∗∗p < 0.005, ∗∗∗p < 0.0005, ##p < 0.0001; n≥3 independent experiments.

4.2.12 Tbx20 is necessary to maintain cardiac function during ER stress *in vivo*

To delineate the necessity of Tbx20 in maintaining cardiac function *in vivo* during ER stress, we looked into the expression of cardiac function markers brain natriuretic peptide (*bnp*), β-myosin heavy chain (*β-mhc*), and sarcoendoplasmic reticulum calcium ATPase 2 (*serca2*). Previous studies have shown *bnp* and *β-mhc* as diagnostic markers for cardiac dysfunction, and cardiac *serca2* was reported as a therapeutic target for heart failure (Cao et al., 2019).

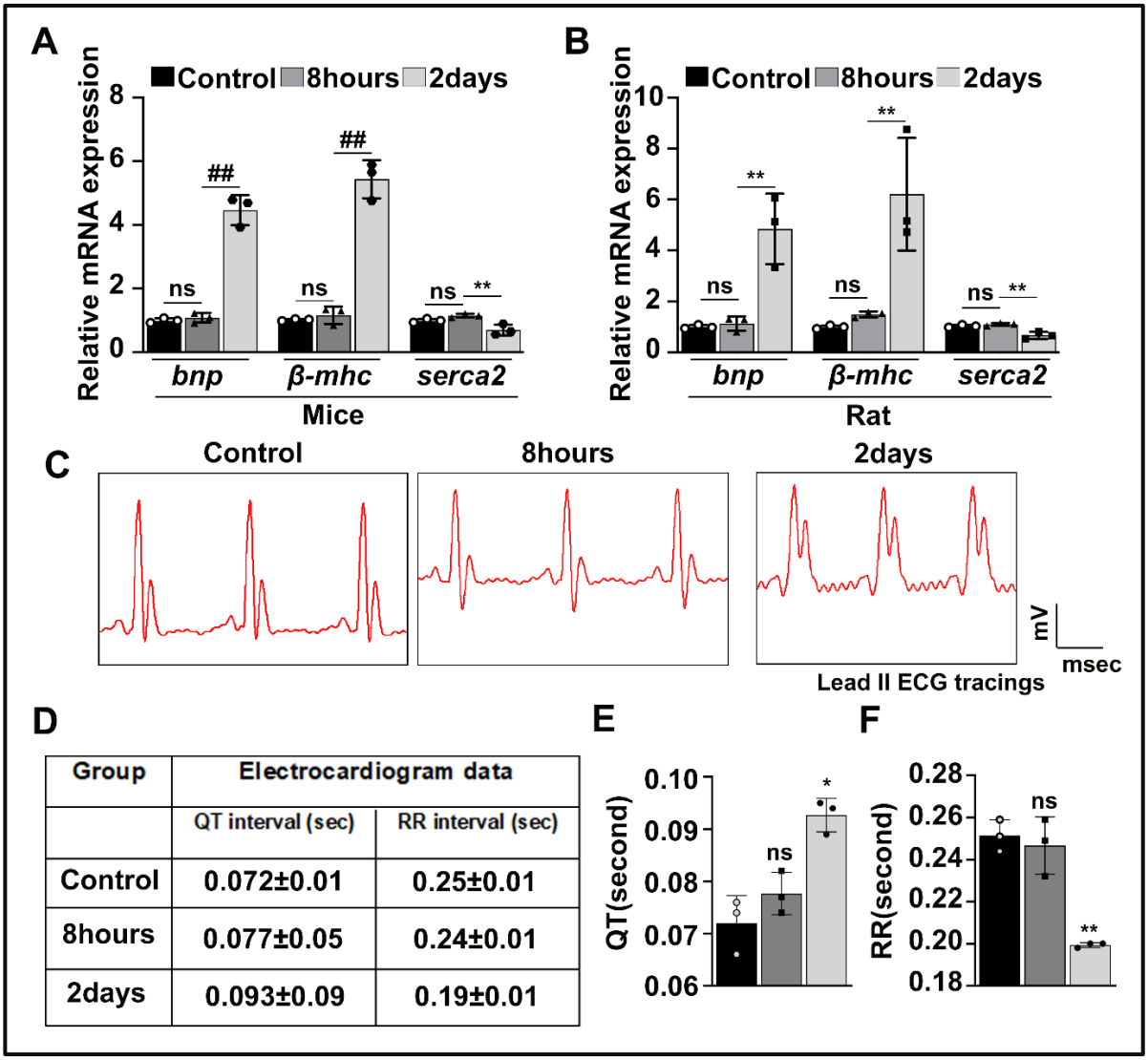

Group	Electrocardiogram data	
	QT interval (sec)	RR interval (sec)
Control	0.072±0.01	0.25±0.01
8hours	0.077±0.05	0.24±0.01
2days	0.093±0.09	0.19±0.01

Figure 12. T-box transcription factor 20 (Tbx20) maintains cardiac function during Endoplasmic reticulum (ER) stress *in vivo*. A, Quantitative RT–PCR (qRT–PCR) analysis showing that prolonged (2 days) ER stress induction resulted in a significant increase in the expression of cardiac function markers *bnp* and *β-mhc* and a significant decrease in the expression of *serca2* as compared with 8 hours ER stress induction and control groups in murine heart. **B,** qRT–PCR analysis showed that prolonged (2 days) ER stress induction resulted in a significant increase in the expression of cardiac function test markers *bnp* and *β-mhc* and a significant decrease in the expression of *serca2* as compared with 8 hours ER stress induction and control groups in rat heart. **C,** Electrocardiograph (ECG) analysis showing altered cardiac function in 2 days Tun-treated group with elevated ST segment as compared to 8 hours

and the control group. **D and E,** Electrocardiograph (ECG) analysis showing altered cardiac function in 2 days Tun-treated group with increased QT interval as compared to the 8 hours and control group. **D and F,** Electrocardiograph (ECG) analysis showing altered cardiac function in the 2 days Tun-treated group with decreased RR interval as compared to the 8 hours and control group. Statistical significance was calculated by one-way ANOVA. Error bars represent SD from three independent biological replicates (n=3); ns, p: nonsignificant, ∗p < 0.05, ∗∗p < 0.005, ∗∗∗p < 0.0005, ##p < 0.0001.

Our study reported upregulation of *bnp* and *β-mhc* mRNA during 2 days of ER stress induction compared to 8 hours and control (Figure 12A). The expression of a therapeutic target of cardiomyopathy, *serca2* decreased significantly during 2 days of ER stress in comparison to 8 hours and the control group (Figure 12A). Therefore, the expression of cardiac function markers is altered significantly in the 2 days ER stress group, where the expression of Tbx20 was also reduced. We observed a similar expression profile of the cardiac function genes in rat hearts (Figure 12B).To further corroborate the importance of Tbx20 in maintaining proper cardiac function, we performed an Electrocardiograph (ECG) of rodents following ER stress induction. ECG recordings showed a significant increase in QT interval (0.093 ± 0.01s) in the 2 days group compared to the 8 hours (0.077 ± 0.01s) and control (0.072 ± 0.01s) groups (Figure 11, C, D and E). The RR interval showed a significant decrease in the 2 days (0.19 ± 0.01s) group compared to the 8 hours (0.24 ± 0.01s) and control (0.25 ± 0.01s) group (Figure 11, C, D and E). The 2 days ER stress group also displayed a significant elevation of the ST segment in comparison to the 8 hours and control group (Figure 11C). Therefore, these observations further potentiate the necessity of Tbx20 in maintaining proper cardiac function during ER stress.

4.2.13 Diabetes/Hyperglycemia-induced upregulation of Tbx20 drives cardiomyocyte proliferation

Diabetic heart disease is responsible for about 80% of deaths in people suffering from diabetes. Among the multiple causes for the pathogenesis of diabetes, ER stress is one such factor that is involved in cardiomyocyte apoptosis in streptozotocin-induced Type 1 diabetic rats as well as during hyperglycemia (Back & Kaufman, 2012; Li et al., 2007). Therefore, to validate our findings in an actual disease condition, we corroborated the results in both diabetes and hyperglycemia conditions. *In vivo,* the establishment of ER stress during diabetes was validated by Western blotting of Atf6 (4.9 ± 0.2-fold; Figure 13, B and C) and Grp78 (3.35 ± 0.5-fold; Figure 13, B and C). Diabetic cardiomyopathy resulted in significant upregulation of *tbx20* and *bmp2* at the mRNA level (Figure A). Western blotting showed that the expression of Tbx20 was increased by (4.4 ± 0.2-fold) during diabetes as compared to control (Figure 13,

B and C). Bmp2 was also increased significantly during diabetes (2.9 ± 0.5-fold) with reference to control (Figure 13, B and C). Thus, diabetes-induced ER stress is accompanied by a concomitant increase in the expression of Tbx20 and Bmp2. Treatment of H9c2 cardiomyocytes with a high concentration of glucose (25 mM) for 2 days (25 mM 2d) resulted in a significant increase in the expression of Tbx20 (4.3 ± 0.5-fold) and Bmp2 (4.4 ± 0.4-fold) compared to control. However, prolonging the hyperglycemic stress for 5 days (25 mM 5d) resulted in a significant decline in the expression of Tbx20 (1.4 ± 0.3-fold) and Bmp2 (2.7 ± 0.4-fold) (Figure 13, D and E).

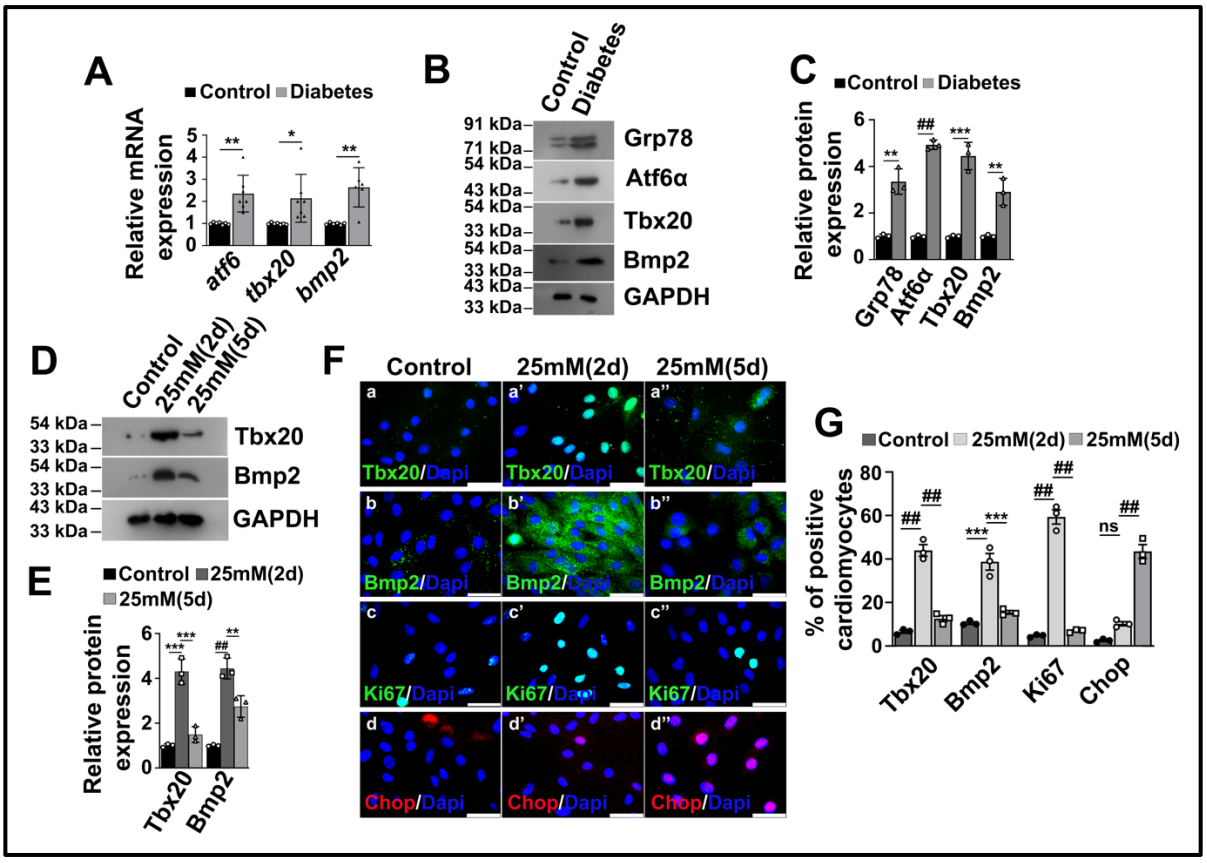

Figure 13. Diabetes/Hyperglycemia-induced upregulation of T-box transcription factor 20 (Tbx20) increases cardiomyocyte proliferation. A, Quantitative RT–PCR (qRT–PCR) analysis showing that induction of diabetes in mice resulted in increased expression of *atf6*, *tbx20*, and *bmp2*. **B,** Western blot analysis showing an increase in the ER stress markers Grp78 and Atf6-p50 upon diabetes induction as compared with control. The expression of Tbx20 and Bmp2 is also increased during diabetes. **C,** Quantitative representation by ImageJ software of the proteins from B. **D,** Western blot analysis showed an increase in the expression of Tbx20 and Bmp2 during hyperglycemia induced for 2 days (25mM 2d). Prolonging the hyperglycemic stress for 5 days (25mM 5d) resulted in a decrease in the expression of Tbx20 and Bmp2**. E,** Quantitative representation by ImageJ software of the proteins from D. **F,** Immunofluorescence staining showing an increase in the expression of Tbx20 (a') and Bmp2 (b') upon hyperglycemia induction for 2 days in comparison to respective controls (a and b). However, prolonging the hyperglycemia (5 days) resulted in a decrease in their expression (a'' and b''). Increase in Tbx20 resulted in a concomitant increase in cardiomyocyte proliferation marked by increased Ki67 (c') as compared with control cells (c). However, prolonging the stress resulted in a decrease in its expression (c''). Prolonged hyperglycemic stress resulted in increased cardiomyocyte apoptosis marked

by increased Chop (d'') expression compared with hyperglycemic stress for 2 days (d') and control. Scale bar represents 50 μm. **G,** Quantitative representation of panels in F. Statistical significance was calculated by one-way ANOVA for three independent biological experiments (n=3). Error bars represent SD from three independent biological replicates. ns, p: nonsignificant, ∗p < 0.05, ∗∗p < 0.005, ∗∗∗p < 0.0005, ##p < 0.0001.

Immunofluorescence staining showed a similar upregulation pattern of Tbx20 and Bmp2 on hyperglycemia induction for 2 days. However, their expression decreased upon prolonging the stress for 5 days (Figure 13, F and G). An increase in the expression of Tbx20 and Bmp2 was accompanied by a concomitant increase of cardiomyocyte proliferation as evidenced by elevated activity of Ki67 during 2 days (59.37 ± 5.7%, Figure 13, Fc' and G) as compared to control (4.66 ± 0.6%; Figure 13, Fc and G). Prolonging the stress response to 5 days caused significant ablation of Ki67 activity (6.92 ± 0.8%; Figure 13, Fc'' and G). On the contrary, the expression of Chop increased significantly during 5 days of hyperglycemia stress (57.97 ± 5.5%; Figure 13, Fd'' and G) in comparison and 2 days stress and control groups. Therefore, prolonged hyperglycemia-mediated ablation of Tbx20 and Bmp2 results in decreased cardiomyocyte proliferation and increased cardiomyocyte apoptosis.

4.3 Discussion

The neonatal heart is highly proliferative; however, with the onset of adulthood, the proliferative capacity of cardiomyocytes ceases as they exit the cell cycle. The limited proliferation of adult cardiomyocytes is one of the main reasons for cardiomyopathy, as the proliferative cardiomyocytes are unable to make restitution for their loss due to injury or stress, and eventually, they are replaced by fibrotic tissues. In our study, we showed ER stress/diabetes-mediated upregulation of Tbx20-Bmp2-pSmad/5/8 signaling results in an elevation in the proliferative capacity of cardiomyocytes, thereby restoring homeostasis. We also showed that Tbx20 maintains homeostasis by upregulating the cardioprotective Atf6 arm of UPR signaling. The critical balance between ER stress-induced cardiomyocyte proliferation and cardiomyocyte apoptosis is essential for driving the cardioprotective function of Tbx20. Prolonging the stress response is associated with decreased expression of Tbx20, and the cause and consequence of the decrease will be discussed in subsequent chapters. Our study showed a persistent and significant increase in the expression of Bmp2 throughout ER stress progression *in vivo.* Since the adult heart is composed of multiple cell types, and in cardiomyocytes we observed a decrease in the expression of Bmp2 upon prolonging ER stress, therefore, we speculated that the increase in the expression of Bmp2 is attributed to other cell

types of the heart. The factors responsible for the gradual increase of Bmp2 throughout disease progression will also be discussed in subsequent chapters.

Since the adult heart lacks proliferative capacity, reinitiating the proliferation of existing cardiomyocytes by modulating the signaling pathway molecules can serve as an effective therapeutic approach for combating cardiomyopathy (Senyo et al., 2013). Tbx20, a cardiac transcription factor, was previously shown to drive adult cardiomyocyte proliferation via inhibiting the cell cycle inhibitors *btg2*, *p21*, and *meis1* post-myocardial infarction, thus making it a crucial mediator of cardiomyocyte proliferation post-stress or injury (Xiang et al., 2016). In another study, Bmp2 was shown to protect cardiomyocytes from ischemia/reperfusion stress via upregulating the Smad1 pathway (Masaki et al., 2005). However, the fact that Tbx20 and Bmp2 play a pivotal role in driving cardiomyocyte proliferation post-ER stress inflicted injury was not known. Our study, for the first time, showed the novel regulatory mechanism whereby ER stress-induced augmentation of Tbx20 drives cardiomyocyte proliferation in both adult mice hearts and H9c2 cardiomyocytes via the Bmp2-pSmad1/5/8 pathway, thereby restoring cardiac homeostasis. Previously, multiple studies have shown the importance of Tbx20 and Bmp2 in reducing fibrosis of tissues. Whereas knockdown of Tbx20 results in extensive fibrosis of the heart in a short duration, overexpression of Tbx20 causes a reduction in fibrotic scar tissue formation (Shen et al., 2011; Xiang et al., 2016). Bmp2 was also shown to reduce fibrosis of liver and renal interstitial cells (Chung et al., 2018; Yang et al., 2011). Here in our study, we showed that in addition to upregulating cardiomyocyte proliferation during ER stress, Tbx20 also restore cardiac homeostasis by restricting the levels of fibrotic markers. In this study, we also showed that though Bmp2 acts downstream of Tbx20 in inducing cardiomyocyte proliferation, it can also impart a synergistic effect on Tbx20 via a feed-forward loop mechanism to further augment cardiomyocyte proliferation. Lastly, we corroborated our results in the actual disease condition, diabetes and observed a similar protective role of Tbx20 and Bmp2 by augmenting cardiomyocyte proliferation. Thus, taken together, our study unveiled a novel regulatory mechanism of Tbx20 and Bmp2-mediated cardiac protection during ER stress by reinitiating cardiomyocyte proliferation (Figure 14).

ER stress results from the progressive accumulation of misfolded or unfolded proteins in the ER, eventually leading to the upregulation of UPR. Among the three pathways of UPR, Atf6 is considered hugely cardio-protective, as multiple studies have highlighted its role in ameliorating cardiac diseases. Here in our study, we provide evidence of the cardioprotective role of Atf6 by increasing the expression of cardiac transcription factor Tbx20 during ER stress.

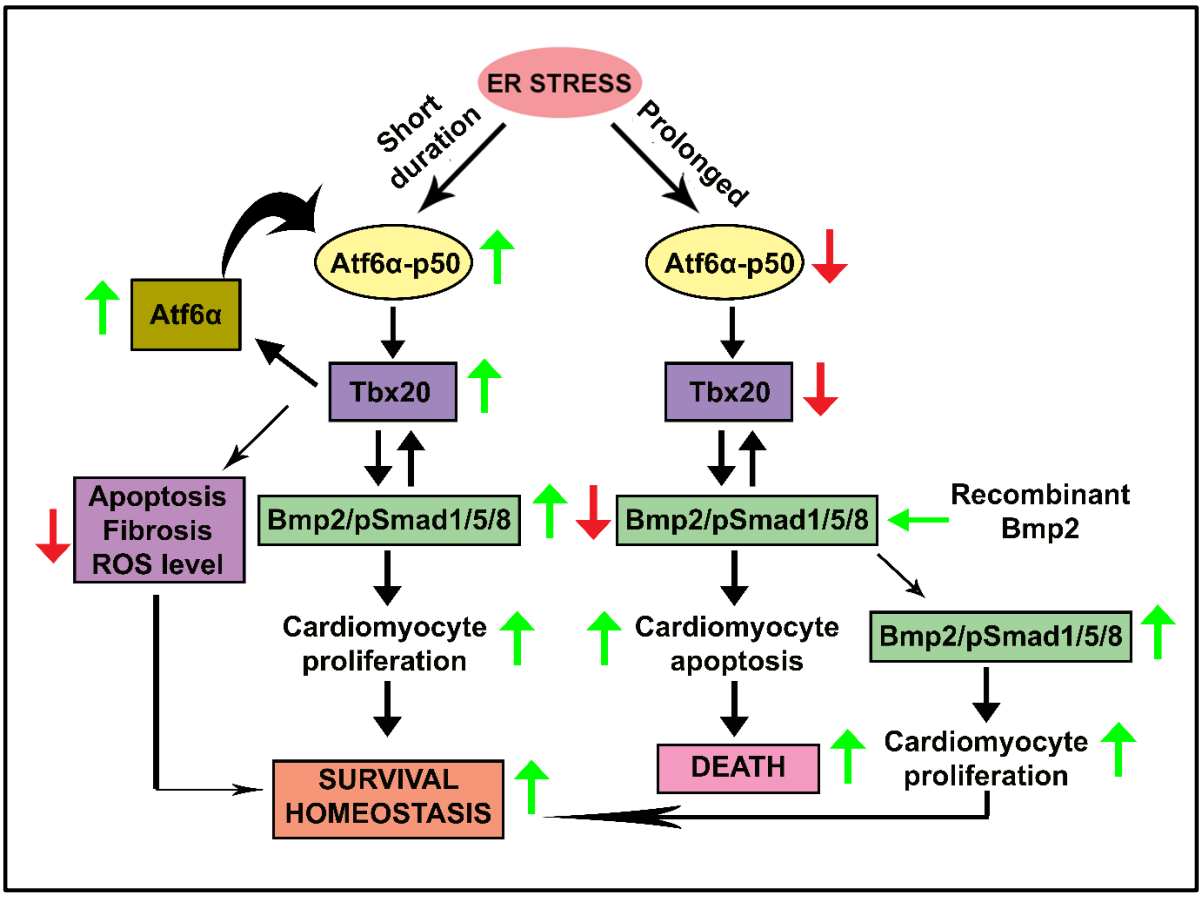

Figure 14. Model for endoplasmic reticulum (ER) stress–mediated upregulation of T-box transcription factor 20 (Tbx20), resulting in increased cardiomyocyte survival. ER stress induction for a short interval results in upregulation of the activating transcription factor 6 (Atf6) pathway of unfolded protein response (UPR). Full-length Atf6 is cleaved (Atf6-p50), and it translocates to the nucleus where it increases the transcription of Tbx20. Increase in the level of Tbx20 results in upregulation of its downstream signaling cascade consisting of bone morphogenetic protein 2 (Bmp2)–pSmad1/5/8. Increased expression of Bmp2–pSmad1/5/8 further results in increased cardiomyocyte proliferation, thereby restoring homeostasis and increasing the survival of cardiomyocytes post ER stress induction. Tbx20 also helps in the restoration of homeostasis by decreasing apoptosis, fibrosis, and reactive oxygen species (ROS) levels during ER stress. Increased expression of Tbx20 during ER stress also helps to maintain the total pool of Atf6 during ER stress. A prolonged ER stress, however, results in decreased expression of cleaved Atf6 (Atf6-p50). This in turn results in a decrease in the expression of Tbx20, and its downstreams Bmp2–pSmad1/5/8 signaling molecules, resulting in decreased cardiomyocyte proliferation and increased cardiomyocyte apoptosis. Ectopic administration of recombinant Bmp2 protein results in upregulation of Bmp2, which in turn upregulates Tbx20 in a feed-forward mechanism, thereby restoring homeostasis by increasing cardiomyocyte proliferation.

We showed direct binding of Atf6 to the *tbx20* promoter, which was further corroborated by treatment with Atf6 inhibitor AEBSF that inhibits the cleavage and nuclear localisation of active Atf6 (Atf6-p50). We also showed the existence of a feedback mechanism between Atf6 and Tbx20, where ChIP analysis revealed direct binding of Tbx20 to the *atf6* promoter, which was further corroborated by siRNA-mediated knockdown of Tbx20. Tbx20 is a cardiac transcription factor that plays a pivotal role in proper cardiac development. Deletion of Tbx20

in cardiomyocytes is associated with embryonic lethality, whereas its loss of function causes a double outlet right ventricle and familial tetralogy of fallot (Huang et al., 2017; Pan et al., 2015). On the contrary, overexpression of Tbx20 results in cardiomyocyte proliferation post-myocardial infarction (Xiang et al., 2016). All these studies highlight the importance of Tbx20 in maintaining cardiac homeostasis. Our study showed that with a decrease in the expression of Tbx20 during prolonged ER stress, there is an alteration of cardiac function as evidenced by increased QT interval, decreased RR interval and elevated ST segment in the electrocardiograph. QT prolongation is associated with malignant arrhythmia and sudden cardiac arrest (Nachimuthu et al., 2012). Whereas decreased RR interval is indicative of increased heart rate, and elevation of the ST segment results due to hypertrophy and acute myocardial infarction (Bahler et al., 1983; Coppola et al., 2013). Since our study reported an alteration of all these established markers of cardiac function upon decreased expression of Tbx20 during prolonged ER stress, therefore our study establishes Tbx20 as a critical factor in maintaining proper cardiac function during ER stress.

ER stress has been associated with the pathogenesis of diabetes, as the ER is an organelle responsible for the folding of proinsulin. Hyperglycemia, a causative factor of diabetes mellitus, was shown to disrupt ER homeostasis, thereby causing ER stress (Back & Kaufman, 2012). Chronic hyperglycemia causes β-cell dysfunction by decreasing Atf6α/Ire1α, resulting in disruption of homeostasis (Walters et al., 2013). In our study, we observed an elevation of ER stress markers during diabetes. The expression of Tbx20 and Bmp2 is also elevated during hyperglycemia with concomitant upregulation of cardiomyocyte proliferation. However, the effect was reversed upon prolonging the hyperglycemic stress, and it resulted in increased cardiomyocyte apoptosis. Therefore, our study showed a novel role of Tbx20 and Bmp2 signaling in imparting cardiomyocyte proliferation during diabetes.

Previously, ER stress was shown to induce ROS generation due to cleavage of the disulfide bonds (Cao & Kaufman, 2014; Zeeshan et al., 2016). Our study also showed a persistent increase in ROS production with the increase in ER stress. However, at a Tun concentration of 50μg/ml, when the expression of both Tbx20 and Bmp2 decreased in cardiomyocytes, the ROS generation increased significantly, and the increase was almost equivalent to the positive control. Tbx20 was shown to limit ROS generation in cardiomyocytes (T. Shen et al., 2013). Our study showed that ablation of Tbx20 during stress was associated with increased ROS generation. Therefore, our study further potentiated the role of Tbc20 as a

driving factor in limiting ROS generation during short-duration stress, thereby maintaining cardiac homeostasis.

In summary, our research indicated that the Tbx20-Bmp2 signaling pathway, mediated by ER stress, helps to restore cardiac balance by promoting the proliferation of cardiomyocytes and reducing apoptosis. Thus, overexpressing Tbx20 or specifically inducing Bmp2 in cardiomyocytes may represent a promising therapeutic strategy for promoting survival in cases of ER stress-induced cardiomyopathy.

Chapter 5

*MiR-101-3p mediated regulation of Tbx20 in cardiomyocytes and Bmp2 in cardiac fibroblasts perturb cardiac homeostasis**

Results from this section is *Under Communication

5.1 Background and Significance of the Study

The importance of cardiogenic transcription factor Tbx20 in driving cardiomyocyte proliferation during ER stress and diabetes via the Bmp2-pSmad 1/5/8 pathway was established in our previous study (Das et al., 2023). However, prolonging the stress resulted in a significant decrease in Tbx20 with a concomitant decrease in cardiomyocyte proliferation. We also observed a persistent and significant elevation of Bmp2 throughout the progression of ER stress. This altered expression of Tbx20 and Bmp2 during prolonged stress led us to discern the plausible factors involved.

In recent times, non-coding RNAs (miRNAs, lncRNAs, circRNAs, etc) have gained immense recognition due to their multi-functional role in different physiological and pathological processes. Among them, microRNAs (miRNAs) play a major role in regulating the expression of a myriad of genes during different diseases like cancer, neurodegenerative diseases, and cardiovascular diseases (Zhou et al., 2018). Multiple studies have shown the involvement of miRNAs in aggravating CVDs, thus making them potential candidates for diagnostic biomarkers and therapeutic targets. Another interesting feature of miRNA is that a single miRNA can regulate the expression of multiple messenger RNAs (mRNAs), thus exacerbating the disease progression (Ikeda et al., 2007). The major features of miRNAs, like stability, sensitivity and sequence specificity, make them ideal candidates for the development of biomarkers (Condrat et al., 2020).

In our study, *in silico* analysis showed the presence of miR-101-3p binding site in the 3' untranslated region (3'UTR) of the *tbx20* gene. Although Bmp2 did not possess miR-101-3p binding sites in its 3'UTR, we observed the presence of miR-101-3p seed sequence in the 3'UTR of the *bmp2* inhibitor noggin (*nog*) gene. Numerous studies have shown the widespread involvement of miR-101-3p in the progression of CVDs. In one study, suppression of miR-101-3p was shown to impart protection against myocardial injury (Bakhshi et al., 2024). Another research study indicated that suppressing miR-101-3p resulted in a reduction of calcification in aortic valve interstitial cells (Chen et al., 2023). Furthermore, miR-101-3p was found to be elevated in the peripheral blood of individuals who have experienced a myocardial infarction (Bakhshi et al., 2024). However, to this point, there have been no studies that have established any correlation between miR-101-3p and Tbx20 or Bmp2 in the context of any disease. Therefore, our study for the first time will unravel the novel role of miR-101-3p as a plausible biomarker regulating the function of cardiac genes to aggravate cardiomyopathy.

In the previous chapter, we showed that a decrease in the expression of Tbx20 during prolonged ER stress was accompanied by a subsequent decrease in cardiomyocyte proliferation. Therefore, we looked into the expression of senescent genes in this study. Senescence is a phenomenon that is characterized by cell-cycle arrest of metabolically active cells in response to endogenous or exogenous stress (Huang et al., 2022). Senescence can be replicative, which generally occurs due to telomere shortening, or it can be premature, which is triggered by stress stimuli (Victorelli & Passos, 2017). Senescent cells often display senescence-associated secretory phenotype (SASP), which is characterized by upregulation and secretion of different matrix metalloproteases and inflammatory molecules like IL-6, IL-11, CXCL1, CXCL2 and M-CSF. These increased SASP factors, in turn, affect the neighbouring cells, thereby adding to the severity of the disease (Han et al., 2024). Multiple studies have shown that the accumulation of senescent cardiac cells is often associated with exacerbation of both the onset as well as the outcome of CVDs. In our study, for the first time, we will show how miR-101-3p mediated regulation of Tbx20 drives cardiac senescence, thereby leading to a detrimental outcome. The discovery of this novel unknown pathway could be exploited further to develop new therapeutics to reduce the burden of senescent cardiac cells, thereby ameliorating cardiomyopathy.

Another unanswered question that has been addressed in this chapter is the persistent and significant increase of Bmp2 throughout the progression of cardiomyopathy. Prolonging stresses like ER stress, Diabetes, Type 2 Myocardial Infarction (T2MI), and High-Fat diet resulted in a similar persistent rise in the levels of Bmp2. We for the first time will show how miR-101-3p indirectly regulates Bmp2 by directly targeting Bmp2 inhibitor Nog, resulting in increased inflammatory response. Our study also showed Bmp2 as a potential candidate for the early detection of CVDs.

Taken together, our study will unwind a novel regulatory pathway where we will show how cross-talk between miR-101-3p, Tbx20 and Bmp2 drives cardiac senescence and inflammation during prolonged cardiac stresses. We will also establish miR-101-3p and Bmp2 as plausible biomarkers for detecting CVDs.

5.2 Results

5.2.1 Prolonged stresses (ER stress, Diabetes, T2MI, High-Fat diet) results in attenuation of Tbx20 with concomitant upregulation of Bmp2 *in vivo*

ER stress was induced by intraperitoneal injection of Tunicamycin (Tun), and the heart tissue was collected after 8 hours (short-duration) and 2 days (prolonged) (Figure 1A). Western blotting showed an initial increase of Tbx20 during the short duration of ER stress (3.22 ± 0.3-fold; Figure 1, B and C). However, prolonging the ER stress resulted in significant attenuation in the expression of Tbx20 (1.29 ± 0.32-fold; Figure 1, B and C). On the contrary, the expression of Bmp2 remained persistently and significantly increasing throughout the progression of ER stress (Figure 1, B and C). To further assess the expression of Tbx20 and Bmp2 during other stresses, we induced diabetes *in vivo* by intraperitoneal injection of Alloxan.

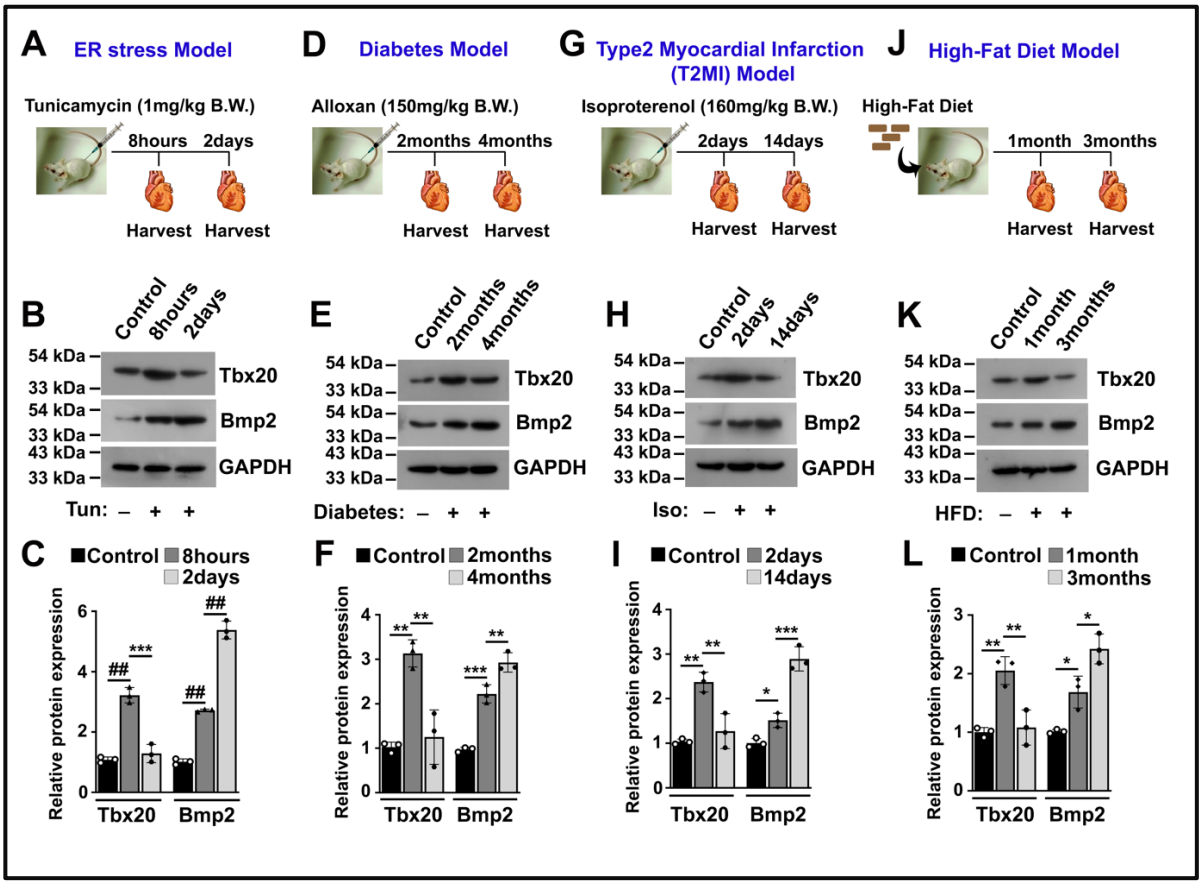

Figure 1. Prolonging Endoplasmic Reticulum (ER) stress, Diabetes, Type 2 Myocardial Infarction (T2MI) and High-Fat diet results in attenuation of T-box transcription factor 20 (Tbx20) with simultaneous upregulation of Bone morphogenetic protein 2 (Bmp2) *in vivo*. A, Schematic diagram of ER stress induction *in vivo*. **B,** Western blot analysis showing an increase in the activity of Tbx20 and Bmp2 in short duration (8 hours) ER stress group. Prolonged (2 days) ER stress caused a significant decrease in Tbx20, whereas the expression of Bmp2 increased significantly. **C,** Quantitative representation of proteins from B. **D,** Schematic diagram of diabetes induction *in vivo*. **E,** Western blot analysis showing elevation of Tbx20 and Bmp2 during diabetes-induced for a shorter duration (2

months). However, prolonging diabetes (4 months) caused decreased expression of Tbx20 and increased expression of Bmp2. **F,** Quantitative representation of proteins from E. **G,** Schematic diagram of T2MI induction *in vivo*. **H,** Western blot analysis showing increased activity of Tbx20 and Bmp2 in the short duration (2 days) T2MI group. Prolonged (14 days) T2MI resulted in a significant decrease in the activity of Tbx20, whereas the expression of Bmp2 increased. **I,** Quantitative representation of proteins from H. **J,** Schematic diagram of High Fat diet administration *in vivo*. **K,** Western blot analysis showing increased activity of Tbx20 and Bmp2 in the short duration (1 month) High-Fat diet administration group. A prolonged (3 months) High-Fat diet resulted in a significant decrease in the activity of Tbx20, whereas the expression of Bmp2 increased. **L,** Quantitative representation of proteins from K. Statistical significance was calculated by one-way ANOVA. Error bars represent SD from three independent biological replicates (n=3); ns, p: nonsignificant, $*p < 0.05$, $**p < 0.005$, $***p < 0.0005$, $##p < 0.0001$.

and we harvested the heart tissue at 2 months (short-duration) and 4 months (prolonged) (Figure 1D). Alloxan induces insulin-dependent diabetes by destroying the pancreatic beta cells, thereby causing insulin deficiency and hyperglycemia, which are typical characteristics of Type 1 Diabetes (Queiroz et al., 2021). Similar to ER stress, diabetes-induced for short duration resulted in a significant increase in the expression of Tbx20 (3.1 ± 0.3-fold) and Bmp2 (2.22 ± 0.21-fold; Figure 1, E and F). However, prolonged diabetes resulted in a significant decrease in the levels of Tbx20 (1.25 ± 0.62-fold), whereas Bmp2 showed a significant increase (2.9 ± 0.2-fold; Figure 1, E and F). T2MI was induced by intraperitoneal injection of isoproterenol, and the heart tissue was collected after 2 days (short-duration) and 14 days (prolonged) (Figure 1G). Isoproterenol is a β-adrenergic agonist that results in increased cardiomyocyte necrosis due to elevated oxygen demand and deregulation of ryanodine receptor 2 (RyR2), resulting in intracellular calcium leakage, all of which mimics the symptoms of T2MI (Forte et al., 2021; Radhakrishnan et al., 2023). The High-Fat diet was fed to mice, and the heart tissue was collected after 1 month (short-term) and 3 months (prolonged) (Figure 1J). During both T2MI and High-Fat diets, we observed a similar decrease in Tbx20 during prolonged stress (Figure 1, H, I, K and L). The expression of Bmp2 similarly showed a stable upregulation throughout the disease progression (Figure 1, H, I, K and L).

The time points chosen during different stresses were selected to depict stress-induced changes for shorter and longer durations to delineate the molecular regulation of Tbx20 and Bmp2 under these conditions. Shorter duration stress does not result in significant alteration of cardiac function, however, prolonged stress is associated with altered cardiac functions (Das et al., 2023; Forte et al., 2021; Hynynen et al., 2020; Lepczynski et al., 2021).

Taken together, our study shows that though prolonging the stress response in cardiac tissue results in decreased expression of Tbx20, the expression of Bmp2 shows a significant

surge. The cause and consequence of the altered expression of the cardiac genes are discussed later in this chapter.

5.2.2 The increase in the expression of Bmp2 during prolonged stresses *in vivo* is attributed to cardiac fibroblasts and not cardiomyocytes

The adult rodent heart is composed of multiple cell types other than cardiomyocytes. Therefore, we speculated that the sustained elevation of Bmp2 during prolonged stress is due

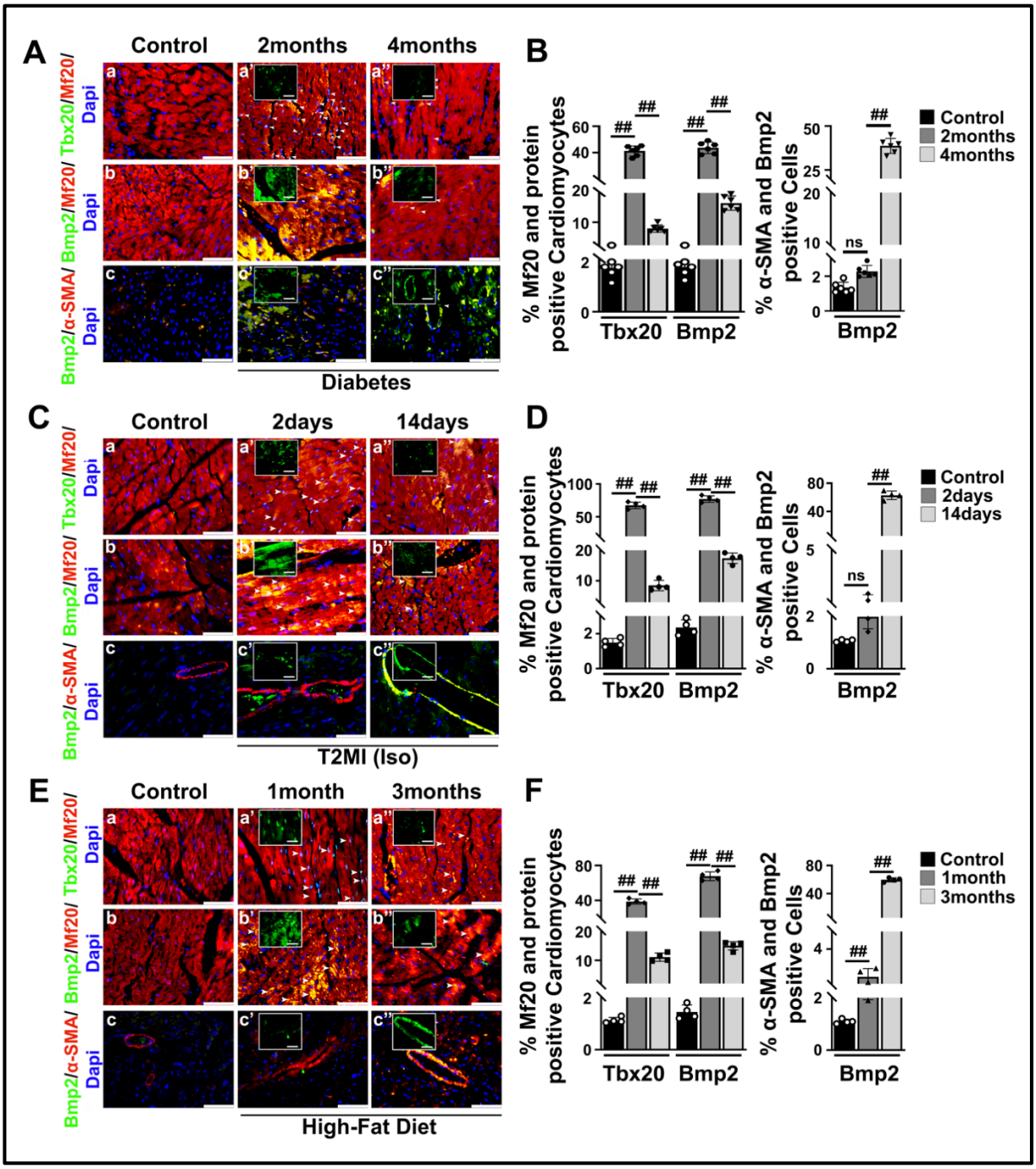

Figure 2. The elevation of Bone morphogenetic protein 2 (Bmp2) during prolonged stresses *in vivo* is attributed to cardiac fibroblasts and not cardiomyocytes. A, Immunostaining showed

prolonged diabetes (4 months) caused amelioration of Tbx20 in cardiomyocytes (a''; Tbx20 (green)/Mf20 (red); white arrows) as compared to diabetes induction for a shorter duration (2 months) (a') and control group (a). The expression of Bmp2 decreased during prolonged diabetes (4 months) in cardiomyocytes (b''; Bmp2 (green)/Mf20 (red); white arrow) compared to diabetes-induced for a shorter duration (2 months) (b') and the control group (b). Bmp2 was shown to colocalize with α-SMA with increased expression during prolonged diabetes (c''; Bmp2 (green)/ α-SMA (red); white arrows) compared to short duration (c') and control group (c). **B,** Quantitative representation of panels in A. **C,** Immunostaining showed prolonged T2MI (14 days) caused downregulation of Tbx20 in cardiomyocytes (a''; Tbx20 (green)/Mf20 (red); white arrows) as compared to T2MI induction for a shorter duration (2 days) (a') and control group (a). The level of Bmp2 also decreased during prolonged T2MI (14 days) in cardiomyocytes (b''; Bmp2 (green)/Mf20 (red); white arrow) compared to T2MI induced for a shorter duration (2 days) (b') and the control group (b). Bmp2 colocalized with α-SMA with increased expression during 14 days of T2MI (c''; Bmp2 (green)/ α-SMA (red); white arrows) compared to 2 days (c') and the control group (c). **D,** Quantitative representation of panels in C. **E,** Immunostaining showed prolonged High-Fat diet (3 months) decreased the expression of Tbx20 in cardiomyocytes (a''; Tbx20 (green)/Mf20 (red); white arrows) as compared High-Fat diet administered for a shorter duration (1 month) (a') and control group (a). The level of Bmp2 also decreased in the prolonged High-Fat diet group (3 months) in cardiomyocytes (b''; Bmp2 (green)/Mf20 (red); white arrow) compared to shorter duration (1 month) (b') and control group (b). Bmp2 was shown to colocalize with α-SMA with increased expression during 3 months High-Fat diet group (c''; Bmp2 (green)/ α-SMA (red); white arrows) compared to 1 month (c') and the control group (c). **F,** Quantitative representation of proteins from E. Statistical significance was calculated by one-way ANOVA. Error bars represent SD from at least three independent biological replicates ($n \geq 3$); ns, p: nonsignificant, $*p < 0.05$, $**p < 0.005$, $***p < 0.0005$, $\#\#p < 0.0001$.

to other cell types of the heart. Colocalization of Tbx20 and $Mf20^{+}$ (cardiomyocyte-specific marker) showed a significant upregulation of Tbx20 in cardiomyocytes in the 2 months diabetic group (41.35 ± 3.8%; Figure 2, Aa' and B) as compared to the control group (1.6 ± 0.34%; Figure 2, Aa and B). However, prolonging diabetes to 4 months resulted in a significant decrease in the expression of Tbx20 (7.82 ± 1.3%; Figure 2, Aa'' and B). Bmp2 also showed an initial increase in expression in cardiomyocytes during 2 months (43.72 ± 4.34%; Figure 2, Ab' and B); however, its expression later decreased in the 4 months diabetes group (16.5 ± 2.4%; Figure 2, Ab'' and B). On the contrary, colocalization of Bmp2 and α-SMA (myofibroblast-specific marker) showed a significant augmentation of Bmp2 in cardiac fibroblasts in the 4 months diabetes group (38.4 ± 4.2%; Figure 2, Ac'' and B) as compared to the 2 months (2.4 ± 0.4%; Figure 2, Ac' and B) and control groups (1.35 ± 0.34%; Figure 2, Ac and B). To further corroborate our findings, we looked into the expression of Tbx20 and Bmp2 during the T2MI and High-Fat diet groups. The expression of Tbx20 increased significantly in cardiomyocytes during a short duration (2 days) of T2MI (67.4 ± 5.0%; Figure 2, Ca' and D) as compared to the control group (1.5 ± 0.24%; Figure 2, Ca and D). However, the expression of Tbx20 significantly declined after extending (14 days) the stress response (8.5 ± 1.7%; Figure 2, Ca'' and D). Similarly, Bmp2 displayed an expression pattern akin to

Tbx20 during T2MI in cardiomyocytes (Figure 2, Cb, Cb', Cb'' and D). Interestingly, colocalization of Bmp2 and α-SMA showed a significant increase of Bmp2 in cardiac fibroblasts during 14 days T2MI induction (63 ± 5.9%; Figure Cc'' and D) as compared to 2 days T2MI (1.9 ± 0.45%; Figure Cc' and D) and control group (1.05 ± 0.04%; Figure Cc and D). In the High-Fat diet group, the expression of Tbx20 (Figure 2, Ea, Ea', Ea'' and F) and Bmp2 (Figure 2, Eb, Eb', Eb'' and F) showed a similar expression profile in cardiomyocytes as that of the other two groups, with an initial upregulation during a short duration of stress, followed by a sharp decline upon prolonging the stress. The expression of Bmp2 showed a similar upregulation in cardiac fibroblasts during 3 months of High-Fat diet administration with respect to 1 month and the control group (Figure 2, Ec, Ec', Ec'' and F).

The similar expression pattern of Tbx20 and Bmp2 in cardiomyocytes and Bmp2 in cardiac fibroblasts during all four stresses substantiates the fact that the significant increase in Bmp2 during prolonged stress is attributed to fibroblasts and not cardiomyocytes. The cause and consequence of this increase are discussed later in this chapter.

5.2.3 The expression of miR-101-3p is increased during prolonged ER stress/diabetes *in vivo*

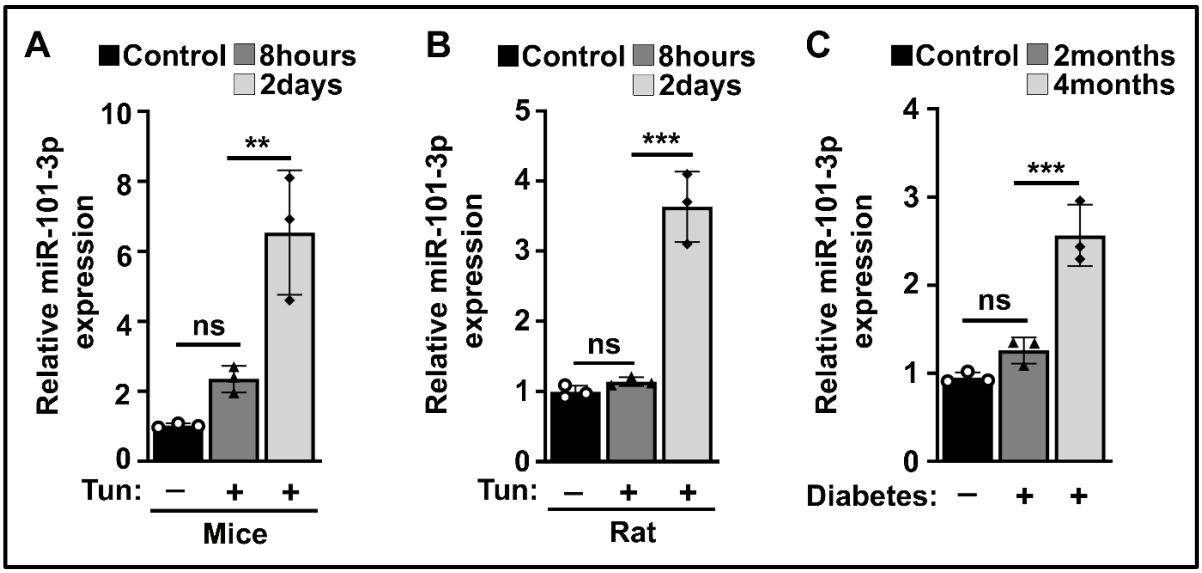

Figure 3. miR-101-3p is elevated during prolonged Endoplasmic Reticulum (ER) stress/diabetes *in vivo*. A, Taqman analysis showing elevation of miR-101-3p during prolonged ER stress (2 days) as compared to short duration (8 hours) and control group in mice. **B,** Taqman analysis showing elevation of miR-101-3p during prolonged ER stress (2 days) as compared to short duration (8 hours) and control group **i**n rats. **C,** Taqman analysis showing elevation of miR-101-3p during prolonged diabetes (4 months) as compared to short duration (2 months) and the control group. Statistical significance was calculated by one-way ANOVA. Error bars represent SD from three independent biological replicates (n=3); ns, p: nonsignificant, ∗p < 0.05, ∗∗p < 0.005, ∗∗∗p < 0.0005, ##p < 0.0001.

The marked decrease of Tbx20 during prolonged stresses (ER/diabetes) prompted us to delineate the factors involved. miR-101-3p was previously shown to be elevated during ER stress in cancer (Park et al., 2022). However, no reports to date have shown their involvement during ER stress in CVDs. *In silico* analysis showed the presence of miR-101-3p binding site on the 3'UTR of the *tbx20* gene, and though we did not find the binding site of miR-101-3p on *bmp2,* interestingly, we observed the presence of miR-101-3p binding sequence in the 3'UTR of the *nog* gene, which is a Bmp2 antagonist. Therefore, we looked into the expression of miR-101-3p during different stresses. Taqman analysis showed significant upregulation in the levels of miR-101-3p in the 2 days ER stress group as compared to 8 hours and control groups. However, the change in the levels of miR-101-3p between 8 hours and the control group was found to be non-significant (Figure 3A). We also observed a similar upregulation of miR-101-3p during prolonged ER stress in rats (Figure 3B). Prolonged diabetes (4 months) also resulted in a significant increase in the expression of miR-101-3p as compared to shorter duration (2 months) and the control group (Figure 3C). These results correlate with the significant decrease of Tbx20 and increase of Bmp2 during prolonged ER stress/diabetes.

Together, these results indicate the possible involvement of miR-101-3p in regulating the expression of Tbx20 and Bmp2 during prolonged ER stress and diabetic cardiomyopathy.

5.2.4 Elevation of miR-101-3p is associated with increased senescence of cardiomyocytes *in vivo*

Next, we sought to determine the consequence of the elevated levels of miR-101-3p during prolonged ER stress/diabetes *in vivo*. In the previous chapter, we showed that with an increase in the expression of Tbx20 during the short duration of ER stress, cardiomyocyte proliferation also increases. However, prolonging the ER stress resulted in a significant decrease of Tbx20 with a concomitant decrease in cardiomyocyte proliferation. This prompted us to look into the expression of senescence marker genes, as cellular senescence is associated with cell cycle arrest, resulting in stalling of proliferation.

The level of senescent marker p21 was significantly elevated in the 2 days ER stress group compared to 8 hours and control groups (Figure 4, A and B), as shown by Western blotting. Another senescent marker, p16, also showed a significant upregulation in the prolonged ER stress group as compared to 8 hours and the control group (Figure 4, A and B). A comparable elevation in the p21 and p16 levels was noted in the 4 months diabetic group when compared to the 2 months and control groups (Figure 4, E and F). The colocalization of

p21 and Mf20^{+} indicated an upregulation of p21 in cardiomyocytes in the 2 days ER stress group (49.36 ± 4.35%; Figure 4, Ca'' and D) relative to the 8 hours (5.7 ± 1.9%; Figure 4, Ca' and D) and control group (1.82 ± 0.7%; Figure 4, Ca and D). Additionally, there was a significant increase in p16 expression in cardiomyocytes during prolonged ER stress (38.77 ± 6.39%; Figure 4, Cb'' and D) as compared to shorter duration (5.2 ± 1.7%; Figure 4, Cb' and D) and control group (1.5 ± 0.6%; Figure 4, Cb and D). Colocalization of p21 and Mf20^{+} also showed elevated expression of p21 in cardiomyocytes during prolonged (4 months) diabetes group (32.41 ± 2.5%; Figure 4, Ga'' and H) in comparison to shorter duration (2 months) diabetes (3.64 ± 1.23%; Figure 4, Ga' and H) and control group (1.26 ± 0.12%; Figure 4, Ga and H). A similar expression profile of p16 was observed during diabetes in cardiomyocytes (Figure 4, Gb, Gb', Gb'' and H).

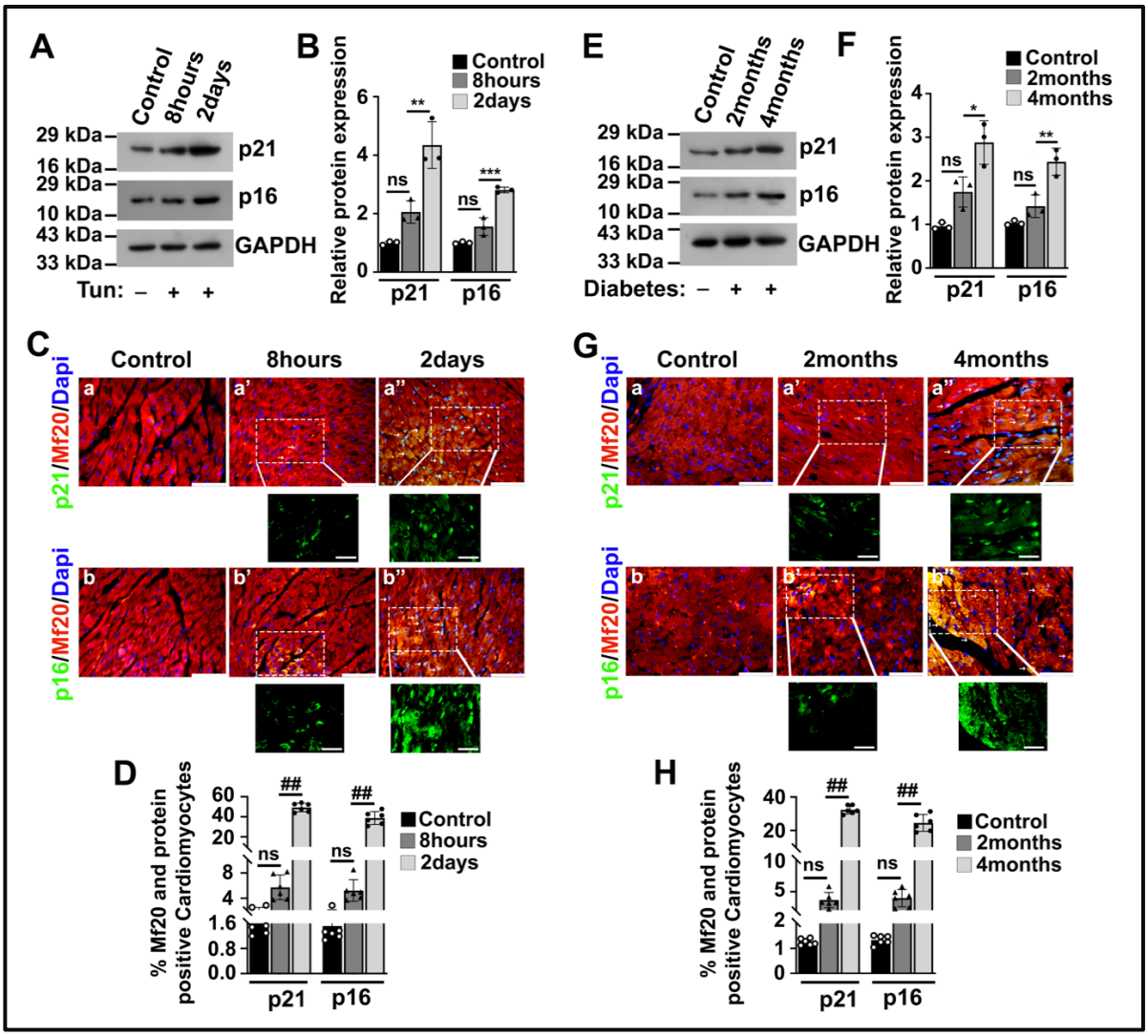

Figure 4. Increased level of miR-101-3p during prolonged Endoplasmic Reticulum (ER) stress/diabetes promotes senescence response in cardiomyocytes *in vivo*. A, Western blot analysis

showing enhanced expression of senescent markers p21 and p16 during prolonged ER stress (2 days), where the expression of miR-101-3p was also increased in contrast to ER stress induction for shorter duration (8 hours) and the control group. **B,** Quantitative representation of proteins from A. **C,** The senescent marker p21 exhibited colocalization in cardiomyocytes with heightened expression during prolonged ER stress (2 days) (a"; p21 (green)/Mf20 (red); white arrows) when compared to a shorter duration (8 hours) (a') and the control group (a). The levels of p16 increased in cardiomyocytes during prolonged ER stress (b"; p16 (green)/Mf20 (red); white arrows) in comparison to the short duration (b') and the control group (b). **D,** Quantitative representation of panels in C. **E,** Western blot analysis showing elevated expression of senescence markers p21 and p16 after prolonged diabetes (4 months), with a corresponding increase in miR-101-3p expression compared to both a shorter duration of diabetes (2 months) and the control group. **F,** Quantitative representation of proteins from E. **G,** The senescent marker p21 was observed to colocalize with elevated expression during prolonged diabetes (4 months) (a"; p21 (green)/Mf20 (red); white arrows) compared to the short duration (2 months) (a') and the control group (a). The level of p16 expression was found to be higher in cardiomyocytes during proonged diabetes (b"; p16 (green)/Mf20 (red); white arrows) relative to the short duration (b') and the control group (b). **H,** Quantitative representation of panels in G. Scale bar of the main image represent 50 μm. The scale bar of the inset represents 20 μm. Statistical significance was calculated by one-way ANOVA. Error bars represent SD from three independent biological replicates (n=3); ns, p: nonsignificant, $*p < 0.05$, $**p < 0.005$, $***p < 0.0005$, $\#\#p < 0.0001$.

This intriguing finding indicates an increase in senescence response upon prolonging ER stress/diabetes when the expression of miR-101-3p was also increased. The role of miR-101-3p in inducing the senescence response in cardiomyocytes and the regulatory pathway involved are discussed later in this chapter.

5.2.5 Increasing ER stress results in an increase in cardiomyocyte senescence *in vitro,* which correlates with a decrease in the expression of Tbx20 and an increase in the expression of miR-101-3p

Next, we wanted to assess the possible mechanism behind the elevated expression of senescent markers during prolonged stresses. For that, we treated H9c2 cardiomyocytes with increasing concentrations (10 μg/ml, 20 μg/ml, and 50 μg/ml) of ER stress inducer Tun. We observed a gradual increase in the expression of Tbx20 with increasing ER stress up to a Tun concentration of 20 μg/ml, as evidenced by Western blotting. However, increasing the concentration of Tun further to 50 μg/ml resulted in a significant decline in the levels of Tbx20 (Figure 5A). Interestingly, at 50 μg/ml Tun concentration, there was a significant upregulation of senescent markers p21 and p16 (Figure 5A). To further corroborate the elevation of senescence response, we performed the Senescence-associated associated-β-galactosidase assay (SA-β-Gal), a hallmark of senescent cells. Our study showed a significant upregulation of SA-β-Gal activity in 50 μg/ml Tun-treated cells (61.7 ± 2.5%; Figure 5, Da''' and E) as compared to 20 μg/ml Tun (3.3 ± 0.6%; Figure 5, Da'' and E), 10 μg/ml Tun (1.6 ± 0.13%; Figure 5, Da' and E) and control cells (1.04 ± 0.04%; Figure 5, Da and E). Immunostaining

studies also showed a significant augmentation in the levels of p21 and γH2AX in 50 µg/ml Tun-treated cells as compared to 20 µg/ml, 10 µg/ml Tun and control cells (Figure 5, F and G). Thus, a decrease in the activity of Tbx20 results in a concomitant increase in cardiomyocyte senescence. To our surprise, in the 50 µg/ml Tun-treated cells, we observed a significant upregulation of miR-101-3p as evidenced by Taqman assay as compared to 20 µg/ml Tun, 10 µg/ml Tun-treated and control cells (Figure 5C).

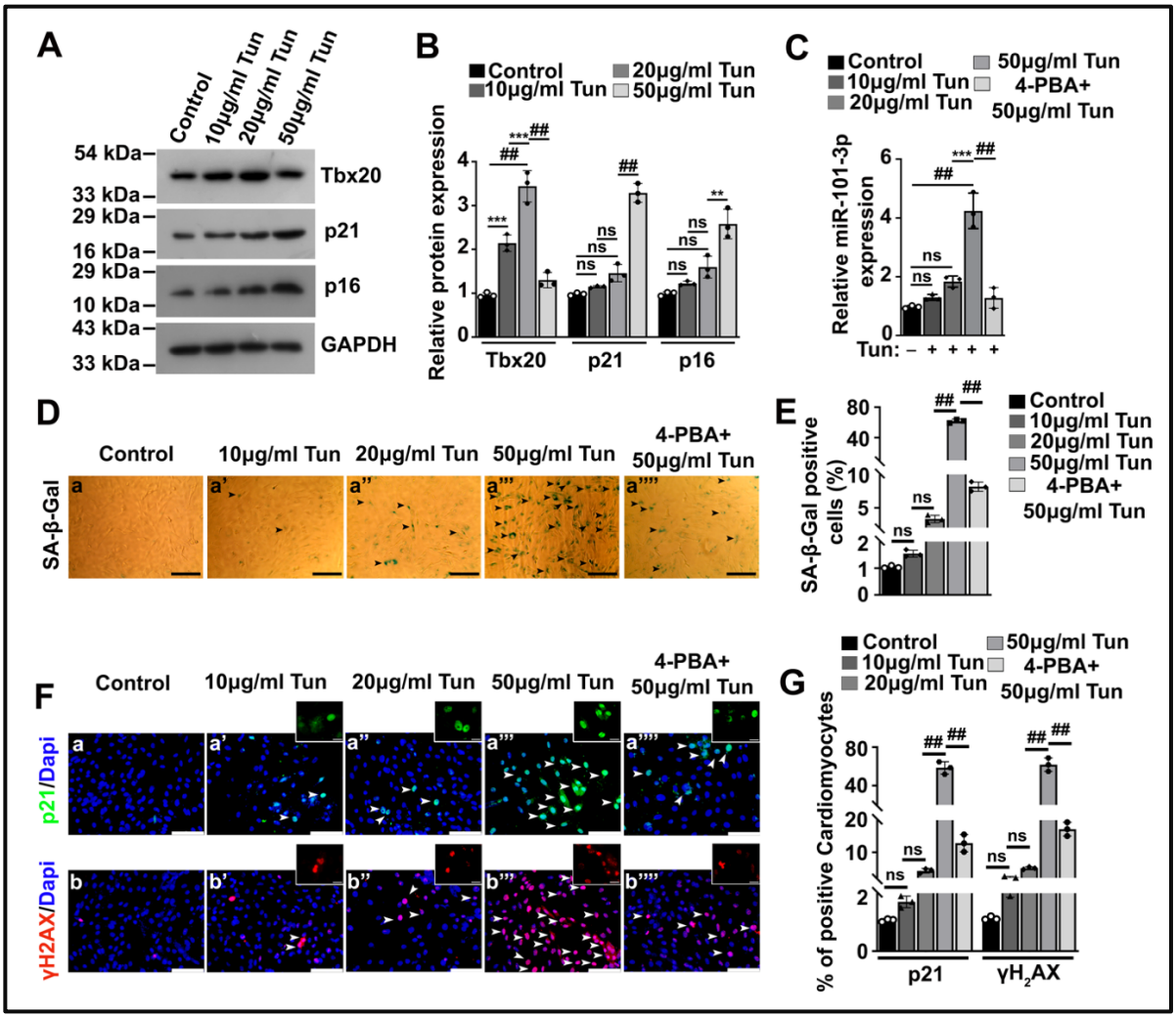

Figure 5. Elevation of Endoplasmic Reticulum (ER) stress causes increased cardiomyocyte senescence, which correlates with a decrease in the expression of T-box transcription factor 20 (Tbx20) and an increase in the expression of miR-101-3p. **A,** Western blot analysis showing a gradual increase in the expression of Tbx20 with increasing ER stress upon administration of ER stress inducer Tunicamycin (Tun) (10 µg/ml Tun, 20 µg/ml Tun). However, its expression decreased in 50 µg/ml Tun-treated H9c2 cardiomyocytes. Increasing the concentration of Tun to 50 µg/ml resulted in significant upregulation of senescent markers p21 and p16. **B,** Quantitative representation of proteins from A. **C,** Taqman analysis showed increased expression of miR-101-3p upon increasing ER stress (50 µg/ml Tun) compared to 20 µg/ml Tun, 10 µg/ml Tun and control cells. **D,** Senescence associated β galactosidase (SA-β-Gal) assay showed increased senescence of cardiomyocytes upon increasing ER stress (50 µg/ml Tun; a''') as compared to (20 µg/ml Tun; a''), (10 µg/ml Tun; a') and control cells (a). Administration of 4-Phenyl butyric acid (4-PBA), an ER stress antagonist, resulted in decreased

senescence of cardiomyocytes (a’’’’). **E,** Quantitative representation of images from D. **F,** Immunofluorescence staining showing an increased expression of senescent markers p21 and γH2AX upon increasing ER stress (50 μg/ml Tun; a’’’, b’’’) as compared to (20 μg/ml Tun; a’’, b’’), (10 μg/ml Tun; a’, b’) and control cells (a, b) respectively. Their expression decreased upon administration of 4-PBA (a’’’’, b’’’’). The scale bar of the main image represents 50 μm. The scale bar of the inset represents 20 μm. **G,** Quantitative representation of images from F. Statistical significance was calculated by one-way ANOVA. Error bars represent SD from three independent biological replicates (n=3); ns, p: nonsignificant, ∗p < 0.05, ∗∗p < 0.005, ∗∗∗p < 0.0005, ##p < 0.0001.

To further evaluate whether the increase in the levels of miR-101-3p is due to ER stress, we treated the cells with ER stress inhibitor 4-Phenylbutyric acid (4-PBA), followed by ER stress induction (50 μg/ml Tun). We observed a significant amelioration in the expression of miR-101-3p upon treatment with 4-PBA, followed by ER stress induction (50 μg/ml Tun) as compared to ER stress induction alone (50 μg/ml Tun) (Figure 5C). These results corroborated our *in vivo* data showing that increasing ER stress resulted in the augmentation of miR-101-3p with a concomitant decrease of Tbx20. 4-PBA treatment followed by ER stress induction also showed decreased SA-β-Gal staining (Figure 5, Da’’’’ and E) and amelioration in the expression of p21 (Figure 5, Fa’’’’ and G) and γH_2AX (Figure 5, Fb’’’’ and G), thus further substantiating our hypothesis.

Therefore, these data hint at a possible involvement of Tbx20 in limiting cardiomyocyte senescence induced by miR-101-3p during increasing ER stress.

5.2.6 Prolonging hyperglycemia causes a decrease in the expression of Tbx20 with concomitant upregulation of cardiomyocyte senescence *in vitro*

To corroborate our findings in another disease model, we induced hyperglycemia in H9c2 cardiomyocytes, and we harvested the cells at two time points, 2 days (25 mM 2d) and 5 days (25 mM 5d). In the previous section, we had already shown that inducing hyperglycemic stress for 2days is associated with a significant increase in the expression of Tbx20 compared to the control. However, prolonging the hyperglycemic stress to 5 days resulted in a significant decrease in the expression of Tbx20. Therefore, here, we looked into the expression of senescent markers in this study. The SA-β-Gal assay showed a significant increase in the SA-β-Gal activity in 5 days hyperglycemic cells compared to 2 days and control cells (Figure 6, A and B). Immunostaining analysis also showed a marked increase in the levels of p21 and γH2AX in the 5 days hyperglycemic cells as compared to 2 days and control cells (Figure 6, C and D). The results were further corroborated by Western blotting of p21 and p16 (Figure 6, E and F). Thus, these data further establish a plausible role of Tbx20 in limiting cardiomyocyte senescence during stress.

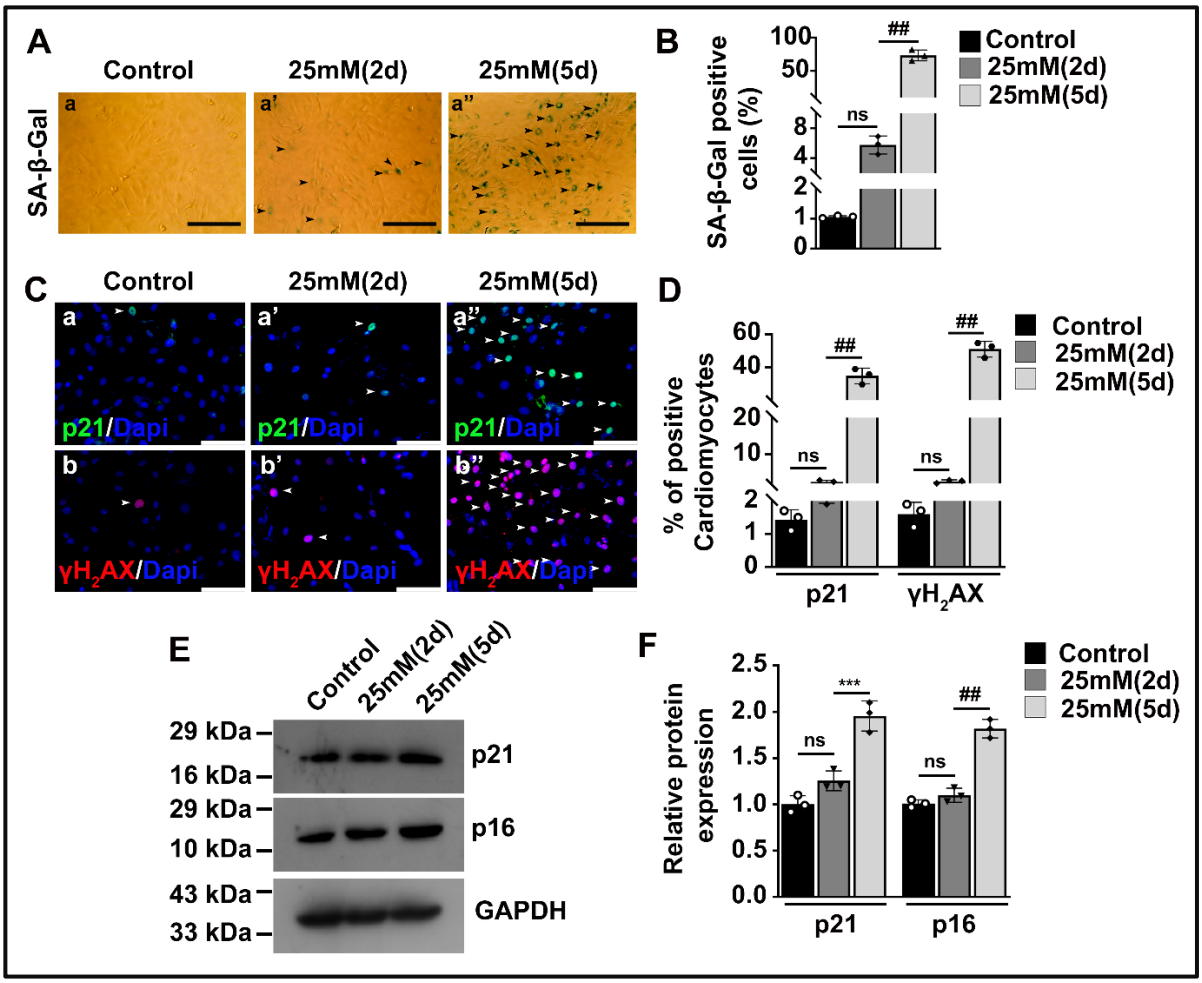

Figure 6. Prolonged hyperglycemia is associated with downregulation of T-box transcription factor 20 (Tbx20) with concomitant upregulation of cardiomyocyte senescence *in vitro* A, During prolonged hyperglycemia (25mM for 5 days), SA-β-Gal exhibited heightened levels of cardiomyocyte senescence (a'') in comparison to a shorter duration (25mM for 2 days) (a') and the control (a). **B,** Quantitative representation of images from A. **C,** Immunofluorescence staining revealed increased levels of senescence markers p21 (a'') and γH2AX (b'') during prolonged hyperglycemia, when compared to shorter durations (a' and b') and the control (a and b). **D,** Quantitative representation of images from C. **E,** Western blot analysis demonstrating elevated levels of senescence markers p21 and p16 during prolonged hyperglycemic stress. **F,** Quantitative representation of proteins from E. The scale bar of the main image represents 50 μm. Statistical significance was calculated by one-way ANOVA. Error bars represent SD from three independent biological replicates (n=3); ns, p: nonsignificant, ∗p < 0.05, ∗∗p < 0.005, ∗∗∗p < 0.0005, ##p < 0.0001.

5.2.7 Tbx20 is necessary and it acts upstream of senescent signaling in protecting cardiomyocytes against ER stress

We have previously shown a plausible role of Tbx20 in attenuating senescence response during ER stress. To further strengthen our findings and to ascertain the molecular hierarchy between Tbx20 and senescent markers, as well as the mechanism of action via which Tbx20 shields the cardiomyocyte against ER stress, we knocked down Tbx20 in H9c2 cardiomyocytes by Tbx20 specific siRNA followed by ER stress induction.

SA-β-Gal staining showed a robust increase in the SA-β-Gal activity in H9c2 cells treated with Tbx20 siRNA followed by ER stress induction (20 µg/ml) (53.3 ± 6.3%; Figure 7, Aa'' and B) in comparison to Tun treatment (20 µg/ml) alone (3.53 ± 0.53%; Figure 7, Aa' and B). siRNA-mediated knockdown of Tbx20 followed by ER stress induction (20 µg/ml) resulted in significant upregulation of p21 and p16 as compared to ER stress induction (20 µg/ml) alone, as evidenced by Western blotting (Figure 7, C and D). The observations were further corroborated by immunostaining, which showed a significant augmentation of p21 in the H9c2 cardiomyocytes transfected with Tbx20 siRNA followed by ER stress induction as compared to ER stress induction alone (Figure 7, E and F). The expression of p16 and γH2AX also showed robust upregulation upon knockdown of Tbx20 followed by ER stress induction with reference to ER stress induction alone (Figure 7, E and F).

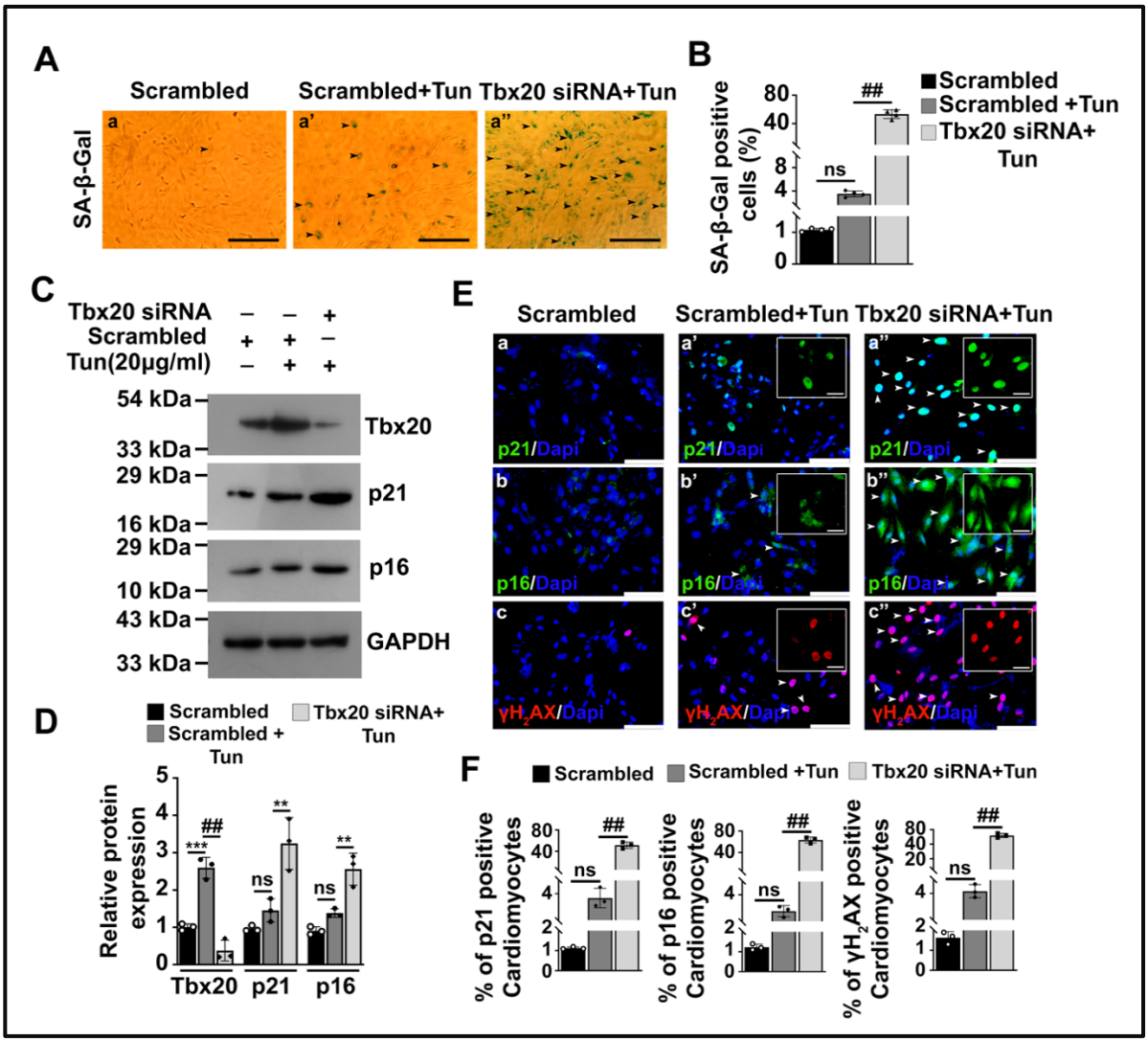

Figure 7. T-box transcription factor 20 (Tbx20) is essential and functions upstream of senescence signaling to safeguard cardiomyocytes from Endoplasmic Reticulum (ER) stress. A, SA-β-Gal staining showing increased senescence response upon siRNA-mediated knockdown of Tbx20 followed

by ER stress induction (20 µg/ml Tun; a'') as compared to scrambled+20 µg/ml Tun (a') and scramble treatment alone (a). Scale bar of the main image represents 50 µm. **B,** Quantitative representation of images from A. **C,** Western blot analysis showing augmentation of p21 and p16 levels upon siRNA-mediated knockdown of Tbx20 followed by ER stress induction (20 µg/ml Tun) as compared to ER stress induction alone. **D,** Quantitative representation of proteins from C. **E,** Immunofluorescence staining showing increased expression of p21 (a''), p16 (b'') and γH2AX (c'') upon siRNA mediated knockdown of Tbx20 followed by ER stress induction as compared scrambled+ER stress induction (a', b', c') and scrambled (a, b, c) alone. Scale bar of the main image represents 50 µm. The scale bar of the inset represents 20 µm. **F,** Quantitative representation of images from E. Statistical significance was calculated by one-way ANOVA. Error bars represent SD from three independent biological replicates (n=3); ns, p: nonsignificant, ∗p < 0.05, ∗∗p < 0.005, ∗∗∗p < 0.0005, ##p < 0.0001.

Together, these data uncover the fact that Tbx20 works upstream of senescent signaling and is necessary for imparting protection against ER stress by ameliorating cardiomyocyte senescence and, in turn, restoring cardiac homeostasis.

5.2.8 MiR-101-3p directly targets Tbx20

The robust increase of miR-101-3p upon prolonged ER stress/diabetes, with concomitant decrease in the expression of Tbx20 and the presence of miR-101-3p binding site in the 3'UTR of the *tbx20* gene, as evidenced by *in silico* analysis, led us to evaluate the direct binding of miR-101-3p to the *tbx20* gene (Figure 8A). For that, we first cloned the *tbx20* 3'UTR containing the miR-101-3p binding site in the pmiRGLO dual-luciferase vector. The direct binding was assessed by luciferase assay, where ectopic transfection of miR-101-3p mimic caused a significant decrease in the relative luciferase activity as compared to scrambled (Figure 8E).

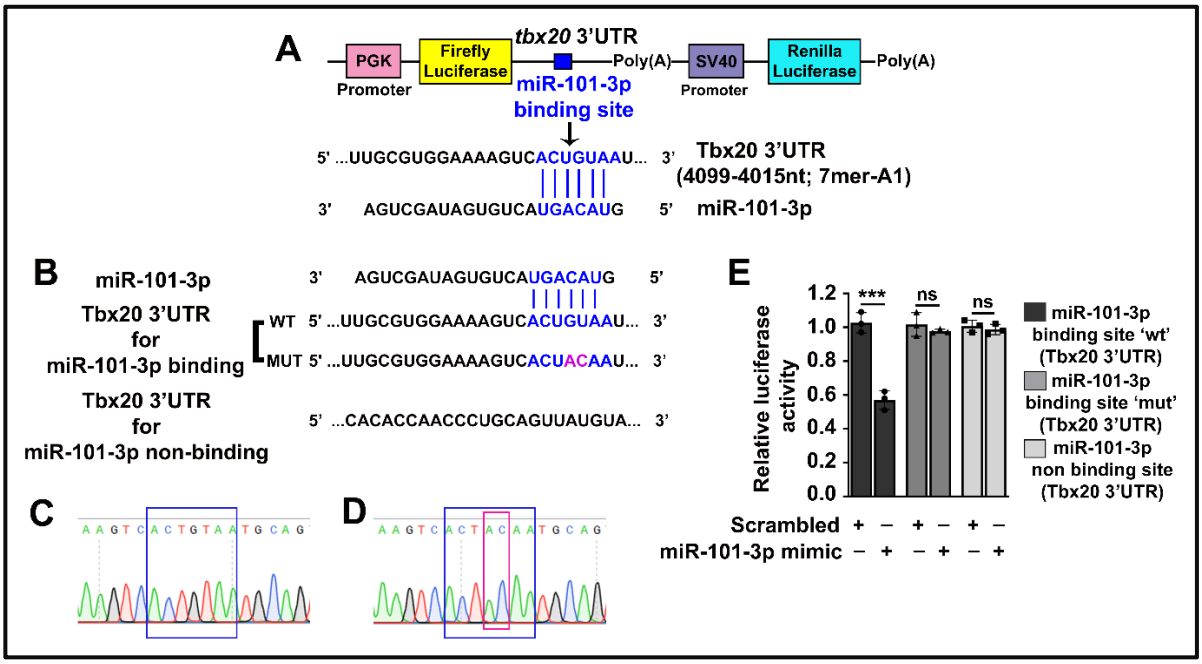

Figure 8. MiR-101-3p targets T-box transcription factor 20 (Tbx20). A, Schematic diagram of pmirGLO-Tbx20-3'UTR reporter construct containing wild type (wt) binding site for miR-101-3p. **B,** Schematic diagram of pmirGLO-Tbx20-3'UTR reporter construct containing wild type (WT) and mutated (MUT) binding site for miR-101-3p. Schematic diagram of pmirGLO-Tbx20-3'UTR reporter constructs that do not contain a binding site for miR-101-3p. **C,** Chromatogram showing pmirGLO-Tbx20-3'UTR containing wild-type binding site for miR-101-3p (marked in blue) after Sanger Sequencing. **D,** Chromatogram showing pmirGLO-Tbx20-3'UTR containing a mutated binding site for miR-101-3p (marked in pink) after Sanger Sequencing. **E,** Relative luciferase activity showed the repressive effect of miR-101-3p on 'wt' Tbx20-3'UTR upon administration of miR-101-3p mimic. However, miR-101-3p mimic administration did not affect Tbx20-3'UTR containing a mutant ('mut') binding site for miR-101-3p. miR-101-3p mimic administration did not affect Tbx20-3'UTR containing a 'non binding site' for miR-101-3p. Statistical significance was calculated by Student's *t*-test. Error bars represent SD from three independent biological replicates (n=3); ns, p: nonsignificant, $*p < 0.05$, $**p < 0.005$, $***p < 0.0005$, $\#\#p < 0.0001$.

The specificity of inhibition was further validated by introducing two point mutations in the seed region of the miR-101-3p binding site in the 3'UTR of the *tbx20* gene (Figure 8B). The introduction of a successful point mutation was corroborated by Sanger sequencing, and the chromatogram represents the wild-type and mutated seed sequence region (Figure 8, C and D). Mutation in the 3'UTR of the *tbx20* gene failed to inhibit luciferase activity upon ectopic addition of miR-101-3p (Figure 8E). To further validate our results, we also cloned a region of the 3'UTR of the *tbx20* gene that does not contain the miR-101-3p binding site. Ectopic administration of miR-101-3p resulted in no significant alteration in the relative luciferase activity (Figure 8E). Therefore, these results unravel the novel regulation of miR-101-3p on *tbx20* by directly binding to its 3'UTR.

5.2.9 MiR-101-3p potentiates cardiomyocyte senescence by targeting Tbx20

After proving the direct binding of miR-101-3p to *tbx20* 3'UTR, we wanted to delineate the physiological relevance of this finding and the effect of miR-101-3p on Tbx20 during ER stress. To decipher that, we transfected H9c2 cells with miR-101-3p mimic or inhibitor followed by ER stress induction and the levels of Tbx20 were assessed. Since previously we had shown that Tbx20 is increased significantly in 20 μg/ml Tun-treated cells, therefore to delineate the effect of miR-101-3p on Tbx20, we transfected H9c2 cardiomyocytes with miR-101-3p mimic followed by ER stress induction (20 μg/ml Tun). The expression of the *tbx20* transcript was decreased significantly in miR-101-3p mimic+20 μg/ml Tun treated cells (3.1 ± 0.37-fold; Figure 9A) as compared to scrambled+20 μg/ml Tun cells (7.9 ± 1.05-fold; Figure 9A). Therefore, our study, for the first time, unravelled miR-101-3p mediated regulation of Tbx20 during ER stress.

To further corroborate our finding, we treated H9c2 cardiomyocytes with miR-101-3p inhibitor followed by ER stress induction (50 µg/ml Tun), since previously we had shown a robust decrease in the expression of Tbx20 at a Tun concentration of 50 µg/ml. We observed a significant upregulation of *tbx20* mRNA upon treatment with the inhibitor followed by ER (6.7 ± 1.3-fold; Figure 9A) stress as compared to ER stress induction alone (2.7 ± 0.72-fold; Figure 9A). Tbx20 protein level also showed a similar expression pattern as that of the transcript upon mimic and inhibitor administration (Figure 9, B and C). Thus, these observations further potentiate our findings that miR-101-3p levels are increased during increasing ER stress, which in turn binds to *tbx20* 3'UTR and degrades the *tbx20* mRNA, resulting in a significant decrease in its expression.

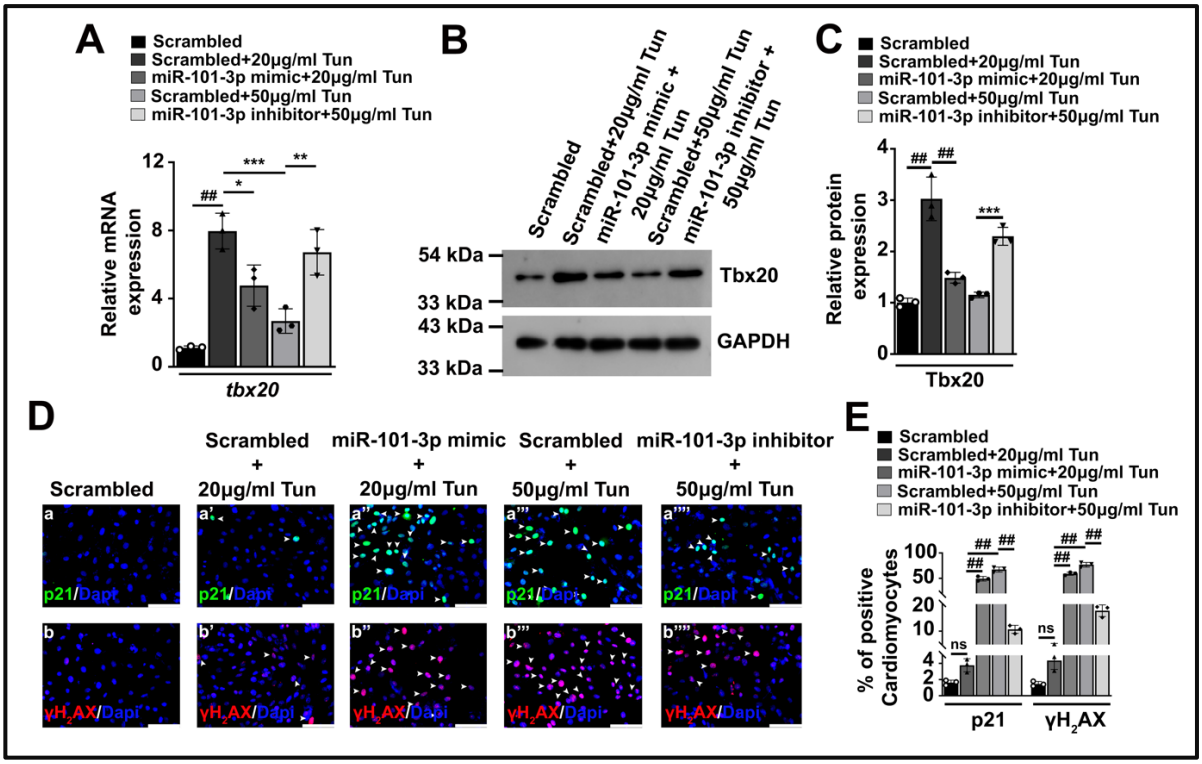

Figure 9. MiR-101-3p mediated suppression of T-box transcription factor 20 (Tbx20) increases cardiomyocyte senescence *in vitro*. A, qRT-PCR showing increased expression of the *tbx20* gene upon treatment with scrambled+20 µg/ml Tun as compared to scramble alone, which was later decreased in scrambled+50 µg/ml Tun-treated cells. miR-101-3p mimic+20 µg/ml Tun administration resulted in a significant decrease in the expression of *tbx20* as compared to 20 µg/ml Tun alone treated cardiomyocytes. miR-101-3p inhibitor+50 µg/ml Tun administration resulted in a significant increase in the expression of *tbx20* compared to only 50 µg/ml Tun-treated cardiomyocytes. **B,** Western blotting analysis showing a significant decrease in the expression of Tbx20 in miR-101-3p mimic+20 µg/ml Tun treated cells as compared to only 20 µg/ml Tun treated cardiomyocytes. miR-101-3p inhibitor+50 µg/ml Tun administration resulted in a significant increase in Tbx20 as compared to only 50 µg/ml Tun-treated cells. **C,** Quantitative representation of proteins from B. **D,** Immunofluorescence staining showing increased expression of senescent markers p21 and γH2AX in miR-101-3p mimic+20 µg/ml Tun treated cells (a'', b'') as compared to scrambled+20 µg/ml Tun (a', b') and scrambled (a, b) treated cells respectively. The expression of senescent markers, however, decreased in miR-101-3p

inhibitor+50 μg/ml Tun treated cells (a’’’’, b’’’’) as compared to scrambled+50 μg/ml Tun (a’’’, b’’’) treated cardiomyocytes. The scale bar of the main image represents 50 μm. **E,** Quantitative representation of images from D. Statistical significance was calculated by one-way ANOVA. Error bars represent SD from three independent biological replicates (n=3); ns, p: nonsignificant, ∗p < 0.05, ∗∗p < 0.005, ∗∗∗p < 0.0005, ##p < 0.0001.

Next, we sought to determine the expression of senescent markers under these conditions. Immunostaining studies showed a robust upregulation in the expression of p21 (Figure 9, Da’’ and E) and γH2AX (Figure 9, Db’’ and E) upon ectopic administration of miR-101-3p mimic followed by ER stress induction (20 μg/ml Tun) as compared to scrambled+ER stress (20 μg/ml Tun) (Figure 9, Da’ and E) and (Figure 9, Db’ and E) respectively in H9c2 cardiomyocytes. However, H9c2 cardiomyocytes transfected with miR-101-3p inhibitor followed by ER stress induction (50 μg/ml Tun) resulted in a significant decrease in the expression of p21 (Figure 9, Da’’’’ and E) and γH2AX (Figure 9, Db’’’’ and E) as compared to scrambled+ER stress induction (50 μg/ml Tun) alone (Figure 9, Da’’’ and E) and (Figure 9, Db’’’ and E). Taken together, these result shows that increased expression of miR-101-3p during increasing ER stress results in an augmentation in the activity of senescent markers by decreasing Tbx20 expression.

5.2.10 Differential expression of Tbx20 and Nog in cardiomyocytes and cardiac fibroblasts

The drastic upregulation of Bmp2 during prolonged stresses (ER stress, Diabetes, T2MI and High-Fat diet administration) *in vivo* led us to unravel the cause and consequence of the increase. Upon colocalization of Bmp2 with α-SMA, we observed increased expression of Bmp2 in cardiac fibroblasts during prolonged stress in all four different stress models. Upon delineating the possible factors that might control the expression of Bmp2 in cardiac fibroblasts upon prolonged stress, we stumbled upon Noggin (Nog), a Bmp2 antagonist, as an *in silico* study showed the presence of miR-101-3p binding site in the 3’UTR of the *nog* gene. Previously, we had shown that in cardiomyocytes, the expression of Bmp2 is decreased during prolonged stress, and its regulation is driven by Tbx20; therefore, we looked into the differential expression of Tbx20 and Nog in cardiomyocytes and fibroblasts. A pure population of cardiac fibroblasts after culturing from rodent hearts was ascertained by immunostaining with fibroblast-specific marker Vimentin (Vim). Next, we assessed the expression of miR-101-3p in fibroblasts upon increasing the concentration of Tun. The expression of miR-101-3p did not increase significantly in 20 μg/ml Tun-treated cells (1.39 ± 0.27-fold; Figure 10B) as compared to the control (0.98 ± 0.11-fold; Figure 10B). However, its expression increased

significantly in 50 µg/ml Tun-treated cells (2.63 ± 0.32-fold; Figure 10B). Thus, the expression of miR-101-3p is upregulated in cardiac fibroblasts upon increasing ER stress.

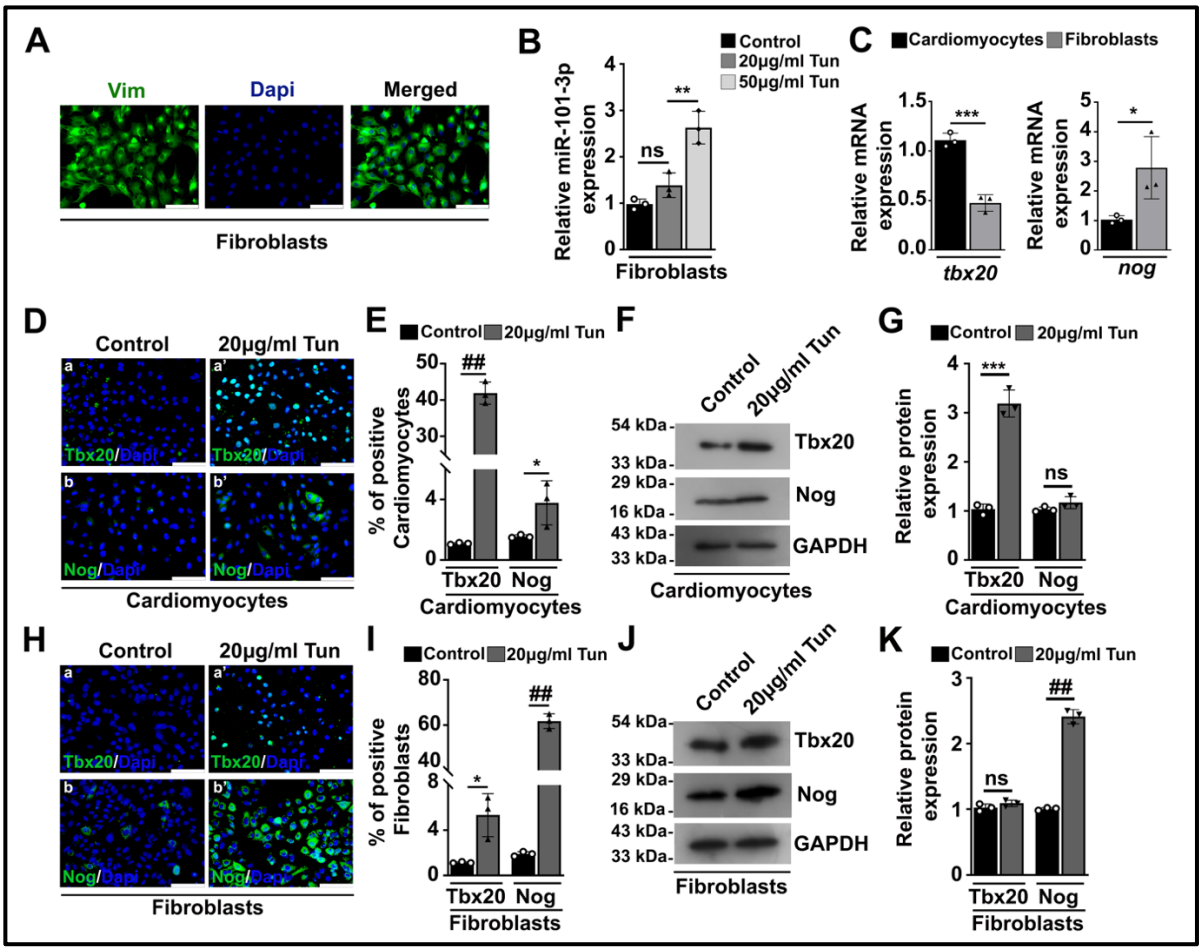

Figure 10. T-box transcription factor 20 (Tbx20) and Noggin (Nog) are differentially expressed in cardiomyocytes and cardiac fibroblasts. A, Immunofluorescence staining of Vimentin (Vim) showing a pure population of isolated cardiac fibroblasts. **B,** Taqman analysis showing increased expression of miR-101-3p in cardiac fibroblasts upon increasing ER stress (50 µg/ml Tun) as compared to 20 µg/ml Tun and control cells.. **C,** Differential expression of Tbx20 and Nog in cardiomyocytes and fibroblasts was determined by qRT-PCR. **D,** Immunofluorescence staining showing increased expression of Tbx20 in cardiomyocytes during ER stress (41.93±3.035%) as compared to control (1.083±0.06%). Nog expression is increased in cardiomyocytes (4.047±1.036%) during ER stress as compared to control (1.553±0.1021%). **E,** Quantitative representation of images from D. **F,** Western blotting showing a significant increase in expression of Tbx20 during ER stress in cardiomyocytes compared to control. The expression of Nog did change significantly during ER stress compared to control in cardiomyocytes. **G,** Quantitative representation of proteins from F. **H,** Immunofluorescence staining showing increased expression of Tbx20 in fibroblasts during ER stress (5.333±1.914%) as compared to control (1.133±0.06%). Nog expression is increased significantly in fibroblasts (61.73±3.253%) during ER stress as compared to control (1.901±0.201%). **I,** Quantitative representation of images from H. **J,** Western blotting showing no significant increase in expression of Tbx20 during ER stress in fibroblasts compared to control. The expression of Nog increased significantly during ER stress compared to control in fibroblasts. **K,** Quantitative representation of proteins from J. The scale bar of the images represents 50 µm. Statistical significance was calculated by one-way ANOVA. Error bars represent SD from three independent biological replicates (n=3); ns, p: nonsignificant, ∗p < 0.05, ∗∗p < 0.005, ∗∗∗p < 0.0005, ##p < 0.0001.

Real-time PCR showed heightened expression of the *tbx20* transcript in cardiomyocytes as compared to fibroblasts at the basal level (Figure 10C). However, *nog* was shown to be expressed more in cardiac fibroblasts as compared to cardiomyocytes (Figure 10C). After showing the basal level distribution of Tbx20 and Nog, next, we wanted to see their differential expression during ER stress. For that, we treated both H9c2 cardiomyocytes and fibroblasts with 20 µg/ml Tun. Immunostaining showed a significant augmentation in the expression of Tbx20 (41.93±3.035%; Figure 10, Da' and E) in cardiomyocytes upon induction of ER stress as compared to control (1.083±0.06%; Figure 10, Da and E). On the contrary, Nog increased only 4.047±1.036% (Figure 10, Db' and E) in cardiomyocytes as compared to control (1.553±0.1021%; Figure 10, Db and E). Immunoblotting also showed a significant increase of Tbx20 in cardiomyocytes upon ER stress, whereas Nog did not show any significant alteration in cardiomyocytes upon ER stress induction as compared to control (Figure 10, F and G). In fibroblasts, the expression of Nog was elevated up to 61.73±3.25% (Figure 10, Hb' and I) as compared to control (1.901±0.201%; Figure 10, Hb and I), whereas the expression of Tbx20 increased only 5.33±0.06% (Figure 10, Ha' and I) as compared to control (1.133±0.066%; Figure 10, Ha and I). Western blotting also showed a significant upregulation of Nog in cardiac fibroblasts during ER stress, whereas Tbx20 displayed no significant alteration (Figure 10, J and K).

Therefore, our study showed elevated levels of miR-101-3p in cardiac fibroblasts upon increasing ER stress. From all the observations, it can be inferred that Tbx20 and Nog are differentially expressed in cardiomyocytes and fibroblasts; Tbx20 is expressed more in cardiomyocytes, whereas Nog is expressed more in cardiac fibroblasts. It is also inferred from our study that the increase in Bmp2 in fibroblasts during prolonged stress is attributed to Nog and not Tbx20.

5.2.11 MiR-101-3p induces senescence in cardiac fibroblasts upon ER stress/hyperglycemia

We have previously demonstrated that miR-101-3p induces cardiomyocyte senescence by directly inhibiting the *tbx20* gene under stress conditions. Additionally, we observed that levels of miR-101-3p are elevated in cardiac fibroblasts when ER stress increases. Thus, we aimed to determine whether miR-101-3p also induces senescence in cardiac fibroblasts.

The SA-β-Gal staining revealed heightened SA-β-Gal activity in 50 µg/ml Tun-treated cells (Figure 11, Aa'' and B) as compared to 20 µg/ml Tun-treated (Figure 11, Aa' and B) and

control cells (Figure 11, Aa and B). Immunostaining also showed increased expression of senescent markers p21 (Figure 11, Ca'' and D) and γH2AX (Figure 11, Ca' and D) in 50 µg/ml Tun-treated cells compared to 20 µg/ml Tun-treated (Figure 11, Ca' and D; Figure 11, Cb' and D) and control cells (Figure 11, Ca and D; Figure 11, Cb and D) respectively. Therefore, from all these observations, we can conclude that miR-101-3p induces senescence of cardiac fibroblasts upon increasing ER stress.

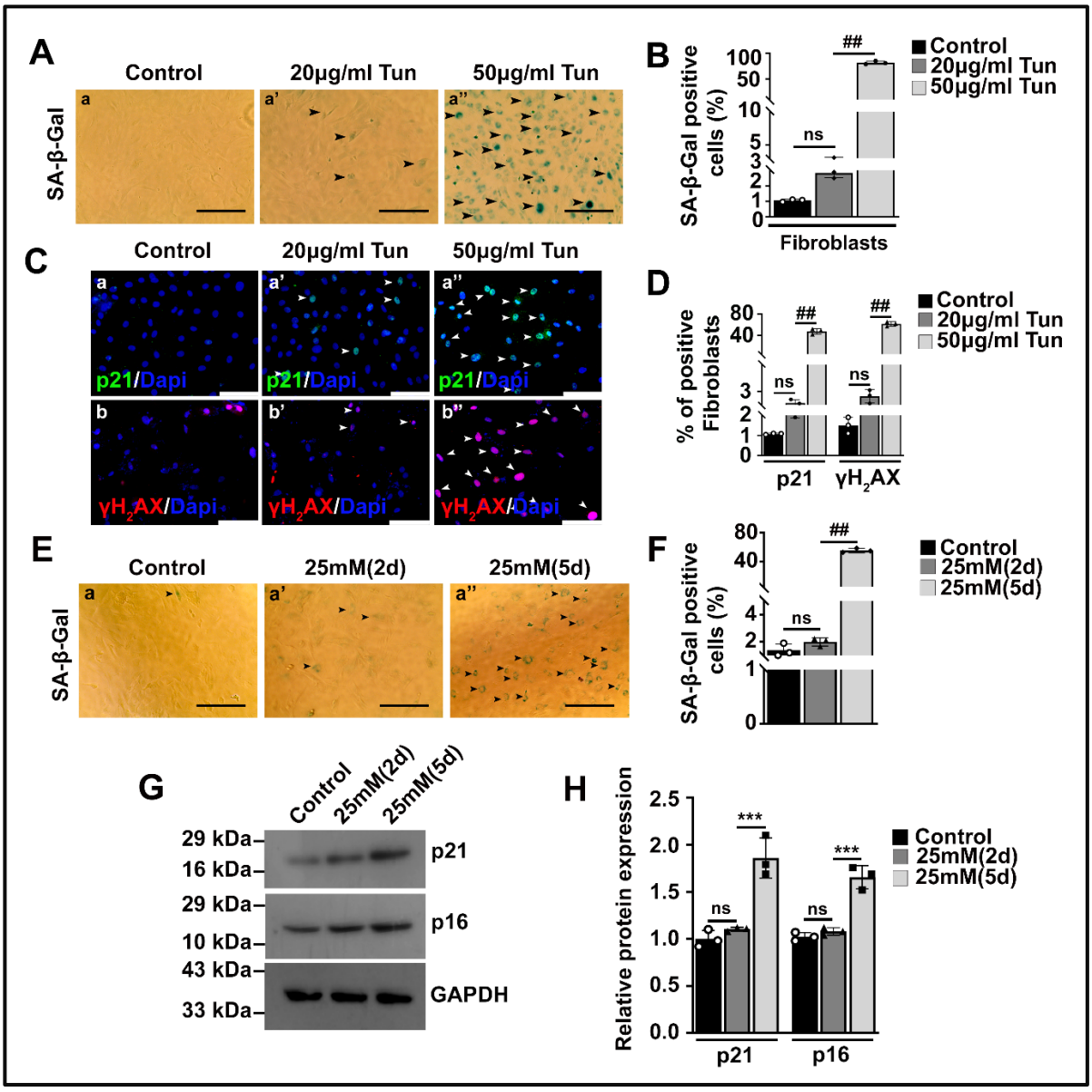

Figure 11. Increase in expression of miR-101-3p induces cardiac fibroblast senescence upon Endoplasmic Reticulum (ER) stress/hyperglycemia. A, SA-β-Gal staining showing increased cardiac fibroblast senescence during increasing ER stress. **B,** Quantitative representation of images from A. **C,** Immunofluorescence staining showing increased expression of senescent markers p21 and γH2AX in miR-101-3p mimic+20 µg/ml Tun treated cells (a'', b'') as compared to scrambled+20 µg/ml Tun (a', b') and scrambled (a, b) treated cells respectively. **D,** Quantitative representation of images from C. **E,** SA-β-Gal staining showing increasing senescence of fibroblasts during prolonged hyperglycemic stress (25mM 5d) compared to short duration (25mM 2d) and control. **F,** Quantitative representation of images

from E. **G,** Western blotting showing increased expression of senescent markers p21 and p16 during prolonged hyperglycemia (5d). **H,** Quantitative representation of proteins from G. The scale bar of the main image represents 50 µm. Statistical significance was calculated by one-way ANOVA. Error bars represent SD from three independent biological replicates (n=3); ns, p: nonsignificant, ∗p < 0.05, ∗∗p < 0.005, ∗∗∗p < 0.0005, ##p < 0.0001.

To further validate our observations, we also looked into the expression of senescent markers during hyperglycemic stress. SA-β-Gal staining showed increased β-Gal activity in hyperglycemia-induced for a longer duration (5 days) (Figure 11, Ea'' and F) as compared to 2 days (Figure 11, Ea' and F) and the control group (Figure 11, Ea and F). Immunostaining also showed significant upregulation of senescent markers p21 and p16 in the prolonged hyperglycemia group as compared to hyperglycemia induced for a shorter duration (2 days) and control group (Figure 11, G and H).

Taken together, our results show the involvement of miR-101-3p in inducing fibroblast senescence upon increasing/prolonging stress.

5.2.12 MiR-101-3p directly targets Nog

Since *in silico* analysis revealed a miR-101-3p binding site in the 3'UTR of the *nog* gene, therefore to ascertain direct binding we cloned the region of the *nog* 3'UTR containing the miR-101-3p seed sequence in pmiRGLO dual-luciferase vector (Figure 12A) and the direct binding was validated by luciferase assay. Ectopic transfection of miR-101-3p mimic along with the "wild-type (wt)" vector in HEK-293T cells resulted in significant downregulation of relative luciferase activity (Figure 12E).

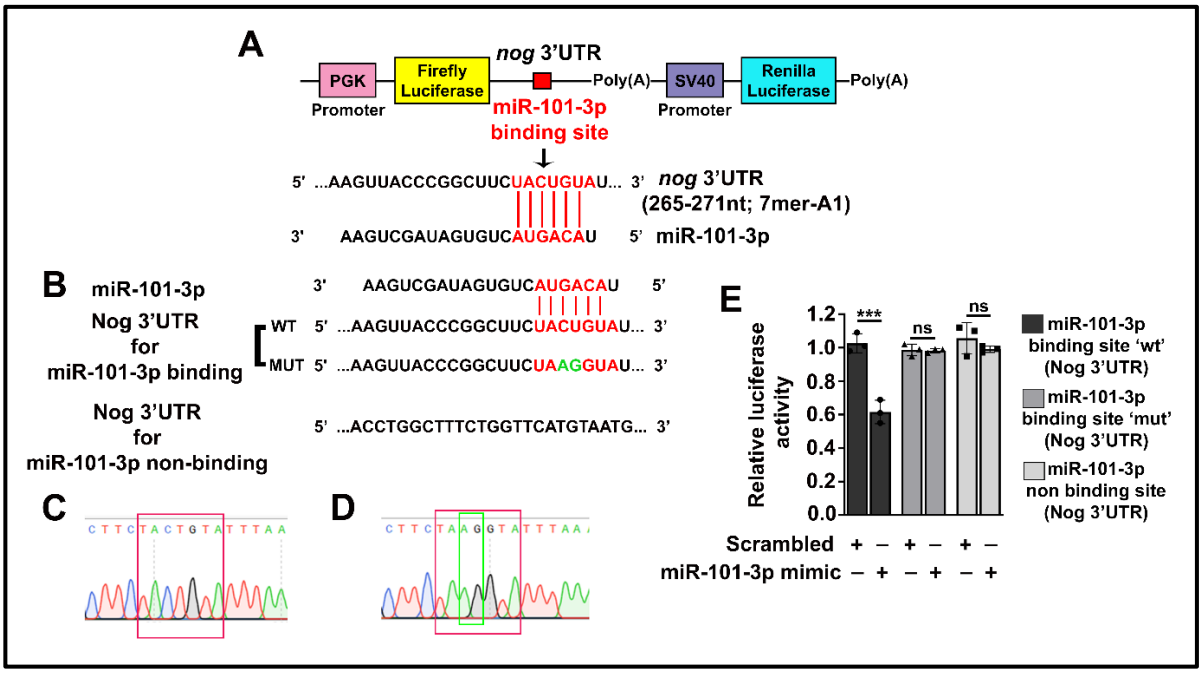

Figure 12. MiR-101-3p targets Noggin (Nog). A, Schematic diagram of pmirGLO-Nog-3'UTR reporter construct containing wild type (wt) binding site for miR-101-3p. **B,** Schematic diagram of pmirGLO-Nog-3'UTR reporter construct containing wild type (WT) and mutated (MUT) binding site for miR-101-3p. Schematic diagram of pmirGLO-Nog-3'UTR reporter constructs that do not contain a binding site for miR-101-3p. **C,** Chromatogram showing pmirGLO-Nog-3'UTR containing wild-type binding site for miR-101-3p (marked in red) after Sanger Sequencing. **D,** Chromatogram showing pmirGLO-Tbx20-3'UTR containing a mutated binding site for miR-101-3p (marked in green) after Sanger Sequencing. **E,** Relative luciferase activity showed the repressive effect of miR-101-3p on 'wt' Nog-3'UTR upon administration of miR-101-3p mimic. However, miR-101-3p mimic administration did not affect Nog-3'UTR containing a 'mut' binding site for miR-101-3p. miR-101-3p mimic administration did not affect Nog-3'UTR containing a 'non binding site' for miR-101-3p. Statistical significance was calculated by Student's *t*-test. Error bars represent SD from three independent biological replicates (n=3); ns, p: nonsignificant, $*p < 0.05$, $**p < 0.005$, $***p < 0.0005$, $\#\#p < 0.0001$.

The specificity of inhibition was further validated by introducing two point mutations in the seed region of the miR-101-3p binding site in the 3'UTR of the *nog* gene (Figure 12B). The introduction of two point mutations was corroborated by Sanger sequencing, and the chromatogram represents the wild-type and mutated seed sequence region (Figure 12, C and D). Ectopic transfection of miR-101-3p mimic along with "mutant (mut)" vector resulted in no significant alteration in luciferase activity compared to scrambled (Figure 12E). The specificity of binding was further validated by cloning a region of the *nog* 3'UTR that does not contain the miR-101-3p seed sequence. Luciferase assay revealed no inhibition of luciferase activity upon transfection of the non-binding construct (Figure 12E).

Therefore, altogether our data provide evidence of the previously unknown mechanism whereby miR-101-3p can bind to the *nog* gene to regulate its expression.

5.2.13 MiR-101-3p indirectly regulates the expression of Bmp2 by targeting Nog in cardiac fibroblasts

Since we established direct binding of miR-101-3p to *nog*, therefore we wanted to decipher the physiological relevance of our finding and the impact of miR-101-3p on both Nog and Bmp2 during ER stress. To achieve that, we transfected cardiac fibroblasts with either miR-101-3p mimic or inhibitor, followed by induction of ER stress and measured the expression level of Nog and Bmp2. Real-time PCR showed a significant decrease in the expression of the *nog* transcript in miR-101-3p mimic, followed by 20 μg/ml Tun-treated cells (2.7 ± 0.34-fold; Figure 13A) as compared to scrambled+20 μg/ml Tun (5.5 ± 1.12; Figure 13A). On the contrary, cardiac fibroblasts transfected with miR-101-3p inhibitor, followed by ER stress induction (50 μg/ml Tun), caused a significant increase in the level of *nog* (3.88 ± 0.45-fold; Figure 13A) transcript as compared to ER stress (50 μg/ml Tun) alone (2.1 ± 0.1-fold; Figure 13A). Immunoblotting also showed a similar regulation of Nog upon transfection

of miR-101-3p mimic or inhibitor (Figure 13B). Taken together, these observations prove that the expression of miR-101-3p is increased during increasing ER stress in cardiac fibroblasts, which in turn binds to *nog* 3'UTR, thereby degrading it and in turn lowering its expression.

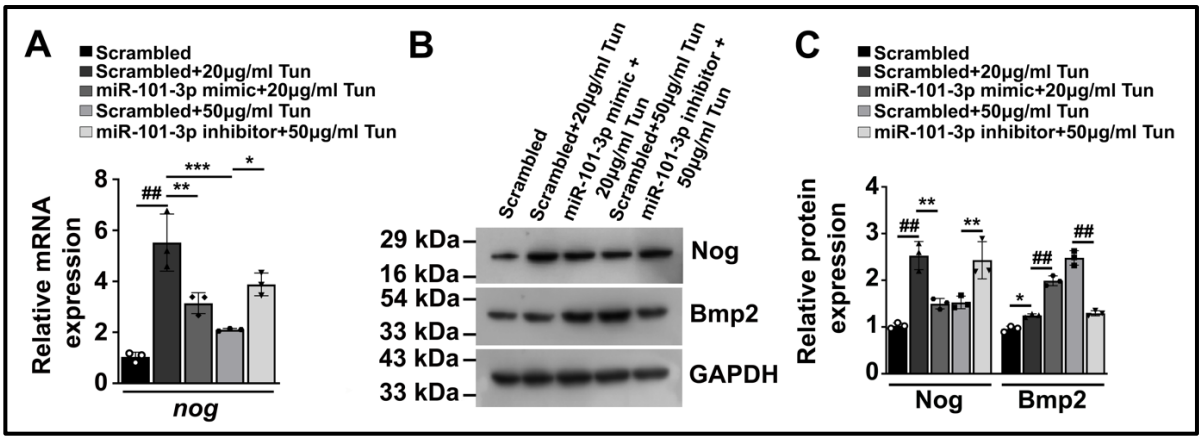

Figure 13. MiR-101-3p targeting of Noggin (Nog) upregulates Bone morphogenetic protein 2 (Bmp2) in cardiac fibroblasts. A, qRT-PCR showing increased expression of the *nog* gene upon treatment with scrambled+20 µg/ml Tun as compared to scramble alone, which was later decreased in scrambled+50 µg/ml Tun-treated cells. miR-101-3p mimic+20 µg/ml Tun administration resulted in a significant decrease in the expression of *nog* as compared to 20 µg/ml Tun alone-treated cardiomyocytes. miR-101-3p inhibitor+50 µg/ml Tun administration resulted in a significant increase in the expression of nog compared to only 50 µg/ml Tun-treated cardiomyocytes. **B,** Western blotting analysis showing a significant decrease in the expression of Nog and an increase of Bmp2 in miR-101-3p mimic+20 µg/ml Tun treated cells as compared to only 20 µg/ml Tun treated cardiomyocytes. miR-101-3p inhibitor+50 µg/ml Tun administration resulted in a significant increase in Nog and a decrease in Bmp2 as compared to only 50µg/ml Tun-treated cells. **C,** Quantitative representation of proteins from B. Statistical significance was calculated by one-way ANOVA Error bars represent SD from three independent biological replicates (n=3); ns, p: nonsignificant, $*p < 0.05$, $**p < 0.005$, $***p < 0.0005$, $##p < 0.0001$.

After discerning the regulation between miR-101-3p and Nog, we looked into the expression of Bmp2 since Nog is a Bmp2 antagonist. Nog regulates the Bmp2 signaling by binding to the Bmp2 ligand, thereby inhibiting it from binding to BMPR and, in turn, impeding the Bmp2 signaling axis (Zhu et al., 2006). Downregulation of Bmp2 signaling in turn results in attenuation in Bmp2 transcript and protein levels, as previous studies have shown that Bmp2 can auto-induce the transcription of its gene (Ghosh-Choudhury et al., 2001). Moreover, an increase in the Bmp2 signaling was shown to activate the transcript and protein levels of Bmp2 by phosphatidylinositol-3-kinase (PI-3-kinase)/Akt signaling via a feedback mechanism (Rogers et al., 2015). Immunoblotting revealed a significant increase in the expression of Bmp2 upon treatment with miR-101-3p mimic, followed by ER stress (20 µg/ml Tun) induction (2.01 ± 0.1-fold; Figure 13C) as compared to ER stress induction (20 µg/ml Tun) alone (1.2 ± 0.03-fold; Figure 13C). However, miR-101-3p inhibitor transfection followed by ER stress

induction (50 µg/ml Tun) resulted in significant downregulation of Bmp2 (2.49 ± 0.15-fold; Figure 13C) compared to ER stress induction (50 µg/ml Tun) alone (1.29 ± 0.05-fold; Figure 13C).

Therefore, our study establishes a novel regulatory pathway where, upon prolonging or increasing ER stress, miR-101-3p is recruited to the 3'UTR of the *nog* gene thereby decreasing its expression in cardiac fibroblasts. Decreased levels of Nog in turn fail to exert their inhibitory effect on Bmp2, thereby increasing its expression in fibroblasts.

5.2.14 MiR-101-3p mediated upregulation of Bmp2 drives inflammation of cardiac fibroblast

After establishing that Bmp2 is increased during prolonged or increasing stress, we wanted to delineate the downstream consequences of this increase. Interestingly, *in vivo,* we observed elevated expression of inflammatory markers *il6* and *tnfα* in murine hearts upon prolonged ER stress as compared to 8 hours and the control group (Figure 14A). To further verify the cell types of the heart where the inflammatory markers are expressed more, we treated both cardiomyocytes and fibroblasts with increasing concentrations of Tun to induce ER stress. The expression of inflammatory markers *il6* and *tnfα* was increased significantly in fibroblasts at a Tun concentration of 50 µg/ml compared to 20 µg/ml Tun and control cells (Figure 14B); however, in cardiomyocytes, we did not observe any significant change in the expression of both the inflammatory markers (Figure 14C). Thus, the increase in the expression of inflammatory markers in murine hearts during prolonged ER stress is attributed to fibroblasts. Previously, multiple studies have shown that elevated levels of Bmp2 result in increased inflammatory response. In our study, Western blotting showed a significant increase in the expression of Bmp2 during increasing ER stress (50 µg/ml Tun) in fibroblasts with a concomitant increase in the expression of inflammatory markers TNFα (Figure 14, D and E). Immunostaining also showed that with the decrease in the expression of Nog at a Tun concentration of 50 µg/ml, the expression of both Bmp2 and TNFα increased significantly (Figure 13, F and G). Therefore, to verify the direct involvement of Bmp2 in inducing inflammation, we induced ER stress (20 µg/ml Tun) in cardiac fibroblasts followed by ectopic administration of Recombinant Bmp2 (RecBmp2) protein. Both Western blotting and Immunostaining showed a significant upregulation in the expression of inflammatory marker TNFα upon RecBmp2 treatment following ER stress induction as compared to ER stress induction alone (Figure 14, H, I, J and K).

Taken together, our results showed that increased expression of miR-101-3p during increasing ER stress (50 µg/ml Tun) results in decreased activity of Nog. Since Nog is an inhibitor of Bmp2, inhibition of Nog by miR-101-3p results in increased expression of Bmp2 with concomitant increase in fibroblast inflammation. Altogether, our study potentiates the role of Bmp2 in inducing inflammation of fibroblasts, resulting in exacerbation of the progression of cardiomyopathy. Our study thus establishes Bmp2 in addition to miR-101-3p as a plausible biomarker for the early detection of cardiomyopathy.

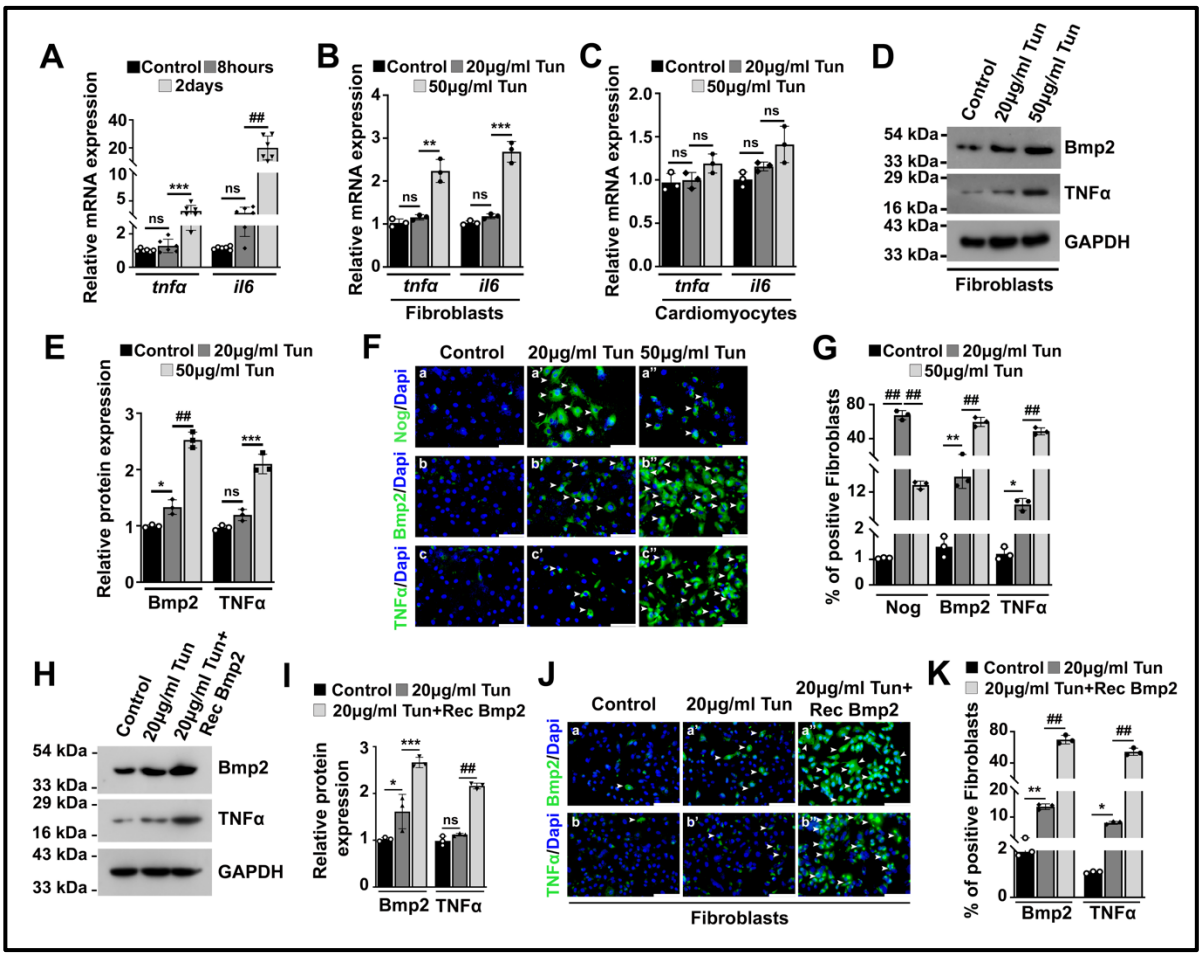

Figure 14. Upregulation of Bone morphogenetic protein 2 (Bmp2) drives inflammation of cardiac fibroblasts. A, qRT-PCR showing increased expression of inflammatory markers *tnfα* and *il6* during prolonged ER stress *in vivo*. **B,** qRT-PCR showing increased expression of inflammatory markers *tnfα* and *il6* during increasing ER stress (50 µg/ml Tun) in cardiac fibroblasts as compared to 20 µg/ml Tun-treated and control cells. **C,** qRT-PCR showing no significant change in the expression of inflammatory markers *tnfα* and *il6* during increasing ER stress (50 µg/ml Tun) in cardiomyocytes as compared to 20 µg/ml Tun-treated and control cells. **D,** Western blotting analysis showing increased expression of Bmp2 and inflammatory marker TNFα upon increasing ER stress (50 µg/ml Tun) as compared to 20 µg/ml Tun-treated and control cells. **E,** Quantitative representation of proteins from D. **F,** Immunofluorescence staining showing upregulation of Nog in 20 µg/ml Tun-treated cells (a') as compared to control (a). However, its expression is decreased in 50 µg/ml Tun-treated fibroblasts (a''). The expression of Bmp2 (b'') and TNFα (c'') is increased in 50 µg/ml Tun-treated fibroblasts as compared to 20 µg/ml Tun-treated (b', c') and control (b, c) cells. **G,** Quantitative representation of

images from F. **H,** Western blotting showing ER stress induction (20 μg/ml Tun) followed by treatment with Recombinant Bmp2 (RecBmp2) protein causes a significant increase in the expression of Bmp2 in cardiac fibroblasts. The expression of inflammatory marker TNFα increased significantly upon ER stress induction (20 μg/ml Tun) followed by RecBmp2 treatment. **I,** Quantitative representation of proteins from H. **J,** Immunofluorescence staining showing ER stress induction (20 μg/ml Tun) followed by treatment with Recombinant Bmp2 (RecBmp2) protein causes a significant increase in the expression of Bmp2 in cardiac fibroblasts. The expression of inflammatory marker TNFα is increased significantly upon ER stress induction (20 μg/ml Tun), followed by RecBmp2 treatment. **K,** Quantitative representation of proteins from C. Scale bar of the main image represents 50 μm. Statistical significance was calculated by Student's *t*-test. Error bars represent SD from three independent biological replicates (n=3); ns, p: nonsignificant, ∗p < 0.05, ∗∗p < 0.005, ∗∗∗p < 0.0005, ##p < 0.0001.

5.3 Discussion

Despite major developments in prognosis and therapeutics, CVD remains a major cause of death worldwide. Therefore, new advancements in the form of identification of early biomarkers are of utmost importance for saving millions of lives. In this study, we show that both *in vivo* and *in vitro,* the level of miR-101-3p is elevated during prolonged or increasing ER stress/diabetes. miR-101-3p, in turn, directly targets the *tbx20* gene in cardiomyocytes by directly binding to its 3'UTR and thereby suppressing it. Decreased levels of Tbx20, in turn, result in the upregulation of senescence response in cardiac cells, resulting in aggravation of cardiomyopathy. Cardiomyocyte-specific knockdown of Tbx20 was shown to elevate senescence, thus highlighting its importance in attenuating cardiac senescence during stress/diseases (Figure 15). We also observed a gradual and persistent augmentation of Bmp2 during different stresses like ER stress, Diabetes, T2MI and High-Fat diet model and this increase of Bmp2 was confined to cardiac fibroblasts and not cardiomyocytes. Upon discerning the cause of this increase in Bmp2, we observed direct binding of miR-101-3p to the 3'UTR of the *nog* gene in cardiac fibroblasts, which is an antagonist of Bmp2. An increase in Bmp2 was accompanied by subsequent upregulation of the inflammatory response in cardiac fibroblasts, thereby exacerbating the progression of cardiac disease (Figure 15). Thus, our study establishes miR-101-3p as a potential biomarker for the detection of cardiomyopathy and can be exploited further for the development of therapeutic interventions.

ER stress is often correlated with the onset and progression of CVDs. Multiple studies have shown that relieving the ER stress response is an effective therapeutic approach for treating cardiac diseases like atherosclerosis, arrhythmia, hypertension and heart failure (Kassan et al., 2012). Nowadays, lifestyle factors have become a cardinal cause for development of CVDs. Diet-induced obesity, which is a lifestyle-induced disease, is often associated with the development of cardiac diseases like atherosclerosis, fibrillation, systemic

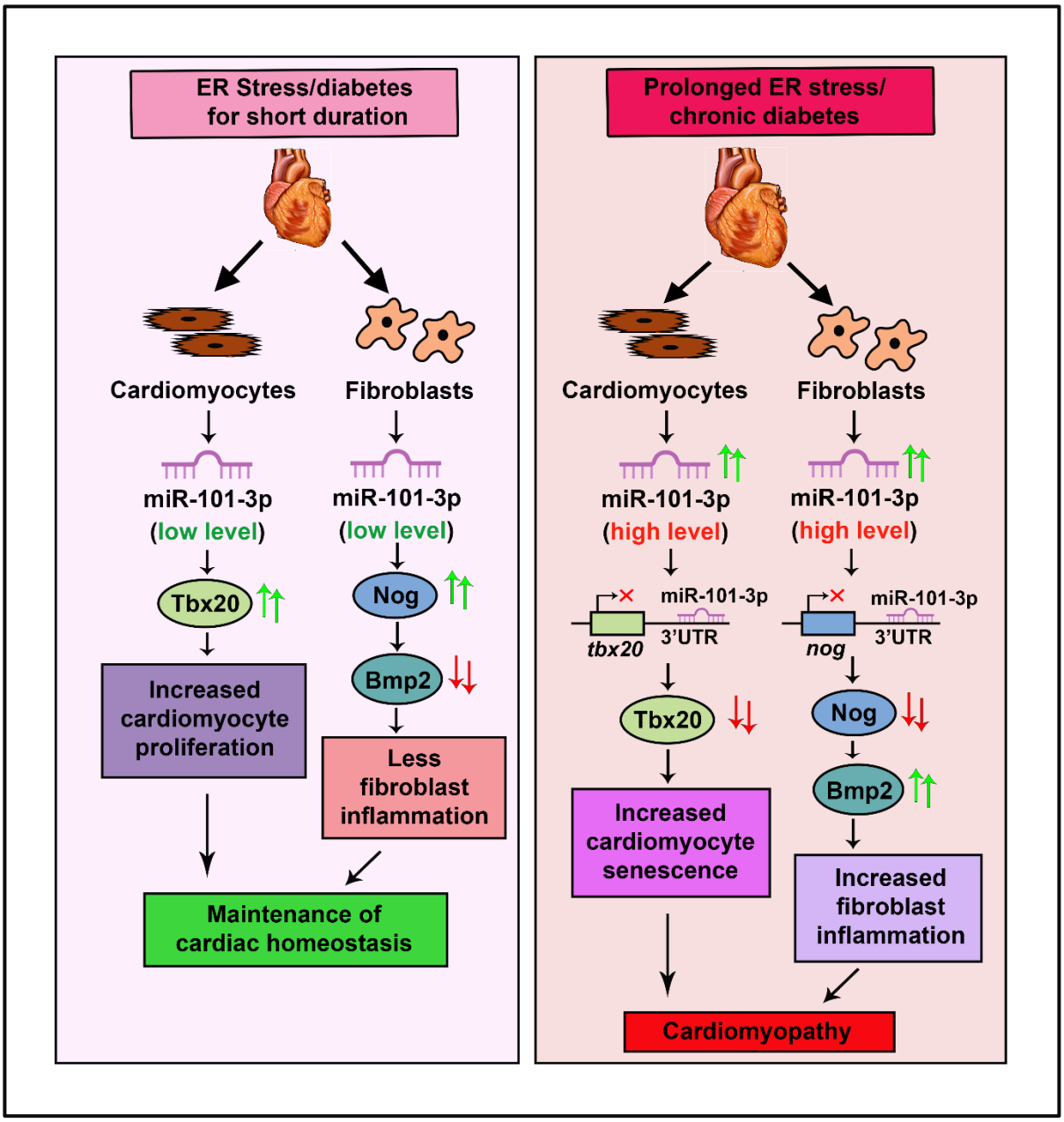

Figure 15. Model for Endoplasmic Reticulum (ER) stress-mediated upregulation of miR-101-3p, resulting in increased cardiomyocyte senescence and inflammation by targeting T-box transcription factor (Tbx20) and Noggin (Nog), respectively. Mild ER/Diabetes is associated with upregulation of Tbx20 and Nog in cardiomyocytes and fibroblasts, respectively, resulting in maintenance of cardiac homeostasis by increasing cardiomyocyte proliferation and decreasing cardiac senescence and inflammation. However, prolonged stress results in significant upregulation of miR-101-3p in cardiac cells. miR-101-3p in turn targets Tbx20 and Nog in cardiomyocytes and fibroblasts, respectively, by directly binding to their 3'UTR. Downregulation of Tbx20 is associated with increased cardiomyocyte senescence, thus resulting in cardiomyopathy. Downregulation of Nog results in concomitant upregulation of Bmp2 in cardiac fibroblasts, which in turn results in increased inflammatory response, thus adding to the severity of cardiomyopathy.

inflammation and heart failure (Joseph et al., 2022). ER stress and obesity, in turn, are associated with the pathogenesis and progression of Type 2 Diabetes Mellitus (T2DM)

(Mustapha et al., 2021; Scherer & Hill, 2016). T2DM, in turn, causes the pathophysiology of atherosclerosis and diabetic cardiomyopathy (De Rosa et al., 2018). Another factor in today's world that is often linked to cardiac diseases is aging. Aging results in the build-up of senescent cells, which is detrimental as it results in cell cycle arrest, upregulation of senescent markers p21, p16, p53, increased DNA damage and elevated secretion of SASPs (Luan et al., 2024). Thus, the identification of common factors that are associated with or contribute to the development of cardiomyopathy due to the above-mentioned stress responses will be invaluable in generating early biomarkers for the detection and cure of CVDs.

Tbx20 plays a pivotal role and is an indispensable factor for proper cardiac development. It interacts with other cardiac genes, such as Nkx2.5, GATA4, and GATA5, to ensure heart development (Stennard et al., 2003). Overexpression of Tbx20 in adult cardiomyocytes leads to an increase in proliferative factors like Cyclin D1, E1, and IGF-1, while decreasing cell cycle inhibitors such as p21 and Meis1 (Xiang et al., 2016). We have also shown that Tbx20 drives adult cardiomyocyte proliferation via the Bmp2-pSmad1/5/8 pathway during ER stress (Das et al., 2023). Therefore, it serves as a crucial mediator for adult cardiac proliferation, and identifying regulatory factors that promote the expression of Tbx20 during various stresses could have significant therapeutic implications for restoring cardiac homeostasis.

In this chapter, we demonstrate that miR-101-3p directly targets Tbx20 during prolonged or chronic stresses (such as ER stress and diabetes) to induce cardiomyocyte senescence. Thus, our study suggests for the first time that miR-101-3p can act as an effective biomarker, as its elevation is associated with increased cardiomyopathy during ER stress and diabetes. Moreover, using a miR-101-3p antagonist may provide an effective therapeutic approach to alleviate the inhibitory effect of miR-101-3p on Tbx20 and reactivate cardiomyocyte proliferation.

Bmp2 is a signaling molecule that belongs to the Transforming growth factor beta (TGFβ) superfamily and has been implicated in proper cardiac development. We have previously shown that Bmp2 augments cardiomyocyte proliferation during ER stress (Das et al., 2023). However, though Bmp2 have many protective roles in cardiac development and proper cardiac function, there are contradicting reports that suggest Bmp2 is involved in the pathogenesis of cardiac diseases. In adult ischemic porcine hearts, Bmp2 gene transfer results in pericardial effusion and increased inflammatory response (Pulkkinen et al., 2023). Increased plasma levels of Bmp2 correlate with atherosclerosis in Type 2 Diabetes patients (Zhang et al., 2015). Gremlin2, a Bmp2 antagonist, was shown to ameliorate Bmp2-mediated inflammation

post MI (Sanders et al., 2016). Here in this study, we found Bmp2 to be significantly upregulated during different stresses (ER stress, Diabetes, T2MI and High-Fat diet model). miR-101-3p mediated targeting of Nog resulted in the upregulation of Bmp2. Here, we show that Bmp2 further accentuates the inflammatory response in cardiac fibroblasts, thereby deteriorating the advancement of cardiomyopathy. Some previous studies have shown that increased Bmp2 mediated inflammation results in seroma, edema and radiculitis (J. Shen et al., 2013). Therefore, the identification of factors that drive Bmp2 towards increased inflammation is important in maintaining a proper balance to restore homeostasis. Another pivotal observation from our study is the gradual and progressive increase in the expression of Bmp2 throughout disease progression. The initial upregulation of Bmp2 in cardiomyocytes is beneficial as it drives cardiomyocyte proliferation; however, the increase later in cardiac fibroblasts is detrimental as it drives an inflammatory response. Therefore, our study also establishes Bmp2 as a plausible early biomarker for the detection of cardiac diseases and warrants further investigation.

Non-coding RNA, specifically miRNAs, can often regulate gene expression. Among the different miRNAs, miR-101-3p can regulate the expression of different genes to induce cardiac diseases. In one study, inhibition of miR-101-3p was shown to ameliorate myocardial injury induced by sepsis by attenuating the MAPK and NF-κB pathway (Xin et al., 2021). In humans, inhibition of miR-101-3p suppresses interstitial cell calcification in the aorta by regulating the CDH11/SOX9 signaling axis (Chen et al., 2023). miR-101-3p was also shown as a plausible biomarker for acute cellular rejection in patients with heart transplantation (Sukma Dewi et al., 2017). There are very few reports of miR-101-3p in regulating cardiac diseases, and its role in regulating cardiomyopathy during ER stress or diabetes is not yet explored. Only a single study has shown elevated levels of circulating miR-101-3p in Type 1 Diabetes patients (Santos et al., 2019). Our overwhelming observations of miR-101-3p directly binding to Tbx20 and Nog, thereby indirectly regulating the expression of Bmp2 and, in turn, increasing the senescence and inflammatory response in cardiac tissue during prolonged stress, makes it a potential biomarker candidate for the detection of cardiomyopathy.

Cardiac senescence is a stress-induced phenomenon that results in cell cycle arrest, DNA damage, telomere attrition, upregulation of tumor suppressor genes, and activation of secretory and inflammatory phenotypes. Senescence is accompanied by an abundance of detrimental consequences, like upregulation of pro-inflammatory factors that in turn infiltrate the neighbouring cells, thereby damaging them and aggravating the progression of disease. ER

stress is shown to cause senescence as senescent cells show abnormalities of the ER and also display increased UPR signaling, which in turn results in aberration of proteostasis in senescent cells (Marino et al., 2022; Pluquet et al., 2015). Diabetes mellitus also causes senescence, which in turn disrupts cardiac regeneration and cardiac function (Marino et al., 2022). However, no studies to date have shown the probable mechanism of how ER stress or diabetes induces cardiac senescence. Here, in this study, we show how miR-101-3p regulates the senescent response in cardiac cells. Senolytic drugs are extensively used to reduce the burden of senescent cells during aging. Dasatinib and quercetin are two drugs whose combinatorial administration has shown promising results in killing senescent cells (Islam et al., 2023). Dasatinib, an anti-neoplastic drug and quercetin, a flavonoid, are currently under clinical trial. Using these drugs in our study can reduce the burden of senescent cells during prolonged stresses and warrants further investigation.

Therefore, in conclusion, this chapter elucidates how miR-101-3p attenuates the expression of Tbx20 in cardiomyocytes to induce senescence. We also show how miR-101-3p attenuates Nog in cardiac fibroblasts to indirectly increase the expression of Bmp2 and, in turn, the inflammatory response. Thus, we substantiate miR-101-3p as a plausible biomarker candidate for the detection of cardiomyopathy. It can also be showcased as a novel target for the development of effective therapeutic interventions. Modulating the levels of miR-101-3p by using antagonists can serve as an effective therapeutic approach for restoring cardiac homeostasis, and it needs further investigation. The gradual and persistently increasing expression of Bmp2 throughout disease progression during all four stresses (ER stress, Diabetes, T2MI and High-Fat diet administration) makes it a potential biomarker for early detection of cardiac disease. Attenuating the progression of Bmp2 during prolonged stresses by using inhibitors can serve as effective therapeutics for reducing the severity of cardiac diseases, and it warrants further studies. Studies in various rodent models subjected to prolonged or chronic stress, along with research on cultured cardiomyocytes, indicate that a proper balance of stress response is crucial for the effective functioning of Tbx20 and the maintenance of cardiac homeostasis.

Chapter 6

Conclusions

The cardiovascular system, which comprises of heart and blood vessels, is responsible for transporting blood, oxygen and nutrients to all parts of the body and removing waste materials from the body. Any perturbation to this system results in the development of cardiovascular diseases (CVDs). It is the foremost cause of death globally, with a death toll of approximately 17.9 million every year. With this death toll rising every year, early identification by the development of biomarkers and proper therapeutic interventions is of utmost importance. Cardiac regeneration is the main arena of CVDs that needs to be addressed, as though the developing heart is highly proliferative, after birth, the proliferation ceases as the cardiomyocyte exits the cell cycle, and they grow primarily by hypertrophy. Upon encountering any stress or injury, the cardiomyocytes eventually die, and the existing ones are unable to make up for the overwhelming loss, eventually resulting in the space being occupied by fibrotic scar. Recently, multiple studies have shown the possibility of adult cardiomyocyte regeneration via regulating different cardiac transcription factors, signaling pathways, as well as stem cell therapies.

Tbx20 is one such cardiac transcription factor that is integral for proper cardiac development, as loss of Tbx20 results in looping defects, hypoplastic heart and embryonic death at day 10.5. Tbx20 was also shown to interact with other cardiac genes like Nkx2.5, GATA4 and GATA5 to synergistically regulate the expression of cardiac genes. Overexpression of Tbx20 in the adult heart was shown to revive cardiomyocyte proliferation post-injury. Therefore, understanding the mechanism behind Tbx20 mediated re-initiation of cardiomyocyte proliferation of the adult heart during different cardiac injuries is invaluable in the field of cardiac regeneration. ER stress is a stress driven phenomenon that has been extensively linked to the development of CVDs. The upregulation of the UPR is driven by ER stress, which is initially advantageous; however, prolonging the stress often leads to a shift towards cell death. Additionally, ER stress has been linked to the development of diabetic cardiomyopathy. However, no study to date has shown any mechanistic role of Tbx20 during ER stress induced cardiomyopathy.

The findings elucidated in this thesis demonstrates a) The role of Tbx20 in inducing adult cardiomyocyte proliferation during ER stress/diabetes via the Bmp2-pSmad1/5/8 pathway, thus shifting the balance towards cardiac homeostasis; b) The involvement of miR-101-3p in regulating the expression of Tbx20 and Bmp2 during prolonged ER stress/diabetes; c) The role of Tbx20 in attenuating senescence response in cardiomyocytes and Bmp2 in upregulating inflammatory response in cardiac fibroblasts during ER stress/diabetes.

Tbx20 was shown to be upregulated during the short duration of ER stress. The Atf6 arm of the UPR resulted in an augmentation in the expression of Tbx20 by directly binding its promoter. Tbx20 was shown to induce cardiomyocyte proliferation both *in vivo* and *in vitro* by upregulating the Bmp2-pSmad1/5/8 signaling axis. Increased expression of Tbx20 during ER stress was shown to maintain normal cardiac function, as evidenced by Electrocardiographic studies as well as cardiac marker studies. Upregulation of Tbx20 during ER stress resulted in limiting cardiomyocyte apoptosis, which was corroborated by knockdown studies. The importance of Tbx20 in restoring homeostasis was also validated by the suppression of ROS generation and fibrotic marker expression upon knockdown of Tbx20 during ER stress. Knockdown of Tbx20, along with overexpression of Bmp2 and Bmp2 antagonist Nog during ER stress, showed the molecular hierarchy between Tbx20 and Bmp2, where Tbx20 was reported to work upstream of Bmp2 in imparting protection during ER stress. Bmp2 was also shown to regulate the expression of Tbx20 via a feed-forward loop mechanism. During diabetes *in vivo* and hyperglycemia *in vitro,* upregulation of Tbx20 resulted in augmentation of cardiomyocyte proliferation. However, prolonging or increasing the stress response caused a downregulation of Tbx20 with a concomitant decrease in cardiomyocyte proliferation. On the contrary, the expression of Bmp2 showed a steady upregulation. A decrease in the expression of Tbx20 was accompanied by an altered cardiac function, increased ROS generation, and increased expression of fibrotic and apoptotic markers. Thus, a decrease in the expression of Tbx20 during prolonged stress results in a shifting of the balance towards pro-apoptosis.

The intriguing finding of altered expression of Tbx20 and Bmp2 during prolonged stress led us to uncover the possible factors involved. The expression of Tbx20 and Bmp2 was also validated during other stresses like Diabetes, T2MI and High-Fat diet. During all the stresses, the expression of Tbx20 initially increased for a short duration, which was reversed upon prolonging the injury. However, the expression of Bmp2 showed a gradual upregulation throughout the injury progression. The involvement of miRNAs in regulating the expression of genes during different pathophysiological conditions prompted us to look for their involvement in the altered expression profile of Tbx20 and Bmp2. miR-101-3p is the one that caught our attention since *in silico* analysis showed the presence of miR-101-3p binding site in the 3'UTR of *tbx20* and *nog* (a Bmp2 antagonist) gene, and very few studies have been done so far to show the involvement of miR-101-3p during CVDs. In our study, the expression of miR-101-3p was elevated during prolonged ER stress and diabetes. miR-101-3p was shown to directly bind to *tbx20* 3'UTR, thereby resulting in augmentation of senescence response in

cardiomyocytes. The negative regulation of Tbx20 on senescence response was corroborated by the knockdown of Tbx20 and miR-101-3p mimic and inhibitor administration.

Upon deciphering the cause for the persistent upregulation of Bmp2 throughout injury progression, we observed upregulation of Bmp2 in cardiac fibroblasts and not cardiomyocytes during prolonged stress. miR-101-3p was shown to be elevated during increasing ER stress in cardiac fibroblasts. The presence of the miR-101-3p binding site in the 3'UTR of the *nog* gene led us to look into the differential expression of Tbx20 and Nog in cardiomyocytes and fibroblasts, since, in cardiomyocytes, Tbx20 regulates the expression of Bmp2. Both at the basal level and during stress, Tbx20 was shown to be expressed more in cardiomyocytes, whereas Nog is expressed more in fibroblasts during these conditions. miR-101-3p was shown to directly bind to the *nog* gene, thereby suppressing its expression and indirectly increasing the expression of Bmp2 in cardiac fibroblasts. Increased expression of Bmp2, in turn, was shown to upregulate the expression of inflammatory markers IL-6 and TNFα , which was corroborated by overexpression of Bmp2 during ER stress.

Therefore, our study unveiled the novel regulatory pathway where miR-101-3p represses the expression of Tbx20 in cardiomyocytes, thereby upregulating the senescence response. miR-101-3p was also shown to suppress the expression of Nog, thereby increasing the levels of Bmp2 and augmenting the inflammatory response in fibroblasts.

In conclusion, it can be inferred from our studies that Tbx20 is an indispensable transcription factor that drives adult cardiomyocyte proliferation during the initial stages of injury response via Bmp2-pSmad1/5/8 signaling. Therefore, we predict that overexpression of Tbx20 or cardiomyocyte-specific upregulation of Bmp2 could serve as a novel therapeutic approach to confer protection against ER stress and shift the balance of UPR towards pro-survival. The downregulation in the expression of Tbx20 during prolonged injury and the concomitant upregulation of Bmp2 were shown to be driven by the elevation of miR-101-3p during prolonged stress induction. miR-101-3p was shown to induce senescence and inflammatory response in cardiac cells by directly regulating Tbx20 and indirectly regulating Bmp2 via Nog, thereby exacerbating cardiomyopathy. Taken together, our study substantiates miR-101-3p as a plausible biomarker for the detection of cardiomyopathy. miR-101-3p could be exploited as a novel target for the development of therapeutics for the treatment of cardiomyopathy. The gradual increase of Bmp2 throughout the disease progression, as corroborated under different stress conditions, establishes Bmp2 as a potential biomarker for early detection of cardiomyopathy. Modulating the levels of miR-101-3p by antagonist or

attenuating the drastic increase of Bmp2 during prolonged stresses by inhibitors could result in the restoration of cardiac homeostasis and warrants further investigation (Figure 1).

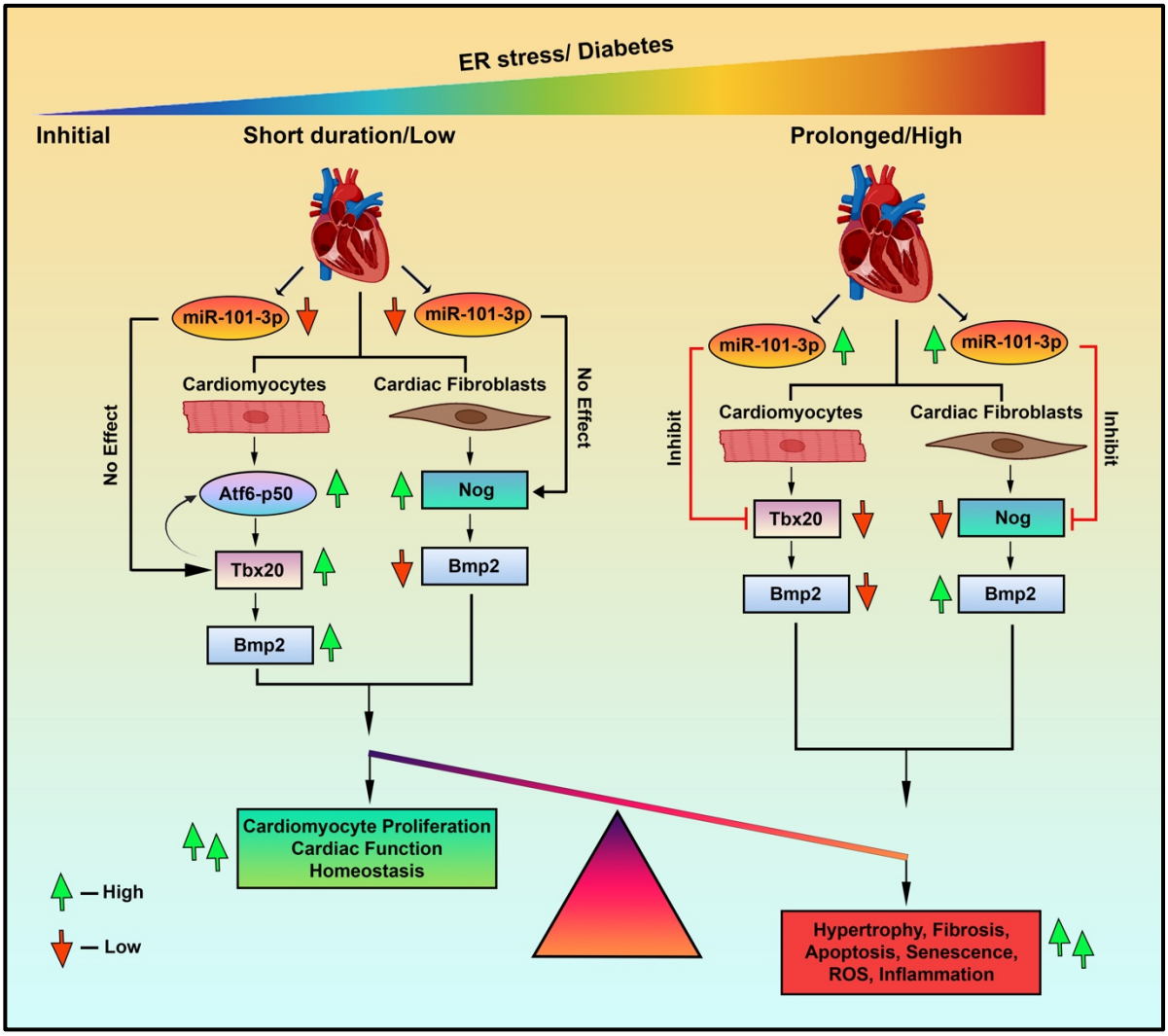

Figure 1. Study Conclusion. Schematic illustration representing the study conclusion. A short duration or low dosage of stress (ER stress/Diabetes) results in no significant alteration of miR-101-3p. Stress induces the upregulation of Tbx20 in cardiomyocytes mediated by the Atf6 arm of UPR signaling. Upregulation of Tbx20 causes a concomitant elevation of Bmp2-pSmad1/5/8 signaling. An increase in Bmp2 signaling results in increased cardiomyocyte proliferation. Upregulation of Tbx20 improves cardiac function and restoration of cardiac homeostasis. Short duration or lower dosage of stress results in upregulation of Nog in cardiac fibroblasts. Increased expression of Nog antagonizes Bmp2 in fibroblasts, thereby restoring homeostasis. A prolonged or high dosage of stress (ER stress/Diabetes) results in a significant increase of miR-101-3p in cardiomyocytes and cardiac fibroblasts. In the cardiomyocytes, miR-101-3p directly binds to Tbx20 and suppresses its expression. Decreased expression of Tbx20 results in a concomitant decrease of Bmp2 with decreased cardiomyocyte proliferation. Decrease in the expression of Tbx20 results in increased hypertrophy, fibrosis, senescence and apoptosis of cardiomyocytes. Reduced expression of Tbx20 also results in altered cardiac functions. In cardiac fibroblasts, increased levels of miR-101-3p suppress Nog, which in turn increases the expression of Bmp2. Increased expression of Bmp2 in cardiac fibroblasts results in increased inflammatory response. miR-101-3p mediated targeting of Tbx20 in cardiomyocytes and Nog in cardiac fibroblasts, thereby causing exacerbation of cardiomyopathy.

Chapter 7

Bibliography

Aanhaanen, W. T. J., Boukens, B. J. D., Sizarov, A., Wakker, V., et al. (2011). Defective Tbx2-dependent patterning of the atrioventricular canal myocardium causes accessory pathway formation in mice. *Journal of Clinical Investigation*, *121*(2), 534–544.

Abdullahi, A., Stanojcic, M., Parousis, A., Patsouris, D., et al. (2017). Modeling Acute ER Stress in Vivo and in Vitro. *Shock*, *47*(4), 506–513.

Acharya, A., Baek, S. T., Huang, G., Eskiocak, B., et al. (2012). The bHLH transcription factor Tcf21 is required for lineage-specific EMT of cardiac fibroblast progenitors. *Development*, *139*(12), 2139–2149.

Aird, W. C. (2001). Vascular bed-specific hemostasis: Role of endothelium in sepsis pathogenesis. *Critical Care Medicine*, *29*, S28–S34.

Aird, W. C. (2007). Phenotypic Heterogeneity of the Endothelium. *Circulation Research*, *100*(2), 158–173.

Aird, W. C. (2012). Endothelial Cell Heterogeneity. *Cold Spring Harbor Perspectives in Medicine*, *2*(1), a006429–a006429.

Alarcón, C. R., Lee, H., Goodarzi, H., Halberg, N., et al F. (2015). N6-methyladenosine marks primary microRNAs for processing. *Nature*, *519*(7544), 482–485.

Allagnat, F., Fukaya, M., Nogueira, T. C., Delaroche, D., et al. (2012). C/EBP homologous protein contributes to cytokine-induced pro-inflammatory responses and apoptosis in β-cells. *Cell Death & Differentiation*, *19*(11), 1836–1846.

Almazloum, A., & Khalil, H. (2023). Isolation of Adult Mouse Cardiac Fibroblasts. *Current Protocols*, *3*(7), e840.

Al-Shabrawey, M., Hussein, K., Wang, F., Wan, M., et al. (2021). Bone Morphogenetic Protein-2 Induces Non-Canonical Inflammatory and Oxidative Pathways in Human Retinal Endothelial Cells. *Frontiers in Immunology*, *11*, 568795.

Anderson, R. H., Mori, S., Spicer, D. E., Brown, N. A., et al. (2016). Development and Morphology of the Ventricular Outflow Tracts. *World Journal for Pediatric and Congenital Heart Surgery*, *7*(5), 561–577.

Aneja, A., Tang, W. H. W., Bansilal, S., Garcia, M. J., et al. (2008). Diabetic Cardiomyopathy: Insights into Pathogenesis, Diagnostic Challenges, and Therapeutic Options. *The American Journal of Medicine*, *121*(9), 748–757.

Antar, S. A., Ashour, N. A., Sharaky, M., Khattab, M., et al. (2023). Diabetes mellitus: Classification, mediators, and complications; A gate to identify potential targets for the development of new effective treatments. *Biomedicine & Pharmacotherapy*, *168*, 115734.

Antzelevitch, C., & Burashnikov, A. (2011). Overview of Basic Mechanisms of Cardiac Arrhythmia. *Cardiac Electrophysiology Clinics*, *3*(1), 23–45.

Avolio, E., Mangialardi, G., Slater, S. C., Alvino, V. V., et al. (2021). Secreted Protein Acidic and Cysteine Rich Matricellular Protein is Enriched in the Bioactive Fraction of the Human Vascular Pericyte Secretome. *Antioxidants & Redox Signaling*, *34*(15), 1151–1164.

Back, S. H., & Kaufman, R. J. (2012). Endoplasmic Reticulum Stress and Type 2 Diabetes. *Annual Review of Biochemistry*, *81*(1), 767–793.

Bahler, R. C., Vrobel, T. R., & Martin, P. (1983). The relation of heart rate and shortening fraction to echocardiographic indexes of left ventricular relaxation in normal subjects. *Journal of the American College of Cardiology*, *2*(5), 926–933.

Bakhshi, A., Khani, M., Alipour Parsa, S., Khaheshi, I., et al. (2024). Investigating the expression level of miR-17-3p, miR-101-3p, miR-335-3p, and miR-296-3p in the peripheral blood of patients with acute myocardial infarction. *Molecular and Cellular Biochemistry*, *479*(4), 859–868.

Banerjee, I., Yekkala, K., Borg, T. K., & Baudino, T. A. (2006). Dynamic Interactions between Myocytes, Fibroblasts, and Extracellular Matrix. *Annals of the New York Academy of Sciences*, *1080*(1), 76–84.

Basatemur, G. L., Jørgensen, H. F., Clarke, M. C. H., Bennett, M. R., et al. (2019). Vascular smooth muscle cells in atherosclerosis. *Nature Reviews Cardiology*, *16*(12), 727–744.

Baudino, T. A., McFadden, A., Fix, C., Hastings, J., Price, R., & Borg, T. K. (2008). Cell Patterning: Interaction of Cardiac Myocytes and Fibroblasts in Three-Dimensional Culture. *Microscopy and Microanalysis*, *14*(2), 117–125.

Bayraktar, M., & Manner, J. (2014). Cardiac looping may be driven by compressive loads resulting from unequal growth of the heart and pericardial cavity. Observations on a physical simulation model. *Frontiers in Physiology*, *5*, 112.

Bernardo, B. C., Gao, X.-M., Winbanks, C. E., Boey, E. J. H., et al. (2012). Therapeutic inhibition of the miR-34 family attenuates pathological cardiac remodeling and improves heart function. *Proceedings of the National Academy of Sciences*, *109*(43), 17615–17620.

Bers, D. M. (2002). Cardiac excitation–contraction coupling. *Nature*, *415*(6868), 198–205.

Bersell, K., Arab, S., Haring, B., & Kühn, B. (2009). Neuregulin1/ErbB4 Signaling Induces Cardiomyocyte Proliferation and Repair of Heart Injury. *Cell*, *138*(2), 257–270.

Bhandary, B., Marahatta, A., Kim, H.-R., & Chae, H.-J. (2012). An Involvement of Oxidative Stress in Endoplasmic Reticulum Stress and Its Associated Diseases. *International Journal of Molecular Sciences*, *14*(1), 434–456.

Bhattarai, K. R., Riaz, T. A., Kim, H.-R., & Chae, H.-J. (2021). The aftermath of the interplay between the endoplasmic reticulum stress response and redox signaling. *Experimental & Molecular Medicine*, *53*(2), 151–167.

Bhimji, S., Godin, D. V., & McNeill, J. H. (1986). Myocardial Ultrastructural Changes in Alloxan-Induced Diabetes in Rabbits. *Cells Tissues Organs*, *125*(3), 195–200.

Blackwood, E. A., Azizi, K., Thuerauf, D. J., Paxman, R. J., et al. (2019). Pharmacologic ATF6 activation confers global protection in widespread disease models by reprograming cellular proteostasis. *Nature Communications*, *10*(1), 187.

Boogerd, C. J., Aneas, I., Sakabe, N., Dirschinger, R. J., et al. (2016). Probing chromatin landscape reveals roles of endocardial TBX20 in septation. *Journal of Clinical Investigation*, *126*(8), 3023–3035.

Boogerd, C. J., Zhu, X., Aneas, I., Sakabe, N., et al. (2018). Tbx20 is required in mid-gestation cardiomyocytes and plays a central role in atrial development. *Circulation Research*, *123*(4), 428–442.

Boon, R. A., & Vickers, K. C. (2013). Intercellular Transport of MicroRNAs. *Arteriosclerosis, Thrombosis, and Vascular Biology*, *33*(2), 186–192.

Boudina, S., Sena, S., Theobald, H., Sheng, X., et al. (2007). Mitochondrial energetics in the heart in obesity-related diabetes: Direct evidence for increased uncoupled respiration and activation of uncoupling proteins. *Diabetes*, *56*(10), 2457–2466.

Braun, J. E., Truffault, V., Boland, A., Huntzinger, E., et al. (2012). A direct interaction between DCP1 and XRN1 couples mRNA decapping to 5′ exonucleolytic degradation. *Nature Structural & Molecular Biology*, *19*(12), 1324–1331.

Briggs, L. E., Burns, T. A., Lockhart, M. M., Phelps, A. L., et al. (2016). Wnt/β-catenin and sonic hedgehog pathways interact in the regulation of the development of the dorsal mesenchymal protrusion. *Developmental Dynamics*, *245*(2), 103–113.

Briggs, L. E., Phelps, A. L., Brown, E., Kakarla, J., et al (2013). Expression of the BMP Receptor Alk3 in the Second Heart Field Is Essential for Development of the Dorsal Mesenchymal Protrusion and Atrioventricular Septation. *Circulation Research*, *112*(11), 1420–1432.

Broughton, J. P., Lovci, M. T., Huang, J. L., Yeo, G. W., et al. (2016). Pairing beyond the Seed Supports MicroRNA Targeting Specificity. *Molecular Cell*, *64*(2), 320–333.

Bryant, D. M., O'Meara, C. C., Ho, N. N., Gannon, J., et al. (2015). A systematic analysis of neonatal mouse heart regeneration after apical resection. *Journal of Molecular and Cellular Cardiology*, *79*, 315–318.

Buckingham, M., Meilhac, S., & Zaffran, S. (2005). Building the mammalian heart from two sources of myocardial cells. *Nature Reviews Genetics*, *6*(11), 826–835.

Bueno Marinas, M., Celeghin, R., Cason, M., Bariani, R., et al. (2020). A microRNA Expression Profile as Non-Invasive Biomarker in a Large Arrhythmogenic Cardiomyopathy Cohort. *International Journal of Molecular Sciences*, *21*(4), 1536.

Buijtendijk, M. F. J., Barnett, P., & van den Hoff, M. J. B. (2020). Development of the human heart. *American Journal of Medical Genetics Part C: Seminars in Medical Genetics*, *184*(1), 7–22.

Burman, A., Tanjore, H., & Blackwell, T. S. (2018). Endoplasmic reticulum stress in pulmonary fibrosis. *Matrix Biology*, *68–69*, 355–365.

Caballero, R., Utrilla, R. G., Amorós, I., Matamoros, M., et al. (2017). Tbx20 controls the expression of the *KCNH2* gene and of hERG channels. *Proceedings of the National Academy of Sciences*, *114*(3), E416–E425.

Cai, C. L., Zhou, W., Yang, L., Bu, L., et al. (2005). T-box genes coordinate regional rates of proliferation and regional specification during cardiogenesis. *Development*, *132*(10), 2475–2487.

Cai, C., Xie, Y., Wu, liangliang, Chen, X., et al. (2017). PLGA-based dual targeted nanoparticles enhance miRNA transfection efficiency in hepatic carcinoma. *Scientific Reports*, *7*(1), 46250.

Cai, C. L., Liang, X., Shi, Y., Chu, P.-H., et al. (2003). Isl1 Identifies a Cardiac Progenitor Population that Proliferates Prior to Differentiation and Contributes a Majority of Cells to the Heart. *Developmental Cell*, *5*(6), 877–889.

Cai, X., Nomura-Kitabayashi, A., Cai, W., Yan, J., et al. (2011). Myocardial Tbx20 regulates early atrioventricular canal formation and endocardial epithelial–mesenchymal transition via Bmp2. *Developmental Biology*, *360*(2), 381–390.

Cai, X., Zhang, W., Hu, J., Zhang, L., et al. (2013). Tbx20 acts upstream of Wnt signaling to regulate endocardial cushion formation and valve remodeling during mouse cardiogenesis. *Development*, *140*(15), 3176–3187.

Calero, A., & Illig, K. A. (2016). Overview of aortic aneurysm management in the endovascular era. *Seminars in vascular surgery*, *29*(1-2), 3–17.

Camenisch, T. D., Schroeder, J. A., Bradley, J., Klewer, S. E., et al. (2002). Heart-valve mesenchyme formation is dependent on hyaluronan-augmented activation of ErbB2–ErbB3 receptors. *Nature Medicine*, *8*(8), 850–855.

Cao, S. S., & Kaufman, R. J. (2014). Endoplasmic Reticulum Stress and Oxidative Stress in Cell Fate Decision and Human Disease. *Antioxidants & Redox Signaling*, *21*(3), 396–413.

Cao, Z., Jia, Y., & Zhu, B. (2019). BNP and NT-proBNP as Diagnostic Biomarkers for Cardiac Dysfunction in Both Clinical and Forensic Medicine. *International Journal of Molecular Sciences*, *20*(8), 1820.

Carabello, B. A. (2002). Concentric versus eccentric remodeling. *Journal of cardiac failure*, *8*(6 Suppl), S258–S263.

Chakraborty, S., Sengupta, A., & Yutzey, K. E. (2013). Tbx20 promotes cardiomyocyte proliferation and persistence of fetal characteristics in adult mouse hearts. *Journal of Molecular and Cellular Cardiology*, *62*, 203–213.

Chen, J., Lin, Y., & Sun, Z. (2023). Inhibition of miR-101-3p prevents human aortic valve interstitial cell calcification through regulation of CDH11/SOX9 expression. *Molecular Medicine*, *29*(1), 24.

Chen, P. Y., Qin, L., Li, G., Malagon-Lopez, J., et al. (2020). Smooth Muscle Cell Reprogramming in Aortic Aneurysms. *Cell Stem Cell*, *26*(4), 542-557.e11.

Chen, S., Puthanveetil, P., Feng, B., Matkovich, S. J., et al. (2014). Cardiac miR-133a overexpression prevents early cardiac fibrosis in diabetes. *Journal of Cellular and Molecular Medicine*, *18*(3), 415–421.

Chen, Y., Xiao, D., Zhang, L., Cai, C. L., et al. (2021). The Role of Tbx20 in Cardiovascular Development and Function. *Frontiers in cell and developmental biology*, *9*, 638542.

Chen, Y., Zhao, Y., Chen, W., Xie, L., et al. (2017). MicroRNA-133 overexpression promotes the therapeutic efficacy of mesenchymal stem cells on acute myocardial infarction. *Stem Cell Research & Therapy*, *8*(1), 268.

Chipurupalli, S., Samavedam, U., & Robinson, N. (2021). Crosstalk Between ER Stress, Autophagy and Inflammation. *Frontiers in medicine*, *8*, 758311.

Chowdhry, M. F., Vohra, H. A., & Galiñanes, M. (2007). Diabetes increases apoptosis and necrosis in both ischemic and nonischemic human myocardium: Role of caspases and poly-adenosine diphosphate-ribose polymerase. *Journal of Thoracic and Cardiovascular Surgery*, *134*(1), 124–131.e1313.

Christie, M., Boland, A., Huntzinger, E., Weichenrieder, O., et al. (2013). Structure of the PAN3 Pseudokinase Reveals the Basis for Interactions with the PAN2 Deadenylase and the GW182 Proteins. *Molecular Cell*, *51*(3), 360–373.

Christoffels, V. M., Habets, P. E. M. H., Franco, D., Campione, M., et al. (2000). Chamber formation and morphogenesis in the developing mammalian heart. *Developmental Biology*, *223*(2), 266–278.

Christoffels, V. M., Smits, G. J., Kispert, A., & Moorman, A. F. M. (2010). Development of the Pacemaker Tissues of the Heart. *Circulation Research*, *106*(2), 240–254.

Chung, Y.-H., Huang, Y.-H., Chu, T.-H., Chen, C.-L., et al. (2018). BMP-2 restoration aids in recovery from liver fibrosis by attenuating TGF-β1 signaling. *Laboratory Investigation*, *98*(8), 999–1013.

Clark, A. L., Maruyama, S., Sano, S., Accorsi, A., et al. (2016). miR-410 and miR-495 Are Dynamically Regulated in Diverse Cardiomyopathies and Their Inhibition Attenuates Pathological Hypertrophy. *PLOS ONE*, *11*(3), e0151515.

Collesi, C., Zentilin, L., Sinagra, G., & Giacca, M. (2008). Notch1 signaling stimulates proliferation of immature cardiomyocytes. *The Journal of Cell Biology*, *183*(1), 117–128.

Condrat, C. E., Thompson, D. C., Barbu, M. G., Bugnar, O. L., et al. (2020). miRNAs as Biomarkers in Disease: Latest Findings Regarding Their Role in Diagnosis and Prognosis. *Cells*, *9*(2), 276.

Coppola, G., Carità, P., Corrado, E., Borrelli, A., et al. (2013). ST segment elevations: Always a marker of acute myocardial infarction? *Indian Heart Journal*, *65*(4), 412–423.

Cossu, G., & Bianco, P. (2003). Mesoangioblasts — vascular progenitors for extravascular mesodermal tissues. *Current Opinion in Genetics & Development*, *13*(5), 537–542.

Crider, A., Nelson, T., Davis, T., Fagan, K., et al. (2018). Estrogen Receptor β Agonist Attenuates Endoplasmic Reticulum Stress-Induced Changes in Social Behavior and Brain Connectivity in Mice. *Molecular Neurobiology*, *55*(9), 7606–7618.

Csiszar, A., Ahmad, M., Smith, K. E., Labinskyy, N., et al. (2006). Bone morphogenetic protein-2 induces proinflammatory endothelial phenotype. *American Journal of Pathology*, *168*(2), 629–638.

Cui, W., Li, J., Ron, D., & Sha, B. (2011). The structure of the PERK kinase domain suggests the mechanism for its activation. *Acta Crystallographica Section D Biological Crystallography*, *67*(5), 423–428.

Cybulsky, A. V., Takano, T., Papillon, J., Khadir, A., et al. (2002). Complement C5b-9 Membrane Attack Complex Increases Expression of Endoplasmic Reticulum Stress Proteins in Glomerular Epithelial Cells. *Journal of Biological Chemistry*, *277*(44), 41342–41351.

da Costa Martins, P. A., Salic, K., Gladka, M. M., Armand, A.-S., et al. (2010). MicroRNA-199b targets the nuclear kinase Dyrk1a in an auto-amplification loop promoting calcineurin/NFAT signalling. *Nature Cell Biology*, *12*(12), 1220–1227.

Dai, Y., & Zhang, X. (2019). MicroRNA Delivery with Bioreducible Polyethylenimine as a Non-Viral Vector for Breast Cancer Gene Therapy. *Macromolecular Bioscience*, *19*(4), e1800445.

Danielson, L. S., Park, D. S., Rotllan, N., Chamorro-Jorganes, A., et al. (2013). Cardiovascular dysregulation of miR-17-92 causes a lethal hypertrophic cardiomyopathy and arrhythmogenesis. *The FASEB Journal*, *27*(4), 1460–1467.

Das, S., Mondal, A., Dey, C., Chakraborty, S., et al. (2023). ER stress induces upregulation of transcription factor Tbx20 and downstream Bmp2 signaling to promote cardiomyocyte survival. *Journal of Biological Chemistry*, *299*(4), 103031.

Das, S., Mondal, A., Samanta, J., Chakraborty, S., et al. (2021). Unfolded protein response during cardiovascular disorders: a tilt towards pro-survival and cellular homeostasis. *Molecular and cellular biochemistry*, *476*(11), 4061–4080.

de Boer, B. A., van den Berg, G., Soufan, A. T., de Boer, P. A. J., et al. (2012). Measurement and 3D-Visualization of Cell-Cycle Length Using Double Labelling with Two Thymidine Analogues Applied in Early Heart Development. *PLOS ONE*, *7*(10), e47719.

De Bono, C., Thellier, C., Bertrand, N., Sturny, R., et al. (2018). T-box genes and retinoic acid signaling regulate the segregation of arterial and venous pole progenitor cells in the murine second heart field. *Human Molecular Genetics*, *27*(21), 3747–3760.

de Rie, D., Abugessaisa, I., Alam, T., Arner, E., et al. (2017). An integrated expression atlas of miRNAs and their promoters in human and mouse. *Nature Biotechnology*, *35*(9), 872–878.

De Rosa, S., Arcidiacono, B., Chiefari, E., Brunetti, A., et al. (2018). Type 2 Diabetes Mellitus and Cardiovascular Disease: Genetic and Epigenetic Links. *Frontiers in Endocrinology*, *9*, 2.

Del Monte-Nieto, G., Ramialison, M., Adam, A. A. S., Wu, B., et al. (2018). Control of cardiac jelly dynamics by NOTCH1 and NRG1 defines the building plan for trabeculation. *Nature*, *557*(7705), 439–445.

Delmar, M., & Liang, F.-X. (2012). Connexin43 and the regulation of intercalated disc function. *Heart Rhythm*, *9*(5), 835–838.

Denli, A. M., Tops, B. B. J., Plasterk, R. H. A., Ketting, R. F., et al. (2004). Processing of primary microRNAs by the Microprocessor complex. *Nature*, *432*(7014), 231–235.

Derynck, R., & Zhang, Y. E. (2003). Smad-dependent and Smad-independent pathways in TGF-β family signalling. *Nature*, *425*(6958), 577–584.

Dhahri, W., Sadikov Valdman, T., Wilkinson, D., Pereira, E., et al. (2022). In Vitro Matured Human Pluripotent Stem Cell–Derived Cardiomyocytes Form Grafts With Enhanced Structure and Function in Injured Hearts. *Circulation*, *145*(18), 1412–1426.

Dill, T. L., & Naya, F. J. (2018). A Hearty Dose of Noncoding RNAs: The Imprinted DLK1-DIO3 Locus in Cardiac Development and Disease. *Journal of Cardiovascular Development and Disease*, *5*(3), 37.

Disertori, M., Masè, M., & Ravelli, F. (2017). Myocardial fibrosis predicts ventricular tachyarrhythmias. *Trends in cardiovascular medicine*, *27*(5), 363–372.

Du, L., Liu, C., Teng, M., Meng, Q., et al. (2016). Anti-diabetic activities of Paecilomyces tenuipes N45 extract in alloxan-induced diabetic mice. *Molecular Medicine Reports*, *13*(2), 1701–1708.

Du, W., Liang, H., Gao, X., Li, X., et al. (2016). MicroRNA-328, a Potential Anti-Fibrotic Target in Cardiac Interstitial Fibrosis. *Cellular Physiology and Biochemistry*, *39*(3), 827–836.

Duan, J., Gherghe, C., Liu, D., Hamlett, E., et al. (2012). Wnt1/βcatenin injury response activates the epicardium and cardiac fibroblasts to promote cardiac repair. *The EMBO Journal*, *31*(2), 429–442.

Ebert, M. S., & Sharp, P. A. (2010). MicroRNA sponges: Progress and possibilities. *RNA*, *16*(11), 2043–2050.

Eguchi, K., Boden-Albala, B., Jin, Z., Rundek, T., et al. (2008). Association Between Diabetes Mellitus and Left Ventricular Hypertrophy in a Multi-Ethnic Population. *The American journal of cardiology*, *101*(12), 1787–1791.

Espinoza-Lewis, R. A., Yu, L., He, F., Liu, H., et al. (2009). Shox2 is essential for the differentiation of cardiac pacemaker cells by repressing Nkx2-5. *Developmental Biology*, *327*(2), 376–385.

Evangelou, K., Vasileiou, P. V. S., Papaspyropoulos, A., Hazapis, O., et al. (2023). Cellular senescence and cardiovascular diseases: moving to the "heart" of the problem. *Physiological Reviews*, *103*(1), 609–647.

Fabiato, A. (1985). Time and calcium dependence of activation and inactivation of calcium-induced release of calcium from the sarcoplasmic reticulum of a skinned canine cardiac Purkinje cell. *The Journal of General Physiology*, *85*(2), 247–289.

Fan, K.-L., Zhang, H.-F., Shen, J., Zhang, Q., et al. (2013). Circulating microRNAs levels in Chinese heart failure patients caused by dilated cardiomyopathy. *Indian Heart Journal*, *65*(1), 12–16.

Fang, L., Ellims, A. H., Moore, X., White, D. A., et al. (2015). Circulating microRNAs as biomarkers for diffuse myocardial fibrosis in patients with hypertrophic cardiomyopathy. *Journal of Translational Medicine*, *13*(1), 314.

Ferron, M., Denis, M., Persello, A., Rathagirishnan, R., et al. (2019). Protein O-GlcNAcylation in Cardiac Pathologies: Past, Present, Future. *Frontiers in Endocrinology*, *9*, 819.

Finney, A. C., Stokes, K. Y., Pattillo, C. B., & Orr, A. W. (2017). Integrin signaling in atherosclerosis. *Cellular and Molecular Life Sciences*, *74*(12), 2263–2282.

Forte, E., Panahi, M., Baxan, N., Ng, F. S., et al. (2021). Type 2 MI induced by a single high dose of isoproterenol in C57BL/6J mice triggers a persistent adaptive immune response against the heart. *Journal of Cellular and Molecular Medicine*, *25*(1), 229–243.

Franco, D., Markman, M. M. W., Wagenaar, G. T. M., Ya, J., et al. (1999). Myosin light chain 2a and 2v identifies the embryonic outflow tract myocardium in the developing rodent heart. *The Anatomical Record*, *254*(1), 135–146.

Franco, D., Meilhac, S. M., Christoffels, V. M., Kispert, A., et al. (2006). Left and right ventricular contributions to the formation of the interventricular septum in the mouse heart. *Developmental biology*, *294*(2), 366–375.

Friedlander, M. R., Lizano, E., Houben, A. J., Bezdan, D., et al. (2014). Evidence for the biogenesis of more than 1,000 novel human microRNAs. *Genome Biology*, *15*(4), R57.

Geng, H., & Guan, J. (2017). MiR-18a-5p inhibits endothelial–mesenchymal transition and cardiac fibrosis through the Notch2 pathway. *Biochemical and Biophysical Research Communications*, *491*(2), 329–336.

Ghannam, S., Bouffi, C., Djouad, F., Jorgensen, C., et al. (2010). Immunosuppression by mesenchymal stem cells: mechanisms and clinical applications. *Stem Cell Research & Therapy*, *1*(1), 2.

Ghosh-Choudhury, N., Ghosh Choudhury, G., Harris, M. A., Wozney, J., et al. (2001). Autoregulation of Mouse BMP-2 Gene Transcription Is Directed by the Proximal Promoter Element. *Biochemical and Biophysical Research Communications*, *286*(1), 101–108.

Greco, S., Fasanaro, P., Castelvecchio, S., D'Alessandra, Y., et al. (2012). MicroRNA Dysregulation in Diabetic Ischemic Heart Failure Patients. *Diabetes*, *61*(6), 1633–1641.

Grego-Bessa, J., Luna-Zurita, L., del Monte, G., Bolos, V., et al. (2007). Notch signaling is essential for ventricular chamber development. *Developmental cell*, *12*(3), 415–429.

Greulich, F., Rudat, C., & Kispert, A. (2011). Mechanisms of T-box gene function in the developing heart. *Cardiovascular research*, *91*(2), 212–222

Groenendyk, J., Sreenivasaiah, P. K., Kim, D. H., Agellon, L. B., et al. (2010). Biology of endoplasmic reticulum stress in the heart. *Circulation research*, *107*(10), 1185–1197.

Guha, P., Kaptan, E., Gade, P., Kalvakolanu, D. V., et al. (2017). Tunicamycin induced endoplasmic reticulum stress promotes apoptosis of prostate cancer cells by activating mTORC1. *Oncotarget*, *8*(40), 68191–68207.

Guijarro-Munoz, I., Compte, M., Alvarez-Cienfuegos, A., Alvarez-Vallina, L., et al. (2014). Lipopolysaccharide Activates Toll-like Receptor 4 (TLR4)-mediated NF-κB Signaling Pathway and Proinflammatory Response in Human Pericytes. *Journal of Biological Chemistry*, *289*(4), 2457–2468.

Guo, R., & Nair, S. (2017). Role of microRNA in diabetic cardiomyopathy: From mechanism to intervention. *Biochimica et biophysica acta. Molecular basis of disease*, *1863*(8), 2070–2077.

Halloran, D., Durbano, H. W., & Nohe, A. (2020). Developmental review bone morphogenetic protein-2 in development and bone homeostasis. *Journal of Developmental Biology*, *8*(3), 19.

Hammer, S., Toenjes, M., Lange, M., Fischer, J. J., et al. (2008). Characterization of TBX20 in human hearts and its regulation by TFAP2. *Journal of Cellular Biochemistry*, *104*(3), 1022–1033.

Han, Z., Wang, K., Ding, S., & Zhang, M. (2024). Cross-talk of inflammation and cellular senescence: a new insight into the occurrence and progression of osteoarthritis. *Bone Research*, *12*(1), 69.

Harvey, R. P. (2002). Patterning the vertebrate heart. *Nature Reviews Genetics*, *3*(7), 544–556.

Hatzopoulos, S., Petruccelli, J., Laurell, G., Finesso, M., et al. (2002). Evaluation of anesthesia effects in a rat animal model using otoacoustic emission protocols. *Hearing Research*, *170*(1–2), 12–21.

Haubner, B. J., Adamowicz-Brice, M., Khadayate, S., Tiefenthaler, V., et al. (2012). Complete cardiac regeneration in a mouse model of myocardial infarction. *Aging*, *4*(12), 966–977.

Hayat, S. A., Patel, B., Khattar Rajdeep S., & Malik, R. A. (2004). Diabetic cardiomyopathy: mechanisms, diagnosis and treatment. *Clinical Science*, *107*(6), 539–557.

Hayflick, L., & Moorhead, P. S. (1961). The serial cultivation of human diploid cell strains. *Experimental Cell Research*, *25*(3), 585–621.

Herrmann, B. G., Labeit, S., Poustka, A., Kingt, T. R., et al. (1990). *Cloning of the T gene required in mesoderm formation in the mouse. Nature*, *343*(6259), 617–622.

Hirai, M., Chen, J., & Evans, S. M. (2016). Tissue-Specific Cell Cycle Indicator Reveals Unexpected Findings for Cardiac Myocyte Proliferation. *Circulation Research*, *118*(1), 20–28.

Hogers, B., DeRuiter, M. C., Baasten, A. M. J., Gittenberger-de Groot, A. C., et al. (1995). Intracardiac Blood Flow Patterns Related to the Yolk Sac Circulation of the Chick Embryo. *Circulation Research*, *76*(5), 871–877.

Houweling, A. C., Somi, S., Van Den Hoff, M. J., Moorman, A. F., et al. (2002). Developmental pattern of ANF gene expression reveals a strict localization of cardiac chamber formation in chicken. *The Anatomical record*, *266*(2), 93–102.

Hu, C., Zhang, X., Teng, T., Ma, Z.-G., et al. (2022). Cellular Senescence in Cardiovascular Diseases: A Systematic Review. *Aging and Disease*, *13*(1), 103.

Huang, R.-T., Wang, J., Xue, S., Qiu, X.-B., et al. (2017). TBX20 loss-of-function mutation responsible for familial tetralogy of Fallot or sporadic persistent truncus arteriosus. *International Journal of Medical Sciences*, *14*(4), 323–332.

Huang, W., Hickson, L. J., Eirin, A., Kirkland, J. L., et al. (2022). Cellular senescence: the good, the bad and the unknown. *Nature Reviews Nephrology*, *18*(10), 611–627.

Huang, Z.-P., & Wang, D.-Z. (2014). miR-22 in cardiac remodeling and disease. *Trends in Cardiovascular Medicine*, *24*(7), 267–272.

Hynynen, H., Mutikainen, M., Naumenko, N., Shakirzyanova, A., et al. (2020). Short high-fat diet interferes with the physiological maturation of the late adolescent mouse heart. *Physiological reports, 8*(13), e14474.

Ieda, M., Tsuchihashi, T., Ivey, K. N., Ross, R. S., et al. (2009). Cardiac Fibroblasts Regulate Myocardial Proliferation through β1 Integrin Signaling. *Developmental Cell*, *16*(2), 233–244.

Ihara, D., Watanabe, Y., Seya, D., Arai, Y., et al. (2020). Expression of Hey2 transcription factor in the early embryonic ventricles is controlled through a distal enhancer by Tbx20 and Gata transcription factors. *Developmental Biology*, *461*(2), 124–131.

Ikeda, S., Kong, S. W., Lu, J., Bisping, E., et al. (2007). Altered microRNA expression in human heart disease. *Physiological Genomics*, *31*(3), 367–373.

Islam, M. M., & Takeyama, N. (2023). Role of Neutrophil Extracellular Traps in Health and Disease Pathophysiology: Recent Insights and Advances. *International journal of molecular sciences*, *24*(21), 15805.

Islam, M. T., Tuday, E., Allen, S., Kim, J., et al. (2023). Senolytic drugs, dasatinib and quercetin, attenuate adipose tissue inflammation, and ameliorate metabolic function in old age. *Aging Cell*, *22*(2), e13767.

Jackson, K. A., Majka, S. M., Wang, H., Pocius, J., et al. (2001). Regeneration of ischemic cardiac muscle and vascular endothelium by adult stem cells. *Journal of Clinical Investigation*, *107*(11), 1395–1402.

Jackson, C. V, McGrath, G. M., Tahiliani, A. G., Vadlamudi, R. V. S. V, et al. (1985). A Functional and Ultrastructural Analysis of Experimental Diabetic Rat Myocardium: Manifestation of a Cardiomyopathy. *Diabetes*, *34*(9), 876–883.

Janssen, R., Zuidwijk, M., Muller, A., Mulders, J., et al. (2013). Cardiac Expression of Deiodinase type 3 (Dio3) Following Myocardial Infarction Is Associated With the Induction of a Pluripotency microRNA Signature from the Dlk1-Dio3 Genomic Region. *Endocrinology*, *154*(6), 1973–1978.

Janssens, S., Pulendran, B., & Lambrecht, B. N. (2014). Emerging functions of the unfolded protein response in immunity. *Nature Immunology*, *15*(10), 910-919.

Japp, A. G., Gulati, A., Cook, S. A., Cowie, M. R., et al. (2016). The Diagnosis and Evaluation of Dilated Cardiomyopathy. *Journal of the American College of Cardiology*, *67*(25), 2996–3010.

Jennings, R. B., & Ganote, C. E. (1974). Structural changes in myocardium during acute ischemia. *Circulation research*, *35* Suppl 3, 156–172.

Jiang, X., Yang, Z., & Dong, M. (2020). Cardiac repair in a murine model of myocardial infarction with human induced pluripotent stem cell-derived cardiomyocytes. *Stem Cell Research & Therapy*, *11*(1), 297.

Jin, J. K., Blackwood, E. A., Azizi, K., Thuerauf, D. J., et al. (2017). ATF6 Decreases Myocardial Ischemia/Reperfusion Damage and Links ER Stress and Oxidative Stress Signaling Pathways in the Heart. *Circulation Research*, *120*(5), 862–875.

Joseph, J. J., Deedwania, P., Acharya, T., Aguilar, D., et al. (2022). Comprehensive Management of Cardiovascular Risk Factors for Adults With Type 2 Diabetes: A Scientific Statement From the American Heart Association. *Circulation*, *145*(9), e722–e759.

Ju, C., Shen, Y., Ma, G., Liu, Y., et al. (2018). Transplantation of Cardiac Mesenchymal Stem Cell-Derived Exosomes Promotes Repair in Ischemic Myocardium. *Journal of Cardiovascular Translational Research*, *11*(5), 420–428.

Julien, O., & Wells, J. A. (2017). Caspases and their substrates. *Cell Death & Differentiation*, *24*(8), 1380–1389.

Kassan, M., Galán, M., Partyka, M., Saifudeen, Z., et al. (2012). Endoplasmic Reticulum Stress Is Involved in Cardiac Damage and Vascular Endothelial Dysfunction in Hypertensive Mice. *Arteriosclerosis, Thrombosis, and Vascular Biology*, *32*(7), 1652–1661.

Katz, T. C., Singh, M. K., Degenhardt, K., Rivera-Feliciano, J., et al. (2012). Distinct Compartments of the Proepicardial Organ Give Rise to Coronary Vascular Endothelial Cells. *Developmental Cell*, *22*(3), 639–650.

Kaur, N., Raja, R., Ruiz-Velasco, A., & Liu, W. (2020). Cellular Protein Quality Control in Diabetic Cardiomyopathy: From Bench to Bedside. *Frontiers in cardiovascular medicine*, *7*, 585309.

Kawamata, T., & Tomari, Y. (2010). Making RISC. *Trends in Biochemical Sciences*, *35*(7), 368–376.

Keith, A., & Flack, M. W. (2004). The auriculo-ventricular bundle of the human heart. *Annals of Noninvasive Electrocardiology*, *9*(4), 400–409.

Kim, H. W., & Weintraub, N. L. (2016). Aortic Aneurysm. *Arteriosclerosis, Thrombosis, and Vascular Biology*, *36*(11), 2138–2140.

Kohl, P. (2003). Heterogeneous Cell Coupling in the Heart. *Circulation Research*, *93*(5), 381–383.

Laflamme, M. A., Chen, K. Y., Naumova, A. V, Muskheli, V., et al. (2007). Cardiomyocytes derived from human embryonic stem cells in pro-survival factors enhance function of infarcted rat hearts. *Nature Biotechnology*, *25*(9), 1015–1024.

Lai, D., Liu, X., Forrai, A., Wolstein, O., et al P. (2010). Neuregulin 1 Sustains the Gene Regulatory Network in Both Trabecular and Nontrabecular Myocardium. *Circulation Research*, *107*(6), 715–727.

Lämmerhirt, L., Kappelmann-Fenzl, M., Fischer, S., Meier, P., et al. (2024). Loss of miR-101-3p in melanoma stabilizes genomic integrity, leading to cell death prevention. *Cellular & Molecular Biology Letters*, *29*(1), 29.

Lawson, W. E., Cheng, D.-S., Degryse, A. L., Tanjore, H., et al. (2011). Endoplasmic reticulum stress enhances fibrotic remodeling in the lungs. *Proceedings of the National Academy of Sciences*, *108*(26), 10562–10567.

Le Garrec, J. F., Ragni, C. V., Pop, S., Dufour, A., et al. (2013). Quantitative analysis of polarity in 3D reveals local cell coordination in the embryonic mouse heart. *Development (Cambridge, England)*, *140*(2), 395–404.

Lee, R. C., Feinbaum, R. L., & Ambros, V. (1993). The C. elegans heterochronic gene lin-4 encodes small RNAs with antisense complementarity to lin-14. *Cell*, *75*(5), 843–854.

Lee, Y., Kim, M., Han, J., Yeom, K.-H., et al. (2004). MicroRNA genes are transcribed by RNA polymerase II. *The EMBO Journal*, *23*(20), 4051–4060.

Lepczyński, A., Ożgo, M., Michałek, K., Dratwa-Chałupnik, A., et al. (2021). Effects of Three-Month Feeding High Fat Diets with Different Fatty Acid Composition on Myocardial Proteome in Mice. *Nutrients*, *13*(2), 330.

Lescroart, F., Kelly, R. G., Le Garrec, J.-F., Nicolas, J.-F., et al. (2010). Clonal analysis reveals common lineage relationships between head muscles and second heart field derivatives in the mouse embryo. *Development*, *137*(19), 3269–3279.

Li, C., Zhang, J., Xue, M., Li, X., et al. (2019). SGLT2 inhibition with empagliflozin attenuates myocardial oxidative stress and fibrosis in diabetic mice heart. *Cardiovascular Diabetology*, *18*(1), 15.

Li, F., Wang, X., Capasso, J., & Gerdes, A. (1996). Rapid Transition of Cardiac Myocytes from Hyperplasia to Hypertrophy During Postnatal Development. *Journal of Molecular and Cellular Cardiology*, *28*(8), 1737–1746.

Li, J., Wu, W., Xin, Y., Zhao, M., et al. (2018). Inhibition of Nogo-B promotes cardiac hypertrophy via endoplasmic reticulum stress. *Biomedicine and Pharmacotherapy*, *104*, 193–203.

Li, S.-C., Chan, W.-C., Hu, L.-Y., Lai, C.-H., et al. (2010). Identification of homologous microRNAs in 56 animal genomes. *Genomics*, *96*(1), 1–9.

Li, Y., Guo, Y., Tang, J., Jiang, J., et al. (2014). New insights into the roles of CHOP-induced apoptosis in ER stress. *Acta biochimica et biophysica Sinica*, *46*(8), 629–640.

Li, Z., Guo, J., Bian, Y., & Zhang, M. (2020). Intermedin protects thapsigargin-induced endoplasmic reticulum stress in cardiomyocytes by modulating protein kinase A and sarco/endoplasmic reticulum Ca $^{2+}$ -ATPase. *Molecular Medicine Reports*, *23*(2), 107.

Li, Z., Zhang, T., Dai, H., Liu, G., et al. (2007). Involvement of endoplasmic reticulum stress in myocardial apoptosis of streptozocin-induced diabetic rats. *Journal of clinical biochemistry and nutrition*, *41*(1), 58–67.

Lipton, M. J., & Coulden, R. (1999). Valvular heart disease. *Radiologic clinics of North America*, *37*(2), 319–vi.

Lima, J. F., Cerqueira, L., Figueiredo, C., Oliveira, C., et al. (2018). Anti-miRNA oligonucleotides: A comprehensive guide for design. *RNA Biology*, *15*(3), 338–352.

Litvinukova, M., Talavera-López, C., Maatz, H., Reichart, D., et al. (2020). Cells of the adult human heart. *Nature*, *588*(7838), 466–472.

Liu, K., Shi, Y., Guo, X., Wang, S., et al. (2014). CHOP mediates ASPP2-induced autophagic apoptosis in hepatoma cells by releasing Beclin-1 from Bcl-2 and inducing nuclear translocation of Bcl-2. *Cell Death & Disease*, *5*(7), e1323–e1323.

Liu, M., López de Juan Abad, B., & Cheng, K. (2021). Cardiac fibrosis: Myofibroblast-mediated pathological regulation and drug delivery strategies. *Advanced Drug Delivery Reviews*, *173*, 504–519.

Liu, X., Xu, Y., Deng, Y., & Li, H. (2018). MicroRNA-223 Regulates Cardiac Fibrosis After Myocardial Infarction by Targeting RASA1. *Cellular Physiology and Biochemistry*, *46*(4), 1439–1454.

Liu, Y., Hu, J., Wang, W., & Wang, Q. (2023). MircroRNA-145 Attenuates Cardiac Fibrosis Via Regulating Mitogen-Activated Protein Kinase Kinase Kinase 3. *Cardiovascular Drugs and Therapy*, *37*(4), 655–665.

Liu, Z., Cai, H., Zhu, H., Toque, H., et al. (2014). Protein kinase RNA-like endoplasmic reticulum kinase (PERK)/calcineurin signaling is a novel pathway regulating intracellular calcium accumulation which might be involved in ventricular arrhythmias in diabetic cardiomyopathy. *Cellular Signalling*, *26*(12), 2591–2600.

Louault, C., Benamer, N., Faivre, J.-F., Potreau, D., et al. (2008). Implication of connexins 40 and 43 in functional coupling between mouse cardiac fibroblasts in primary culture. *Biochimica et Biophysica Acta (BBA) - Biomembranes*, *1778*(10), 2097–2104.

Lu, L., Liu, M., Sun, R., Zheng, Y., et al. (2015). Myocardial Infarction: Symptoms and Treatments. *Cell Biochemistry and Biophysics*, *72*(3), 865–867.

Luan, Y., Zhu, X., Jiao, Y., Liu, H., et al. (2024). Cardiac cell senescence: molecular mechanisms, key proteins and therapeutic targets. *Cell Death Discovery*, *10*(1), 78.

Luyckx, I., Kumar, A. A., Reyniers, E., Dekeyser, E., et al. (2019). Copy number variation analysis in bicuspid aortic valve-related aortopathy identifies TBX20 as a contributing gene. *European Journal of Human Genetics*, *27*(7), 1033–1043.

Ma, L., Lu, M.-F., Schwartz, R. J., & Martin, J. F. (2005). *Bmp2* is essential for cardiac cushion epithelial-mesenchymal transition and myocardial patterning. *Development*, *132*(24), 5601–5611.

Mahmoud, A. I., Kocabas, F., Muralidhar, S. A., Kimura, W., et al. (2013). Meis1 regulates postnatal cardiomyocyte cell cycle arrest. *Nature*, *497*(7448), 249–253.

Marciniak, S. J., Yun, C. Y., Oyadomari, S., Novoa, I., et al. (2004). CHOP induces death by promoting protein synthesis and oxidation in the stressed endoplasmic reticulum. *Genes and Development*, *18*(24), 3066–3077.

Marian, A. J., & Braunwald, E. (2017). Hypertrophic Cardiomyopathy. *Circulation Research*, *121*(7), 749–770.

Marino, F., Scalise, M., Salerno, N., Salerno, L., et al. (2022). Diabetes-Induced Cellular Senescence and Senescence-Associated Secretory Phenotype Impair Cardiac Regeneration and Function Independently of Age. *Diabetes*, *71*(5), 1081–1098.

Marsh, K. G., Arrieta, A., Thuerauf, D. J., Blackwood, E. A., et al. (2021). The peroxisomal enzyme, FAR1, is induced during ER stress in an ATF6-dependent manner in cardiac myocytes. *American Journal of Physiology-Heart and Circulatory Physiology*, *320*(5), H1813–H1821.

Martindale, J. J., Fernandez, R., Thuerauf, D., Whittaker, R., et al. (2006). Endoplasmic reticulum stress gene induction and protection from ischemia/reperfusion injury in the hearts of transgenic mice with a tamoxifen-regulated form of ATF6. *Circulation Research*, *98*(9), 1186–1193.

Masaki, M., Izumi, M., Oshima, Y., Nakaoka, Y., et al. (2005). Smad1 Protects Cardiomyocytes From Ischemia-Reperfusion Injury. *Circulation*, *111*(21), 2752–2759.

Maurel, M., Dejeans, N., Taouji, S., Chevet, E., et al. (2013). MicroRNA-1291-mediated silencing of IRE1α enhances Glypican-3 expression. *RNA*, *19*(6), 778–788.

Mazurek, S. R., Calway, T., Harmon, C., Farrell, P., et al. (2017). MicroRNA-130a Regulation of Desmocollin 2 in a Novel Model of Arrhythmogenic Cardiomyopathy. *MicroRNA*, *6*(2), 143–150.

Meijer, H. A., Smith, E. M., & Bushell, M. (2014). Regulation of miRNA strand selection: follow the leader? *Biochemical Society Transactions*, *42*(4), 1135–1140.

Menu, P., Mayor, A., Zhou, R., Tardivel, A., et al. (2012). ER stress activates the NLRP3 inflammasome via an UPR-independent pathway. *Cell Death and Disease*, *3*(1), e261.

Michler, R. E. (2018). The current status of stem cell therapy in ischemic heart disease. *Journal of Cardiac Surgery*, *33*(9), 520–531.

Miquerol, L., Moreno-Rascon, N., Beyer, S., Dupays, L., et al. (2010). Biphasic development of the mammalian ventricular conduction system. *Circulation research*, *107*(1), 153–161.

Molkentin, J. D., Bugg, D., Ghearing, N., Dorn, L. E., et al. (2017). Fibroblast-Specific Genetic Manipulation of p38 Mitogen-Activated Protein Kinase In Vivo Reveals Its Central Regulatory Role in Fibrosis. *Circulation*, *136*(6), 549–561.

Mommersteeg, M. T. M., Domínguez, J. N., Wiese, C., Norden, J., et al. (2010). The sinus venosus progenitors separate and diversify from the first and second heart fields early in development. *Cardiovascular Research*, *87*(1), 92–101.

Mommersteeg, M. T. M., Hoogaars, W. M. H., Prall, O. W. J., de Gier-de Vries, C., et al. (2007). Molecular Pathway for the Localized Formation of the Sinoatrial Node. *Circulation Research*, *100*(3), 354–362.

Mondal, A., Das, S., Samanta, J., Chakraborty, S., et al. (2022). YAP1 induces hyperglycemic stress-mediated cardiac hypertrophy and fibrosis in an AKT-FOXM1 dependent signaling pathway. *Archives of Biochemistry and Biophysics*, *722*, 109198.

Moorman, A. F. M., & Christoffels, V. M. (2003). Cardiac Chamber Formation: Development, Genes, and Evolution. *Physiological Reviews*, *83*(4), 1223–1267.

Moorman, A. F. M., Christoffels, V. M., Anderson, R. H., & van den Hoff, M. J. B. (2007). The heart-forming fields: one or multiple? *Philosophical Transactions of the Royal Society B: Biological Sciences*, *362*(1484), 1257–1265.

Moorman, A. F. M., Schumacher, C. A., de Boer, P. A. J., Hagoort, J., et al. (2000). Presence of Functional Sarcoplasmic Reticulum in the Developing Heart and Its Confinement to Chamber Myocardium. *Developmental Biology*, *223*(2), 279–290.

Morikawa, Y., Heallen, T., Leach, J., Xiao, Y., et al. (2017). Dystrophin–glycoprotein complex sequesters Yap to inhibit cardiomyocyte proliferation. *Nature*, *547*(7662), 227–231.

Murray, I. R., Baily, J. E., Chen, W. C. W., Dar, A., et al. (2017). Skeletal and cardiac muscle pericytes: Functions and therapeutic potential. *Pharmacology & Therapeutics*, *171*, 65–74.

Mustapha, S., Mohammed, M., Azemi, A. K., Jatau, A. I., et al. (2021). Current Status of Endoplasmic Reticulum Stress in Type II Diabetes. *Molecules*, *26*(14), 4362.

Muthusamy, S., DeMartino, A. M., Watson, L. J., Brittian, K. R., et al. (2014). MicroRNA-539 Is Up-regulated in Failing Heart, and Suppresses O-GlcNAcase Expression. *Journal of Biological Chemistry*, *289*(43), 29665–29676.

Nachimuthu, S., Assar, M. D., & Schussler, J. M. (2012). Drug-induced QT interval prolongation: mechanisms and clinical management. *Therapeutic Advances in Drug Safety*, *3*(5), 241–253.

Naiche, L. A., Harrelson, Z., Kelly, R. G., & Papaioannou, V. E. (2005). T-box genes in vertebrate development. *Annual review of genetics*, *39*, 219–239.

Nakanishi, K. (2022). Anatomy of four human Argonaute proteins. *Nucleic Acids Research*, *50*(12), 6618–6638.

Nehme, A., & Edelman, J. (2008). Dexamethasone Inhibits High Glucose–, TNF-α–, and IL-1β–Induced Secretion of Inflammatory and Angiogenic Mediators from Retinal Microvascular Pericytes. *Investigative Opthalmology & Visual Science*, *49*(5), 2030.

Nicoletti, L., Paoletti, C., Tarricone, G., Andreana, I., et al. (2022). Lipoplexes for effective in vitro delivery of microRNAs to adult human cardiac fibroblasts for perspective direct cardiac cell reprogramming. *Nanomedicine: Nanotechnology, Biology and Medicine*, *45*, 102589.

Nishitoh, H., Matsuzawa, A., Tobiume, K., Saegusa, K., et al. (2002). ASK1 is essential for endoplasmic reticulum stress-induced neuronal cell death triggered by expanded polyglutamine repeats. *Genes and Development*, *16*(11), 1345–1355.

Obernosterer, G., Martinez, J., & Alenius, M. (2007). Locked nucleic acid-based in situ detection of microRNAs in mouse tissue sections. *Nature Protocols*, *2*(6), 1508–1514.

O'Brien, J., Hayder, H., Zayed, Y., & Peng, C. (2018). Overview of MicroRNA Biogenesis, Mechanisms of Actions, and Circulation. *Frontiers in Endocrinology*, *9*, 402.

Ohoka, N., Yoshii, S., Hattori, T., Onozaki, K., et al. (2005). TRB3, a novel ER stress-inducible gene, is induced via ATF4-CHOP pathway and is involved in cell death. *EMBO Journal*, *24*(6), 1243–1255.

Okada, T., Haze, K., Nadanaka, S., Yoshida, H., et al. (2003). A Serine Protease Inhibitor Prevents Endoplasmic Reticulum Stress-induced Cleavage but Not Transport of the Membrane-bound Transcription Factor ATF6. *Journal of Biological Chemistry*, *278*(33), 31024–31032.

Onrat, S. T., Onrat, E., Ercan Onay, E., Yalım, Z., et al. (2018). The Genetic Determination of the Differentiation Between Ischemic Dilated Cardiomyopathy and Idiopathic Dilated Cardiomyopathy. *Genetic Testing and Molecular Biomarkers*, *22*(11), 644–651.

Ooi, D. S., Isotalo, P. A., & Veinot, J. P. (2000). Correlation of antemortem serum creatine kinase, creatine kinase-MB, troponin I, and troponin T with cardiac pathology. *Clinical chemistry*, *46*(3), 338–344.

Oostra, R. J., Steding, G., Lamers, W. H., & Moorman, A. F. (2007). *Steding's and Virágh's Scanning Electron Microscopy Atlas of the Developing Human Heart*. (ISBN: 978-0-387-68272-3) Springer New York.

O'Rahilly, R., & Muller, F. (2010). Developmental Stages in Human Embryos: Revised and New Measurements. *Cells Tissues Organs*, *192*(2), 73–84.

Orlic, D., Kajstura, J., Chimenti, S., Jakoniuk, I., et al. (2001). Bone marrow cells regenerate infarcted myocardium. *Nature*, *410*(6829), 701–705.

Ortega, A., Roselló-Lletí, E., Tarazón, E., Molina-Navarro, M. M., et al. (2014). Endoplasmic reticulum stress induces different molecular structural alterations in human dilated and ischemic cardiomyopathy. *PLOS ONE*, *9*(9), e107635.

Pagoni, M., Cava, C., Sideris, D. C., Avgeris, M., et al. (2023). miRNA-Based Technologies in Cancer Therapy. *Journal of Personalized Medicine*, *13*(11), 1586.

Pan, Y., Geng, R., Zhou, N., Zheng, G., et al. (2015). TBX20 loss-of-function mutation contributes to double outlet right ventricle. *International Journal of Molecular Medicine*, *35*(4), 1058–1066.

Papaioannou, V. E. (2001). *T-box genes in development: from hydra to humans. International review of cytology, 207*, 1–70.

Park, J., Cho, M., Cho, J., Kim, E. E., et al. (2022). MicroRNA-101-3p Suppresses Cancer Cell Growth by Inhibiting the USP47-Induced Deubiquitination of RPL11. *Cancers*, *14*(4), 964.

Park, J. K., Shao, M., Kim, M. Y., Baik, S. K., et al. (2017). An endoplasmic reticulum protein, Nogo-B, facilitates alcoholic liver disease through regulation of kupffer cell polarization. *Hepatology*, *65*(5), 1720–1734.

Passer, D., van de Vrugt, A., Atmanli, A., & Domian, I. J. (2016). Atypical Protein Kinase C-Dependent Polarized Cell Division Is Required for Myocardial Trabeculation. *Cell reports*, *14*(7), 1662–1672.

Pasumarthi, K. B. S., & Field, L. J. (2002). Cardiomyocyte Cell Cycle Regulation. *Circulation Research*, *90*(10), 1044–1054.

Pizzo, P., & Pozzan, T. (2007). Mitochondria-endoplasmic reticulum choreography: structure and signaling dynamics. *Trends in cell biology, 17*(10), 511–517.

Plageman, T. F., & Yutzey, K. E. (2004). Differential Expression and Function of Tbx5 and Tbx20 in Cardiac Development. *Journal of Biological Chemistry*, *279*(18), 19026–19034.

Pluquet, O., Pourtier, A., & Abbadie, C. (2015). The unfolded protein response and cellular senescence. A Review in the Theme: Cellular Mechanisms of Endoplasmic Reticulum Stress Signaling in Health and Disease. *American Journal of Physiology-Cell Physiology*, *308*(6), C415–C425.

Porrello, E. R., Mahmoud, A. I., Simpson, E., Hill, J. A., et al. (2011). Transient Regenerative Potential of the Neonatal Mouse Heart. *Science*, *331*(6020), 1078–1080.

Posch, M. G., Gramlich, M., Sunde, M., Schmitt, K. R., et al. (2010). A gain-of-function TBX20 mutation causes congenital atrial septal defects, patent foramen ovale and cardiac valve defects. *Journal of Medical Genetics*, *47*(4), 230–235.

Prados, B., Gomez-Apinaniz, P., Papoutsi, T., Luxan, G., et al. (2018). Myocardial Bmp2 gain causes ectopic EMT and promotes cardiomyocyte proliferation and immaturity article. *Cell Death and Disease*, *9*(3), 399.

Pulkkinen, H. H., Kivisto-Rahnasto, A., Korpela, H., Heikkila, M., et al. (2023). BMP2 gene transfer induces pericardial effusion and inflammatory response in the ischemic porcine myocardium. *Frontiers in Cardiovascular Medicine*, *10*, 1279613.

Queiroz, L. A. D., Assis, J. B., Guimaraes, J. P. T., Sousa, E. S. A., Milhomem,. (2021). Endangered Lymphocytes: The Effects of Alloxan and Streptozotocin on Immune Cells in Type 1 Induced Diabetes. *Mediators of Inflammation*, *2021*, 1–15.

Radhakrishnan, A., Ensam, B., Moody, W. E., & Ludman, P. F. (2023). Isoprenaline induced myocardial infarction in a patient with high-grade atrioventricular block: a case report. *European Heart Journal - Case Reports*, *7*(8), ytad358.

Rainer, J., Meraviglia, V., Blankenburg, H., Piubelli, C.,et al. (2018). The arrhythmogenic cardiomyopathy-specific coding and non-coding transcriptome in human cardiac stromal cells. *BMC Genomics*, *19*(1), 491.

Ramdas Nair, A., Lakhiani, P., Zhang, C., Macchi, F., et al. (2022). A permissive epigenetic landscape facilitates distinct transcriptional signatures of activating transcription factor 6 in the liver. *Genomics*, *114*(1), 107–124.

Rana, M. S., Horsten, N. C. A., Tesink-Taekema, S., Lamers, W. H., et al. (2007). Trabeculated Right Ventricular Free Wall in the Chicken Heart Forms by Ventricularization of the Myocardium Initially Forming the Outflow Tract. *Circulation Research*, *100*(7), 1000–1007.

Regan, T. J., Lyons, M. M., Ahmed, S. S., Levinson, G. E., et al. (1977). Evidence for Cardiomyopathy in Familial Diabetes Mellitus. *Journal of Clinical Investigation*, *60*(4), 885–899.

Rentschler, S., Harris, B. S., Kuznekoff, L., Jain, R., et al. (2011). Notch signaling regulates murine atrioventricular conduction and the formation of accessory pathways. *Journal of Clinical Investigation*, *121*(2), 525–533.

Ridker, P. M. (2014). Targeting inflammatory pathways for the treatment of cardiovascular disease. *European heart journal, 35*(9), 540–543.

Rijzewijk, L. J., van der Meer, R. W., Smit, J. W. A., Diamant, M., Bax, et al. (2008). Myocardial Steatosis Is an Independent Predictor of Diastolic Dysfunction in Type 2 Diabetes Mellitus. *Journal of the American College of Cardiology*, *52*(22), 1793–1799.

Rivera-Feliciano, J., & Tabin, C. J. (2006). Bmp2 instructs cardiac progenitors to form the heart-valve-inducing field. *Developmental Biology*, *295*(2), 580–588.

Rogers, M. B., Shah, T. A., & Shaikh, N. N. (2015). Turning Bone Morphogenetic Protein 2 (BMP2) on and off in Mesenchymal Cells. *Journal of Cellular Biochemistry*, *116*(10), 2127–2138.

Rojas, A., Kong, S. W., Agarwal, P., Gilliss, B., et al. (2008). GATA4 Is a Direct Transcriptional Activator of *Cyclin D2* and *Cdk4* and Is Required for Cardiomyocyte Proliferation in Anterior Heart Field-Derived Myocardium. *Molecular and Cellular Biology*, *28*(17), 5420–5431.

Rojas, S. V., Kensah, G., Rotaermel, A., Baraki, H., et al. (2017). Transplantation of purified iPSC-derived cardiomyocytes in myocardial infarction. *PLOS ONE*, *12*(5), e0173222.

Roncarati, R., Viviani Anselmi, C., Losi, M. A., Papa, L., et al. (2014). Circulating miR-29a, Among Other Up-Regulated MicroRNAs, Is the Only Biomarker for Both Hypertrophy and Fibrosis in Patients With Hypertrophic Cardiomyopathy. *Journal of the American College of Cardiology*, *63*(9), 920–927.

Rubler, S., Dlugash, J., Yuceoglu, Y. Z., Kumral, T., et al. (1972). New type of cardiomyopathy associated with diabetic glomerulosclerosis. *The American Journal of Cardiology*, *30*(6), 595–602.

Ruby, J. G., Jan, C. H., & Bartel, D. P. (2007). Intronic microRNA precursors that bypass Drosha processing. *Nature*, *448*(7149), 83–86.

Ruiz-Villalba, A., Hoppler, S., & van den Hoff, M. J. B. (2016). Wnt signaling in the heart fields: Variations on a common theme. *Developmental Dynamics*, *245*(3), 294–306.

Ryota, M. (2023). Outcomes Following Management of Congenital and Acquired Diaphragmatic Hernia in a Tertiary Care Centre-A Case Series. In *OPINION ARTICLE Journal of Interdisciplinary Histopathology* (Vol. 11).

Safiedeen, Z., Rodríguez-Gómez, I., Vergori, L., Soleti, R., et al. (2017). Temporal Cross Talk Between Endoplasmic Reticulum and Mitochondria Regulates Oxidative Stress and Mediates Microparticle-Induced Endothelial Dysfunction. *Antioxidants & Redox Signaling*, *26*(1), 15–27.

Saguner, A. M. (2014). Arrhythmogenic ventricular cardiomyopathy: A paradigm shift from right to biventricular disease. *World Journal of Cardiology*, *6*(4), 154.

Sanders, L. N., Schoenhard, J. A., Saleh, M. A., Mukherjee, A., et al. (2016). BMP antagonist gremlin 2 limits inflammation after myocardial infarction. *Circulation Research*, *119*(3), 434–449.

Sanderson, T. H., Gallaway, M., & Kumar, R. (2015). Unfolding the unfolded protein response: unique insights into brain ischemia. *International journal of molecular sciences, 16*(4), 7133–7142.

Santos, A. S., Cunha Neto, E., Fukui, R. T., Ferreira, L. R. P., et al. (2019). Increased Expression of Circulating microRNA 101-3p in Type 1 Diabetes Patients: New Insights Into miRNA-Regulated Pathophysiological Pathways for Type 1 Diabetes. *Frontiers in Immunology*, *10*, 1637.

Schaufelberger, M. (2019). Cardiomyopathy and pregnancy. *Heart (British Cardiac Society)*, *105*(20), 1543–1551.

Scherer, P. E., & Hill, J. A. (2016). Obesity, Diabetes, and Cardiovascular Diseases. *Circulation Research*, *118*(11), 1703–1705.

Schmidt, P. J., Ezri, M. D., & Denes, P. (1987). Cardiac arrhythmias--update 1987. *Disease-a-month : DM*, *33*(7), 365–432.

Sen-Chowdhry, S., Syrris, P., Prasad, S. K., Hughes, S. E., et al. (2008). Left-Dominant Arrhythmogenic Cardiomyopathy. *Journal of the American College of Cardiology*, *52*(25), 2175–2187.

Sengupta, A., Molkentin, J. D., Paik, J.-H., DePinho, R. A., et al. (2010). FoxO Transcription Factors Promote Cardiomyocyte Survival upon Induction of Oxidative Stress. *Journal of Biological Chemistry*, *286*(9), 7468–7478.

Senyo, S. E., Steinhauser, M. L., Pizzimenti, C. L., Yang, V. K., et al. (2013). Mammalian heart renewal by pre-existing cardiomyocytes. *Nature*, *493*(7432), 433–436.

Shelton, E. L., & Yutzey, K. E. (2007). Tbx20 regulation of endocardial cushion cell proliferation and extracellular matrix gene expression. *Developmental Biology*, *302*(2), 376–388.

Shen, E., Li, Y., Li, Y., Shan, L., et al. (2009). Rac1 is required for cardiomyocyte apoptosis during hyperglycemia. *Diabetes*, *58*(10), 2386–2395.

Shen, J., James, A. W., Zara, J. N., Asatrian, G., et al. (2013). BMP2-Induced Inflammation Can Be Suppressed by the Osteoinductive Growth Factor NELL-1. *Tissue Engineering Part A*, *19*(21–22), 2390–2401.

Shen, T., Aneas, I., Sakabe, N., Dirschinger, R. J., et al. (2011). Tbx20 regulates a genetic program essential to adult mouse cardiomyocyte function. *Journal of Clinical Investigation*, *121*(12), 4640–4654.

Shen, T., Yang, C., Ding, L., Zhu, Y., et al. (2013). Tbx20 functions as an important regulator of estrogen-mediated cardiomyocyte protection during oxidative stress. *International Journal of Cardiology*, *168*(4), 3704–3714.

Sid-Otmane, C., Perrault, L. P., & Ly, H. Q. (2020). Mesenchymal stem cell mediates cardiac repair through autocrine, paracrine and endocrine axes. *Journal of Translational Medicine*, *18*(1), 336.

Siedner, S., Kruger, M., Schroeter, M., Metzler, D., et al. (2003). Developmental changes in contractility and sarcomeric proteins from the early embryonic to the adult stage in the mouse heart. *The Journal of Physiology*, *548*(2), 493–505.

Singh, R., Horsthuis, T., Farin, H. F., Grieskamp, T., et al. (2009). Tbx20 Interacts With Smads to Confine *Tbx2* Expression to the Atrioventricular Canal. *Circulation Research*, *105*(5), 442–452.

Sizarov, A., Lamers, W. H., Mohun, T. J., Brown, N. A., et al. (2012). Three-dimensional and molecular analysis of the arterial pole of the developing human heart. *Journal of Anatomy*, *220*(4), 336–349.

Sizarov, A., Ya, J., de Boer, B. A., Lamers, W. H., et al. (2011). Formation of the Building Plan of the Human Heart. *Circulation*, *123*(10), 1125–1135.

Snarr, B. S., Kern, C. B., & Wessels, A. (2008). Origin and fate of cardiac mesenchyme. *Developmental Dynamics*, *237*(10), 2804–2819.

Sommariva, E., D'Alessandra, Y., Farina, F. M., Casella, M., et al. (2017). MiR-320a as a Potential Novel Circulating Biomarker of Arrhythmogenic CardioMyopathy. *Scientific Reports*, *7*(1), 4802.

Sozen, E., Yazgan, B., Tok, O. E., Demirel, T., et al. (2020). Cholesterol induced autophagy via IRE1/JNK pathway promotes autophagic cell death in heart tissue. *Metabolism: Clinical and Experimental*, *106*, 154205.

Speakman, J. R. (2019). Use of high-fat diets to study rodent obesity as a model of human obesity. *International Journal of Obesity*, *43*(8), 1491–1492.

Stefanovic, S., Barnett, P., van Duijvenboden, K., Weber, D., et al. (2014). GATA-dependent regulatory switches establish atrioventricular canal specificity during heart development. *Nature Communications*, *5*(1), 3680.

Stein, G. H., Drullinger, L. F., Soulard, A., & Dulić, V. (1999). Differential Roles for Cyclin-Dependent Kinase Inhibitors p21 and p16 in the Mechanisms of Senescence and Differentiation in Human Fibroblasts. *Molecular and Cellular Biology*, *19*(3), 2109–2117.

Stempien-Otero, A., Kim, D.-H., & Davis, J. (2016). Molecular networks underlying myofibroblast fate and fibrosis. *Journal of Molecular and Cellular Cardiology*, *97*, 153–161.

Stennard, F. A., Costa, M. W., Elliott, D. A., Rankin, S., et al. (2003). Cardiac T-box factor Tbx20 directly interacts with Nkx2-5, GATA4, and GATA5 in regulation of gene expression in the developing heart. *Developmental Biology*, *262*(2), 206–224.

Stenvang, J., Petri, A., Lindow, M., Obad, S., et al. (2012). Inhibition of microRNA function by antimiR oligonucleotides. *Silence*, *3*(1), 1.

Strungs, E. G., Ongstad, E. L., O'Quinn, M. P., Palatinus, J. A., et al. (2013). Cryoinjury models of the adult and neonatal mouse heart for studies of scarring and regeneration. *Methods in molecular biology (Clifton, N.J.), 1037*, 343–353.

Sucharov, C., Bristow, M. R., & Port, J. D. (2008). miRNA expression in the failing human heart: Functional correlates. *Journal of Molecular and Cellular Cardiology*, *45*(2), 185–192.

Sugi, Y., Yamamura, H., Okagawa, H., & Markwald, R. R. (2004). Bone morphogenetic protein-2 can mediate myocardial regulation of atrioventricular cushion mesenchymal cell formation in mice. *Developmental Biology*, *269*(2), 505–518.

Sukma Dewi, I., Hollander, Z., Lam, K. K., McManus, J.-W., et al. (2017). Association of Serum MiR-142-3p and MiR-101-3p Levels with Acute Cellular Rejection after Heart Transplantation. *PLOS ONE*, *12*(1), e0170842.

Sukumaran, V., Watanabe, K., Veeraveedu, P. T., Gurusamy, N., et al. (2011). Olmesartan, an AT 1 Antagonist, Attenuates Oxidative Stress, Endoplasmic Reticulum Stress and Cardiac Inflammatory Mediators in Rats with Heart Failure Induced by Experimental Autoimmune Myocarditis. *International journal of biological sciences, 7*(2), 154–167.

Sylva, M., van den Hoff, M. J. B., & Moorman, A. F. M. (2014). Development of the human heart. *American Journal of Medical Genetics Part A*, *164*(6), 1347–1371.

Takeuchi, J. K., Mileikovskaia, M., Koshiba-Takeuchi, K., Heidt, A. B., et al. (2005). Tbx20 dose-dependently regulates transcription factor networks required for mouse heart and motoneuron development. *Development*, *132*(10), 2463–2474.

Tâlvan, C.-D., Tâlvan, E.-T., Mohor, C. I., Budișan, L., et al. (2024). Exploring miRNA Profiles in Colon Cancer: A Focus on miR101-3p, miR106a-5p, and miR326. *Cancers*, *16*(12), 2285.

Tan, Y., Zhang, Z., Zheng, C., Wintergerst, K. A., et al. (2020). Mechanisms of diabetic cardiomyopathy and potential therapeutic strategies: preclinical and clinical evidence. *Nature reviews. Cardiology, 17*(9), 585–607.

Tanjore, H., Lawson, W. E., & Blackwell, T. S. (2013). Endoplasmic reticulum stress as a pro-fibrotic stimulus. *Biochimica et Biophysica Acta (BBA) - Molecular Basis of Disease*, *1832*(7), 940–947.

Tanzer, A., & Stadler, P. F. (2004). Molecular Evolution of a MicroRNA Cluster. *Journal of Molecular Biology*, *339*(2), 327–335.

Tao, L., Bei, Y., Chen, P., Lei, Z., et al. (2016). Crucial Role of miR-433 in Regulating Cardiac Fibrosis. *Theranostics*, *6*(12), 2068–2083.

Terentyev, D., Belevych, A. E., Terentyeva, R., Martin, M. M., et al. (2009). *miR-1* Overexpression Enhances Ca^{2+} Release and Promotes Cardiac Arrhythmogenesis by Targeting PP2A Regulatory Subunit B56α and Causing CaMKII-Dependent Hyperphosphorylation of RyR2. *Circulation Research*, *104*(4), 514–521.

Theveniau-Ruissy, M., Dandonneau, M., Mesbah, K., Ghez, O., et al. (2008). The del22q11.2 Candidate Gene *Tbx1* Controls Regional Outflow Tract Identity and Coronary Artery Patterning. *Circulation Research*, *103*(2), 142–148.

Thottakara, T., Lund, N., Krämer, E., Kirchhof, P., et al. (2021). A Novel miRNA Screen Identifies miRNA-4454 as a Candidate Biomarker for Ventricular Fibrosis in Patients with Hypertrophic Cardiomyopathy. *Biomolecules*, *11*(11), 1718.

Thuerauf, D. J., Hoover, H., Meller, J., Hernandez, J., et al. (2001). Sarco/endoplasmic reticulum calcium ATPase-2 expression is regulated by ATF6 during the endoplasmic reticulum stress response: Intracellular signaling of calcium stress in a cardiac myocyte model system. *Journal of Biological Chemistry*, *276*(51), 48309–48317.

Thygesen, K., Alpert, J. S., Jaffe, A. S., Chaitman, B. R., et al. (2018). Fourth Universal Definition of Myocardial Infarction (2018). *Circulation*, *138*(20), e618–e651.

Tijsen, A. J., Creemers, E. E., Moerland, P. D., de Windt, L. J., et al. (2010). MiR423-5p As a Circulating Biomarker for Heart Failure. *Circulation Research*, *106*(6), 1035–1039.

Toko, H., Takahashi, H., Kayama, Y., Okada, S., et al. (2010). ATF6 is important under both pathological and physiological states in the heart. *Journal of Molecular and Cellular Cardiology*, *49*(1), 113–120.

Totland, M. Z., Rasmussen, N. L., Knudsen, L. M., & Leithe, E. (2020). Regulation of gap junction intercellular communication by connexin ubiquitination: physiological and pathophysiological implications. *Cellular and Molecular Life Sciences*, *77*(4), 573–591.

Tsai, C. T., Tseng, C. D., Hwang, J. J., Wu, C. K., et al. (2011). Tachycardia of atrial myocytes induces collagen expression in atrial fibroblasts through transforming growth factor β1. *Cardiovascular research*, *89*(4), 805–815.

Uranbileg, B., Yamamoto, H., Park, J., Mohanty, A. R., et al. (2012). Cdc6 Protein Activates p27KIP1-bound Cdk2 Protein Only after the Bound p27 Protein Undergoes C-terminal Phosphorylation. *Journal of Biological Chemistry*, *287*(9), 6275–6283.

Valkov, N., King, M. E., Moeller, J., Liu, H., et al. (2019). MicroRNA-1-Mediated Inhibition of Cardiac Fibroblast Proliferation Through Targeting Cyclin D2 and CDK6. *Frontiers in Cardiovascular Medicine*, *6*, 65.

Van den Bergh, A., Vanderper, A., Vangheluwe, P., Desjardins, F., et al. (2008). Dyslipidaemia in type II diabetic mice does not aggravate contractile impairment but increases ventricular stiffness. *Cardiovascular Research*, *77*(2), 371–379.

Van Rooij, E., Sutherland, L. B., Qi, X., et al. (2007). Control of Stress-Dependent Cardiac Growth and Gene Expression by a MicroRNA. *Science*, *316*(5824), 575–579.

Van Rooij, E., Sutherland, L. B., Thatcher, J. E., DiMaio, J. M., et al. (2008). Dysregulation of microRNAs after myocardial infarction reveals a role of miR-29 in cardiac fibrosis. *Proceedings of the National Academy of Sciences*, *105*(35), 13027–13032.

Victorelli, S., & Passos, J. F. (2017). Telomeres and Cell Senescence - Size Matters Not. *EBioMedicine*, *21*, 14–20.

Vincentz, J. W., Barnes, R. M., & Firulli, A. B. (2011). Hand factors as regulators of cardiac morphogenesis and implications for congenital heart defects. *Birth defects research. Part A, Clinical and molecular teratology*, *91*(6), 485–494.

Von Gise, A., & Pu, W. T. (2012). Endocardial and epicardial epithelial to mesenchymal transitions in heart development and disease. *Circulation Research*, *110*(12), 1628–1645.

Walters, S. N., Luzuriaga, J., Chan, J. Y., Grey, S. T., et al. (2013). Influence of chronic hyperglycemia on the loss of the unfolded protein response in transplanted islets. *Journal of Molecular Endocrinology*, *51*(2), 225–232.

Wang, H., Chen, F., Tong, J., Li, Y., et al. (2017). Circulating microRNAs as novel biomarkers for dilated cardiomyopathy. *Cardiology Journal*, *24*(1), 65–73.

Wang, H., Liu, S., Jia, L., Chu, F., et al. (2018). Nanostructured lipid carriers for MicroRNA delivery in tumor gene therapy. *Cancer Cell International*, *18*(1), 101.

Wang, H., Xiao, R., & Yang, B. (2021). MiR-101-3p Suppresses Progression of Cervical Squamous Cell Carcinoma by Targeting and Down-Regulating KPNA2. *Technology in Cancer Research & Treatment*, *20*, 15330338211055948.

Wang, J., Huang, W., Xu, R., Nie, Y., et al. (2012). MicroRNA-24 regulates cardiac fibrosis after myocardial infarction. *Journal of Cellular and Molecular Medicine*, *16*(9), 2150–2160.

Wang, L., Liu, J., Xu, B., Liu, Y., et al. (2018). Reduced exosome miR-425 and miR-744 in the plasma represents the progression of fibrosis and heart failure. *The Kaohsiung Journal of Medical Sciences*, *34*(11), 626–633.

Wang, Y., Shen, J., Arenzana, N., Tirasophon, W., et al. (2000). Activation of ATF6 and an ATF6 DNA binding site by the endoplasmic reticulum stress response. *Journal of Biological Chemistry*, *275*(35), 27013–27020.

Way, K. J., Isshiki, K., Suzuma, K., Yokota, T., et al. (2002). Expression of Connective Tissue Growth Factor Is Increased in Injured Myocardium Associated With Protein Kinase C β2 Activation and Diabetes. *Diabetes*, *51*(9), 2709–2718.

Webb, S., Qayyum, S. R., Anderson, R. H., Lamers, W. H., et al. (2003). Septation and separation within the outflow tract of the developing heart. *Journal of Anatomy*, *202*(4), 327–342.

Wei, H., Zhang, R., Jin, H., Liu, D., et al. (2010). Hydrogen Sulfide Attenuates Hyperhomocysteinemia-Induced Cardiomyocytic Endoplasmic Reticulum Stress in Rats. *Antioxidants & Redox Signaling*, *12*(9), 1079–1091.

Wei, J., Zhao, Y., Liang, H., Du, W., et al. (2022). Preliminary evidence for the presence of multiple forms of cell death in diabetes cardiomyopathy. *Acta pharmaceutica Sinica. B*, *12*(1), 1–17.

Wei, Y., Yan, X., Yan, L., Hu, F., et al. (2017). Inhibition of microRNA-155 ameliorates cardiac fibrosis in the process of angiotensin II-induced cardiac remodeling. *Molecular Medicine Reports*, *16*(5), 7287–7296.

Wessels, A., Anderson, R. H., Markwald, R. R., Webb, S., et al. (2000). Atrial development in the human heart: An immunohistochemical study with emphasis on the role of mesenchymal tissues. *The Anatomical Record*, *259*(3), 288–300.

Wessels, A., van den Hoff, M. J. B., Adamo, R. F., Phelps, A. L., Lockhart, et al. (2012). Epicardially derived fibroblasts preferentially contribute to the parietal leaflets of the atrioventricular valves in the murine heart. *Developmental Biology*, *366*(2), 111–124.

Wessels, A., Vermeulen, J. L. M., Verbeek, F. J., Virágh, S. Z., et al. (1992). Spatial distribution of "tissue-specific" antigens in the developing human heart and skeletal muscle III. An immunohistochemical analysis of the distribution of the neural tissue antigen G1N2 in the embryonic heart; implications for the development of the atrioventricular conduction system. *The Anatomical Record*, *232*(1), 97–111.

Wiese, C., Grieskamp, T., Airik, R., Mommersteeg, M. T. M., et al. (2009). Formation of the Sinus Node Head and Differentiation of Sinus Node Myocardium Are Independently Regulated by Tbx18 and Tbx3. *Circulation Research*, *104*(3), 388–397.

Wightman, B., Ha, I., & Ruvkun, G. (1993). Posttranscriptional regulation of the heterochronic gene lin-14 by lin-4 mediates temporal pattern formation in C. elegans. *Cell*, *75*(5), 855–862.

Woodall, M. C., Woodall, B. P., Gao, E., Yuan, A., et al. (2016). Cardiac Fibroblast GRK2 Deletion Enhances Contractility and Remodeling Following Ischemia/Reperfusion Injury. *Circulation Research*, *119*(10), 1116–1127.

Wu, D. H., & Hatzopoulos, A. K. (2019). Bone morphogenetic protein signaling in inflammation. *Experimental biology and medicine (Maywood, N.J.), 244*(2), 147–156.

Wu, J., Yang, J., Cho, W. C., & Zheng, Y. (2020). Argonaute proteins: Structural features, functions and emerging roles. *Journal of Advanced Research*, *24*, 317–324.

Wu, S. pin, Cheng, C. M., Lanz, R. B., Wang, T., et al. (2013). Atrial Identity Is Determined by a COUP-TFII Regulatory Network. *Developmental Cell*, *25*(4), 417–426.

Xiang, F., Guo, M., & Yutzey, K. E. (2016). Overexpression of Tbx20 in Adult Cardiomyocytes Promotes Proliferation and Improves Cardiac Function After Myocardial Infarction. *Circulation*, *133*(11), 1081–1092.

Xiang, F. L., Fang, M., & Yutzey, K. E. (2017). Loss of β-catenin in resident cardiac fibroblasts attenuates fibrosis induced by pressure overload in mice. *Nature Communications*, *8*(1), 712.

Xiang, X. Y., Yang, X. C., Su, J., Kang, J. S., et al. (2016). Inhibition of autophagic flux by ROS promotes apoptosis during DTT-induced ER/oxidative stress in HeLa cells. *Oncology Reports*, *35*(6), 3471–3479.

Xiao, Y., Hill, M. C., Li, L., Deshmukh, V., et al. (2019). Hippo pathway deletion in adult resting cardiac fibroblasts initiates a cell state transition with spontaneous and self-sustaining fibrosis. *Genes & Development*, *33*(21–22), 1491–1505.

Xie, M., Li, M., Vilborg, A., Lee, N., et al. (2013). Mammalian 5′-Capped MicroRNA Precursors that Generate a Single MicroRNA. *Cell*, *155*(7), 1568–1580.

Xin, W., Li, X., Lu, X., Niu, K., et al. (2011). Involvement of endoplasmic reticulum stress-associated apoptosis in a heart failure model induced by chronic myocardial ischemia. *International Journal of Molecular Medicine*, *27*(4), 503–509.

Xin, W., Lu, X., Li, X., Niu, K., et al. (2011). Attenuation of endoplasmic reticulum stress-related myocardial apoptosis by SERCA2a gene delivery in ischemic heart disease. *Molecular Medicine*, *17*(3–4), 201–210.

Xin, Y., Tang, L., Chen, J., Chen, D., et al. (2021). Inhibition of miR-101-3p protects against sepsis-induced myocardial injury by inhibiting MAPK and NF-κB pathway activation via the upregulation of DUSP1. *International Journal of Molecular Medicine*, *47*(3), 20.

Xu, F. P., Chen, M. S., Wang, Y. Z., Yi, Q., et al. (2004). Leptin induces hypertrophy via endothelin-1-reactive oxygen species pathway in cultured neonatal rat cardiomyocytes. *Circulation*, *110*(10), 1269–1275.

Ya, J., van den Hoff, M. J. B., de Boer, P. A. J., Tesink-Taekema, S., et al. (1998). Normal Development of the Outflow Tract in the Rat. *Circulation Research*, *82*(4), 464–472.

Yamada, S., Hsiao, Y. W., Chang, S. L., Lin, Y. J., et al. (2018). Circulating microRNAs in arrhythmogenic right ventricular cardiomyopathy with ventricular arrhythmia. *EP Europace*, *20*(FI1), f37–f45.

Yamamoto, T., Mukai, Y., Wada, F., Terada, C., et al. (2021). Highly Potent GalNAc-Conjugated Tiny LNA Anti-miRNA-122 Antisense Oligonucleotides. *Pharmaceutics*, *13*(6), 817.

Yang, J. S., Maurin, T., Robine, N., Rasmussen, K. D., et al. (2010). Conserved vertebrate *mir-451* provides a platform for Dicer-independent, Ago2-mediated microRNA biogenesis. *Proceedings of the National Academy of Sciences*, *107*(34), 15163–15168.

Yang, Y., Ju, H., Liu, S., Lee, T., et al. (2011). BMP-2 suppresses renal interstitial fibrosis by regulating epithelial–mesenchymal transition. *Journal of Cellular Biochemistry*, *112*(9), 2558–2565.

Yoshida, M., Stadler, J., Bertholdt, G., & Gerisch, G. (1984). Wheat germ agglutinin binds to the contact site A glycoprotein of *Dictyostelium discoideum* and inhibits EDTA-stable cell adhesion. *The EMBO Journal*, *3*(11), 2663–2670.

Yu, Y., Liu, H., Yang, D., He, F., et al. (2019). Aloe-emodin attenuates myocardial infarction and apoptosis via up-regulating miR-133 expression. *Pharmacological Research*, *146*, 104315.

Yutzey, K. E. (2017). Cardiomyocyte Proliferation. *Circulation Research*, *120*(4), 627–629.

Zeeshan, H., Lee, G., Kim, H. R., & Chae, H. J. (2016). Endoplasmic Reticulum Stress and Associated ROS. *International Journal of Molecular Sciences*, *17*(3), 327.

Zhang, C., Tang, Y., Li, Y., Xie, L., et al. (2017). Unfolded protein response plays a critical role in heart damage after myocardial ischemia/reperfusion in rats. *PLOS ONE*, *12*(6).

Zhang, H., & Bradley, A. (1996). Mice deficient for BMP2 are nonviable and have defects in amnion/chorion and cardiac development. *Development*, *122*(10), 2977–2986.

Zhang, H., & Dhalla, N. S. (2024). The Role of Pro-Inflammatory Cytokines in the Pathogenesis of Cardiovascular Disease. *International journal of molecular sciences, 25*(2), 1082.

Zhang, H., Kolb, F. A., Jaskiewicz, L., Westhof, E., et al. (2004). Single Processing Center Models for Human Dicer and Bacterial RNase III. *Cell*, *118*(1), 57–68.

Zhang, M., Sara, J. D., Wang, F. L., Liu, L. P., et al. (2015). Increased plasma BMP-2 levels are associated with atherosclerosis burden and coronary calcification in type 2 diabetic patients. *Cardiovascular Diabetology*, *14*(1), 64.

Zhang, P., Su, J., & Mende, U. (2012). Cross talk between cardiac myocytes and fibroblasts: from multiscale investigative approaches to mechanisms and functional consequences. *American journal of physiology. Heart and circulatory physiology*, *303*(12), H1385–H1396.

Zhang, X., He, X., Liu, Y., Zhang, H., et al. (2017). MiR-101-3p inhibits the growth and metastasis of non-small cell lung cancer through blocking PI3K/AKT signal pathway by targeting MALAT-1. *Biomedicine & Pharmacotherapy*, *93*, 1065–1073.

Zhou, Z., Wang, J., Guo, C., Chang, W., et al. (2017). Temporally Distinct Six2-Positive Second Heart Field Progenitors Regulate Mammalian Heart Development and Disease. *Cell reports*, *18*(4), 1019–1032.

Zhou, Q., Schötterl, S., Backes, D., Brunner, E., et al. (2017). Inhibition of miR-208b improves cardiac function in titin-based dilated cardiomyopathy. *International Journal of Cardiology*, *230*, 634–641.

Zhou, S., Jin, J., Wang, J., Zhang, Z., et al. (2018). miRNAS in cardiovascular diseases: potential biomarkers, therapeutic targets and challenges. *Acta Pharmacologica Sinica*, *39*(7), 1073–1084.

Zhu, F., Meng, Q., Yu, Y., Shao, L., et al. (2021). Adult Cardiomyocyte Proliferation: a New Insight for Myocardial Infarction Therapy. *Journal of Cardiovascular Translational Research*, *14*(3), 457–466.

Zhu, W., Kim, J., Cheng, C., Rawlins, B. A., et al. (2006). Noggin regulation of bone morphogenetic protein (BMP) 2/7 heterodimer activity in vitro. *Bone*, *39*(1), 61–71.

Zhu, W., Ni, Q., Wang, Z., Zhang, R., et al. (2025). MiR-101-3p targets the PI3K-AKT signaling pathway via Birc5 to inhibit invasion, proliferation, and epithelial–mesenchymal transition in hepatocellular carcinoma. *Clinical and Experimental Medicine*, *25*(1), 88.

Zhuge, Y., Zhang, J., Qian, F., Wen, Z., et al. (2020). Role of smooth muscle cells in Cardiovascular Disease. *International Journal of Biological Sciences*, *16*(14), 2741–2751.

Zou, T., Zhu, M., Ma, Y. C., Xiao, F., et al. (2018). MicroRNA-410-5p exacerbates high-fat diet-induced cardiac remodeling in mice in an endocrine fashion. *Scientific Reports*, *8*(1), 8780.

Licenses

License for reuse of image in Chapter 1: Review of Literature

License Number	6021220051524
License date	May 03, 2025
Licensed Content Publisher	John Wiley and Sons
Licensed Content Publication	American Journal of Medical Genetics Part A
Licensed Content Title	Development of the human heart
Licensed Content Author	Marc Sylva, Maurice J.B. van den Hoff, Antoon F.M. Moorman
Licensed Content Date	Apr 30, 2013
Licensed Content Volume	164
Licensed Content Issue	6
Licensed Content Pages	25
Type of use	Dissertation/Thesis
Requestor type	University/Academic
Format	Print and electronic
Portion	Figure/table
Number of figures/tables	1
Will you be translating?	No
Title of new work	The interplay of cardiac developmental factors T- box transcription factor 20 (Tbx20) and Bone morphogenetic protein2 (Bmp2) and their cross-talk with miR-101-3p in regulating cardiac homeostasis in rodent cardiomyopathy model
Institution name	Jadavpur University
Expected presentation date	Jun 2025
Portions	Figure 3
The Requesting Person / Organization to Appear on the License	Ms Shreya Das
Requestor Location	188, Raja Subodh Chandra Mallick Rd, Jadavpur, Kolkata, 700032, India
Publisher Tax ID	EU826007151
Billing Type	Invoice
Billing Address	188, Raja Subodh Chandra Mallick Rd, Jadavpur, Kolkata, 700032, India
Total	0.00 USD

List of Publications & Conferences

***Book Chapters**:*

1. **Das, S.**, Dey, C., Chakraborty, S., & Sengupta, A. (2024). RNA Interference (RNAi): A Boon to Medical Biotechnology. ***Exploring Medical Biotechnology- in vivo, in vitro, in silico***. (ISBN: 9781003302131) Taylor & Francis Group.

2. **Das, S.**, Mondal, A., Samanta, J., Chakraborty, S., & Sengupta, A. (2022). Tale of Viruses in Male Infertility. ***Advances in experimental medicine and biology***, *1358*, 275–323.

***Review Article**:*

1. **Das, S.**, Mondal, A., Samanta, J., Chakraborty, S., & Sengupta, A. (2021). Unfolded protein response during cardiovascular disorders: a tilt towards pro-survival and cellular homeostasis. ***Molecular and cellular biochemistry***, *476*(11), 4061–4080.

***Research Article**:*

1. **Das, S.**, Mondal, A., Dey, C., Chakraborty, S., Bhowmik, R., Karmakar, S., & Sengupta, A. (2023). ER stress induces upregulation of transcription factor Tbx20 and downstream Bmp2 signaling to promote cardiomyocyte survival. ***Journal of Biological Chemistry***, *299*(4), 103031.

2. **Das, S.**, Das, M., Chakraborty, S., & Sengupta, A. (2025). MiR-101-3p mediated regulation of Tbx20 in cardiomyocytes and Bmp2 in cardiac fibroblasts perturb cardiac homeostasis. (***Manucript Under Communication)***.

3. Mukherjee, S*., **Das, S***., Das, S., Gupta, S., Hui, S. P., Sengupta, A., & Ghosh, A. (2025). Pyruvate plus uridine augment mitochondrial respiration and prevent cardiac hypertrophy in zebrafish and H9c2 cells. ***Journal of Cell Science***, jcs.263653. Advance online publication. **(equal contribution)**.

4. Mondal, A., **Das, S.**, Das, M., Chakraborty, S., & Sengupta, A. (2024). YAP1-mediated dysregulation of ACE-ACE2 activity augments cardiac fibrosis upon induction of hyperglycemic stress. ***Biochimica et biophysica acta. General subjects***, *1868*(9), 130666.

5. Mondal, A., **Das, S.**, Samanta, J., Chakraborty, S., & Sengupta, A. (2022). YAP1 induces hyperglycemic stress-mediated cardiac hypertrophy and fibrosis in an AKT-FOXM1 dependent signaling pathway. ***Archives of biochemistry and biophysics***, *722*, 109198.

6. Samanta, J., Mondal, A., **Das, S.**, Chakraborty, S., & Sengupta, A. (2021). Induction of cardiomyocyte calcification is dependent on FoxO1/NFATc3/Runx2 signaling. ***In vitro cellular & developmental biology. Animal***, *57*(10), 973–986.

7. Mondal, A., **Das, S.**, Banerjee, A., Sengupta, A., & Molla, M. R. (2025). Amphiphilic poly(disulfide)s by a three-component Cascade reactions: a therapeutic architecture for redox-responsive intracellular drug delivery. ***Journal of Macromolecular Science, Part A***, *62*(3), 212–223.

8. Mukherjee, A., Kar, S., **Das, S.**, Bera, T., Mondal, A., Sengupta, A., & Guha, S. (2024). Design of an Acidic pH-Activated NIR Fluorescent Convertible Rhodamine-Hemicyanine

Probe-Peptide Conjugate for Living Cancer Cell Active Targeted Selective Tracking of Lysosomes. ***Chemistry (Weinheim an der Bergstrasse, Germany)***, *30*(51), e202402146.

9. Santra, S., **Das, S.**, Dey, S., Sengupta, A., Giri, B., & Molla, M. R. (2024). Degradable Polymer-Based Nanoassemblies for Precise Targeting and Drug Delivery to Breast Cancer Cells without Affecting Normal Healthy Cells. ***Biomacromolecules***, *25*(3), 1724–1737.

10. Maiti M., **Das, S.**, Panda J., Karmakar D., Pal A., Guha S., Sengupta A., Paul S., & Paul PM (2024). Spectrofluorometric detection of mercury ions in aqueous medium and cellular milieu using MoS2 nanoflakes. ***Journal of Physics and Chemistry of Solids***, *184*, 111680.

11. Santra, S., **Das, S.**, Sengupta, A., & Molla, M. R. (2023). Tumor acidity-induced surface charge modulation in covalent nanonetworks for activated cellular uptake: targeted delivery of anticancer drugs and selective cancer cell death. ***Biomaterials science***, *11*(16), 5549–5559.

12. Mondal, A., **Das, S.**, Ali, S. M., Kolay, S., Sengupta, A., & Molla, M. R. (2023). Bioderived Lipoic Acid-Based Dynamic Covalent Nanonetworks of Poly(disulfide)s: Enhanced Encapsulation Stability and Cancer Cell-Selective Delivery of Drugs. ***Bioconjugate chemistry***, *34*(3), 489–500.

13. Saha, P. C., Das, R. S., **Das, S.**, Sepay, N., Chatterjee, T., Mukherjee, A., Bera, T., Kar, S., Bhattacharyya, M., Sengupta, A., & Guha, S. (2023). Live-Cell Mitochondrial Targeted NIR Fluorescent Covalent Labeling of Specific Proteins Using a Dual Localization Effect. ***Bioconjugate chemistry***, *34*(8), 1407–1417.

14. Das, R. S., Mukherjee, A., Kar, S., Bera, T., **Das, S.**, Sengupta, A., & Guha, S. (2022). Construction of Red Fluorescent Dual Targeting Mechanically Interlocked Molecules for Live Cancer Cell Specific Lysosomal Staining and Multicolor Cellular Imaging. ***Organic letters***, *24*(32), 5907–5912.

***Conference Article*:**

1. **Das, S.**, Chakraborty, S., & Sengupta, A. (2024). MicroRNA-101-3p regulates gene signatures of murine heart to induce senescence and inflammation: a plausible biomarker of cardiomyopathy. ***Journal of Biological Chemistry*,** *300*(3), 106727.

***Conference Proceedings*:**

1. **Das, S.**, Chakraborty, S., & Sengupta, A. (2025). MicroRNA-101-3p mediated alteration of Tbx20 and Bmp2 augments cardiac injury by elevating senescence and inflammation. ***Proceedings of 1st Symposium on Emerging Frontiers of Biotechnology*,** held at Jadavpur University, Kolkata. Page no: 18, Poster no: 02.

2. **Das, S.**, Chakraborty, S., & Sengupta, A. (2024). MicroRNA-101-3p regulates gene signatures of murine heart to induce senescence and inflammation: a plausible biomarker of cardiomyopathy. ***Proceedings of DiscoverBMB 2024, organized by American Society of Biochemistry and Molecular Biology (ASBMB)*,** held at Henry B. Gonzalez Convention Centre, San Antonio, Texas, USA. Abstract No. 1068, Poster no: 309.

3. **Das, S.**, Chakraborty, S., & Sengupta, A. (2024). MicroRNA-101-3p regulates the expression of Tbx20 and Bmp2 to augments cardiac injury by modulating senescence and inflammation: a plausible biomarker of cardiomyopathy. ***Proceedings of 7th Regional Science & Technology Congress*****,** held at Presidency University, Kolkata.

4. **Das, S.**, Chakraborty, S., & Sengupta, A. (2023). Role of cardiogenic transcription factor Tbx20 in promoting cardiomyocyte survival post Endoplasmic Reticulum (ER) stress mediated cardiomyopathy. ***Proceedings of Physiology to Pathology: Finding the Therapeutic Roadmap*****,** National Conference organized by Amity University, Kolkata.

5. **Das, S.**, Chakraborty, S., & Sengupta, A. (2023). Atf6 mediated novel role of Tbx20 in promoting cardiomyocyte survival post Endoplasmic Reticulum (ER) stress mediated cardiomyopathy. ***Proceedings of 45th All India Cell Biology Conference and International Symposium on Biology of Development and Disease***, held at BHU.

6. **Das, S.**, Chakraborty, S., & Sengupta, A. (2022). Atf6 mediated novel role of Tbx20 in promoting cardiomyocyte survival post Endoplasmic Reticulum (ER) stress mediated cardiomyopathy. ***Proceedings of International Seminar on Emerging Fields of Research in Biotechnology and Biomedicine***, held at Jadavpur University, Kolkata. IAPST/2022/O/16

7. **Das, S.**, Chakraborty, S., & Sengupta, A. (2022). Role of Bmp2 in regulating cardiac remodelling post Endoplasmic Reticulum (ER) stress. ***Proceedings of Cardiovascular Research Convergence***, held at CSIR-IICB, Kolkata.

8. **Das, S.**, Chakraborty, S., & Sengupta, A. (2022). Role of cardiac transcription factor Tbx20 and Bmp2 signalling in regulating cardiac remodelling post Endoplasmic stress (ER) induced cardiomyopathy. ***Proceedings of 6th International Anatomical Sciences and Cell Biology Conference (IASCBC)***, organised by National University of Singapore, Singapore. Page no: 67, Poster no: P033.

9. **Das, S.**, Mondal, A., Chakraborty, S., & Sengupta, A. (2020). Dynamics of Tbx20 in maintaining cellular homeostasis during Endoplasmic reticular (ER) stress induced diseases. ***UGC-SAP (DRS-II) Sponsored National Conference on Stress Response and Diseases***, organised by Department of Biochemistry and Biophysics, University of Kalyani, India. Page no: 58, Poster no: ST-05.

Selected Publications

JBC RESEARCH ARTICLE

ER stress induces upregulation of transcription factor Tbx20 and downstream Bmp2 signaling to promote cardiomyocyte survival

Received for publication, November 21, 2022, and in revised form, February 3, 2023 Published, Papers in Press, February 16, 2023,
https://doi.org/10.1016/j.jbc.2023.103031

Shreya Das[1], Arunima Mondal[1], Chandrani Dey[1], Santanu Chakraborty[2], Rudranil Bhowmik[3], Sanmoy Karmakar[3], and Arunima Sengupta[1,*]

From the [1]Department of Life Science and Biotechnology, Jadavpur University, Kolkata, India; [2]Department of Life Sciences, Presidency University, Kolkata, India; [3]Bioequivalence Study Centre, Department of Pharmaceutical Technology, Jadavpur University, Kolkata, India

Reviewed by members of the JBC Editorial Board. Edited by Ronald Wek

In the mammalian heart, fetal cardiomyocytes proliferate prior to birth; however, they exit the cell cycle shortly after birth. Recent studies show that adult cardiomyocytes re-enters the cell cycle postinjury to promote cardiac regeneration. The endoplasmic reticulum (ER) orchestrates the production and assembly of different types of proteins, and a disruption in this machinery leads to the generation of ER stress, which activates the unfolded protein response. There is a very fine balance between ER stress–mediated protective and proapoptotic responses. T-box transcription factor 20 (Tbx20) promotes embryonic and adult cardiomyocyte proliferation postinjury to restore cardiac homeostasis. However, the function and regulatory interactions of Tbx20 in ER stress–induced cardiomyopathy have not yet been reported. We show here that ER stress upregulates Tbx20, which activates downstream bone morphogenetic protein 2 (Bmp2)-pSmad1/5/8 signaling to induce cardiomyocyte proliferation and limit apoptosis. However, augmenting ER stress reverses this protective response. We also show that increased expression of *tbx20* during ER stress is mediated by the activating transcription factor 6 arm of the unfolded protein response. Cardiomyocyte-specific loss of Tbx20 results in decreased cardiomyocyte proliferation and increased apoptosis. Administration of recombinant Bmp2 protein during ER stress upregulates Tbx20 leading to augmented proliferation, indicating a feed-forward loop mechanism. In *in vivo* ER stress, as well as in diabetic cardiomyopathy, the activity of Tbx20 is increased with concomitant increased cardiomyocyte proliferation and decreased apoptosis. These data support a critical role of Tbx20-Bmp2 signaling in promoting cardiomyocyte survival during ER stress–induced cardiomyopathies.

In mammals, the developing heart is highly proliferative prior to birth, and it involves the interplay of multiple signaling pathways. However, after birth, the cardiomyocytes lose its plasticity, exit the cell cycle, its proliferative capacity dissipates, and the cells grow in size primarily by hypertrophy (1). In the neonates, post 1 week after birth, the cardiomyocytes become binucleated, express adult contractile protein isoforms, and lose its ability to regenerate (2–4). The notion that adult cardiomyocytes lose their capacity to proliferate because of cell cycle arrest was revoked by growing studies showing that resident adult myocardial cardiomyocyte re-enters cell cycle following myocardial injury by regulating key regulatory pathways (5).

T-box transcription factor 20 (Tbx20) is a member of the Tbx1 subfamily of T-box–containing genes and plays pivotal roles in development and maintenance of heart by driving cardiomyocyte proliferation (6). Loss of function of Tbx20 leads to unlooped and severely hypoplastic heart with embryonic lethality (7–9). Ablation of Tbx20 in adult cardiomyocytes leads to severe cardiomyopathy with arrhythmias and death (10). Gain of function of Tbx20 leads to increased cardiomyocyte proliferation in fetal heart development (11).

Endoplasmic reticulum (ER) is an organelle that mediates production and folding of different secretory and membrane proteins (12). Any sort of dysregulation in the machinery of the ER because of external factors or internal stimulus leads to accumulation of misfolded protein leading to generation of ER stress. ER stress activates the adaptive cellular response signaling cascade known as unfolded protein response (UPR), which consists of three pathways, activating transcription factor 6 (ATF6), inositol-requiring enzyme 1 alpha (IRE1α), and protein kinase RNA-activated-like ER kinase (PERK). The protective UPR is initially beneficial as it works for restoration of homeostasis; however, a severe ER stress leads to cell death *via* apoptosis. There is a very delicate balance between ER stress–induced prosurvival and proapoptosis (13). Tbx20 overexpression was previously shown to induce proliferation of cardiomyocytes during oxidative stress and hypoxia (14); however, its mechanistic role during ER stress–mediated cardiomyopathy is still elusive.

Our study for the first time identified the novel unknown function of Tbx20 that is able to directly enhance the protective responses of the UPR for restoration of ER homeostasis in the milieu of cardiac injury. Since ER stress have been

* For correspondence: Arunima Sengupta, arunimasengupta2013@gmail.com.

Molecular and Cellular Biochemistry (2021) 476:4061–4080
https://doi.org/10.1007/s11010-021-04223-0

Unfolded protein response during cardiovascular disorders: a tilt towards pro-survival and cellular homeostasis

Shreya Das[1] · Arunima Mondal[1] · Jayeeta Samanta[1] · Santanu Chakraborty[2] · Arunima Sengupta[1]

Received: 12 March 2021 / Accepted: 8 July 2021 / Published online: 14 July 2021

Abstract

The endoplasmic reticulum (ER) is an organelle that orchestrates the production and proper assembly of an extensive types of secretory and membrane proteins. Endoplasmic reticulum stress is conventionally related to prolonged disruption in the protein folding machinery resulting in the accumulation of unfolded proteins in the ER. This disruption is often manifested due to oxidative stress, Ca^{2+} leakage, iron imbalance, disease conditions which in turn hampers the cellular homeostasis and induces cellular apoptosis. A mild ER stress is often reverted back to normal. However, cells retaliate to acute ER stress by activating the unfolded protein response (UPR) which comprises three signaling pathways, Activating transcription factor 6 (ATF6), inositol requiring enzyme 1 alpha (IRE1α), and protein kinase RNA-activated-like ER kinase (PERK). The UPR response participates in both protective and pro-apoptotic responses and not much is known about the mechanistic aspects of the switch from pro-survival to pro-apoptosis. When ER stress outpaces UPR response then cell apoptosis prevails which often leads to the development of various diseases including cardiomyopathies. Therefore, it is important to identify molecules that modulate the UPR that may serve as promising tools towards effective treatment of cardiovascular diseases. In this review, we elucidated the latest advances in construing the contribution imparted by the three arms of UPR to combat the adverse environment in the ER to restore cellular homeostasis during cardiomyopathies. We also summarized the various therapeutic agents that plays crucial role in tilting the UPR response towards pro-survival.

Keywords ER stress · Unfolded protein response · Cardiovascular diseases · Cardioprotective · Chemical · Natural products

Introduction

The endoplasmic reticulum (ER) serves as the primary gateway for protein synthesis [1]. It is involved in a multitudinal array of cellular processes including protein folding, serving as a site for synthesis of both secretory and membrane proteins as well as many steroids, cholesterol and lipids [1, 2]. The endoplasmic reticulum is an organelle that houses escalating demand for protein folding. However, any kind of dysregulation in proper protein folding due to any extracellular stimuli or intracellular loss of equilibrium often leads to the accumulation of misfolded proteins in the ER [3]. Glucose-regulated protein 78 (GRP78), an ER chaperone plays a critical role in gauging the intensity of insult done to ER due to accumulation of misfolded proteins. It acts as a protein quality control agent of the ER. A mild insult to the ER is often reverted by the chaperone function of GRP78. However, an intense disruption of the ER homeostasis causes GRP78 to activate ER transmembrane signaling molecules. The stress caused due to the accumulation of misfolded proteins is perceived by three ER resident proteins namely PERK, IRE1α and ATF6α which in turn triggers the activation of an adaptive cellular response signaling cascade known as the unfolded protein response (UPR) [4]. All the three resident proteins initially remains bound to GRP78. The UPR recruits various molecules to revert back the damaged caused and restore the cellular homeostasis. However, prolonged ER stress often leads to cell death [5]. There is a delicate balance between adaptation and apoptosis due to the upregulation of UPR during ER stress.

Cardiovascular diseases are one of the leading causes of death worldwide [6, 7]. Compelling evidences suggests that

✉ Arunima Sengupta
arunimasengupta2013@gmail.com

[1] Department of Life Science and Biotechnology, Jadavpur University, 188, Raja S. C. Mallick Road, Kolkata, West Bengal 700032, India

[2] Department of Life Sciences, Presidency University, Kolkata, India

© 2025. Published by The Company of Biologists | Journal of Cell Science (2025) 138, jcs263653. doi:10.1242/jcs.263653

RESEARCH ARTICLE

SPECIAL ISSUE
CELL BIOLOGY OF MITOCHONDRIA

Pyruvate plus uridine augments mitochondrial respiration and prevents cardiac hypertrophy in zebrafish and H9c2 cells

Soumyajit Mukherjee[1,2,*], Shreya Das[3,*], Surajit Das[1], Samudra Gupta[4], Subhra Prakash Hui[4], Arunima Sengupta[3,‡] and Alok Ghosh[1,‡]

ABSTRACT

Dysfunction of mitochondrial pyruvate oxidation and aberrant respiratory chain components are common in cardiac defects. However, the precise role of mitochondrial respiration in cardiomyocyte hypertrophy is unclear. Phenylephrine (PE) treatment of rat neonatal H9c2 cardiomyocytes promotes significant hypertrophy with decreased mitochondrial oxygen consumption rate (OCR), membrane potential, respiratory subunit NDUFB8, UQCRC2 and ATP5A (ATP5F1A) expression, and accumulation of reactive oxygen species (ROS). Surprisingly, a 60% reduction in cell survival was observed in PE-treated cells relative to control cells when grown under the respiratory-proficient galactose medium. To revert H9c2 hypertrophy and increase survival, we performed a screening with compounds that boost mitochondrial OCR and scavenge ROS, and identified pyruvate plus uridine as the best hit. As corroboration of the *in vitro* study, supplementation of pyruvate plus uridine significantly prevented PE-induced cardiac hypertrophy, pericardial edema and bradycardia symptoms in zebrafish embryos. Moreover, pyruvate plus uridine decreased the ventricular and atrial area in cardiomyocyte-specific GFP transgenic *Tg (myl7:HRAS-EGFP)* lines. Using *in vitro* and *in vivo* models, we show that boosting of mitochondrial respiration through pyruvate supplementation and scavenging ROS through uridine supplementation jointly ameliorate cardiac hypertrophy and bradycardia symptoms.

KEY WORDS: Mitochondria, Respiration, Cardiomyocyte hypertrophy, Zebrafish, Phenylephrine, Pyruvate, Uridine

INTRODUCTION

Hypertrophy in cardiac muscle leads to chronic heart failure and mortality, with a prevalence of 1 in 500 among humans (Frey et al., 2004). Cardiac hypertrophy (CH) is characterized by increased cardiomyocyte size, altered protein synthesis and defects in sarcomeric organization in heart muscle. It results as an adaptive response to different physiological and pathological factors, such as stress, mutation in sarcomeric proteins, toxicity of drugs etc. (reviewed in Metra and Teerlink, 2017; Wilcox et al., 2015). The interventricular septum and ventricles of the heart are mostly affected (Wigle et al., 1995). Transcriptional elevations of two peptides, atrial natriuretic peptide and brain/B type natriuretic peptide (BNP, encoded by *NPPB*), secreted from the cardiac atria and ventricles, decrease blood pressure and promote CH (Colucci et al., 1997; Bernardo et al., 2010). BNP modulates the levels of the transforming growth factor (TGF)-β gene, which in turn increases cardiac fibrosis and hypertrophy (Kapoun et al., 2004), thus acting as a potential biomarker of cardiovascular disease. CH is also accompanied by the activation of the rennin–angiotensin system and increased level of catecholamine in the circulatory system (Rapacciuolo et al., 2001; Scheuer, 1999). Several cardiac toxicants stimulate the release of hypertrophy inducing endocrine hormones, endothelin 1 (ET-1; also known as EDN1) and/or catecholamines (reviewed in Chen et al., 2001). Moreover, the production of high cellular reactive oxygen species (ROS) and hypoxia might also trigger CH (Chen et al., 2001; Sutton and Sharpe, 2000). Interestingly, consuming a diet rich in unsaturated fatty acids, as an antioxidant, protects against CH (Al-Shudiefat et al., 2013; Samanta et al., 2020).

A recent study claims that mitochondrial dysfunction has a role in the development of CH (Li et al., 2017). Active mitochondrial oxidative phosphorylation generates ATP essential for pumping blood by the heart (Barger and Kelly, 1999). The disparity of mitochondrial function causes ectopic ATP consumption and a large increase in lactate dehydrogenase (LDH) release, which contributes to the apoptosis of cardiomyocytes (Li et al., 2020). We previously showed that arsenic treatment inhibits the downstream target of transcription factor FoxO1, and hypertrophy inducer NFATc3 in the rat H9c2 cell line (Samanta et al., 2020). Arsenate is a well-known inhibitor of the mitochondrial pyruvate dehydrogenase complex (Bae et al., 2019; Luz et al., 2016).

Mitochondrial pyruvate oxidation and oxidative phosphorylation (OXPHOS) are known to be severely inhibited in different CH models. Similar to what is seen in cancer cells, hypertrophic cardiac cells rely on glycolysis rather than OXPHOS (Bhullar and Dhalla, 2023). Downregulation of mitochondrial pyruvate carrier 1 (MPC1) and MPC2 were observed in humans and mice with failing hearts (Fernandez-Caggiano and Eaton, 2021). Moreover, knockout of normal cardiomyocytes *MPC1* or *MCP2* genes resulted in severe hypertrophy. Impaired cardiac metabolism contributes to the deterioration of contractile function, which leads to heart failure. Studying metabolic intermediate using [1-^{13}C]pyruvate indicated that metabolic flux through pyruvate dehydrogenase (PDH) is significantly decreased despite an increased rate of glycolysis, referred to as the uncoupling of glycolysis and mitochondrial OXPHOS (Bøgh et al., 2020; Doenst et al., 2010; Schroeder et al., 2013). Interestingly, an increase of PDH flux was able to protect heart by coupling glycolysis with OXPHOS (Bøgh et al., 2020). Similarly,

[1]Department of Biochemistry, University of Calcutta, 35, Ballygunge Circular Road, Kolkata 700019, India. [2]Department of Biochemistry, Indian Institute of Science, Bangalore 560012, India. [3]Department of Life Science and Biotechnology, Jadavpur University, Kolkata 700032, India. [4]S.N. Pradhan Centre for Neurosciences, University of Calcutta, 35, Ballygunge Circular Road, Kolkata 700019, India.
*These authors contributed equally to this work

‡Authors for correspondence (arunima.sengupta@jadavpuruniversity.in; agbiochem@caluniv.ac.in)

A.S., 0000-0002-0014-3242; A.G., 0000-0001-8916-7381

Handling Editor: Ana García-Saéz
Received 31 October 2024; Accepted 15 April 2025

BBA - General Subjects 1868 (2024) 130666

Contents lists available at ScienceDirect

BBA - General Subjects

journal homepage: www.elsevier.com/locate/bbagen

YAP1-mediated dysregulation of ACE-ACE2 activity augments cardiac fibrosis upon induction of hyperglycemic stress

Arunima Mondal [a], Shreya Das [a], Madhuchhanda Das [a], Santanu Chakraborty [b], Arunima Sengupta [a,*]

[a] Department of Life Science and Biotechnology, Jadavpur University, Kolkata, India
[b] Department of Life Sciences, Presidency University, Kolkata, India

ARTICLE INFO

Keywords:
Diabetes
Cardiac fibrosis
YAP1
ACE
ACE2

ABSTRACT

Background: Diabetic stress acts on the cardiac tissue to induce cardiac hypertrophy and fibrosis. Diabetes induced activated renin angiotensin system (RAS) has been reported to play a critical role in mediating cardiac hypertrophy and fibrosis. Angiotensin converting enzyme (ACE) in producing Angiotensin-II, promotes cardiomyocyte hypertrophy and fibrotic damage. ACE2, a recently discovered molecule structurally homologous to ACE, has been reported to be beneficial in reducing the effect of RAS driven pathologies.

Methods: In vivo diabetic mouse model was used and co-labelling immunostaining assay have been performed to analyse the fibrotic remodeling and involvement of associated target signaling molecules in mouse heart tissue. For *in vitro* analyses, qPCR and western blot experiments were performed in different groups for RNA and protein expression analyses.

Results: Fibrosis markers were observed to be upregulated in the diabetic mouse heart tissue as well as in high glucose treated fibroblast and cardiomyocyte cells. Hyperglycemia induced overexpression of YAP1 leads to increased expression of β-catenin (CTNNB1) and ACE with downregulated ACE2 expression. The differential expression of ACE/ACE2 promotes TGFB1-SMAD2/3 pathway in the hyperglycemic cardiomyocyte and fibroblast resulting in increased cardiac fibrotic remodeling.

Conclusion: In the following study, we have reported YAP1 modulates the RAS signaling pathway by inducing ACE and inhibiting ACE2 activity to augment cardiomyocyte hypertrophy and fibrosis in hyperglycemic condition. Furthermore, we have shown that hyperglycemia induced dysregulation of ACE-ACE2 activity by YAP1 promotes cardiac fibrosis through β-catenin/TGFB1 dependent pathway.

1. Introduction

Diabetic cardiomyopathy is currently one of the major metabolic disorders worldwide leading to increased rate of heart failure in patients. Hypertrophy of cardiomyocyte and increased collagen deposition which leads to fibrosis in the myocardium are common occurrence in the hyperglycemic stressed heart [1,2]. Recent research has focused extensively to understand how the hyperglycemic stimulus is perceived at the molecular level in cardiac tissue to induce the pathogenesis of hypertrophy and fibrosis. In our previous study we have reported an altered fetal gene expression such as YAP1, FOXM1 under hyperglycemic stress acts as one of the major contributing factor in cardiomyocyte hypertrophy induction [3]. High glucose in the adult cardiomyocyte resulted in increased YAP1 activation through both downregulating the phosphorylation of YAP1 and increased N acetyl glycosylation of YAP1. YAP1 overexpression under hyperglycemia in turn leads to FOXM1 accumulation in the cardiac tissue, promoting pathological hypertrophy of heart [3]. However, the specific functions of YAP1 in inducing cardiac fibrosis through aberrant regulation of RAS (renin- angiotensin system) signaling molecules in the heart are not well understood.

Activated Angiotensin-II (Ang-II), the main component of RAS signaling has been well known to induce cardiomyocyte hypertrophy and fibrosis. ACE (Angiotensin converting enzyme) promotes the production of Ang-II and hence, the blocking of upregulated ACE is

Abbreviations: EMT, epithelial-mesenchymal transition; RAS, renin angiotensin system; NG, normal glucose (5 mM); HG, high glucose (25 mM); VP, verteporfin; ACE, angiotensin converting enzyme.

* Corresponding author at: 188, Raja S.C. Mullick Road, Jadavpur University, Kolkata 700032, India.
E-mail address: arunima.sengupta@jadavpuruniversity.in (A. Sengupta).

https://doi.org/10.1016/j.bbagen.2024.130666
Received 7 February 2024; Received in revised form 20 June 2024; Accepted 27 June 2024
Available online 30 June 2024

Archives of Biochemistry and Biophysics 722 (2022) 109198

Contents lists available at ScienceDirect

Archives of Biochemistry and Biophysics

journal homepage: www.elsevier.com/locate/yabbi

YAP1 induces hyperglycemic stress-mediated cardiac hypertrophy and fibrosis in an AKT-FOXM1 dependent signaling pathway

Arunima Mondal [a], Shreya Das [a], Jayeeta Samanta [a], Santanu Chakraborty [b], Arunima sengupta [a,*]

[a] Department of Life Science and Biotechnology, Jadavpur University, Kolkata, India
[b] Department of Life Sciences, Presidency University, Kolkata, India

ARTICLE INFO

Keywords:
Diabetes
Cardiac hypertrophy
Fibrosis
YAP1
FOXM1

ABSTRACT

Cardiac disease is one of the most common complications associated with diabetes. Cardiac hypertrophy and fibrosis often lead to structural and functional abnormalities leading to risks of heart failure. Several regulatory molecules related to major signaling pathways have been found to overexpress in different tissues during diabetes which show very low level of expression in non-diabetic condition. YAP1 and FOXM1 are recently being reported to play important role in various hypertrophic and fibrotic disorders. But, very limited information is still known regarding their roles in cardiomyopathies especially in the context of diabetes and hyperglycemic stress. YAP1 is known to be associated with AKT- GSK3β signaling that is one of the important regulatory pathways in glucose and lipid metabolism. On the other hand, the expression of FOXM1 has been found to be significantly upregulated in adult lung tissue with induction of fibrosis but little is known about their role in cardiac diseases. In our study, YAP1 and FOXM1 have been found to overexpress in cardiac tissue under hyperglycemic condition leading to cardiomyocyte hypertrophy and increased fibrotic response. Further YAP1 inhibition has resulted in a reduced expression of FOXM1 pointing to a possible association of YAP1 and FOXM1 in high glucose-stressed cardiomyocyte. As mechanism we have found that YAP1 undergoes reduced ser127 phosphorylation as well as extensive O-GlcNAcylation mediated activation under hyperglycemia. Upregulated YAP1 further acts through increased AKT phosphorylation causing inhibition of GSK3β that in turn results in increased FOXM1 expression, leading to cardiomyocyte hypertrophy and fibrosis.

1. Introduction

Cardiac diseases are currently one of the major health issues especially in urban areas with modern lifestyle and food habits [11]. Currently, diabetes is considered as one of the leading causes of cardiac disease across the globe. This metabolic disease leads to inefficient uptake of glucose by the cells resulting in persistent high glucose content in the blood, which often leads to cardiac hypertrophy and associated fibrotic damages [7,16]. During diabetes, the continuous hyperglycemic stress to the primary contractile cells of heart, the cardiomyocyte results in increased cellular apoptosis, which in turn leads to cardiomyocyte hypertrophy and fibrosis [10,16]. Within the cells an extensive reactivation of fetal genes causes significant alteration in transcriptional activity of different important genes responsible for the pathogenesis [23,27,36].

YAP1 is an important regulatory molecule which is known to be expressed largely during the developmental stages of various organs and subsequently its expression declines with postnatal growth. Interestingly, increased expression of YAP1 has been found in some pathologically stressed adult organs including fibrotic lung and kidney [21,30,36]. In both human hypertrophic cardiomyopathy (HCM) patient and experimental mice, YAP1 overexpression has been shown to be associated with pathological cardiac hypertrophy [32]. Several studies have recently reported an important glucose mediated activation of YAP1, however, very little information has been known regarding the role of YAP1 in the induction of cardiac hypertrophy especially in the context of diabetic cardiomyopathy [34]. In our study we have reported that hyperglycemia increases O-GlcNAcylation of YAP1 as well as inhibits phosphorylation at ser127 thereby dramatically increasing the YAP1 level within the cardiomyocyte. Along with this we observed a high level of FOXM1 that correlated with cardiomyocyte hypertrophy and fibrosis induction.

* Corresponding author.
E-mail address: arunima.sengupta@jadavpuruniversity.in (A. sengupta).

https://doi.org/10.1016/j.abb.2022.109198
Received 18 October 2021; Received in revised form 25 March 2022; Accepted 25 March 2022
Available online 28 March 2022

In Vitro Cellular & Developmental Biology - Animal (2021) 57:973–986
https://doi.org/10.1007/s11626-021-00623-0

Induction of cardiomyocyte calcification is dependent on FoxO1/NFATc3/Runx2 signaling

Jayeeta Samanta[1] · Arunima Mondal[1] · Shreya Das[1] · Santanu Chakraborty[2] · Arunima Sengupta[1]

Received: 6 July 2021 / Accepted: 17 September 2021 / Published online: 29 November 2021 / Editor: Tetsuji Okamoto

Abstract

Cardiovascular disorders (CAVDs) being a major concern over the past several years due to the huge number of morbidity and mortality worldwide, a number of studies have been done on the various aspects of cardiac problems. One of the various CAVDs is cardiovascular calcification. A number of investigations and research work have been done previously on the molecular mechanism of vascular and heart valve calcification but the mechanism of myocardial and cardiomyocyte calcification has remained uninvestigated. A number of case studies have shown the presence of calcific deposits in the myocardial/ventricular region of the heart in fetal condition as well as in individuals of different ages but no detailed studies have been done yet. In this study, we have mainly investigated the role of Forkhead box transcription factor FoxO1 and nuclear factor of activated T-cells NFATc3 in cardiomyocyte calcification. Our studies in H9c2 cardiomyocytes show that calcific deposition in cardiomyocytes does not occur in 15 d but upon osteogenic induction for 1 mo where FoxO1 expression gets reduced thereby increasing the expression of its downstream target NFATc3, thus increasing the expression of the osteogenic marker Runx2. Detailed studies on the molecular mechanism of cardiomyocyte calcification will help in finding out therapeutic strategies in the treatment of cardiac calcification.

Keywords Cardiovascular · Cardiomyocyte · Calcification · FoxO1 · NFATc3

Introduction

Cardiovascular disorders (CAVDs) are a very common pathological condition that leads to mortality of a number of people worldwide. Various studies are being done extensively on the various types of CAVDs like cardiac hypertrophy, fibrosis and myocardial infarction, cardiomyocyte apoptosis, and arterial and valvular calcification. Another known CAVD that has been detected in a number of cases not only in adult hearts but also in fetal condition is cardiac/myocardial calcification. Many case studies have been done so far on the aspect of cardiac calcification but very few detailed studies have been done on the molecular mechanism that leads to the calcific deposition in the cardiomyocytes/myocardium/ventricular region of the heart (Ivandic *et al*. 1996; Korff *et al*. 2006; Elsherif *et al*. 2008). A number of case studies have shown that calcific deposition occurs in the ventricular region in the case of renal disorder patients. Cardiac calcification has also been detected in heart failure and in other pathological condition (Lasser 1983; Catellier *et al*. 1990; Olbrich *et al*. 1990; Aras *et al*. 2006; Lee *et al*. 2007; Kruijsdijk *et al*. 2011; Rios *et al*. 2014). Myocardial/cardiomyocyte calcification is a delayed process and is often detected in patients with sepsis and other complications as observed in a number of case studies like postoperative complications and kidney disorders. For example, a patient with acute myeloid leukemia (AML) developed myocardial calcification after several weeks of suffering from sepsis.

✉ Arunima Sengupta
arunimasengupta2013@gmail.com

Jayeeta Samanta
jayeeta1993@gmail.com

Arunima Mondal
mondal.arunima18@gmail.com

Shreya Das
shreyadas1991@gmail.com

Santanu Chakraborty
santanu.dbs@presiuniv.ac.in

[1] Department of Life Science and Biotechnology, Jadavpur University, 188, Raja S. C. Mallick Road, Kolkata 700032, West Bengal, India

[2] Department of Life Sciences, Presidency University, 86/1, College Street, Kolkata 700073, India

Conference Publication

Theme: Signaling Mechanisms in the Nucleus

Abstract 1068

MicroRNA-101-3p regulates gene signatures of murine heart to induce senescence and inflammation: a plausible biomarker of cardiomyopathy

Shreya Das, *Jadavpur University*

Santanu Chakraborty and Arunima Sengupta

Keywords: miRNA, cardiomyopathy, Tbx20, senescence, inflammation

Cardiovascular diseases (CVDs) are the leading cause of death globally. Therefore early detection of the disease is pivotal in saving millions of lives. In mammalian heart, the cardiomyocytes (CM) exit cell cycle soon after birth. T-box transcription factor 20 (Tbx20) stimulates adult CM proliferation post-injury to restore homeostasis. Recently we have shown that during ER stress induced cardiomyopathy and diabetes, Tbx20 and Bmp2 signaling is upregulated with concomitant increase in CM proliferation. However, prolonged ER stress resulted in downregulation of Tbx20 whereas the expression of Bmp2 is augmented in murine heart (Das et al., J Biol Chem 2023). This led us to unravel the mechanism behind the differential regulation of Tbx20 and Bmp2 during ER stress in murine heart (approved by Institutional Animal Ethics Committee). CM and fibroblasts are the most abundant cell types present in the heart. Using real-time PCR analysis we observed higher levels of Tbx20 in CM compared to fibroblasts. On the contrary, Bmp2 inhibitor Noggin is expressed more in fibroblasts compared to CM. Since miRNAs often control gene signatures during cardiomyopathy, therefore, we hypothesized that miRNAs regulates this differential expression profile of Tbx20 and Bmp2 in murine heart during ER stress mediated cardiomyopathy and diabetes. In silico analysis revealed miR-101-3p targets both Tbx20 and Bmp2 inhibitor Noggin. Upregulation of miR-101-3p in murine heart during prolonged ER stress and diabetes is associated with concomitant decrease in expression of Tbx20. In vitro, treatment of CM and fibroblast with increasing concentration of ER stress inducer tunicamycin and prolonged hyperglycemic stress resulted in upregulation of miR-101-3p. Treatment with chemical chaperone 4-Phenylbutyric acid, a selective inhibitor of ER stress resulted in downregulation of miR-101-3p in CM as compared to cells treated with increasing concentration of tunicamycin thus potentiating that increase in the level of miR-101-3p is mediated by ER stress. Immunofluorescence analysis and immunoblotting showed decrease in the levels of miR-101-3p in vitro resulted in augmented expression of Tbx20. Since downregulation of Tbx20 resulted in decreased proliferation, therefore, we looked into the expression of senescent markers. Tbx20 downregulation is accompanied with heightened expression of senescent markers p21, p16 in murine heart as evidenced by immunoblotting and co-labelling experiments. In CM, siRNA mediated knockdown of Tbx20 resulted in increased senescence. Thus, ER stress induced augmentation of Tbx20 suppresses senescence phenotype which is reversed upon prolonging the stress. Furthermore, in fibroblasts, miRNA mediated decrease in Noggin resulted in increased expression of Bmp2 with concomitant augmentation of inflammatory markers Tnfα and Il6. Taken together, our data shows the novel function of miR-101-3p in regulating the expression of Tbx20 and Bmp2 to induce senescence and inflammation of murine heart during ER stress mediated cardiomyopathy and diabetes. Cure for CVDs are one of the important aspects of modern translational medicine, therefore development of therapeutic strategies for the treatment of adult cardiovascular diseases is invaluable. Our study showed a gradual increase in the expression of Bmp2 throughout the progression of cardiomyopathy, therefore the study establishes miR-101-3p and Bmp2 as plausible biomarkers for early detection of cardiomyopathy.

The work was supported by project grant sponsored by the Department of Science and Technology-Science and Engineering Research Board to AS (DST-SERB, grant no.: CRG/2020/000348). Shreya Das is a Senior Research Fellow funded by University Grant Commission, India.

106727, https://doi.org/10.1016/j.jbc.2024.106727

Conferences

SAN ANTONIO | MARCH 23–26

Discover BMB | 2024

American Society for Biochemistry and Molecular Biology

The American Society for Biochemistry and Molecular Biology

hereby awards this certificate to

SHREYA DAS

in recognition of being an attendee at **Discover BMB 2024**

Ann Stock

Ann Stock, Ph.D.
President

ASBMB
American Society for Biochemistry and Molecular Biology

Stephen T Miller

Stephen Miller
Executive Director

45th All India Cell Biology Conference

International Symposium on Biology of Development and Disease

2023

Certificate of Participation

This is to certify that

Shreya Das

Delivered a *Poster Presentation* at "All India Cell Biology Conference & International Symposium on Biology of Development and Disease"

held at

Department of Zoology, Institute of Science, Banaras Hindu University on

20th–22nd January 2023

Convener | Organizing Secretary | Treasurer

Poster Presentation 2nd Prize Award

Presented to

Shreya Das

at the

6th International Anatomical Sciences and Cell Biology Conference

held virtually in Singapore from 21 February to 23 February 2022

Associate Professor S Thameem Dheen
Chairman
Organizing Committee, 6th IASCBC 2022

NUS National University of Singapore | Department of Anatomy, Yong Loo Lin School of Medicine

NUHS National University Health System

Singapore Neuroscience Association

INTERNATIONAL SEMINAR ON

"EMERGING FIELDS OF RESEARCH IN BIOTECHNOLOGY & BIOMEDICINE"

CERTIFICATE OF APPRECIATION

THIS CERTIFICATE RECOGNIZES THE CONTRIBUTION OF

Prof/Dr./Mr./Ms./Miss Shreya Das

as Invited Speaker/Chair Person/Co-Chair Person/Evaluator/Delegate/Presenter(Oral/Poster)

In the International Seminar Jointly Organized by Dr. V. Ravi Chandran Centre for Advanced Research in Pharmaceutical Sciences, Jadavpur University, Kolkata, India & Indian Association of Pharmaceutical Scientists and Technologists (IAPST), Kolkata, India. held at Jadavpur University, Kolkata, India on 16 November 2022.

Prof.Dr.Biswajit Mukherjee
Coordinator,
Dr. V. Ravi Chandran Centre for Advanced Research in Pharmaceutical Sciences, Jadavpur University, Kolkata, India.

Dr.N.Udupa
President,
Indian Association of Pharmaceutical Scientists and Technologists (IAPST), Kolkata, India.

CERTIFICATE

OF PARTICIPATION

Cardiovascular Research Convergence 2022

This is to certify that Dr./Mr./Ms. ✓

Shreya Das has participated in Poster Presentation in the Cardiovascular Research Convergence 2022, held on 25th June 2022 at CSIR-IICB, Kolkata.

Arun Bandyopadhyay

Dr. Arun Bandyopadhyay
Chairman, CRC 2022

Partha Chakrabarti Sanjay Banerjee

Dr. Partha Chakrabarti and Sanjay K Banerjee
Convenors, CRC-2022

Sandeep Seth

Prof. Sandeep Seth
Chief Editor, JPCS

CSIR-IICB

KOLKATA

NIPER GUWAHATI

Journal of the PRACTICE OF CARDIOVASCULAR SCIENCES

AMITY UNIVERSITY
KOLKATA

AUK/AIBNK/Conference
Sl. No./AC/23/069

Physiology to Pathology: Finding the Therapeutic Roadmap

National Conference Organized by
Amity Institute of Biotechnology

February 16 and 17, 2023

This is to certify that, Shreya Das (Second Prize) has **participated/ presented poster/ delivered lecture** in the National Conference on "Physiology to Pathology: Finding the Therapeutic Roadmap" organized by Amity Institute of Biotechnology, Amity University, Kolkata.

Dr Ashima Bhattacharjee
(Associate Professor & Joint convener)

Dr Swatilekha Ghosh
(Assistant Professor & Joint convener)

Dr Santanu Palchaudhuri
(Advisor, Deputy Director & Head of Institution, Amity Institute of Biotechnology Amity University, Kolkata)

Prof. (Dr.) Sanjay Kumar
(Hon'ble Vice-Chancellor, Amity University, Kolkata)

1st Symposium on Emerging Frontiers of Biotechnology

Organized by

Department of Life Science and Biotechnology, Jadavpur University
188, Raja Subodh Chandra Mallick Rd, Jadavpur, Kolkata, West Bengal 700032

Certificate of Merit

This certificate is awarded to Shreya Das

for securing First / Second / Third position in poster presentation for the paper entitled

MicroRNA-101-3p mediated alteration of Tbx20 & Bmp2 ... senescence & inflammation

in the "1st Symposium on Emerging Frontiers of Biotechnology" on 30th January 2025

Biswadip Das	Ratan Gachhui	Satarupa Das	Gouranga Upadhyaya
Prof. Biswadip Das (Convenor)	*Prof. Ratan Gachhui* (Convenor)	*Dr. Satarupa Das* (Secretary)	*Dr. Gouranga Upadhyaya* (Secretary)

7th Regional Science & Technology Congress, 2024-25

Comprising Districts of the Region: 6 (Kolkata Region)

PRESIDENCY UNIVERSITY
KOLKATA

Certificate of Presentation

Certified that

Shreya Das

affiliated with

Jadavpur University

has presented a Paper titled

miR-101-3p regulates the expression of Tbx20 & Bmp2 to augment cardiac injury by modulating senescence & inflammation: a plausible biomarker of cardiomyopathy

authored by

in Biotechnology *(Scientific Discipline) of 7th Regional Science & Technology Congress, 2024-25 held on17th - 18th January, 2025 at Presidency University, Kolkata.*

Dr. Sharmistha Paul
Nodal Officer of the DSTBT, GoWB
& Joint Organising Secretary

Prof. Soumendu Chatterjee
Joint Organising Secretary

N. N. Chakraborty

Prof. Nirmalya Narayan Chakraborty
Vice-Chancellor

Jointly Organised by : Presidency University, Kolkata
And
Department of Science and Technology and Biotechnology, Government of West Bengal

UGC-SAP (DRS II) Sponsored National Conference on Stress Responses and Diseases (SR&D)

06TH & 07TH MARCH, 2020

ORGANIZED BY

DEPARTMENT OF BIOCHEMISTRY AND BIOPHYSICS, UNIVERSITY OF KALYANI

This is to certify that Prof./Dr./Mr./Mrs./Ms. Shreya Das

participated in the UGC-SAP (DRS II) sponsored National Conference on SR&D, as Invited Speaker/Presenter of an Abstract (Oral/Speed Talk/Poster) /Organiser/Participant held on 06th and 7th March, 2020 at the Department of Biochemistry and Biophysics, University of Kalyani, West Bengal.

Dr. Angshuman Bagchi
Joint Convener

Prof. Tapati Chakraborti
HOD, Dept. of Biochem. & Biophys.

Dr. Jishu Naskar
Joint Convener

The interplay of cardiac developmental factors T-box transcription factor 20 (Tbx20) and Bone morphogenetic protein 2 (Bmp2) and their cross-talk with miR-101-3p in regulating cardiac homeostasis in rodent cardiomyopathy model

ORIGINALITY REPORT

4%
SIMILARITY INDEX

PRIMARY SOURCES

1	pure.uva.nl Internet	697 words — 1%
2	www.ncbi.nlm.nih.gov Internet	572 words — 1%
3	www.biorxiv.org Internet	475 words — 1%
4	link.springer.com Internet	385 words — 1%

EXCLUDE QUOTES	OFF	EXCLUDE SOURCES	< 1%
EXCLUDE BIBLIOGRAPHY	OFF	EXCLUDE MATCHES	< 9 WORDS